Chemically Reactive Polymeric Dip/Spray-Coatings for Developing Durable and Functional Bio-inspired Interfaces

thesis submitted by

Kousik Maji

Roll No. 166122034

to

Indian Institute of Technology Guwahati

for

the award of the degree

of

Doctor of Philosophy

Department of Chemistry

Indian Institute of Technology Guwahati

Guwahati- 781039, Assam

India

13th April 2021

Dedicated to My Parents……

Indian Institute of Technology
Guwahati
Department of Chemistry

STATEMENT

I hereby proclaim that the work presented in the thesis entitled **"Chemically Reactive Polymeric Dip/Spray-Coatings for Developing Durable and Functional Bio-inspired Interfaces"** is the result of investigations of research work accomplished by me in the Department of Chemistry, under the supervision of Dr. Uttam Manna, Associate Professor, Department of Chemistry, Indian Institute of Technology Guwahati, Assam, India.

Research works used in this thesis from any other source has been fully cited and acknowledged. This work is original and has not been submitted elsewhere for the award of any degree.

13th April 2021
IIT Guwahati

Kousik Maji

Kousik Maji

Indian Institute of Technology
Guwahati
Department of Chemistry

CERTIFICATE

This is to certify that the work introduced in this thesis entitled **"Chemically Reactive Polymeric Dip/Spray-Coatings for Developing Durable and Functional Bio-inspired Interfaces"** by **Kousik Maji**, a Ph.D. student of Department of Chemistry, Indian Institute of Technology Guwahati, for the degree of Doctor of Philosophy has been carried out under my supervision and this work has not been submitted elsewhere for the award of any degree.

13th April, 2021

Dr. Uttam Manna
Associate Professor
Department of Chemistry
Indian Institute of Technology Guwahati
Assam, India

Acknowledgment

First of all, I would like to express my sincere gratitude to my supervisor Dr. Uttam Manna for his expert supervision, encouragement, motivation, advice and judicious suggestions throughout this journey. I am fortunate enough to have worked under his guidance which has enlightened me about scientific research and life in general. I am grateful to my doctoral committee members, Prof. Prof. Mohammad Qureshi (Chairperson), Dr. Lal Mohan Kundu and Dr. Sunanda Chatterjee for their valuable advice, suggestions and critiques which helped me in improving the thesis work. I am grateful to all the faculty members of Department of Chemistry, IIT Guwahati for their timely help and encouragement along with the non-teaching staff of the department for their technical support throughout my research work. I am also thankful to Central Instruments Facility (CIF), IIT Guwahati for the instrumental facilities. I gratefully acknowledge Indian Institute of Technology Guwahati for funding without which my Ph.D. work would not have been possible.

Thanks are due to all my lovable lab mates and project students for creating an environment that felt like a home away from home. Their assistance helped me a lot in completing projects in time. Staffs, students and fellows at Indian Institute of Technology, Guwahati have helped a lot in many ways and also make my tenure really memorable. My heartiest thanks to all my friends and all my teachers for being extremely supportive which makes my five years of journey truly enjoyable.

I would like to take this opportunity to thank each one of my family for their unwavering moral and emotional support whenever required.

Table of Contents

Abstract

Over the last few years, both the lotus leaf-inspired superhydrophobic surface and Nepenthe's pitcher plant-inspired slippery liquid-infused porous surfaces (SLIPS) have been emerged as a prospective avenue to design different functional materials that are useful for various relevant applications—including remediation of oil-spillages, self-cleaning, anti-biofouling, anti-corrosion, water harvesting, etc. In the past, various approaches were introduced for developing smart interfaces embedded with desired bio-inspired wettability; however, the lack of a simple and scalable fabrication process and the poor durability of the reported bio-inspired interfaces appeared as major obstacles in their practical applications. Moreover, the conventional design of SLIPS required the complete and high hydrophobization of selected porous matric before lubrication, which provided a chemically inert interface. The design of chemically reactive SLIPS is extremely challenging. In this synopsis report, I have introduced simple and scalable fabrication methods (dip coating and spray coating) for preparing an abrasion tolerant superhydrophobic and a chemically reactive SLIPS through the strategic use of a porous and chemically reactive coating, which is derived following the 1,4-conjugate addition reaction. While a stable dispersion of chemically reactive polymeric nanocomplex (CRPNC) allowed achieving chemically reactive coating on large and porous objects, the accelerated growth of the same CRPNC provided a facile basis for developing a substrate independent, porous, thick, and chemically reactive coating. Abrasion tolerant, and chemically reactive coatings were successfully prepared and further extended for developing durable and functional bio-inspired coatings for remediation of oil spillage, self-cleaning and efficient water harvesting. The synopsis report entitled **"Chemically Reactive Polymeric Dip/Spray-Coatings for Developing Durable and Functional Bio-inspired Interfaces"** has been presented with six chapters. ***Chapter 1*** introduced the fundamentals of lotus leaf and nepenthes pitcher plant-inspired liquid wettability. A brief overview of the different synthesis processes has been included. The examples of existing synthetic methodologies and the practical limitations of such techniques are discussed in chapter 1. While the facile fabrication processes suffered from durability issues, some complex and tedious approaches provided promising direction for achieving tolerant bio-inspired wettability. In the past, 1,4-conjugate addition reaction between branched polyethyleneimine (BPEI) and dipentaerithritol penta/hexa acrylate (5-Acl) was successfully exploited to achieve chemically reactive polymeric nanocomplex (CRPNC). The optically transparent reaction mixture of BPEI/5Acl in ethanol yielded a turbid solution of growing CRPNC—which was further transformed into a free-standing gel within 3h. ***Chapter 2*** introduced a simple dilution process to stabilize such CRPNC in ethanol. Simple and single dip-coating of a commercially available and highly deformable spongy substrate, i.e., melamine sponge (MS) in the ethanolic solution of CRPNC

allowed to develop a chemically reactive polymeric coating on the MS. The same dipping solution of CPRNC was successfully re-used to achieve chemically reactive coating on bare MS. Further, the post-covalent modification of the chemically reactive coating with octadecylamine yielded the superhydrophobic sponge with a water contact angle of 159°. The synthesized superhydrophobic MS remained highly abrasion tolerant and sustained different kinds of harsh physical and chemical exposures without compromising the embedded water repellence property. This highly deformable and robust superhydrophobic MS selectively absorbed oil/oily phase with the capacity of 70 gg^{-1}, was extended for separating oil-spillages from an aqueous phase. Furthermore, the oil/water separation efficiency remains unaltered at practically relevant different severe aqueous mediums. ***Chapter 3*** accounted for a simple spray deposition of CPRNC for preparing a thick (254 ± 10 μm), porous, and chemically reactive polymeric coating on various substrates. A simple alteration of the reaction medium (from ethanol to pentanol) for the same reactant composition of BPEI/5Acl accelerated the sol-gel transition. A rapidly growing and turbid solution of CRPNC in pentanol was spray deposited onto a glass substrate to yield a thick, three-dimensionally (3D) chemically reactive and porous polymeric coating—which was found to be inherently hydrophilic. However, the appropriate post covalent modification through 1,4- conjugate addition reaction allowed to tailor the fraction of contact area between the beaded water droplet and the porous polymeric coating. Eventually, a wide range of water wettabilities—including non-adhesive superhydrophobicity (NASH) and controlled-adhesive superhydrophobicity (CASH), were achieved using the same chemically reactive spray coating. The synthesized coating survived the severe physical abrasions and the exposures to harsh aqueous phases. Such an approach was successfully applied to coat various other relevant substrates. Moreover, the self-cleaning performance of the robust superhydrophobic coatings was demonstrated in detail. In ***chapter 4,*** the same hydrophilic and chemically reactive porous coating that was loaded with residual acrylate groups as described in chapter 3 was directly lubricated with silicone oil; and the post covalent modification of the polymeric coating was not incurred. Interestingly, the hydrophilic and chemically reactive porous coating displayed the slippery property, where the beaded water droplet (WCA of 83.7°) slipped away on the tilted (2.1°) interface. The residual acrylate groups in the chemically reactive coating played a crucial role in achieving essential chemical compatibility to attain the slippery property. Further, such a slippery interface remained chemically reactive towards amine-containing small molecules. Eventually, a spatially selective chemical modulation was demonstrated using organic solvents. Further, the impact of chemistry on the design of SLIPS was examined in detail. During the study, I found that the spray coating of CRPNC was loaded with two distinct residual functional groups—i.e., amine and acrylate. In ***chapter 5,*** this dual chemically reactive polymeric

coating was strategically utilized to achieve different types of bio-inspired liquid wettability—including superhydrophobic interface (SHI), hydrophobic SLIPS (HB-SLIPS), hydrophilic SLIPS (HL-SLIPS), chemically patterned superhydrophobic interface (CP-SHI), chemically patterned hydrophobic SLIPS (CP-HB-SLIPS) and chemically patterned hydrophilic SLIPS (CP-HL-SLIPS). The residual chemically reactive groups (amine and acrylate) present in the same polymeric coating allowed to associate diverse and desired chemistries through post modification, and the appropriate choice of lubricants allowed to achieve both hydrophilic-SLIPS and hydrophobic SLIPS. Further, the water harvesting performance of all the interfaces was examined under the identical experimental conditions. The specific arrangement of chemically modulated hydrophilic patterns on hydrophilic-slippery background accelerated both the growth and shedding of the condensed water droplets. Furthermore, an array of hydrophilic spots on a physically confined hydrophilic-SLIPS yielded the most efficient water harvesting SLIPS with an unprecedented efficiency of 4400 ± 190 mg cm^{-2} h^{-1}. Finally, in ***chapter 6,*** the summary of my thesis work has been described, and the prospects of the current design have also been accounted for.

Chapter 1: Introduction

The understanding of the wetting behavior of a liquid on a solid surface is centuries aged concept that has enormous potential for various relevant applications—starting from cave arts in ancient history to microfluidic devices in modern life.[1,2] The lotus leaf-inspired extreme water-repellence[3], which is widely recognized as superhydrophobicity[4], requires essential hierarchical features (also known as micro/nano topography) that are topped with waxy-like coating.[5] In general, various types of hydrophilic buildings blocks were commonly used to develop appropriate hierarchical topography for synthesizing artificial superhydrophobic surfaces. Further, the hydrophilic hierarchical topography was decorated with inert low surface energy coating—mostly through weak physical interactions/bonding for the entrapment of external meta stable air phase that reduces the interaction between the solid surface and the beaded water phase.[6] However, such surfaces are highly susceptible to mechanical deformations, and the physical abrasion leads to alteration of both the surface topography as well as the surface chemistry.[6,7] Eventually, the embedded anti-wetting property is compromised, as shown in Fig. 1E, F. The compromised embedded anti-wetting property due to abrasive physical/chemical exposures can be repaired or self-healed by adopting some complex and unconventional designs of superhydrophobicity. However, the limited healing/repairing cycles restricted the prolonged and unperturbed performance.[8,9] Recently, the concept of bulk-superhydrophobicity has been introduced in the literature where the embedded anti-wetting property is present in the synthesized material three-dimensionally, i.e., in the top surface as well as the interior

of the material. The synthesized bulk superhydrophobic material can withstand various harsh physical and chemical exposures without perturbing the extreme water repellence property. Furthermore, the meta-stable trapped air in superhydrophobic interfaces is inherently labile to displace, and the extreme water repellence property compromise at severe conditions. Recently, Aizenberg *et al*. introduced

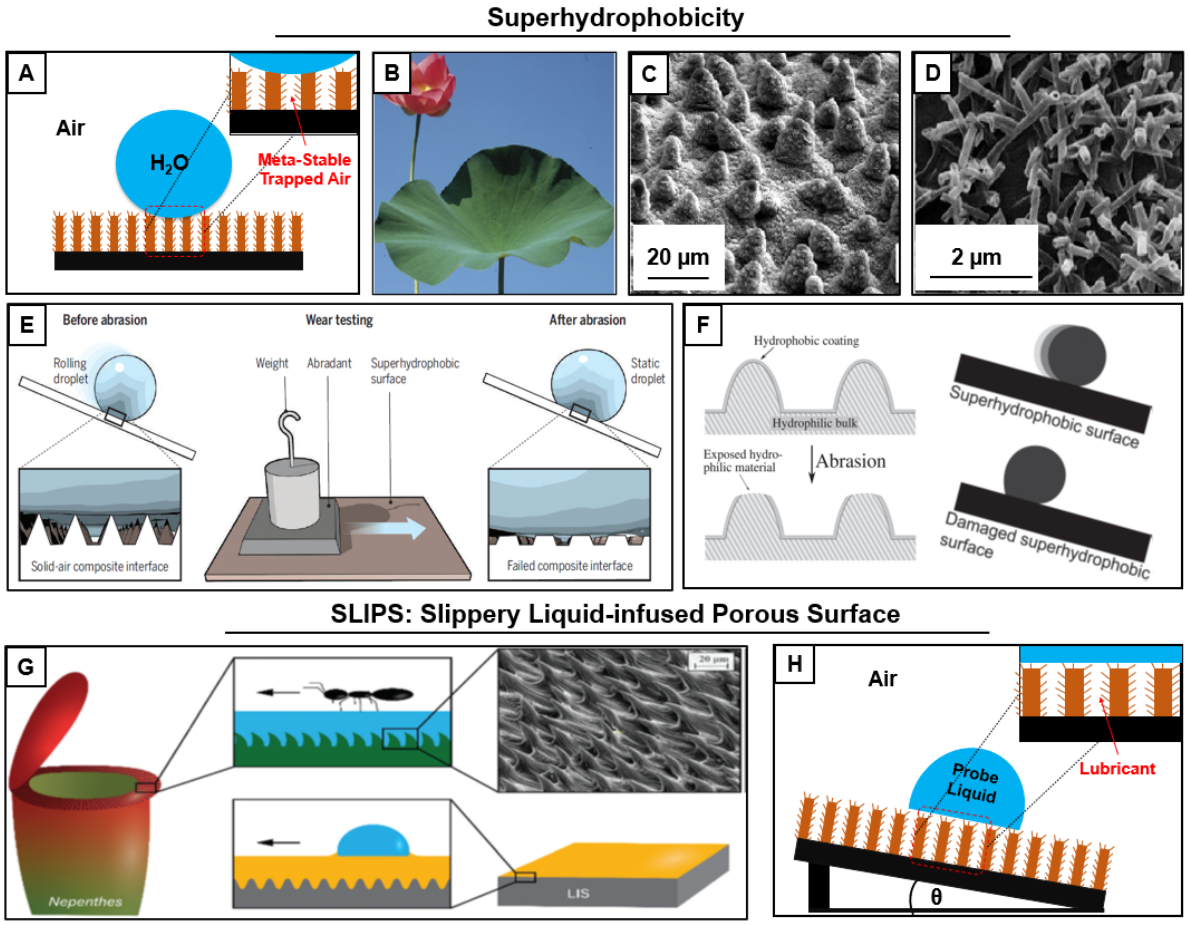

Figure 1. (A) Schematic demonstration of lotus leaf-inspired superhydrophobic surface. (B-D) Digital and (B) FESEM images (C, D) of the lotus leaf. (Reprinted with permission from *Progress in Materials Science* **2009**, *54*, 137–178. Copyright 2009, Elsevier). (E, F) Traditional superhydrophobic surfaces lose their anti-wetting property by the destruction of hierarchical feature (E) (Reprinted with permission from *Science* **2016**, *352*, 142. Copyright 2016, Science) or surface chemistry (F) (Reprinted with permission from *Adv. Mater.* **2011**, *23*, 673–678. Copyright 2011, Wiley-VCH) due to mechanical abrasion. (G) A nepenthes pitcher traps a thin layer of lubricating water phase through its rough surface structure which helps to slide insects towards the digestive bottom of the plant (top). A traditional approach for artificial development of SLIPS (bottom). (Reprinted with permission from *Chem. Soc. Rev.*, **2020**, *49*, 3688−3715. Copyright 2020, Royal Society of Chemistry) (H) Schematic representation of nepenthes pitcher plant-inspired SLIPS.

slippery liquid-infused porous surface (SLIPS), which is inherently capable of sustaining exposures of extremes of pressure, temperature, and so on.[10] The carnivorous nepenthes pitcher plant survives in nutrient-deficient environments and evolved with a specialized trapping organ, known as a pitcher. The special structures of the peristome surface play an important role in slippery property. In the rainy season, when insects step on the surface at the rim of the pitcher, they will slide down into digestive

juices at the bottom, as shown in Fig. 1G.[11] The slippery nature of the peristome appeared due to the lubrication of a thin layer of aqueous phase into the rough surface structure; eventually, the lubricated interface exhibited slipperiness towards oily insect's feet.[11] The surface roughness, chemical composition, and proper choice of lubricant are the essential criteria for synthesizing artificial SLIPS. Traditionally, SLIPS were prepared by lubricating a chemically inert, highly hydrophobic, and hierarchical interface with selected lubricants, where the selected lubricant was immiscible with probe liquid (i.e., mostly water).[11] Thus, in the past, chemically inert SLIPS are mostly reported in the literature. However, the design and synthesis of chemically reactive SLIPS remained a challenge, and such an interface would be useful for various relevant applications.

Both superhydrophobic and SLIPS are with potential for applications[12-32] *including self-cleaning,[14-15] oil/water separation,[16-19] drug delivery,[20] anti-corrosion,[21-23] anti-biofouling[24-26] anti-icing,[27,28] water harvesting[29,] and many more.[30-32]* Over the past two decades, several methods like *Plasma Treatment,[33] Lithographic Technique,[34] Template Based Technique,[35] Chemical vapor deposition,[36,37] layer by layer method,[38] Spin Coating,[39] spray deposition technique[40] and so on[41-45]* were introduced to prepare hierarchical topography (micro/nano features), which is the common and essential requirement for achieving both superhydrophobicity and SLIPS. Despite having potential for prospective applications, such bio-inspired surfaces are commonly suffered from the lack of a simple fabrication process to provide durable and uninterrupted liquid wettability. In this thesis work, the scalable and durable bio-inspired water repellent interfaces were fabricated following a simple synthetic procedure for relevant outdoor applications such as oil/water separation, self-cleaning surfaces, and water harvesting. Previously, Rather *et al.* had developed an artificial bulk-superhydrophobic monolith by exploiting mutual chemical reactivity of acrylate and amine groups following the catalyst-free 1,4- conjugate addition reaction. The reaction mixture of branched poly-(ethyleneimine) (BPEI) and dipentaerythritol penta/hexa acrylate (5Acl) in ethanol transformed into a chemically reactive and free-standing gel via the formation of chemically reactive polymeric nano complex (CRPNC). Further, the salt-assisted accelerated gelation of the CRPNC provided appropriate topography to achieve desired superhydrophobicity after post-covalent modification of the chemically reactive gel with decylamine.[46] In my thesis work, I have extended this CRPNC for developing durable and scalable bio-inspired coatings following the facile deposition (i.e., dip-coating or spray coating) processes. Further, the synthesized coating has been extended for various relevant and outdoor applications—including oil/water separation, self-cleaning and water harvesting.

Chapter 2: Synthesis of Scalable and Durable Superhydrophobic Melamine Sponge for Efficient Oil/Water Separation

In this chapter, I have formulated a simple dip-coating methodology for achieving a durable lotus leaf-inspired superhydrophobic coating on a commercially available melamine sponge for oil/water separation application. In this work, a stable dispersion of chemically reactive polymeric nano-complexes was achieved by adopting a simple half dilution process. The reaction mixture of BPEI and 5Acl in ethanol was diluted to half with the same solvent after 1 h of mutual reaction between the selected reactants at ambient conditions.[47] The half dilution of the reaction mixture led to the reduction of uncontrolled aggregation of reactive nano complexes in the solution, whereas the mixture of BPEI/5Acl led to the formation of a reactive polymeric gel without dilution shown in Fig. 2D-I. The size of the nanocomplex in the half diluted reaction mixture remained steady at 465 nm over 48 h. Then, the native melamine sponge (MS), which is inherently hydrophilic as well as oleophilic, was dipped in the stable dispersion of the nanocomplexes for 3 h. Further, the covalent modification of the chemically reactive coating with octadecylamine (ODA) through the 1,4- conjugate addition reaction provided a durable superhydrophobic coating, as shown in Fig. 2J-N. The successful deposition of chemically reactive nanocomplexes on the MS and its post covalent modification with ODA was investigated through field emission scanning electron microscope (FESEM) and Fourier-transform infrared (FTIR) analysis. The smooth and featureless domains of highly porous native MS (Fig. 2O) were uniformly covered with random granular features of chemically reactive polymeric nanocomplexes, as evident from FESEM images (Fig. 2P). Further, the chemical reactivity of the deposited nanocomplexes on the MS was confirmed by the FTIR analysis. The peaks at 1410 cm^{-1} and 1735 cm^{-1} indicated the characteristics C-H stretching of β-carbon of the vinyl group and C=O stretching, respectively, and revealed the presence of residual acrylate group in the dip-coated MS, as shown in Fig. 2Q (red). Further, the depletion of IR peak intensity at 1410 cm^{-1} with respect to normalized IR peak for carbonyl stretching at 1735 cm^{-1} was noted, which unambiguously indicated the successful post-chemical modification of the residual acrylates on the chemically reactive dip-coating with ODA through 1,4- conjugate addition reaction as shown in Fig. 2Q (black). Moreover, the synthesized superhydrophobic melamine sponge (SMS) was exposed to several harsh physical (sandpaper abrasion, sand drop test, scratching, prolonged UV irradiation) and chemical (exposed to pH=1, pH=13, river water, DTAB solution, seawater, etc.) conditions, however, the embedded anti-wetting property was found to be unperturbed. This impeccable physical and chemical durability can be attributed to the strategic use of facile and robust Michael addition reaction between amine and

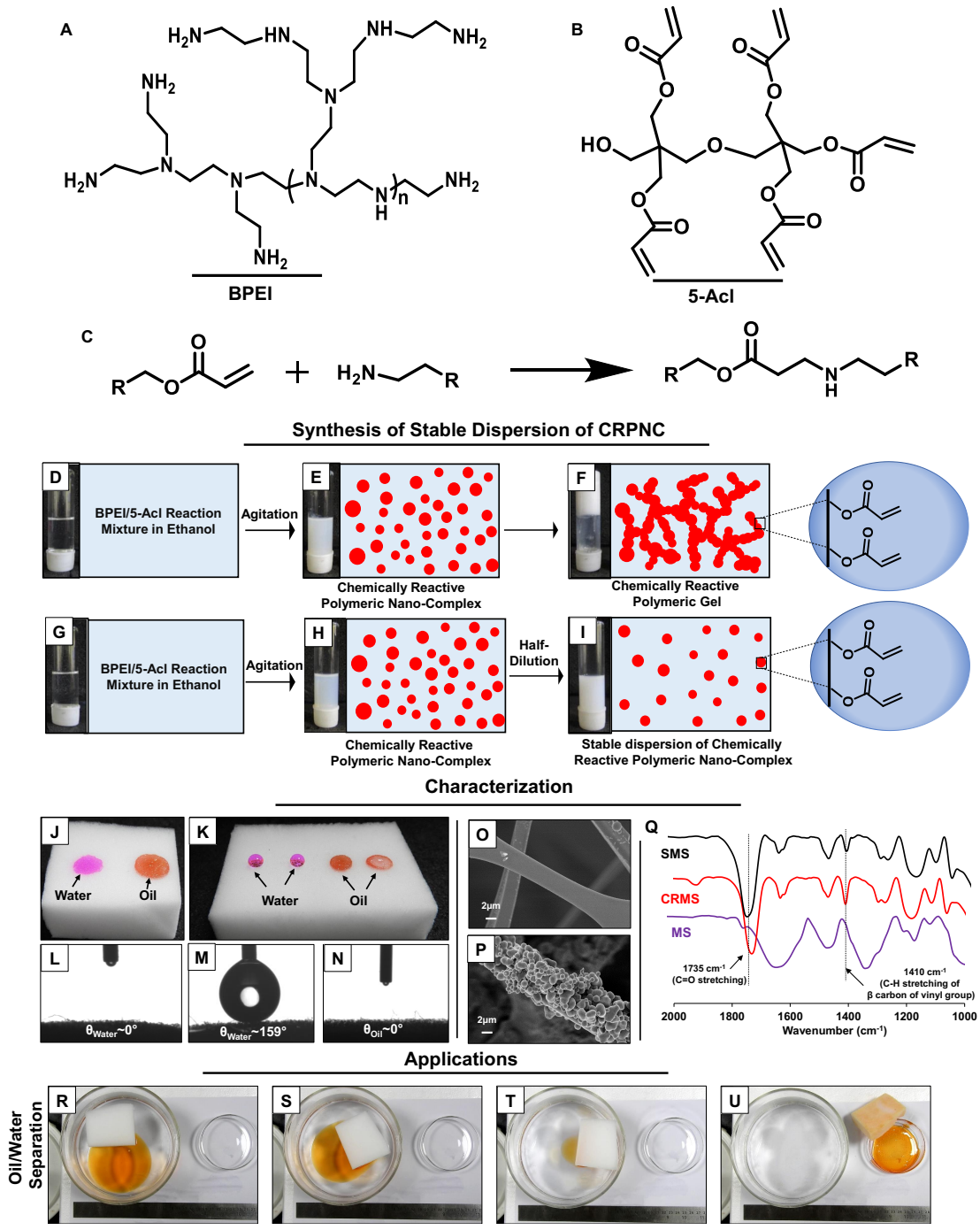

Figure 2. (A-B) Chemical structure of poly(ethyleneimine) branched (BPEI) (A), and dipentaerythritol penta/hexa acrylate (5Acl) (B). C) Chemical reaction between acrylate and amine functionalities through a 1,4-conjugate addition reaction. (D-I) The reaction mixture of BPEI and 5Acl transformed into a reactive polymeric gel and a stable dispersion of CRPNC without (D-F) and with (G-I) dilution. (J-K) Digital images of native melamine sponge (J), as prepared superhydrophobic melamine sponge (K) which repelled beaded water droplet selectively (K). (L, M) Water contact angle image of native (L) and superhydrophobic melamine sponge (SMS, M). (N) Oil contact angle image on as prepared SMS. (O, P) FESEM images of bare MS (O) and synthesized SMS (P). (Q) FTIR spectra of native melamine sponge (MF, purple), chemically reactive melamine sponge (CRMS, red), and superhydrophobic melamine sponge (SMS, black) where the signal at 1735 cm^{-1} and 1410 cm^{-1} corresponds to C=O stretching frequency of carbonyl group and C-H stretching frequency of β carbon of vinylic group respectively. (R-U) Snapshot images of superhydrophobic melamine sponge during absorption-based oil/water separation.

acrylate moieties at ambient conditions for optimizing both appropriate topography and essential low

surface energy. The embedded extreme water repellence, along with the excellent mechanical and chemical durability of the SMS made it an ideal candidate for selective absorption-based oil/water separation at practically relevant settings. For proof of demonstration, some motor oil having density less than water was placed at the water interface. A piece of SMS selectively absorbed the motor oil from the aqueous phase, as shown in Fig. 2R-U. Thereafter, oil/water separation was repeated with other water-immiscible liquids having wide ranges of densities. SMS successfully and selectively collected oil from the oil/water interface with more than 90% separation efficiency at practically relevant diverse and severe settings.

Chapter 3: Chemically Reactive Spray Coating for Achieving Durable and Bulk Superhydrophobicity

In this Chapter, we have utilized the same catalyst-free, rapid, and mutual reactivity between amine and acrylate groups of branched poly(ethyleneimine) (BPEI) and dipentaerythritol penta/hexa acrylate (5Acl), respectively for synthesizing a three-dimensionally 'chemically-reactive', scalable, and porous polymeric coating on various relevant substrates.[48] The dip-coating method, as demonstrated in chapter 2 was not suitable for the preparation of a thick polymeric coating on rigid and flexible flat substrates. In this context, the reaction mixture of BPEI/5Acl was shaken vigorously in a commercially available spraying bottle, prior to spray deposit (Fig. 3A) onto the selected substrates. The reaction medium played an important role in accelerating the growth of CRPNC. The lower analogs of pentanol yielded inhomogeneously deposited (ethanol), peeled off (propanol), and cracked (butanol) coatings, whereas the spray deposition of the same reaction mixture prepared in pentanol provided a homogenous and stable polymeric coating as shown Fig. 3B-E. The synthesized porous and covalently cross-linked polymeric coating possessed 'chemically-reactive' residual acrylate functionality three-dimensionally, including the surface and interior of the coating as confirmed by the FTIR study as shown in Fig. 3G. The appearance of IR peaks at 1410 cm^{-1} and 1732 cm^{-1} signified the existence of residual acrylate moiety in the polymeric coating. The entire polymeric coating was post-modified through a simple 1,4- conjugate addition reaction under ambient conditions.[43] In general, the controlled regulation of adhesive interaction between a beaded water droplet and superhydrophobic coating is highly challenging. The synthesized ‘chemically-reactive’ polymeric coating allowed to adopt addition reaction with appropriately selected alkylamine. A non-adhesive superhydrophobicity (NASH; with $\theta_{roll\text{-}off.}$ below 5°) was achieved after covalent modification of the chemically reactive coating with alkylamine having long hydrocarbon tails (octadecylamine ($\theta_{roll\text{-}off.}$ ~ 3°), dodecylamine ($\theta_{roll\text{-}off.}$ ~ 4°), decylamine ($\theta_{roll\text{-}off.}$ ~ 4.5°)). Whereas, controlled adhesive superhydrophobicity (CASH; with $\theta_{roll\text{-}off.}$ above 10°) was obtained after chemical modification of the same coating with alkylamines having

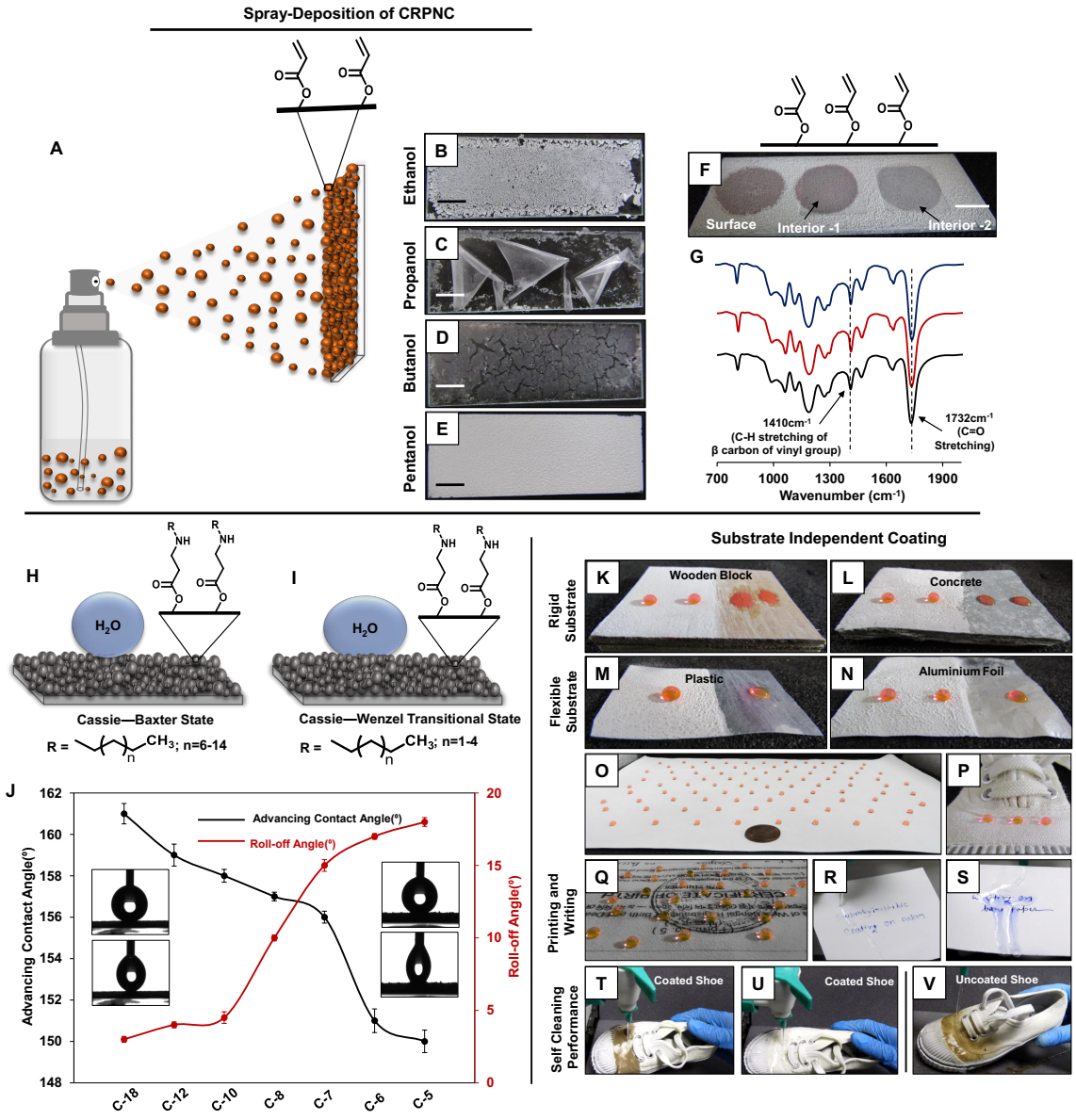

Figure 3. (A) Schematic representation of spray deposition process. (B-E) Reactive polymeric interfaces were obtained from spray deposition of CRPNC from ethanol (B), propanol (C), butanol (D), and pentanol (E). (F) Digital image of the soaked water droplet on the reactive polymeric interface which is obtained from spray deposition of CPRNC in pentanol where residual acrylate groups present three-dimensionally including surface, interior 1, and interior 2. (Interior 1 and Interior 2 obtained through single and double adhesive tape peeling process). (G) FTIR spectra obtained from three different regions of the same reactive polymeric coating including surface, interior 1, and interior 2 where peaks at 1732 cm^{-1} and 1410 cm^{-1} correspond to stretching frequency of C=O of the carbonyl group and C-H stretching of β carbon of vinyl group respectively. (H, I) Schematic representation of the Cassie–Baxter (non-adhesive superhydrophobicity; NASH) (H) and Cassie–Wenzel transitional states (controlled adhesive superhydrophobicity; CASH) (I). (J) A plot showing the chemically tailored wettability, where black and red lines indicate a decrease in the advancing contact angle and an increase in the roll-off angle, respectively, on reducing the carbon chain length of the covalently attached small molecules. (K-P) Digital images of the coated wooden block (K), concrete (L), a plastic (M), aluminum foil (N), A-4 size paper (O) and shoe (P) with non-adhesive superhydrophobicity which repels beaded water droplets (red color aids visual inspection). (Q-S) Digital images of water droplets on superhydrophobic printed paper (Q), water stream on a superhydrophobic (R), and uncoated paper (S) written with a fountain pen. (T, U) Snapshot images of self-cleaning process on the coated superhydrophobic shoe where deposited dust cleaned under the stream of water without wetting the shoe. (V) Digital image of the uncoated shoe which became muddy during the process of self-cleaning.

comparatively shorter hydrocarbon tails length (octylamine ($\theta_{roll\text{-}off.}$ ~10°), heptylamine ($\theta_{roll\text{-}off.}$ ~ 15°),

hexylamine ($\theta_{roll\text{-}off.}$ ~ 17°), pentylamine ($\theta_{roll\text{-}off.}$ ~ 18°)), as shown in Fig. 3H-J. Then, this synthetic approach was extended to coat various relevant objects –including wooden block, concrete, plastic, aluminum foil, A4 size paper, shoe, etc. to obtain the superhydrophobicity (Fig 3K-P) with different roll-off angles. Further, printing and writing have been conducted on the synthesized non-adhesive superhydrophobic paper with a regular printing machine and fountain pen, respectively, as shown in Fig 3Q, R. The deposited ink on a bare paper spread arbitrarily under the stream of water, as shown in Fig 3S, whereas, such spillage and spreading of deposited ink was not observed for superhydrophobic coating. Further, the self-cleaning ability of the superhydrophobic interfaces was demonstrated, where a shoe was decorated with non-adhesive superhydrophobicity and a substantial amount of dust particles deposited on the coated shoe before exposing it to an aqueous stream. In the end, a self-cleaned and dry shoe was recovered, whereas the uncoated shoe became muddy and wet under the identical exposures as described in Fig. 3T-V. Thus, the current design of synthesizing artificial bio-mimicking wettability made it possible to develop some smart materials for convenient and relevant uses in practical settings.

Chapter 4: Design of Chemically Reactive Slippery Liquid Infused Porous Surfaces

In this chapter, the hydrophilic and chemically reactive porous polymeric coating introduced in chapter 3, was extended for evaluating the impact of chemistry for designing slippery liquid-infused porous surfaces (SLIPS). During the course of the study, the chemically reactive, porous, and hydrophilic interface, as described in chapter 3, has been lubricated directly with various ranges of natural and synthetic liquid lubricants. Surprisingly, the lubricated interfaces displayed slippery property—without requiring any additional prior hydrophobization. In contrast, in the past, hydrophobic post modification, prior to lubrication, was routinely adopted as an essential component for designing SLIPS.[49,50] In our current design of SLIPS, it is experimentally validated that the residual acrylate groups help to anchor the water-immiscible lubricating phase,[51] even though the entire porous polymeric coating remained highly hydrophilic (with a water contact angle (WCA) of ~20°). The same porous polymeric coating failed to show slippery property once residual acrylate groups were consumed by D-glucamine through 1,4- conjugate addition reaction prior to the lubrication (Fig. 4C). The porous polymeric coating remained highly efficient to show slippery property after post covalent modification with the higher analog of butylamine prior to lubrication, as shown in Fig. 4D. However, modification with propylamine and butylamine led to the loss in the slippery property of the porous polymeric coating after lubrication (Fig. 4E). Thus, the chemical compatibility of the lubricants with the porous matrix is essential to confer slippery property. Again, the chemical compatibility with the lubricants has been demonstrated in the following section. At first, the as-prepared reactive hydrophilic

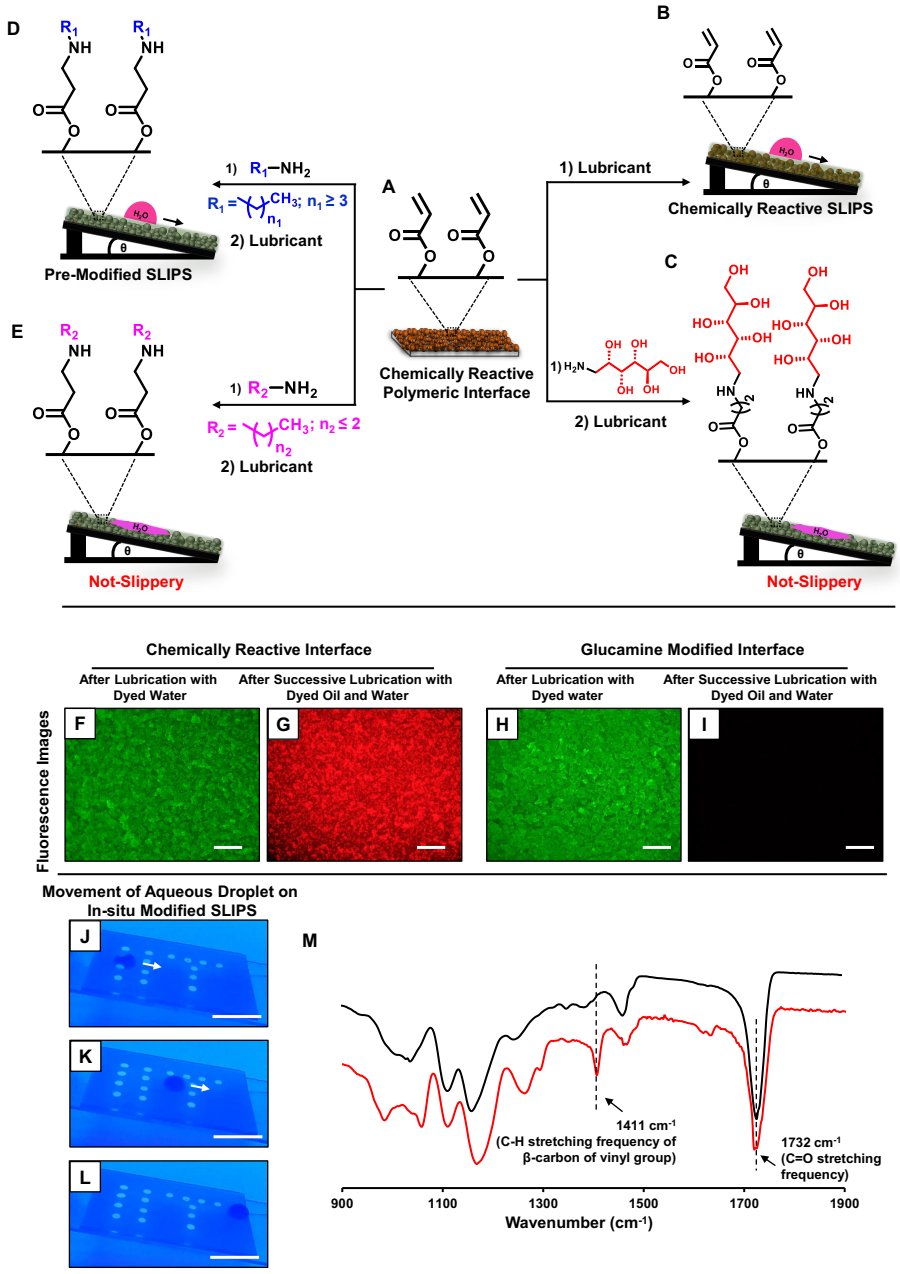

Figure 4. (A-E) Schematic representation of various lubricated interfaces, where the lubrication on the chemically reactive interface and post modified interfaces with higher analogues of butylamine able to show slippery property (B, D), whereas the glucamine, propylamine, and butylamine treated polymeric interfaces unable to display slippery property (C, E) on lubrication. (F-I) Fluorescence microscopic images of the chemically reactive (F-G) and glucamine-modified polymeric coating (H-I) after immersion in dyed (fluorescein, water-soluble) aqueous phase (F, H; scale bar: 500 µm) and successive immersion in dyed (Nile red, water-immiscible) silicone oil and DI water (G, I; scale bar: 500 µm), DI water used for washing the interface. (J-L) Movement of the aqueous droplet on in-situ modified (direct modification on the amine-reactive lubricated surface with dansyl cadaverine through 1,4-conjugate addition reaction) SLIPS. Snapshots are taken under UV lamp; Scale Bar is 1 cm. (M) FTIR spectra of chemically reactive SLIPS with (black) and without (red) in-situ modification with DC.

polymeric interface submerged into an aqueous solution of fluorescein for 30s for complete infiltration of dyed water into the polymeric matrix. The green fluorescence signal confirmed the infiltration of dyed water into the matrix, as shown in Fig. 4F. Then, the wet polymeric matrix immersed in Nile red

(water-immiscible) added solution of silicone oil followed by washing with DI water (to remove loosely held silicone oil). The only red fluorescence signal implied a complete displacement of dyed water from the reactive polymeric coating by silicone oil, as shown in Fig. 4G. Under the identical experiment as described above, the glucamine treated polymeric coating immediately soaked the dyed water as described in Fig. 4H, but silicone oil failed to displace the impregnated aqueous phase from the glucamine treated polymeric matrix. No fluorescence signal was observed for Nile red, as shown in Fig. 4I. Further, the residual acrylate moieties present in the polymeric coating have been utilized for in-situ modification of chemically reactive SLIPS. The pattern in the form of 'IIT' has been generated by transferring a series of droplets (0.7 μL) of dansyl cadaverine (DC) in MeOH on the reactive polymeric coating after lubrication without spillage of the organic medium. However, the slippery property was found to be unaltered after in-situ modification, as revealed under a UV lamp in Fig. 4J-L. The modification of the same interface before lubrication without lubricants led to arbitrary spillage of DC on the reactive polymeric coating. After DC treatment, the significant depletion of IR peak intensity at 1411 cm^{-1} with respect to normalized C=O stretching at 1732 cm^{-1} suggested successful in-situ modification of the chemically reactive SLIPS. However, such spatially selective chemical modulation on the hydrophilic and chemically reactive coating was not possible to achieve with an aqueous phase both in the presence and absence of lubrication.

Chapter 5: Design of Chemically Patterned Hydrophilic SLIPS for Achieving Efficient Water Harvesting

During the course of the current study,[52] the same spray deposited porous polymeric coating, which is demonstrated in chapter 3, was found to be loaded with two distinct and residual groups, amine and the acrylate, as shown in Fig. 5A, and the coating is denoted as DCRPPI (dual chemically reactive porous polymeric interface). The two distinct chemically reactive groups were exploited to optimize different degrees of bio-inspired liquid wettability on DCRPPI through the appropriate selection of the post-chemical modifications and (or) lubricants. The DCRPPI inherently displayed hydrophilicity with a water contact angle (WCA) of approximately 20° and became superhydrophobic with a WCA of approximately 154º after the post covalent modification with octadecyl acrylate (ODAC). The ODAC treated superhydrophobic polymeric coating became super-hydrophilic upon treatment with D-glucamine. This simple post modification process can be adopted with spatial selectively for developing a hydrophilic/superhydrophobic pattern interface (denoted as CP-SHI; Fig. 5A) without having any arbitrary spillage of the aqueous solution of small molecules (i.e. D-glucamine). The patterned hydrophilic spots on the ODAC treated SHI background were obtained by transfer of tiny aqueous droplet of D-glucamine (doped with 20% Ethanol) using a fountain pen where the primary

amine group of the selected D-glucamine readily reacted with the residual acrylate groups of the SHI through the 1,4-conjugate addition reaction. Further, lubrication of CP-SHI with olive oil (natural) and krytox (synthetic) led to the synthesis of both CP-HL-SLIPS and CP-HB-SLIPS, respectively. Then, the water harvesting efficiency of the prepared interfaces has been investigated thoroughly. The shedding and growth of condensed water droplets were much faster for HL-SLIPS in comparison to

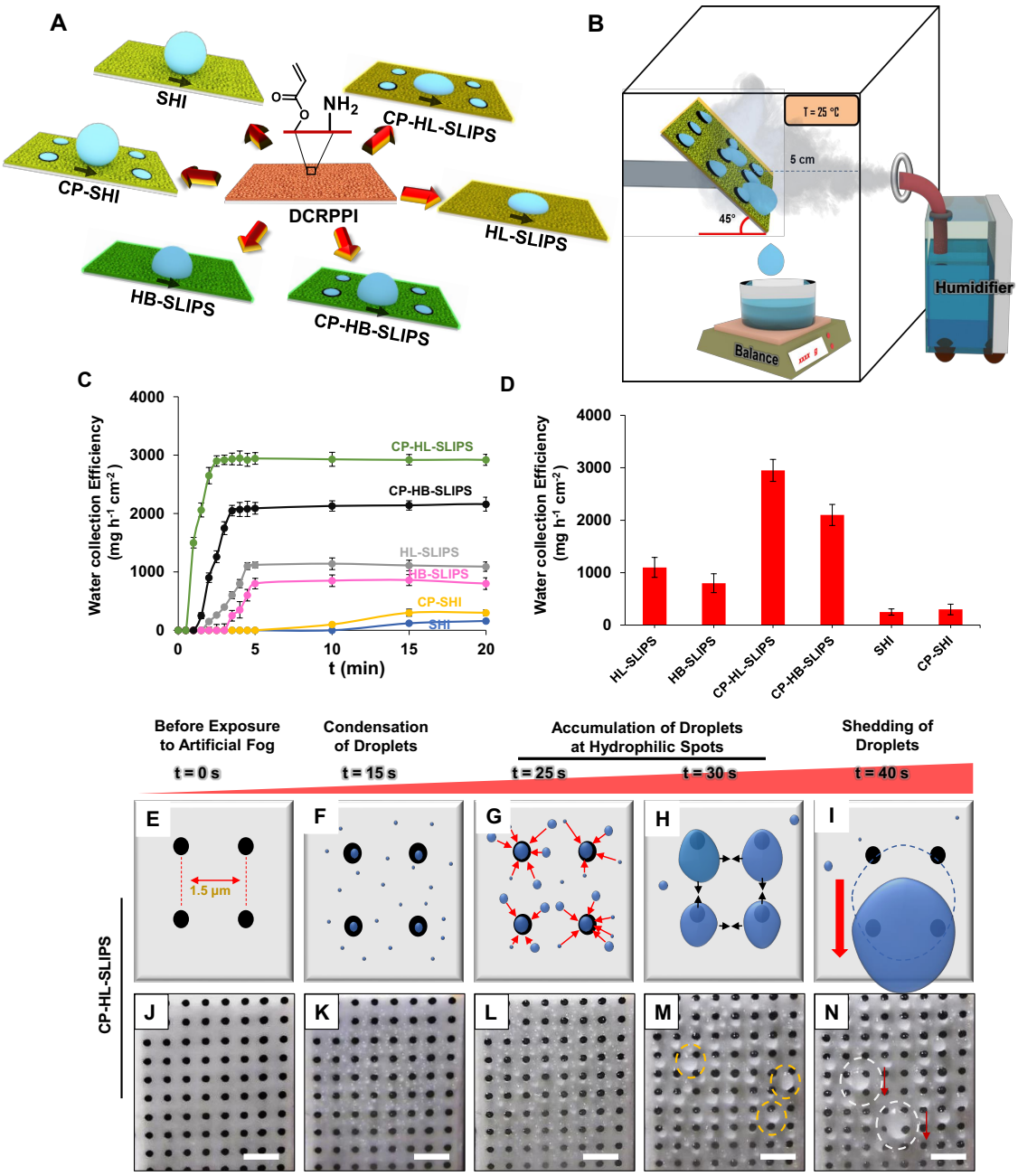

Figure 5. (A, B) Schematic representations of various bio-inspired wettabilities from a dual chemically reactive porous polymeric interface (A) and an artificial water harvesting setup (B). (C, D) Plots illustrating the initial rate of water collection (C) and water collection efficiency for the different kinds of bio-mimicked interfaces including SHI, CP-SHI, HB-SLIPS, HL-SLIPS, CP-HB-SLIPS, and CP-HL-SLIPS. (E-I) Schematic representation of water harvesting process on a bio-inspired patterned interface. (J-N) Different stages of water harvesting process from the artificial fog on chemically patterned hydrophilic SLIPS (CP-HL-SLIPS) where continuous shedding of aqueous droplets strated after 40 secs.

both SHI and HB-SLIPS. Therefore, water harvesting efficiency was found to be much higher for HL-SLIPS (1100 mg cm^{-2} h^{-1}) compared to both HB-SLIPS (800 mg cm^{-2} h^{-1}) and SHI (250 mg cm^{-2} h^{-1}) as shown in Fig. 5C, D. Interestingly, much faster growth and shedding of aqueous droplets observed in the case of CP-HL-SLIPS compared to other interfaces, where hydrophilic spots were incorporated on HL-SLIPS (Fig. 5J-N). Therefore, a maximum water harvesting efficiency was observed for CP-HL-SLIPS (2950 mg cm^{-2} h^{-1}). Further, the physical confinement of the patterned SLIPS has a crucial role in water harvesting efficiency. Once the edge-to-edge distance was maintained at 2 mm, a significantly high-water harvesting efficiency, 4400 ± 190 mg cm^{-2} h^{-1}, was observed for CP-HL-SLIPS.

Chapter 6: Conclusion & Future Directions

In conclusion, I have developed a simple dilution technique for the preparation of a stable dispersion of chemically reactive nano-complex, which is useful to coat a porous and spongy substrate (i.e., MS). Further, the post-chemical modification of the coated MS with long-chain hydrocarbon provided durable superhydrophobicity. The embedded superhydrophobicity sustained different harsh physical/chemical exposures, making the material more appropriate for oil/water separation in practical settings. Further, I have tailored the growth of the chemically reactive nano complex for constructing a thick and porous chemically reactive coating following a facile spray deposition technique. Again, the chemical reactivity of the porous polymeric coating has been utilized for the preparation of both non-adhesive superhydrophobicity (NASH) and controlled adhesive superhydrophobicity (CASH) via post chemical modification with a different primary amine-containing small molecule. The thickness of the coating, as well as hydrophobicity of the coating, can be varied simultaneously by varying the spraying time and chain length of the primary amine-containing small molecule. The same porous chemically reactive hydrophilic polymeric coating was exploited to design a chemically reactive slippery surface without requiring any prior hydrophobization, where the residual acrylate groups on polymeric coating played a crucial for achieving essential chemical compatibility with selected lubricants. The reactive slippery interface was extended for in-situ patterning on the lubricated interface without compromising its slippery property. Finally, a dual chemically reactive and porous polymeric interface (DCRPPI) was extended for preparing various bio-mimicked interfaces, including (i) superhydrophobic interface (SHI), (ii) hydrophobic SLIPS (HB-SLIPS), and (iii) hydrophilic SLIPS (HL-SLIPS). Again, a spatially selective controlled chemical modulation on the chemically reactive interface allowed to develop of (iv) chemically patterned superhydrophobic interface (CP-SHI), and the selection of appropriate lubrication yielded (v) chemically patterned hydrophobic SLIPS (CP-HB- SLIPS) and (vi) chemically

patterned hydrophilic SLIPS (CP-HL-SLIPS). The water harvesting efficiency of these bio-inspired interfaces was examined at the identical experimental set-up. Further, such an approach could be extended to develop various desirable functional materials that would be appropriate for relevant applications in practical settings.

Introduction

1.1 Inspiration from the Nature

Nature has always been the source of inspiration for the design of various modern scientific technologies. Over the last 3.8 billion years of rigorous research and development, nature has become the unbeaten and unprofitable inspiration for contemporary achievements like an aeroplane,[1] bullet train,[2] bionic arms,[3] injection needles,[4] swimsuit,[5] robotic legs,[6] turbine blades, etc. Starting from the invention of the aircraft which was originally inspired by an eagle, nature has continuously and constantly provided insights on how to make the aircraft lighter and faster . The front of the bullet train was inspired by the beak of the kingfisher bird which not only helped to significantly reduce the sound pollution but also ensured 10-15% energy saving owing to aerodynamics. Several other technologies for the advancement of humankind like bionic arms were developed mimicking the elephant's trunk, painless injection needles inspired by mosquito bites, design of swimsuits mimicking the shark skin structure for drag reduction, and so on.

Therefore, bio-inspiration appears to be the common and versatile manifesto to address critical challenges daily.[7] The inspiration from nature provided the opportunity to solve complex problems through imitating the shape, element, or background features. Moreover, several bio-inspired smart materials embedded with lotus leaf-inspired superhydrophobicity and nepenthes pitcher plant-inspired slippery liquid-infused porous surface (SLIPS) were fabricated for various practical applications like oil/water separation, self-cleaning and artificial water harvesting, etc. A detailed discussion about various bio-inspired anti-wetting interfaces have been outlined in the following sections.

1.2 Liquid Wettability

The understanding of the wetting behaviour of a liquid on a solid surface is a centuries aged concept that has gained widespread attention in recent decades due to their enormous applicability in various fields, from cave arts in ancient history to microfluidic devices in modern life.[8-10] The wetting of a solid surface by liquids is mainly governed by two attractive forces namely cohesive force and adhesive force. The cohesive force is defined as the attraction force between similar kinds of molecules which is fundamental to describe the lowering in the contact area between solid and liquid interface. On the other side adhesive force is the attraction force between unlike molecules which is relevant to explain the spreading behaviour of a liquid droplet on a solid surface. Once a liquid droplet is beaded on a solid surface, the degree of spreading of the liquid droplet depends on these two forces of attraction, and the extent of wetting of the solid surface by a liquid droplet is measured in terms of contact angles once these forces are in equilibrium. The contact angle (CA) or static contact angle is

the tangential angle of the liquid/vapor interface, made by the liquid droplet at the three-phase boundary as shown in Fig. 1A. The advancing and the receding contact angles are known as dynamic contact angles which are useful to explain extreme liquid repellence. The advancing angle is the

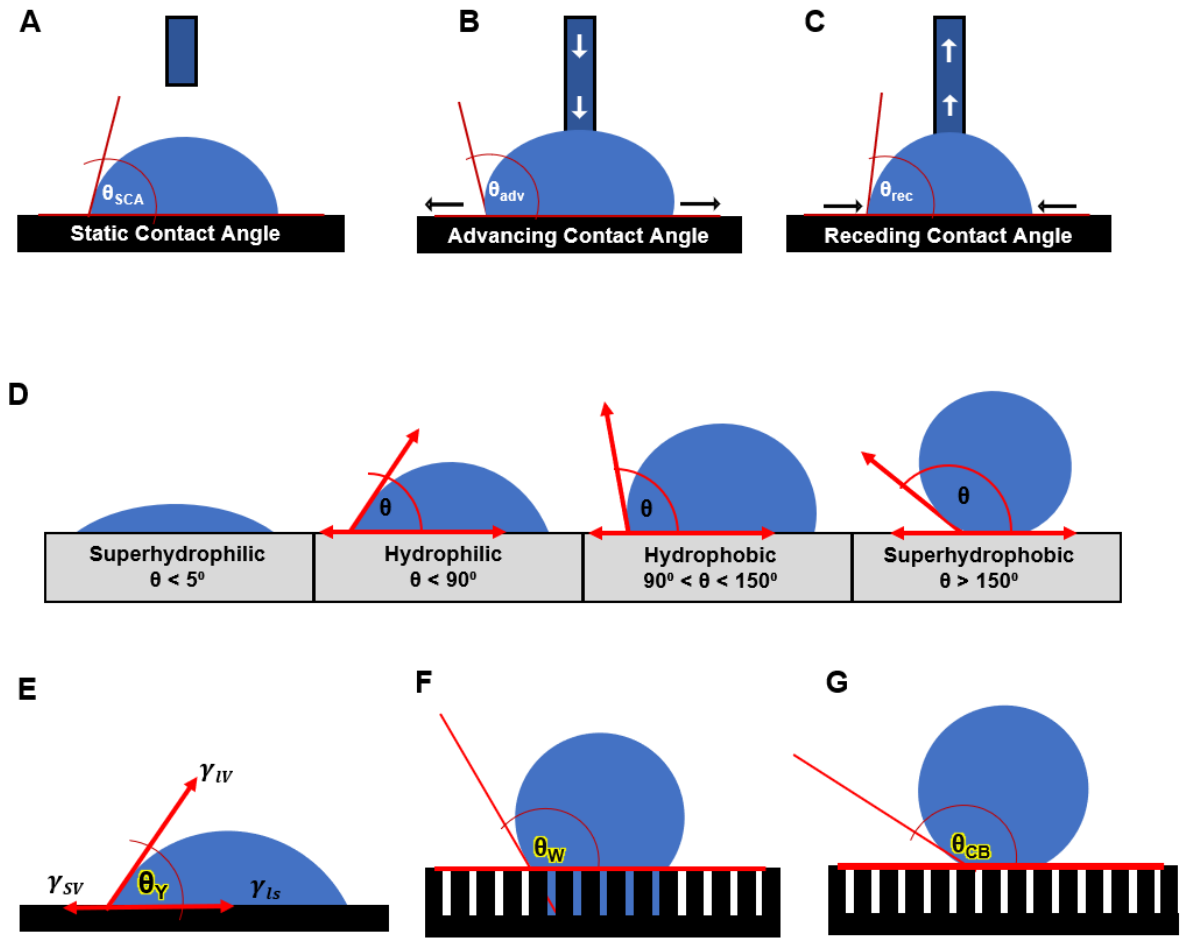

Figure 1.1. (A-C) Schematic representation of various contact angles including static contact angle (A), advancing contact angle (B) and receding contact angle (C). (D) Classification of solid substrates according to contact angles. (E-G) Various wetting model of liquid droplet on solid surfaces. (E) Young's model depicting the behaviour of aqueous droplet on a smooth solid surface. (F, G) Wenzel (F) and Cassie-Baxter (G) model for the interpretation of contact angle of aqueous droplet on hydrophobic and superhydrophobic surface respectively.

maximum contact angle which is measured once the liquid droplet (Fig. 1B) is growing on the solid surface while the receding contact angle is measured during the process of withdrawal of the liquid droplet from the solid surface as shown in Fig. 1C. The difference between advancing and receding contact angles is known as contact angle hysteresis which is a measure of adhesiveness between the solid surface and the probe liquid.[11] Based on contact angle measurements solid surfaces are broadly classified as superhydrophilic, hydrophilic, hydrophobic, and superhydrophobic. In general, solid surfaces having CA < 5^0 are known as superhydrophilic, hydrophilic surfaces have CA < 90^0, and those surfaces having CAs > 90^0 are hydrophobic whereas a superhydrophobic surface displays water

CA >150^0 (Fig. 1.1 D).[12-14] In the past different wettability models have been introduced to explain both homogeneous and heterogenous wetting of a liquid on a solid surface.

1.2.1 Young Model

In 1805, Thomas Young described the equilibrium state of a droplet on an ideal smooth solid surface. When a liquid water droplet is beaded on a solid smooth surface, the adhesive force between the solid surface and the liquid water droplet exceeds the cohesive force and the water droplet starts spreading until the two forces reach an equilibrium (Fig. 1.1 E) and the interfacial contact angle is measured by Young's equation as follows [15]

$$cos\,\theta_Y = \frac{\gamma_{sv}-\gamma_{sl}}{\gamma_{lv}} \quad \ldots\ldots\ldots\ldots\ldots\ldots\ldots\ldots \quad (1)$$

Where γ_{sv}, γ_{sl}, γ_{lv} are the interfacial surface energies of solid-vapor, solid-liquid, and liquid-vapor interfaces respectively and θ_Y represent Young's contact angle.

1.2.2 Wenzel Model

Young's model is the general theoretical model to explain contact angle on a smooth solid surface by calculating the respective interfacial energies. Young's model failed to explain liquid wettability on most of the practically relevant surfaces due to the existence of surface roughness. Later, Wenzel[16] explained the contribution of roughness to the wettability for rough surfaces in 1936. Wenzel modified Young's equation to calculate contact angle on the rough surface following equation 2 (Fig. 1.1 F)

$$cos\theta_W = r cos\theta_Y \quad \ldots\ldots\ldots\ldots\ldots\ldots\ldots\ldots \quad (2)$$

Where θ_W is the Wenzel contact angle on a rough surface and θ_Y is Young's contact angle on a smooth surface, r is the roughness factor which is defined as the ratio of the actual surface area to the projection area. Therefore, according to the Wenzel model, the hydrophilic/hydrophobic surface will be more hydrophilic/hydrophobic on the incorporation of roughness.

1.2.3 Cassie-Baxter Model

Both Young and Wenzel's model failed to explain the wetting of a liquid droplet on a solid surface with contact angle is more than 150^0. In case of Young's and Wenzel models, there exists continuous wetting of the solid surface by the beaded liquid droplet. However, Cassie-Baxter introduced a fundamentally different concept of liquid wettability on a solid surface where a trapped external third phase in between the solid asperities, minimized the contact area of the beaded liquid droplet with the solid interface as shown in Fig 1.1 G. The external third phase is the metastable trapped air which is

responsible for super-liquid repellence where contact angle is more than 150^0. The apparent contact angle of this vapor/liquid/solid is given by Cassie-Baxter equation as follows[17]

$$cos\theta_{CB} = f_{sl}cos\theta_{sl} + f_{lv}cos\theta_{lv} \quad \ldots\ldots\ldots\ldots\ldots\ldots\ldots\ldots\ldots (3)$$

The f_{sl} and f_{lv} are the geometrical fractional area between solid/liquid and liquid/vapor interface (where $f_{sl} + f_{lv} = 1$) respectively. θ_{sl} and θ_{lv} are the contact angle of the beaded liquid droplet on solid and vapor phase respectively. Since liquid droplet suspended on a vapor phase, it forms a contact angle of 180^0 ($\theta_{lv} = 180^0$; $cos\theta_{lv} = -1$). Therefore, the modified Cassie-Baxter equation can be written as

$$cos\theta_{CB} = f_{sl}cos\theta_{sl} + f_{sl} - 1 \ldots\ldots\ldots\ldots\ldots\ldots\ldots\ldots\ldots (4)$$

$$cos\theta_{CB} = f_{sl}(cos\theta_{sl} + 1) - 1 \ldots\ldots\ldots\ldots\ldots\ldots\ldots\ldots\ldots (5)$$

The values of f_{sl} is varied from 0 to 1. When $f_{sl} = 1$, there occurs complete wetting of the surface by the liquid droplet whereas $f_{sl} = 0$, signifies absolutely no contact between the beaded liquid on solid surface.

1.3 Bio-Inspired Anti-Wetting Interfaces

Since ancient times, through evolution, natural organisms have learnt to adapt to the earth's harsh environments not only for survival but as an inspiration for researchers for the development of artificial functional materials for upgrading the lifestyle of humankind also. Therefore, biomimetic research opens a new window to encounter several limitations in numberless events like self-cleaning behaviour on a lotus leaf [18] and cicada wings, [19] water collection by Namib desert beetle, [20] and prey trapping mechanism by Nepenthe's pitcher plant, [21,] etc. A huge number of relevant artificial smart materials have been developed by mimicking the superhydrophobic nature of the lotus leaf and the slippery behaviour of the Nepenthes pitcher plant.

1.3.1 Superhydrophobicity

The evolution of extreme water-repellence interfaces started back in 1997 when two German scientists Barthlott and Neinhuis first discovered the self-cleaning behaviour of lotus leaves without traces of water.[18] The presence of micro/nano features and low surface epicuticular wax coating laid the foundation of extreme water repellence exhibited by the sacred lotus leaf with water contact angle

greater than 150^0 and roll off-angle below 5^0, and the corresponding phenomenon was formally recognized as

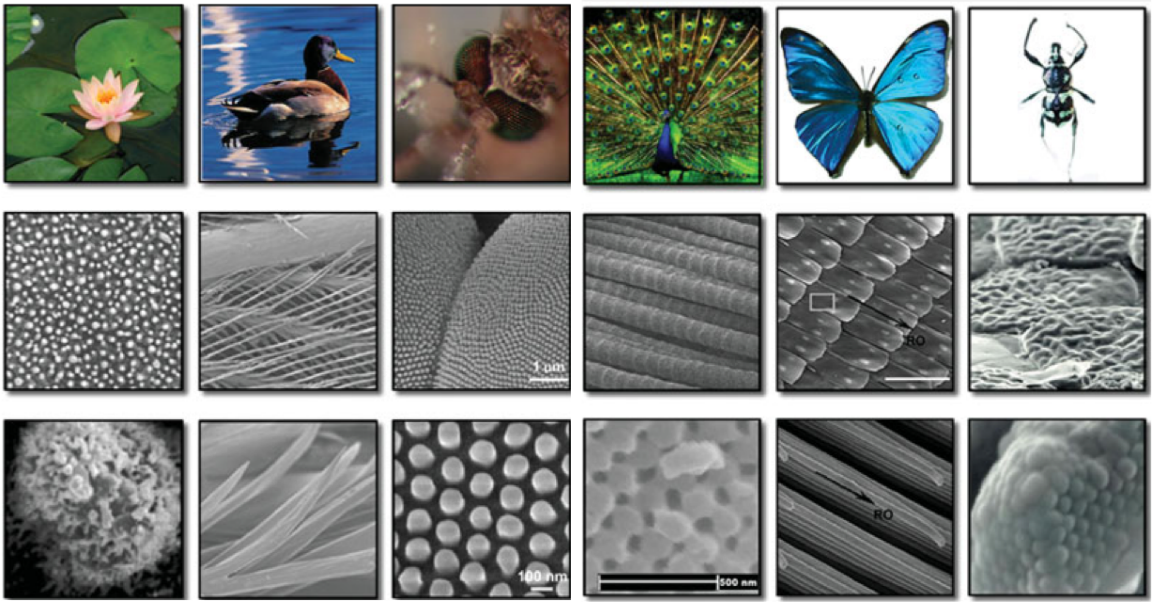

Figure 1.2. Top panel showing digital photograph of several natural anti-wetting organism. Middle panel showing FESEM images of corresponding surfaces in low magnification which revels the existence of micro features. Bottom panel describes the presence nano structure over the micro feature at high magnification. Reprinted with permission from *Adv. Mater*. **2008**, *20*, 2842–2858. Copyright 2008, Wiley-VCH.

superhydrophobicity. The air/aqueous interface of the rolling water droplets on the lotus leaf carried away the deposited dust and dirt particles and the lotus leaf was self-cleaned. In nature, there are several examples of superhydrophobic surfaces. [22-24] As for example superhydrophobic the feathers of Duck prevent the feathers from becoming waterlogged. [25] The presence of closed packed hexagonal microfeatures and non-closed packed nanostructure are responsible for the anti-fogging properties of mosquito eyes. [26] The superhydrophobic legs of the water striders help them to walk freely on water. The SEM images suggest the existence of micro/nano features which are further decorated with waxy-like nano-featured coating on the water strider's leg [27] are responsible for non-wetting legs as shown in Fig 1.2. Similarly, peacock feathers, [28] butterfly wing [29,] and Namib beetle [20] possess the special anti-wetting property for their survival strategies, and in each case, dual degrees of roughness and waxy-like coating have been found to exist.

1.3.2 Slippery Liquid Infused Porous Surface (SLIPS)

On the other hand, a conceptually different type of anti-wetting surface was first introduced by Aizenberg [30] in 2011, namely slippery liquid-infused porous surface (SLIPS), inspired by prey trapping ability of Nepenthes pitcher plant. The carnivorous Nepenthes that survives in nutrient-deficient

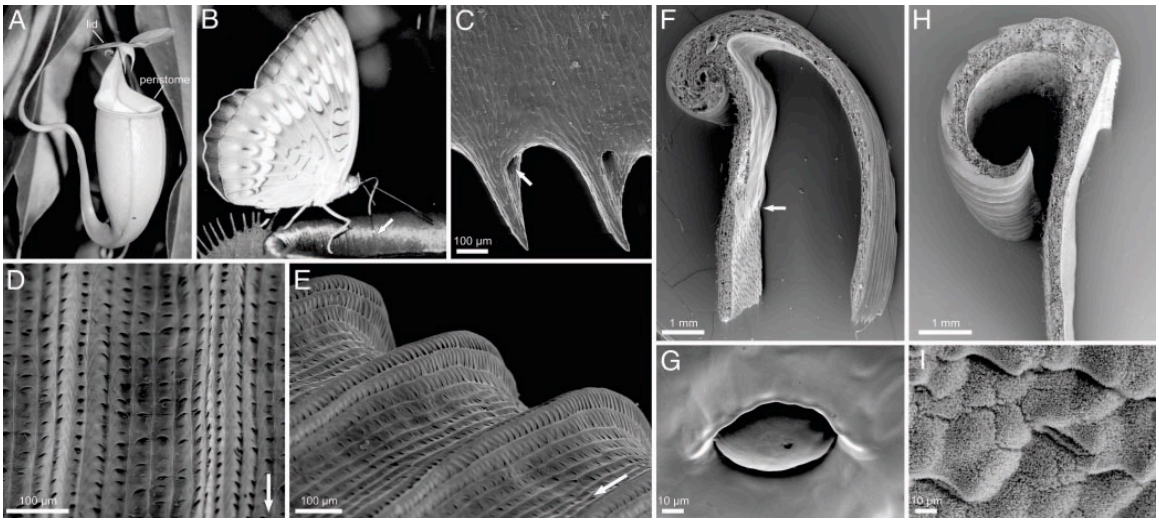

Figure 1.3. Nepenthe's pitcher and peristome morphology. (A–G) N. bicalcarata. (A) Pitcher. (B) Butterfly (probably Tanaecia pelea) harvesting nectar from the peristome surface. Note the visible line of peristome channels filled with nectar secreted from pores at the inner margin of the peristome (arrow). (C)Underside of inner margin of peristome with tooth-like projections and nectar pores (arrow). (D and E) Peristome surface with first- and second-order radial ridges. Arrows indicate direction toward the inside of the pitcher (F) Transverse section of peristome.Note the transition from the digestive zone to the smooth surface under the peristome (arrow). (G) Inner pitcher wall with digestive gland at the height of the inner peristome margin (H and I) N. alata. (H) Transverse section of peristome. (I) Waxy inner pitcher wall at the height of the inner peristome margin. Reprinted with permission from *Proceedings of the National Academy of Sciences* **2004**, *101*, 14138–14143. Copyright 2004, PNAS. United States of America.

environments consists of a specialized trapping organ, known as pitcher. During the dry season the insects can easily walk around the peristome of the pitcher (Fig. 1.3 A) but during rainy season, insects slide towards the digestive bottom of the pitcher. The SEM study revealed the peristome of the pitcher, consists of microfeature (Fig 1.3 D-E) which enables to form a stable continuous thin layer of lubricating water during rainy days and oily legs of the insects slipped in towards the bottom of the peristome.

1.4 Essential Criteria to Develop Artificial Anti-Wetting Surfaces

These two distinct bio-inspired heterogeneous and homogeneous liquid wettability require different chemical and physical optimizations. In the past, different experiments were designed to investigate the essential criteria to develop artificial superhydrophobic coating and slippery liquid-infused porous surface (SLIPS).

1.4.1 Design of Artificial Superhydrophobicity

In 2009, Koch *et al* [31] mimicked the hierarchical structure of lotus leaf by adapting first and precise moulding technology followed by deposition of natural lotus wax through thermal evaporation method to develop nano waxy features. Then, they have demonstrated the wetting behaviour of aqueous droplets either on micro or nano featured surface as shown in Fig. 1.4 A, B. Interestingly, the

hierarchical surface (micro/nano) able to show non-adhesive superhydrophobicity as lotus leaf whereas either micro or nano featured surface showed adhesive superhydrophobicity. In another separate experiment in 2016, Nishimura et al, [32] have synthesized both single and dual roughness surfaces along with low surface energy coating. The surface with a combination of micro and nanostructures

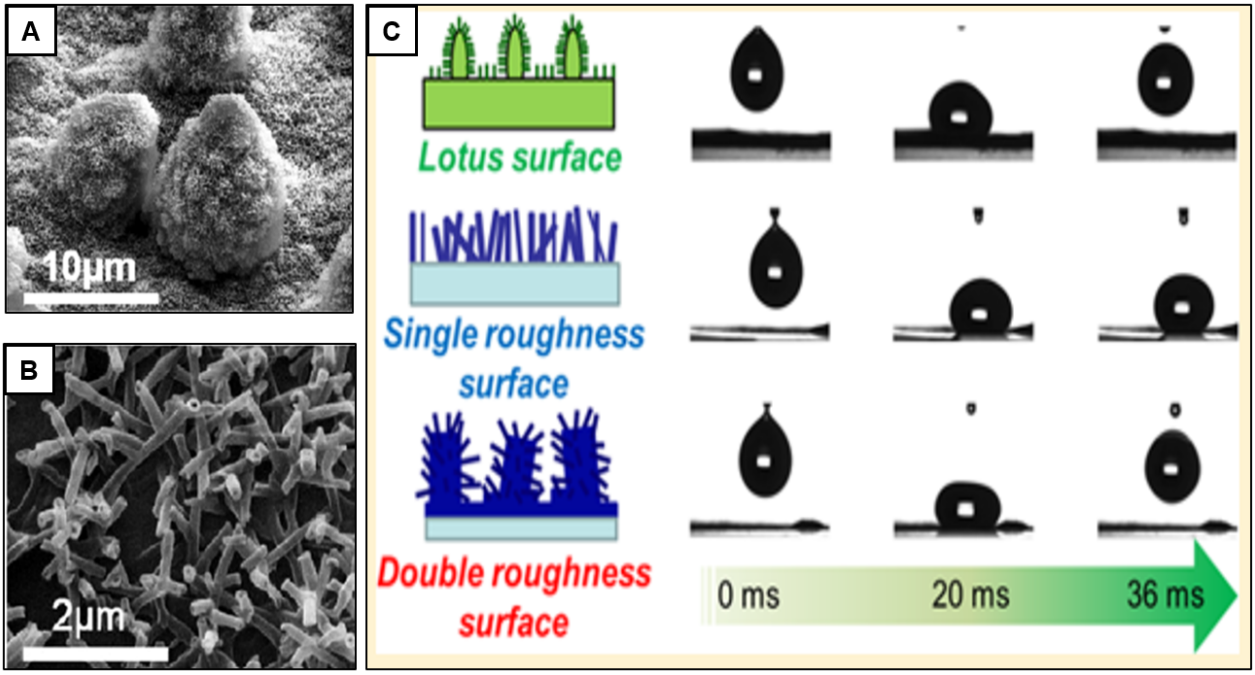

Figure 1.4. (A, B) Scanning electron microscope (SEM) images of lotus leaf at low (A) and high (B) magnifications. Reprinted with permission from *Progress in Materials Science*, **2009**, *54*, 137–178. Copyright 2009, Elsevier. (C)Bouncing behaviour of aqueous droplet on lotus leaf, artificial single roughness surface and double (hierarchical) roughness surface. Reprinted with permission from *J. Am. Chem. Soc.* **2016,** *138,* 10299-10303. Copyright 2016, American Chemical Society.

(hierarchical) were able to mimic the extreme water repellence property lotus leaf whereas the single featured surface ended up with adhesive superhydrophobicity as shown in Fig. 1.4 C. Therefore, from these experiments it was undoubtedly proven that the essential criteria for achieving artificial superhydrophobicity are (1) dual degree of roughness (hierarchical) (2) presence of low surface energy coating on top.

1.4.2 Design of Artificial Slippery Liquid Infused Porous Surfaces (SLIPS)

In 2011, Aizenberg et al, [30] introduced nepenthes pitcher plant-inspired slippery liquid-infused porous surface (SLIPS). In this report they have synthesized two different types of porous/textured matrix, periodically ordered and random nano-posts on a Teflon surface followed by post functionalization with low surface energy poly-fluoroalkyl silane for desired hydrophobization. Then both the functionalized porous interfaces were lubricated with low surface tension per-fluorinated liquids

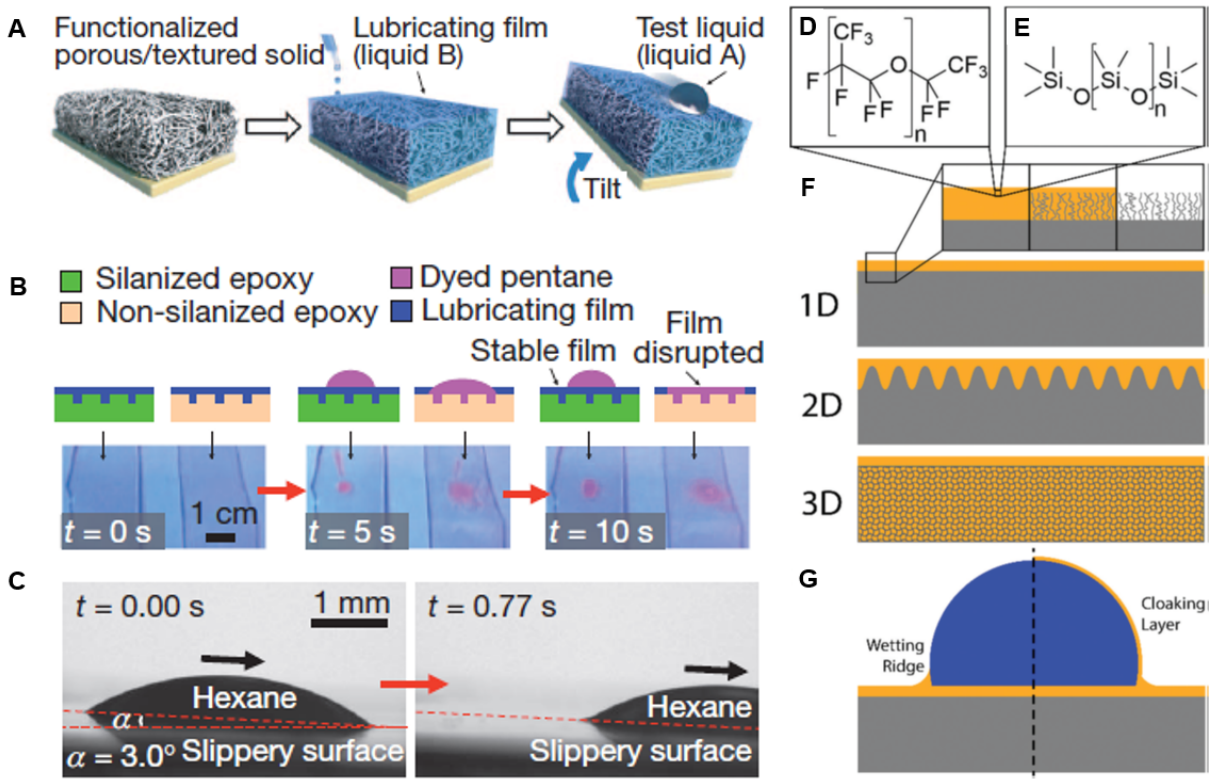

Figure 1.5. (A) Schematic representation for the fabrication of SLIPS by infusing the inert lubricant on the porous functionalized matrix. (B) Behaviour of dyed pentane droplet on lubricated functionalized and non-functionalized surface. (C) Time-lapse image of hexane droplet on SLIPS. Reprinted with permission from *Nature* **2011**, *477*, 443–447. Copyright 2011, Nature. (D, E) Chemical structures of commonly used lubricating fluids, krytox (D) and Silicone oil (E). (F) Schematics of various type of slippery surfaces including one-dimensional (1D), two-dimensional (2D) and three-dimensional (3D). (G) Behaviour of aqueous droplet on a typical SLIPS. Reprinted with permission from *Chem. Soc. Rev.* **2020**, *49*, 3688-3715. Copyright 2020, Royal Society of Chemistry.

(Dupont Krytox oils) which are non-volatile, immiscible with both aqueous and hydrocarbon phases. Thus, the lubricating fluid formed a stable film within the porous matrix and displayed desired slippery property towards various types of working liquids like water, acids, bases, ketones, alkanes, etc (Fig. 1.5 A-C). At the same, time non-functionalized porous surfaces failed to exhibit similar slippery property upon lubrication with the same lubricant towards various working liquids (Fig. 1.5 A-C). From this experiment, they have hypothesized three essential criteria based on interfacial surface energies of the lubricating liquid, probe liquid, and the porous solid surface for the synthesis of artificial SLIPS, namely

1) The lubricating liquid must wick into, wet, and stably adhere within the solid featured surface (the presence of micro/nanostructure satisfy this criterion).
2) The lubricating liquid and the working liquid must be immiscible to each other.
3) The solid surface must be preferentially wetted by the lubricating liquid rather than by the working liquid (also known as probe liquid); this criterion accounted for the formation of a

stable lubricating film within the solid substrate owing to the chemical compatibility of the lubricating liquid with the solid surface.

The absence of any criterion leads to failure of producing stable SLIPS. The chemical compatibility of the solid matrix with the lubricating liquid and the working liquid is expressed as the following equations. [33]

$$R(\gamma_l \cos\theta_l - \gamma_w \cos\theta_w) - \gamma_{lw} > 0 \quad \text{..... (6)}$$

$$R(\gamma_l \cos\theta_l - \gamma_w \cos\theta_w) + \gamma_w - \gamma_l > 0 \quad \text{..... (7)}$$

Where R is the roughness factor which is the ratio of actual surface area and the projected surface area of the solid, γ_l , γ_w are the surface tension of the lubricating liquid and working liquid respectively and γ_{lw} is the interfacial surface tension between the working liquid and the lubricating liquid. Whereas θ_l and θ_w representing the static contact angles of the lubricating liquid and the working liquid on the flat solid surface respectively. Along with these criteria for SLIPS, beaded working liquid

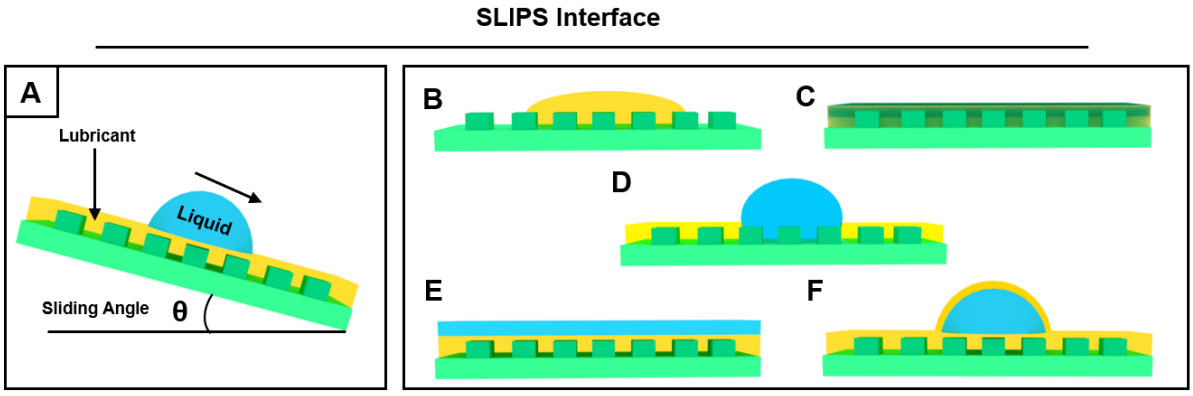

Figure 1.6. A) Schematic representation of sliding behaviour of a liquid droplet on slippery liquid infused porous surface (SLIPS). (B-F) Schematic illustration of various circumstances which are not able form stable SLIPS, including porous solid surface is not wetted by the lubricating fluid (B); lubricating liquid and the working liquid miscible to each other (C); lubricating liquid is displaced by the working liquid (D); working liquid spreads over the lubricating liquid (E); lubricating liquid forms a cloaking layer over the working liquid. Reprinted with permission from *J. Mater. Chem. A* **2021**, *9*, 824–856. Copyright 2020, Royal Society of Chemistry.

on the lubricating film must form discrete droplets without spreading and cloaking as shown in Fig. 1.6 A-F. [34] From these hypotheses most artificial SLIPS were prepared through lubrication of a hydrophobic or superhydrophobic interface with selected natural and synthetic lubricants.

1.5 Different Approaches to Synthesize Bio-inspired Artificial Anti-Wetting Surfaces

In the past various top-down and bottom-up approaches were introduced to develop bio-inspired superhydrophobicity and slippery liquid-infused porous surface (SLIPS). Here, I have briefly accounted for some of these well-recognized approaches.

1.5.1 Superhydrophobic Surfaces

The hierarchical topography and suitable low surface energy coating are recognized as the essential criteria for achieving superhydrophobicity. Therefore, there are mainly two different ways to fabricate superhydrophobic surfaces 1) introduce roughness on the hydrophobic material (top-down method). 2) decorate the rough surface made up of hydrophilic components with low surface energy materials (bottom-up). Here I have categorized exiting approaches in three different methods 1) traditional methods, 2) self-healable/post-repairable superhydrophobic surfaces and 3) bulk superhydrophobicity.

1.5.1.1 Traditional Methods

In traditional methods, mostly the anti-wetting surface coating was achieved by depositing chemically inert low energy material on hierarchical structures. Here, I have highlighted a few important traditional methods to prepare superhydrophobic surfaces.

1.5.1.1.1 Plasma Treatment

The plasma technique is a simple way to introduce hierarchical topography. This technique involves etching of the surface. During this process, several reactive ions or atoms, or radicals are generated which can cause a significant change in the surface morphology because of the anisotropic etching on the surface layers. [35-43] Plasma etching technique was used to increase the roughness of polymeric surfaces generally followed by low surface energy material coating by the chemical vapor deposition technique. Youngblood *et al*, [37] reported the preparation of hierarchical surface (Fig. 1.7 A, B), which exhibit both high advancing and high receding water contact angles, by simultaneous etching of polypropylene and sputtering of poly(tetrafluoroethylene) (PTFE) using inductively coupled radio frequency plasmas argon plasmas.

1.5.1.1.2 Lithographic Technique

The lithography technique remained a great advantage over plasma etching to allow the control of the morphology of the solid surface (Fig. 1.7 C). This technique provided a facile basis to achieve patterns with squared pillars, circular pillars, star-shaped pots, indented square pots, with different diameters, heights, and spacing.[44-54] In photolithographic approaches, X-ray or e-beam is irradiated on the selected surface through a photoresist mask. Oner and McCrathy *et al* [54] reported a photolithographic technique to obtain different sized/shaped micropillar onto the silicon wafer, and further deposition of low surface energy coating to achieve desired superhydrophobicity. The major disadvantages of this method are substrate dependency and expensive instrumental setup.

1.5.1.1.3 Template Based Technique

Various patterns with multiscale structures can act as a template to produce design rough surfaces. [55-57] Bartell and Shepard fabricated a tetrahedral rough olefin surface by casting blocks of paraffin in molds constructed from heavy gauge aluminum foil. [55] Sun *et al* [56] have used templating technique to prepare artificial lotus leaf. They have demonstrated a PDMS surface with essential topography replicated from a lotus leaf to achieve superhydrophobic property similar to lotus leaf as shown in Fig. 1.7 C-G. The templating method suffers from scalability issues.

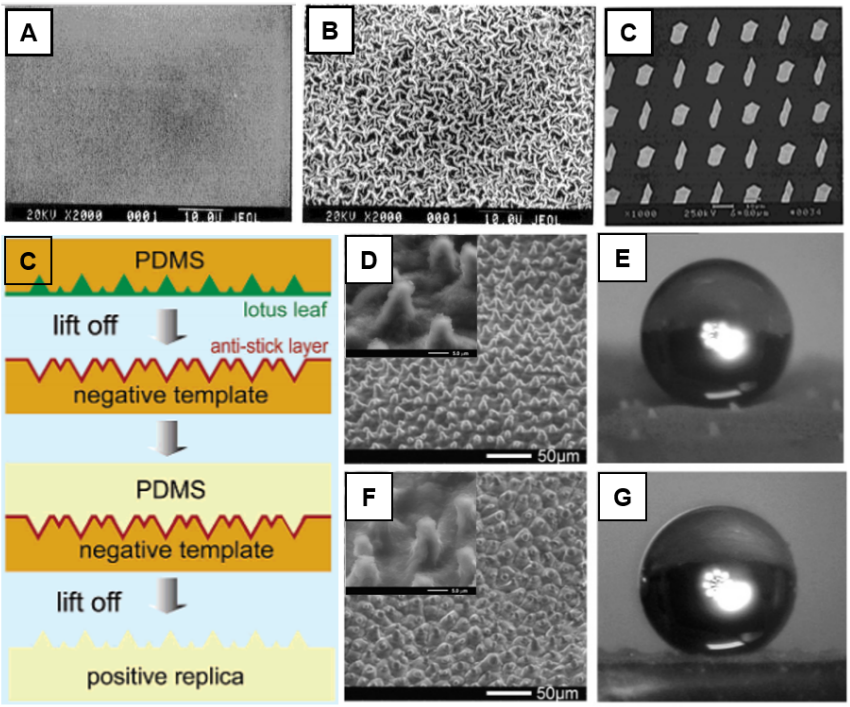

Figure 1.7. (A, B) Scanning Electron Micrograph on silicon wafer before (A) and after (B) plasma etching process. Reprinted with permission from *Macromolecules* **1999,** *32,* 6800–6806. Copyright 1999, American Chemical Society. (C) FESEM images of silicone water after precise lithographic etching process. Reprinted with permission from *Langmuir* **2000**, *16,* 7777–7782. Copyright 2000, American Chemical Society. (C) Schematic representation for the structural surface through template-based technique. (D, F) FESEM images of lotus leaf (D) and positive replica on PDMS (F) respectively. (E, G) Water contact angle images on lotus leaf (E) and superhydrophobic PDMS surface (G). Reprinted with permission from *Langmuir,* **2005**, *21,* 8978−8981. Copyright 2005, American Chemical Society.

1.5.1.1.4 Chemical Vapour Deposition

Chemical vapor deposition (CVD) is a technique where a chemical precursor (mainly liquid) was vaporized to decompose or react and condense back onto the selected solid surface to form a thin film. Chemical vapor deposition can be applied to create rough surfaces or to depose a thin layer of hydrophobic compound on a rough surface. [58-64] Yao *et al* [61] reported the formation of ZnS hierarchical structures on Au-coated silicon substrates by chemical vapor deposition technique. Lau *et al* [65] have created a superhydrophobic surface by CVD deposition of hydrophobic PTFE

(polytetrafluoroethylene) on a vertically aligned carbon nanotube forest. Jiang *et al* [66] have prepared various kinds of ACNTs films on quartz-glass substrates by applying the method of CVD. Chemical vapor deposition processes run at higher temperatures between 300° to 900°c temperature, all substrates cannot tolerate such high temperatures treatments.

1.5.1.1.5 Layer-by-Layer Method

Layer-by-layer (LbL) deposition method is one of the most studied method for the preparation of featured surfaces for its ease of controlling the thickness and surface topography.[67-79] In a traditional

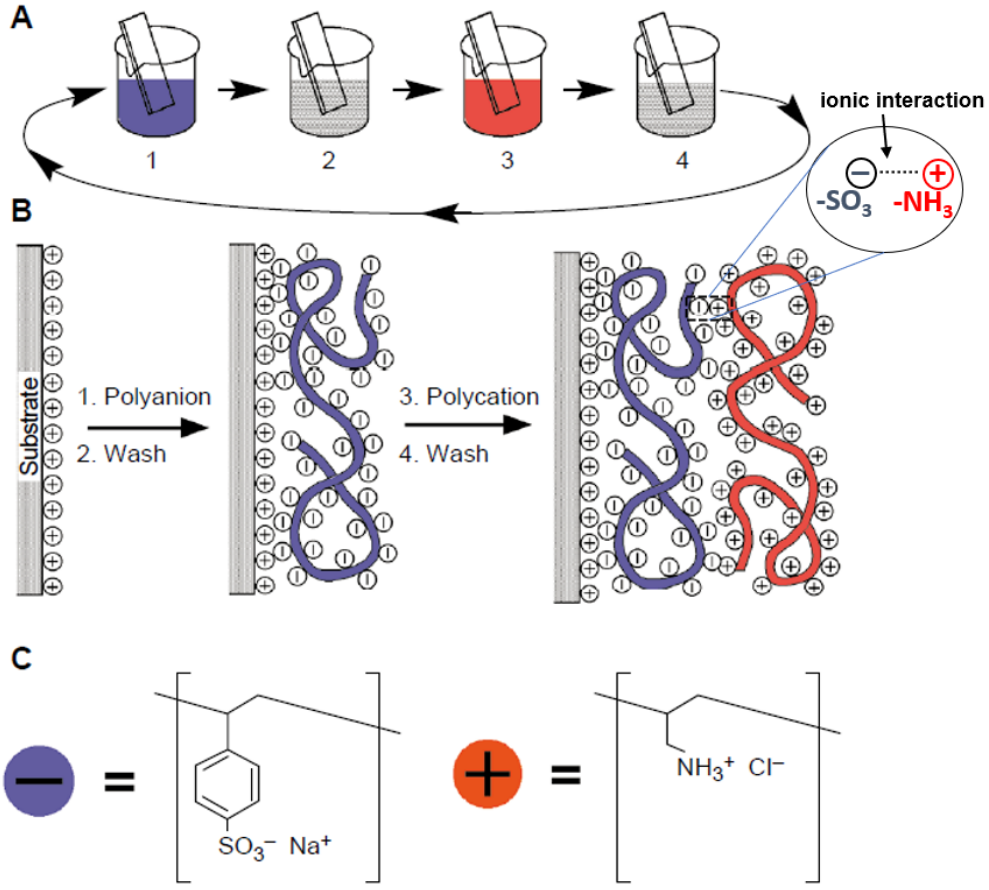

Figure 1.8. (A, B) A schematic representation of layer-by-layer (LbL) deposition process through typical dip coating. (C) Chemical structure of representative oppositely charged poly electrolytes namely poly (allylamine hydrochloride) (PAH) and poly acrylic acid (PAA). Reprinted with permission from *Science* **1997**, *277*, 1232−1237. Copyright 1997, American Association for the Advancement of Science.

LbL approach oppositely charged polyelectrolytes were alternatively deposited onto the selected substrate with appropriate association of washing steps in between to remove loosely bound polyelectrolytes as shown in Fig. 1.8 A, B. [67-69] The bilayer formations and washing steps can be accomplished by various techniques including dip coating, spin coating, spray coating, etc. The LbL coatings were initially built-up mostly based on electrostatic interactions, but later, a wide range of other attractive interactions and bonding like hydrogen bonding, covalent bonding, etc were associated

for the fabrication of various smart and functional materials following the LbL technique. [70-79] In 2009, Ji *et al* [80] fabricated featured multilayer surface by alternative deposition of an aqueous solution of polyacrylic acid (PAA) and polyethyleneimine (PEI) where pH of the solution plays a crucial role for controlling the porosity of the coating. Further the use of silver ion which forms metal-ligand complex (Ag-PAA/PEI) allowed to expedite the growth of the multilayer as shown Fig. 1.9 A, B. Furthermore, the chemical vapor deposition of fluorinated silane yielded a lotus leaf-inspired non-adhesive superhydrophobicity. In another report, Li *et al* [81] reported a seminal work for the preparation of

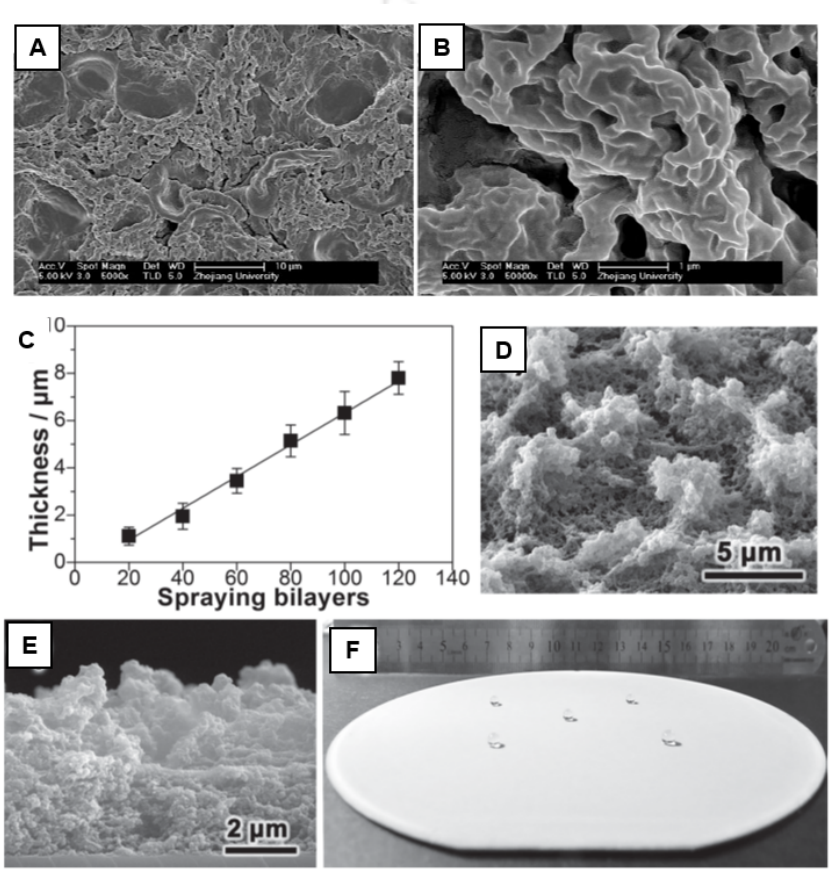

Figure 1.9. (A, B) FESEM images of the multilayers formed by alternative deposition of polyetheleneimine (PEI) and poly acrylic acid (PAA) in absence (A) and presence (B) of Ag ion respectively through Dip coating method. (Reprinted with permission from *Adv. Mater.* **2006**, *18*, 1441–1444. Copyright 2006, Wiley-VCH. (C) A plot describing increment of thickness of the multilayers with increase of no of spraying bilayers. (D, E) FESEM images of the multilayers (Top view: D; side view: E) formed by alternative spray deposition of poly (allylamine hydrochloride) –sulfonated poly (ether ether ketone) (PAH–SPEEK) and poly acrylic acid (PAA). (F) Digital photograph of aqueous droplets on a superhydrophobic watch-glass. (Reprinted with permission from *Adv. Mater.* **2014**, *26*, 3344–3348. Copyright 2014, Wiley-VCH.

hierarchical featured surface by LbL spray deposition technique. The multilayer was fabricated by alternative spraying of polyelectrolyte complexes of poly (allylamine hydrochloride) –sulfonated poly (ether ether ketone) (PAH–SPEEK) and polyacrylic acid (PAA) following a washing step in between with DI water. After 120 bilayers of deposition, the multilayer coating was modified with

perfluorooctanesulfonic acid lithium salt (PFOS) and 1H,1H,2H,2H-perfluorooctyltriethoxysilane (POTS) for preparing superhydrophobic interface (Fig. 1.9 C-F). Here, I have highlighted only a few traditional methods for the fabrication of hierarchical structure followed by association of inert coating to achieve superhydrophobicity. But there are other methods like sol-gel [82-89] approach to create micro/nanostructures, electrochemical method which was known for coating on a geometrically complex object, [90] phase separation methods, [91] electrospinning, [92-94] self-assembly methods [95], and so on.

1.5.1.1.6 Limitations of Traditional Methods

Conventional methods for the fabrication of superhydrophobic surfaces involves (i) the development of hierarchical topography from hydrophilic building blocks followed by (ii) inert low surface energy coating on top of the hydrophilic topography mainly through weak physical interaction for the entrapment of thin layer of metastable air. But such an approach remained highly labile towards

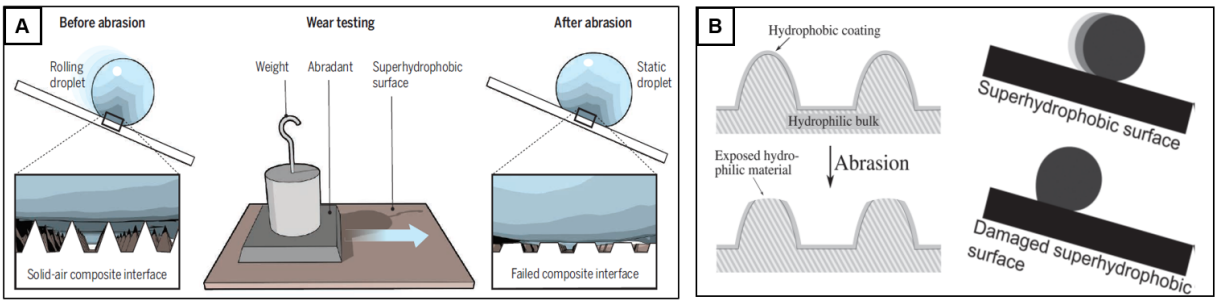

Figure 1.10. (A, B) schematic illustration of physical abrasion process on traditional superhydrophobic surfaces resulted in loss of anti-wetting property. Reprinted with permission from *Science* **2016**, *352*, 142. Copyright 2016, American Association for the Advancement of Science. Reprinted with permission from *Adv. Mater*. **2011**, *23*, 673–678. Copyright 2011, Wiley-VCH.

physical abrasions, and both topography [96] as well as surface chemistry [97] are likely to be compromised as shown in Fig. 1.10 A, B. Therefore, anti-wetting property fail to survive in harsh condition. To combat poor durability issues of traditional methods some sophisticated methods including self-healable and post-repairable methods were introduced in the recent past.

1.5.1.2 Self-healing and Post-Repairable Methods

In nature, plants such as lotus leaves maintain their superhydrophobic property very well by regenerating the epicuticular wax layer after damage, which is well known as self-healing property. The first time, *Li et al* [98] prepared self-healing superhydrophobic coatings through LbL assembly of polyelectrolyte complexes of poly (allylamine hydrochloride) and sulfonated poly (ether ether ketone) with poly (acrylic acid) followed by chemical vapor deposition of 1H,1H,2H,2H perfluorooctyltriethoxysilane (POTS). In this approach, the designing of the self-healing

superhydrophobic coating was in such a way that the essential low surface energy molecules (POTS) were deposited in the bulk of the coating. The bulk deposited molecules diffused out in a humid ambient environment when the multilayer coating was damaged through O_2 plasma etching or

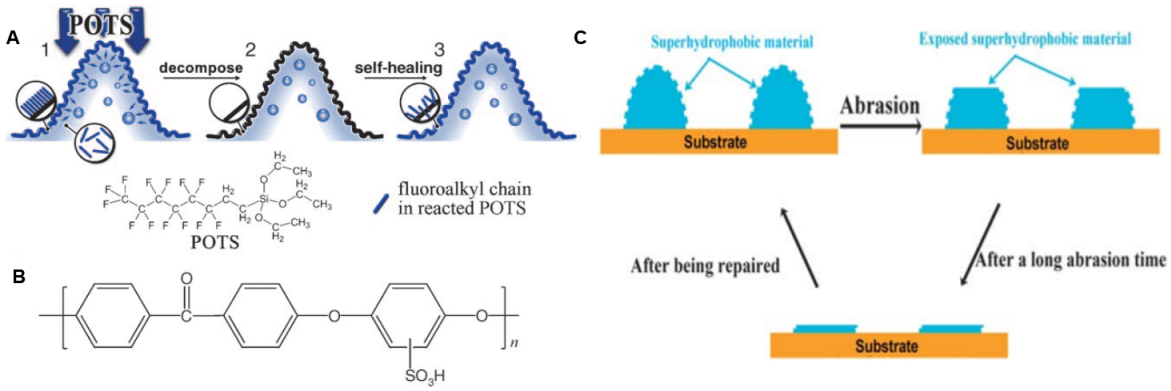

Figure 1.11. (A) Schematic representation of self-healing method where healing agents diffused back to the top of the surface to regenerate the extreme anti-wetting property in presence of external stimuli. (B) Chemical structure of sulfonated poly (ether ether ketone). Reprinted with permission from *Angew. Chem. Int. Ed.* **2010**, *49*, 6129–6133. Copyright 2010, Wiley-VCH. (C) Schematic representation of post-repairable approach for the fabrication of superhydrophobic surface. Reprinted with permission from *J. Mater. Chem.* **2011**, *21*, 15793–15797. Copyright 2011, Royal Society of Chemistry.

scratching, which results in healing of the superhydrophobic property as shown in Fig. 1.11 A-B. One of the major concerns about this method is the limited number of healing cycles and requirement of an external stimuli for the healing process. In case of post-repairable approach, both topography and the essential low surface energy coating were generated on the damaged surface again for restoring the anti-wetting property as shown in Fig. 1.11 C. For instance, Zhu *et al* [99] fabricated mechanical abrasion tolerant and easily repairable superhydrophobic surface by hot pressing of polymer/metal composite. The deposition of silver ion onto the polymer resulted in a hierarchical featured surface whereas further fluorination generated the desired superhydrophobicity. However, the prolonged mechanical abrasion led to destruction of the surface roughness and chemistry, but the damaged interface was repaired by the silver ion deposition followed by fluorination. The major disadvantage of post-repairable methods is the continuous regeneration of both appropriate surface topography and the surface chemistry on the damaged interface.

1.5.1.3 Bulk Superhydrophobic Methods

To encounter the durability of superhydrophobic surfaces (both physical and chemical), a very recent and unique approach has been developed in the literature, which is recognized as bulk superhydrophobicity, where the anti-wetting property is not only limited to the surface but is present

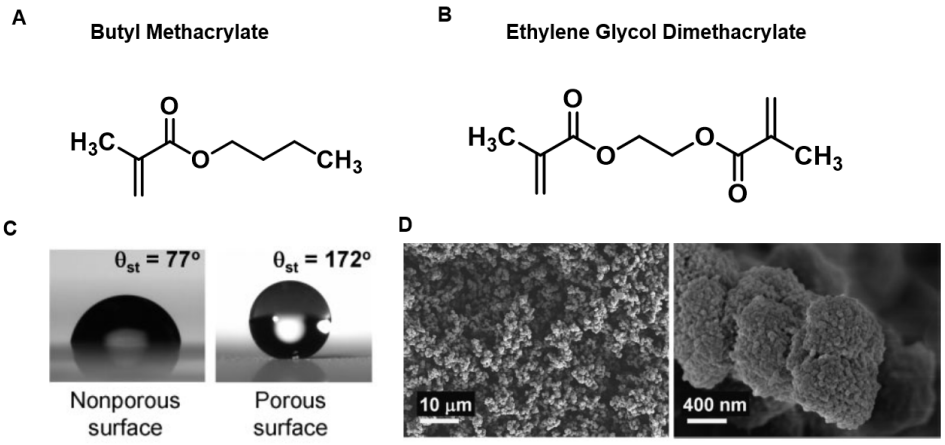

Figure 1.12. (A, B) Chemical structure of the precursor compounds, butyl methacrylate (A) and ethylene glycol di-methacrylate (B). (C) Water contact angle images on nonporous and porous surface. (D) FESEM images of the porous surface at low and high magnification. Reprinted with permission from *Adv. Funct. Mater.* **2009**, *19*, 1993–1998. Copyright 2009, Wiley-VCH.

three-dimensionally (i,e. both surface and bulk). Various bulk superhydrophobic materials have been fabricated by different research groups following different synthetic approaches. This approach was first developed by Levkin *et al*, [100] where a copolymerization of two monomers followed by phase separation was introduced to achieve bulk superhydrophobicity. The porous polymeric coating was prepared using the photoinitiated copolymerization of butyl methacrylate and ethylene dimethacrylate displayed static (θ_{st}), advancing (θ_{adv}), and receding (θ_{rec}) water contact angles (WCA) of 172º, 174º, and 171º, respectively as shown in Fig. 1.12 A-D. In another report, Yohe *et al* [101] have fabricated biocompatible bulk superhydrophobic material for controlled release of bioactive molecules where the trapped air inside the matrix delayed the penetration of water molecules. In this report, they used poly (ε-caprolactone) as the base material for electrospinning and poly (glycerol monostearate *co*-ε-caprolactone) as a hydrophobic dopant for the fabrication of bulk superhydrophobic material. Later, Manna *et al* [102] fabricated porous and reactive polymeric multilayers (~ 80 μm thick) by layer-by-layer deposition of branched poly(ethyleneimine) (PEI) and the amine-reactive polymer poly(vinyl-4,4-dimethyl azlactone) (PVDMA). The covalently crosslinked PEI/PVDMA multilayer coating was loaded with residual amine-reactive azlactone groups that were used to immobilize secondary functionality. When the multi-layered coating was reacted with the hydrophobic small molecule n-decylamine, it displayed superhydrophobicity with an advancing water contact angle (θ_{adv}) of 156° and roll-off angles of 1°. The bulk superhydrophobic coating is inherently capable of sustaining severe physical abrasions.

1.5.2 Slippery Liquid Infused Porous Surfaces (SLIPS)

Along with hierarchical topography and essential low surface energy coating, slippery surfaces required chemically compatible lubricant. Therefore, traditionally, SLIPS were fabricated through lubrication of a superhydrophobic/hydrophobic surface. Therefore, many strategies which were applied for the fabrication of superhydrophobic surfaces can also be useful for the development of slippery liquid-infused porous surfaces (SLIPS). In general fabrication methodology of SLIPS can broadly be categorized into three strategies as 1) substrate structuring 2) in situ growth of structures and 3) surface compositing and coating. [103]

1.5.2.1 Substrate Structuring

Substrate structuring is a common approach for the preparation of featured morphology on solid substrates. The chemical/physical etching, lithography (photolithography, electron-beam lithography, and soft-lithography), laser ablation processes are mainly involved in the sculpturing on the solid surface. A general schematic has been represented in Fig. 1.13 A that depicts the process of substrate structuring. [103] For instance, Li *et al* [104] fabricated cylindrical arrays of micropillar having a different radius on aluminum alloy through laser pulses. Then, a proper mixture of kaolin particles and fluoroalkyl silane in polydimethylsiloxane (PDMS) was used to fill the gaps which were created during

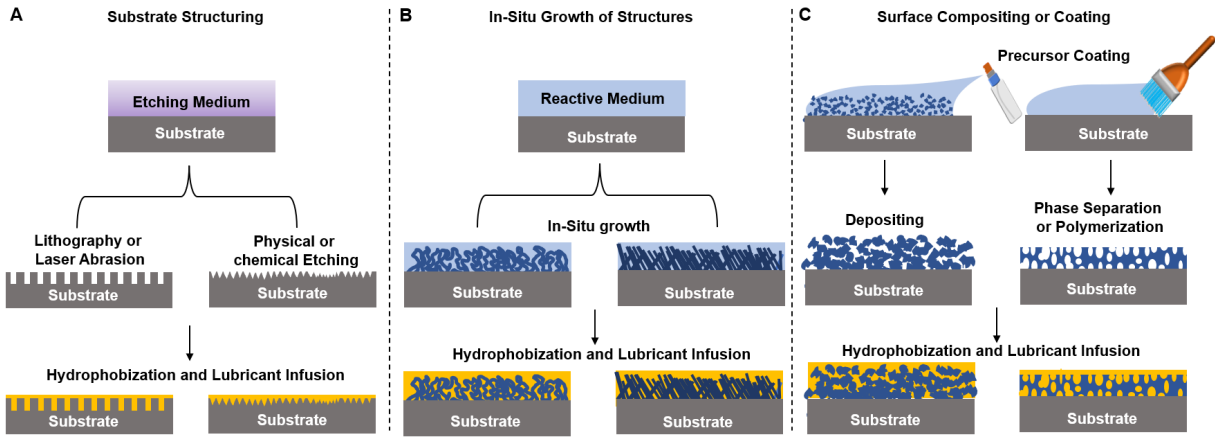

Figure 1.13. Schematic representation for the preparation of slippery liquid infused surface through substrate structuring method (A), in situ growth of structure method (B) and surface compositing or coating method (C). Reprinted with permission from *J. Mater. Chem. A* **2020**, *8*, 7536–7547. Copyright 2011, Royal Society of Chemistry.

laser lithography. Then anti-icing property of these substrates was investigated after lubricating the interface. In another report, Boreyko *et al* [105] synthesized silicon nanopillars using a lithography-free technique for the creation of lubricant-infused slippery surfaces to investigate the coalescence of water droplets. In a typical synthetic procedure, they have thermally grown 100 nm silicon dioxide (SiO_2) onto a silicon substrate followed by deposition of 5 nm platinum onto the SiO_2 using an electron beam evaporator. Then the samples were etched with O_2, SF_6 and C_4H_8 subsequently immersed in

(tridecafluoro-1,1,2,2-tetrahydrooctyl) triethoxysilane in hexane to render superhydrophobicity. The superhydrophobic surfaces were lubricated with different lubricants for the preparation of SLIPS. For metal substrates, a structured feature was mostly achieved by electrolysis [106] and chemical etching [107] processes for the preparation of SLIPS. The advantages of lithography techniques are programmability and tunability of the topography of the featured structure while high cost and poor scalability limit this method for practical applications.

1.5.2.2 In Situ Growth of Structures

Along with substrate sculpting for the generation of structured surfaces, in-situ growth of a porous or rough architecture on a solid substrate (as shown in Fig. 1.13 B) can also be achieved by several methods including sol-gel methods, [108] LbL assembly, [109-113] chemical vapor deposition and atomic layer deposition, etc. [114-116] All these methods for the synthesis of micro/nano featured surface on solid substrate require immersion of the whole substrate in the reaction mixture, therefore formed SLIPS area is dependent on the size of the container or the facilities available. As an example, You *et al* [117] fabricated omniphilic/omniphobic patterned SLIPS for droplet mixing. They have grown TiO_2 nanostructure in-situ on polydopamine coated aluminum alloy followed by post-modification with low surface energy fluorinated molecules for hydrophobization. Then, those surfaces were lubricated with krytox for the preparation of desired SLIPS. In another literature, Zhang *et al* [118] reported in situ growth of silicone nanofilaments on glass substrates by the hydrolysis and condensation of trichloromethylsilane in a toluene-water solution. The in situ grown nanofilaments were then post functionalized with 1H,1H,2H,2H perfluorodecyltrichlorosilane after activating the surface with O_2 plasma followed by lubrication with fluorinated lubricants. Inorganic materials also used as building structures which were mostly developed on the selective substrates through hydrothermal or solvothermal reaction. In 2013, Ma *et al* [119] demonstrated the facile synthesis of nano-structure of alumina sol-gel coating on various substrates via post-hydrothermal treatment. Then the nanostructures were modified with perfluorinated compound, 1H,1H,2H,2H-perfluorodecylphosphonic acid for low surface energy coating followed by lubrication with perfluoropolyether (PFPE) for desired SLIPS. In 2015 Manna *et al* [120] has designed a slippery surface based on silicone oil infusion into a porous polymeric multilayer, fabricated by reactive covalent LbL assembly. In brief, porous multilayers by LbL assembly of poly(vinyl-4,4-dimetylazalactone) (PVDMA) and branched poly(etheleneimine) (PEI) was synthesized through a covalent 1,4 conjugate addition reaction between azalactone group of the PVDMA and amine group of PEI. Further, the reactive multilayer was post functionalized with amine-containing small molecules before lubrication with silicone oil (AR 20). The variations of the chain length of the alkylamines displayed a significant impact on the sliding behavior of the aqueous

droplets through the slippery interface. It was also demonstrated the chemically patterned sticky regions on the oil-infused SLIPS which can arrest the sliding of aqueous droplets.

1.5.2.3 Surface Compositing and Coating

Porous microstructures can also be created by coating or composting precursor solution on the solid substrate directly as demonstrated in Fig. 1.13 C. The major concern of direct compositing of a structural interface on a solid substrate is the poor adhesion between the structured layer and the substrate. But, the proper choice of substrate and the precursor compositing solution can provide a robust durable structural coating on the solid substrates. Compared to in situ growth strategies for the fabrication of micro/nano featured solid surfaces, surface compositing and coating methods are not limited to fabrication area and preparation facilities for construction of SLIPS. In 2016, Wang *et al* [121] fabricated nano featured surfaces on various substrates by phase separation method. In a typical synthetic procedure, they have prepared hydrophobic nanocomposite slurries by mixing hydrophobic SiO_2 and perfluoroalkyl methacrylic copolymer in acetone/water solvent mixture followed by brushing the polymeric solution onto the selected substrates to generate nano featured surface. Then the featured surfaces were lubricated with krytox for the fabrication of desired SLIPS. [122] Liu et al developed hierarchical featured SLIPS on aluminum substrates by electro-spraying silicone rubber onto the selected substrate followed by hydrophobization with fluorinated molecules before lubrication. [123] Electrospinning methods were also used for the construction of micro/nano featured surfaces. As an example, Wu *et al* [124] demonstrated the fabrication of multifunctional SLIPS by associating electrospinning method. For the fabrication of featured surface, they have simultaneously and separately electro spun both polyvinylidene fluoride (PVDF) and polyvinyl acetate (PVAc) onto the selected substrates prior to lubrication with perfluoropolyether. Yuan *et al* also reported fabrication of microstructure by depositing poly(styrene-b-isobutylene-b-styrene) onto the solid substrates through solution blow spraying method followed by fluorination and lubrication to achieve SLIPS. [125]

1.5.2.4 Limitations of Existing Methods for the Fabrication of SLIPS

Most of the existing methods for the construction of SLIPS always lead to formation of chemically inert SLIPS since a chemically inert superhydrophobization/hydrophobization process was mostly associated prior to lubrication as discussed in earlier sections. The effect of roughness factor on slippery property of SLIPS has been studied in the past. However, the effect of surface chemistry has rarely been reported in the earlier literatures. The design of chemically reactive and functional SLIPS is rare in the literature. I aimed to introduce a facile approach for a detailed investigation of the impact

of chemical modifications on slippery property. Further, a chemically reactive SLIPS has been successfully developed to develop patterned interfaces.

1.6 Applications of Water-Repellent Surfaces

During the past two decades, many different synthesis strategies have been developed to fabricate functional surfaces with anti-wetting properties for applications in different fields. Nowadays, a huge number of water-repellent interfaces (including superhydrophobic and SLIPS) have been introduced for different applications at practically relevant scenarios including self-cleaning,[126-131] oil/water separation,[132-136] drug delivery, [101, 137-138] anti-corrosion,[139-146] anti-biofouling,[147-152] anti-icing,[153-157] water harvesting [158-161] and various other relevant applications.[162-164] Self-cleaning coating is the class of material having the ability to remove deposited/contaminated dust/dirt without external intervention. The living example having this kind of self-cleaning property is lotus leaf where rolling water droplet collects the deposited contaminants on the surface and keep the surface clean and dry.[127] This feature arises due to superhydrophobicity of the lotus leaf where water droplet behaves as an elastic ball on the surface of lotus leaf rather than a fluid.

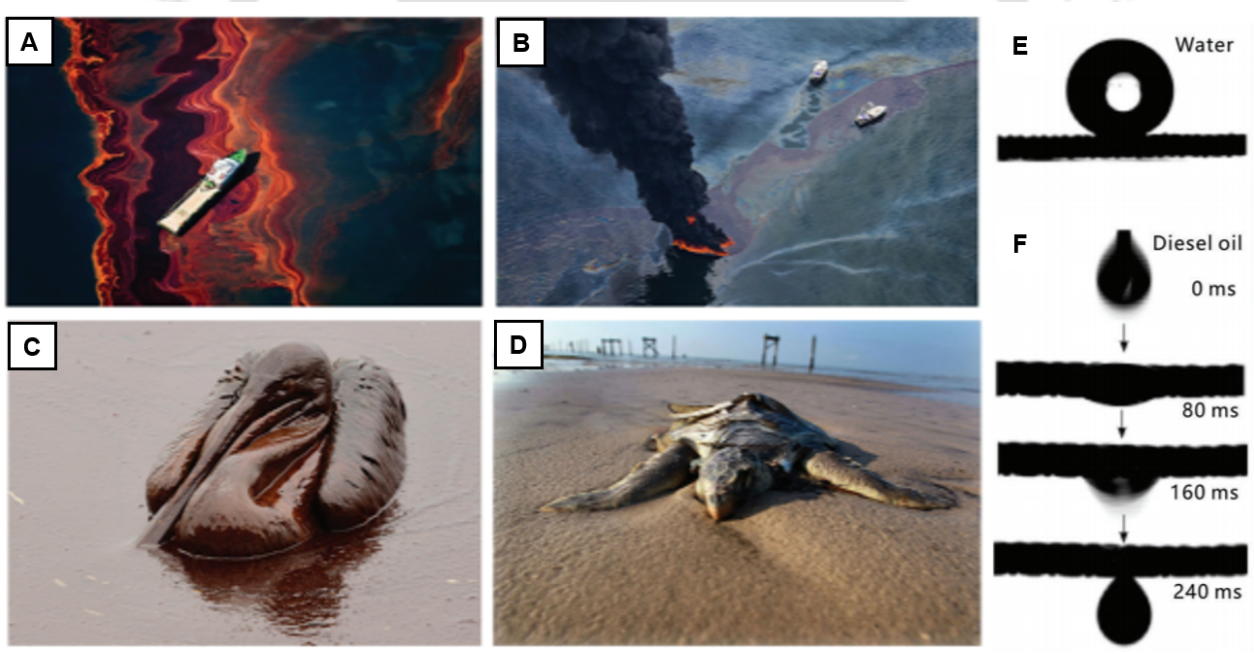

Figure 1.14. (A-D) Photograph of oil spillage accident on Gulf of Mexico which perturbed both aqua and coastal eco-system. Reprinted with permission from *Phys. Chem. Chem. Phys.* **2018**, *20*, 25140. Copyright 2018, Royal Society of Chemistry. (E, F) A superhydrophobic membrane which selectively allow oil to pass while aqueous phase arrested. Reprinted with permission from *Angew. Chem. Int. Ed.* **2004**, *43,* 2012 –2014, Copyright 2004, Wiley-VCH.

For example, Lu et al,[131] introduced instant fabrication of abrasion tolerant superhydrophobic surfaces which can act either in air or in oil for self-cleaning of contaminated dust particles. The same anti-wetting property is useful for protecting metals from harsh outside environments. At present, corrosion

is one of the most serious issues which cause the loss of billions of dollars each year. Anti-corrosion coating paid attention due to its ability to protect the metal from the outside environment. Recently, the chromium treatment of surface was found to be one of the major successes to prepare anti-corrosion coating but one can't neglect the side effect of chromium on health and the environment. It was found that superhydrophobic surfaces could be another alternative solution for anticorrosion coating since anti-wetting surfaces can protect the metals from aqueous environments. Jiang *et al* [142] synthesized Mg alloy surfaces with durable superhydrophobicity for enhanced corrosion resistance. The extreme water repellence property is an alternative solution for fogging especially in the winter season. Fogging is omnipresent as it habitually occurs in mirrors, glasses, and many other substrates and causes inconvenience in daily life and many technological devices. It was observed that fog droplets could be seen in between micro papillae of lotus leaf and therefore superhydrophobic surfaces cannot be an ideal candidate for antifogging coating. But inspired by mosquito compound eye, the artificial compound superhydrophobic interface has been introduced for achieving antifogging properties through adopting a soft lithography technique followed by low-surface-energy fluoroalkylsilane post-modification. The anti-wetting interface selectively repels water while it absorbs oily phases. This property is extremely useful for selective the separation of oil from oil/water interfaces. The separation of oil/water mixture in the recent days is one of the major challenges worldwide due to frequent oil spill accidents and the increasing industrial oily wastewater discharge in the open water resources including river and seashore, which would affect the aqua eco-system as shown in Fig. 1.14. For example, the oil flood in the Gulf of Mexico was one of the most serious pollutions in the last decades. Since superhydrophobic surfaces not only selectively repels aqueous medium but absorb oils at the

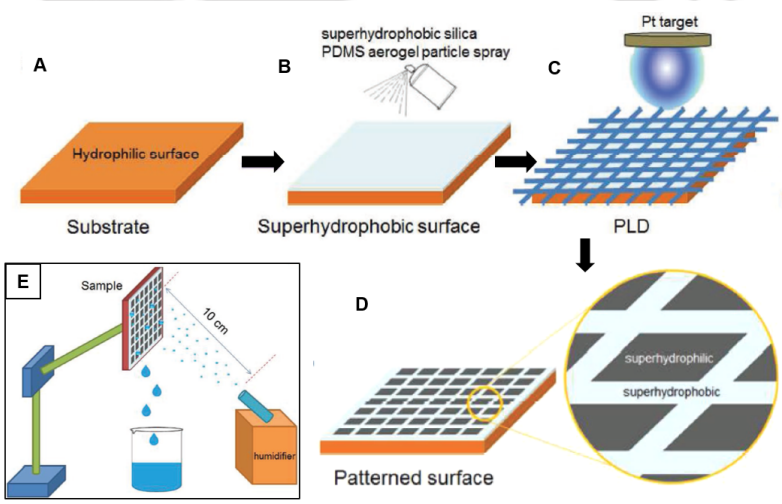

Figure 1.15. (A-D) Schematic representation of systematic preparation of superhydrophobic /superhydrophilic patterned surface for artificial water harvesting. Reprinted with permission from *small* **2017**, *13,* 1701403. Copyright 2017, Wiley-VCH.

same time. An appropriate association of this superhydrophobicity with fibrous/spongy substrates or metal mesh allowed selective absorption-based and filtration-based oil/water separation. Nearly four billion people all over the world are suffering from scarcity of drinkable water. The proper combination of wetting/anti-wetting interfaces is also useful for collecting fog from atmospheres without requiring any desorption process. Several patterned superhydrophobic/superhydrophilic (Fig. 1.15) interfaces were introduced for desorption-free artificial water collection. But, over time superhydrophobicity compromises its extreme water repellence property at high humid conditions. To encounter such limitations of superhydrophobic interfaces, slippery surfaces have appeared as an alternative approach for artificial fog harvesting. Previously, various bio-inspired architects were incorporated with slippery interfaces for the improvement of water-harvesting efficiency from the atmospheric fog. For example, in 2015, Park *et al* [164] incorporated the beetle's bumpy geometry and apex geometry of the cactus spine with a slippery interface for achieving better shedding of water droplets as shown in Fig. 1.16 A. In

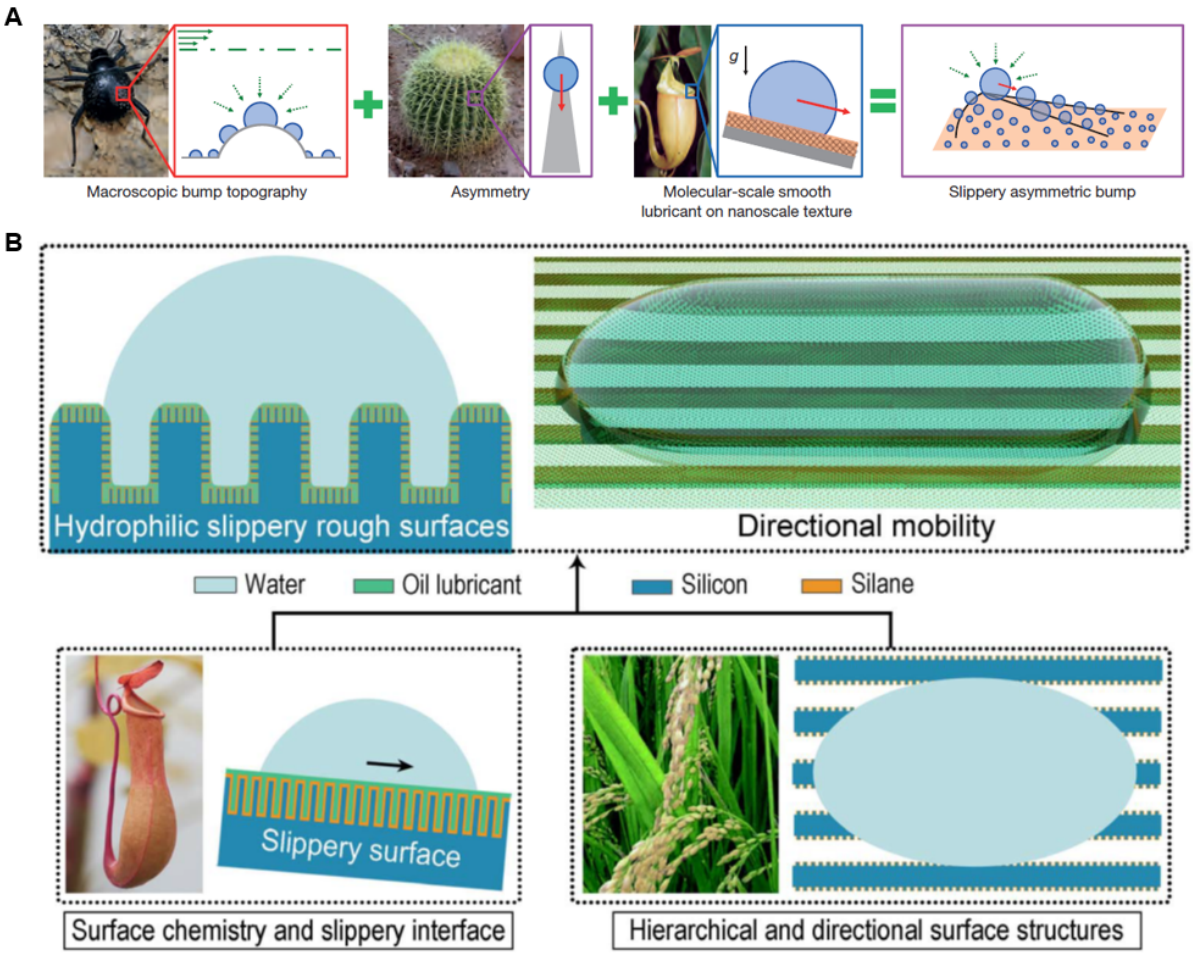

Figure 1.16. (A) Schematic representation for the preparation of slippery asymmetric bump for artificial fog harvesting. Reprinted with permission from *Nature* **2016**, *531*, 78–82. Copyright 2016, Nature. (B) A schematic formulation of directional hydrophilic slippery surface where rice leaf architect was incorporated into the nepenthes-inspired slippery surface. Reprinted with permission from Sci. Adv. **2018,** *4*, eaaq0919. Copyright 2018, American Association for the Advancement of Science.

another report, Dai *et al* investigated the impact of rice leaf geometry into a slippery interface. A hydrophilic directional slippery rough surface (SRS) was developed by combining salient features of rice leaf and pitcher plant. [163] The synthesized SRS outperformed both traditional SLIPS and superhydrophobic surfaces when it comes to water harvesting performance. However, the water harvesting performance of such an approach remained overall low and further development is essential for practically relevant applications (Fig. 1.16 B). Drag is one of the major obstacles for ships, submarines, aircraft, and microfluidic devices. It was found that anti-wetting interfaces provided a suitable avenue for drag reduction due to the existence of its extreme repellences towards water which draws a boundary between the aqueous fluid and solid, and dramatically minimizes the liquid-solid interaction. For instance, Watanabe *et al* [165] first observed a drag reduction phenomenon for Newtonian fluids when water passed through a 16 mm-diameter pipe with superhydrophobic walls. The accumulations of ice on solid surfaces are a common hindrance that causes a serious problem. The addition of extra weight can interfere with the operation of aircraft wings, wind turbine blades, and transmission and telecommunication equipment. Moreover, ice accumulation on roads, roofs, and windshields is a daily inconvenience, especially in cold regiments. Several methods have been incorporated including scraping or spraying warm de-icing fluids which is time and energy-intensive and highly expensive. Recently, some anti-wetting interfaces including superhydrophobic and slippery surfaces have been reported in the literature for the prevention of ice accumulations. [153-157] The presence of the third phase in between the solid surface and the water delays the nucleation of water and eventually prevents ice formation on the respective surfaces.

1.7 Objectives and Motivations

The earlier discussions and substantial investigations revealed that two essential criteria were found to play an important role in developing bio-inspired extreme anti-wetting surfaces and they are 1) essential topography 2) low surface energy coating. Moreover, lubrication on a porous and rough hydrophobic/superhydrophobic surface provides SLIPS. Superhydrophobic coating following a scalable and facile synthesis process is challenging to achieve and the development of functional, chemically reactive SLIPS are rare in literature. Earlier 1,4 conjugate addition reaction was found to be extensively used for developing hierarchical topography through various methods like sol-gel conversion and LbL deposition process. In the past Rather *et al* [166] developed polymeric free-standing superhydrophobic monolith via formation of chemically reactive polymeric nano complex (CRPNC) where a branched poly(etheleneimine) (BPEI) and dipentaerithritol penta/hexa acrylate (5Acl) readily reacted through the catalyst-free 1,4-conjugate addition reaction. The solution of CRPNC eventually transformed into a reactive polymeric gel (Fig. 1.17) which was further post modified for desired

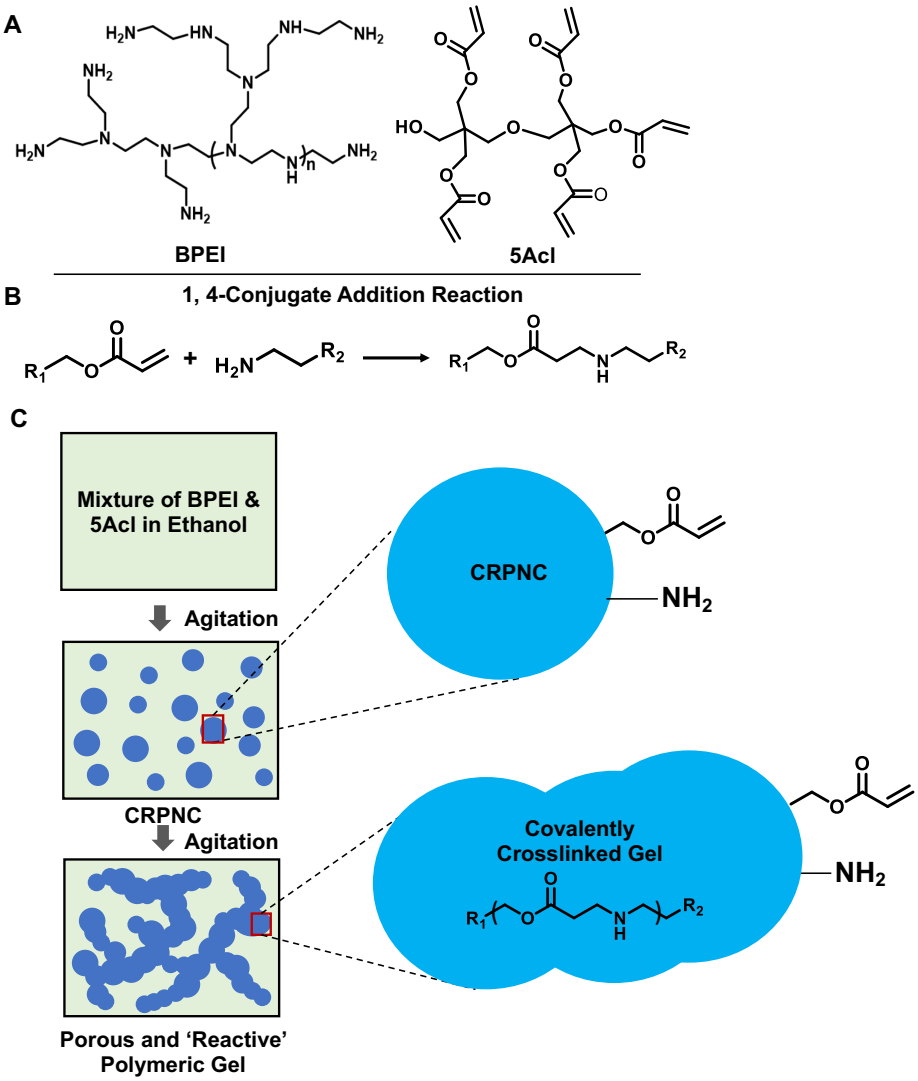

Figure 1.17. (A) Chemical structure of the precursor molecules. (B) 1,4-conjugate addition reaction between BPEI and 5 Acl. (C) Schematic representation for the process of porous reactive polymeric gel through the formation of chemically reactive polymeric nano-complex (CRPNC). Reprinted with permission from *Chem. Mater.* **2016**, *28*, 8689. Copyright 2016, American Chemical Society.

superhydrophobicity. The salt-assisted gelation approach remained inappropriate for coating on various substrates for practical applications. Later on, Parbat *et al* [167] synthesized reactive polymeric multi-layered coatings based on similar the chemistry to achieve extreme liquid wettability. But again, LbL deposition technique is time-consuming and laborious which is one of the major hindrances for real world applications. In this regard, I have assumed that the growth rate of the chemically reactive nano complex (CRPNC) has an important role in developing chemically reactive coating on both flat and porous substrates for practical applications. Based on this hypothesis, I have used a similar chemical reaction for manipulating the growth of CRPNC. A stable dispersion of CRPNC was prepared by introducing *in situ* dilution process. On the other side, the growth of CRPNC was accelerated by selecting an appropriate reaction medium without the addition of external additives. In

my current thesis work, I have introduced the scalable synthesis of abrasion tolerant superhydrophobic interface and chemically reactive SLIPS through the strategic use of CRPNC by dip/spray deposition technique for various applications including oil/water separation, self-cleaning interface, and fog-harvesting.

1.8 References

1. Wilbur and Orville Wright *U.S. Patent* 821, **1906**, 393–395.
2. Verbrugge, K. *Harvard Review* **2011**, 16–19.
3. Schweitzer, W.; Thali, M. J.; Egger, D. *J Neuroeng Rehabil.* **2018**, 15, 1.
4. Oka, K.; Aoyagi, S.; Arai, Y.; Isono, Y.; Hashiguchi, G.; Fujita, H. *Sens. Actuator. A* **2002**, *97*, 478–485.
5. Oeffner, J.; Lauder, G. V. *Journal of Experimental Biology* **2012**, *215*, 785-795.
6. Melingui, A.; Escande, C.; Benoudjit, N.; Merzouki, R.; Mbede, J. B. *IFAC* **2014**, *47*, 9353-9358
7. Aziz, M. S.; El sheriff, A. Y. *Alexandria Engineering Journal* **2016**, *55*, 707–714.
8. Liu, M.; Wang,S.; Jiang, L. *Nat. Mater. Reviews* **2017**, *2,* 17036.
9. Wang, S.; Liu, K.; Yao, X.; Jiang, L. *Chem. Rev.* **2015,** *115,* 8230−8293.
10. Kreder, M.; Alvarenga, J.; Kim, P.; Aizenberg, J. *Nat. Mater. Reviews* **2016**, *1*, 15003.
11. S. Li, J. Huang, Z. Chen, G. Chen and Y. Lai, *J. Mater. Chem. A*, 2017, **5**, 31.
12. Nuraje, N.; Khan, W. S.; Lei, Y.; Ceylan, M.; Asmatulu, R. *J. Mater. Chem. A* **2013**, *1*, 1929–1946.
13. Vogler, E. A. *Adv. Colloid Interface Sci.* **1998**, *74*, 69–117.
14. Su, B.; Tian, Y.; Jiang, L. *J. Am. Chem. Soc.* **2016**, *138*, 1727–1748.
15. Young, T. *Phil. Trans. R. Soc. Lond.* **1805,** *95*, 65–87.
16. Wenzel, R. N. *Ind. Eng. Chem.* **1936**, *28*, 988–994.
17. Cassie A. B. D.; Baxter, S. *Trans. Faraday Soc.* **1944**, *40*, 546–551.
18. Barthlott, W.; Neinhuis, C. *Planta* **1997**, *202*, 1–8.
19. Sun, M.; Watson, G. S.; Zheng, Y.; Watson, J. A.; Liang, A. *Journal of Experimental Biology* **2009**, *212*, 3148–3155.
20. Parker, A. R.; Lawrence, C. R. *Nature* **2001**, *414*, 33–34.
21. Bauera, U.; Paulinc, M.; Roberta, D.; Suttona, G. P. *PNAS* **2015**, *112*, 13384–13389.
22. Feng, L.; Li, S. H.; Li, Y. S.; Li, H. J.; Zhang, L. J.; Zhai, J.; Song, Y. L.; Liu, B. Q.; Jiang, L.; Zhu, D. B. *Adv. Mater*. **2002**, *14*, 1857−1860.

23. Zheng, Y. M.; Gao, X. F.; Jiang, L. *Soft Matter* **2007**, *3*, 178−182.
24. Liu, K. S.; Du, J. X.; Wu, J. T.; Jiang, L. *Nanoscale* **2012**, *4*, 768−772.
25. Neinhuis, C.; Barthlott, W. *Ann. Bot.* **1997**, *79*, 667−677.
26. Gao, X.; Yan, X.; Yao, X.; Xu, L.; Zhang, K.; Zhang, J.; Yang, B.; Jiang, L. *Adv. Mater.* **2007**, *19*, 2213−2217.
27. Gao, X.; Jiang, L. *Nature* **2004**, *432*, 36.
28. Zheng, Y.; Gao, X.; Jiang, L. *Soft Matter* **2007**, *3*, 178 −182.
29. Parker, A. R.; Welch, V. L.; Driver, D. *Nature* **2003**, *426*, 786−787.
30. Kreder, M.; Alvarenga, J.; Kim, P.; Aizenberg, J. *Nature* **2011**, *477*, 443–447.
31. Koch, K.; Bhushan, B.; Jung Y. C.; Barthlott W. *Soft Matter* **2009**, *5*, 1386–1393.
32. Nishimura, R.; Hyodo, K.; Sawaguchi, H.; Yamamoto, Y.; Nonomura, Y.; Mayama, H.; Yokojima, S.; Nakamura, S.; Uchida, K. *J. Am. Chem. Soc.* **2016**, *138*, 10299−10303.
33. Peppou, C. S.; Hong, J. K.; Waterhouse, A. Neto, C. *Chem. Soc. Rev.,* **2020**, *49*, 3688−3715.
34. Das, A.; Shome, A.; Manna, U. *J. Mater. Chem. A* **2021**, *9*, 824–856.
35. Coburn, J. W.; Winters, H. F. *J. Vac. Sci. Technol.* **1979**, *16*, 391–403.
36. Cardinaud, C.; Peignon, M.-C.; Tessier. P.-Y. *Appl Surface Sci*. **2000**, *164*, 72–83.
37. Youngblood, J. P.; McCarthy, T. J. *Macromolecules* **1999**, *32,* 6800–6806.
38. Celia, E.; Givenchy, E.T. de.; Amigoni, S.; Guittard, F. *Soft Matter* **2011**, *7*, 10057–10062.
39. Lee, E. J.; Jung, C.H.; Hwang, I. T.; Choi, J. H.; Cho, S. O.; Nho, Y. C. *ACS Appl. Mater. Interfaces* **2011**, *3*, 2988–2993.
40. Vandencasteele, N.; Nisol, B.; Viville P.; Lazzaroni, R.; Castner D. G.; Reniers, F. *Plasma Process. Polym.* **2008**, *5*, 661–671.
41. Minko, S.; Muller, M.; Motornov, M.; Nitschke, M.; Grundke, K.; Stamm, M. *J. Am. Chem. Soc.* **2003**, *125*, 3896–3900.
42. Vandencasteele, N.; Merche, D.; Reniers, F. *Surf. Interface Anal*. **2006**, *38*, 526–530.
43. Tsougeni, K.; Vourdas, N.; Tserepi, A.; Gogolides, E. *Langmuir* **2009**, 25, 11748–11759.
44. Chou, S. Y.; Krauss, P. R.; Zhang, W.; Guo, L. G.; Zhuang, L. *Vac. J. Sci. Technol. B* **1997,** *15,* 2897–2904.
45. Herbertson, D. L.; Evans, C.R.; Shirtcliffe, N. J.; McHale, G.; Newton, M. I. *Sens. Actuators, A* **2006**, *130*, 189–193.
46. Callies, M.; Chen, Y.; Marty, F.; Pepin, A.; Quere, D. *Microelectron Eng*. **2005**, *78,* 100–105.
47. Martines, E.; Seunarine, K.; Morgan, H.; Gadegaard, N.; Wilkinson, C. D. W.; Riehle, M. O. *Nano Lett*. **2005**, *5*, 2097–2103.

48. Fresnais, J.; Benyahia, L.; Poncin-Epaillard, F. *Surf. Interface Anal*. **2006**, *38*, 144–149.
49. Chou, S.Y.; Keimel, C.; Gu, J. *Nature* **2002**, *417*, 835–837.
50. Zhu, L.; Feng, Y.; Ye, X.; Zhou, Z. *Sens. Actuators, A* **2006**, *130,* 595–600.
51. Furstner, R.; Barthlott, C.; Neinhuis, C.; Walzel, P. *Langmuir* **2005**, *21*, 956–961.
52. Pozzato, A.; Zilio, S. D.; Fois, G.; Vendramin, D.; Mistura, G.; Belotti, M.; Chen, Y.; Natali, M. *Microelectron. Eng.* **2006,** *83,* 884–888.
53. Kawai, A.; Nagata, H. *Jpn. J. Appl. Phys.* **1994**, *33*, 1283–1285.
54. Oner, D. and T. J. McCarthy, *Langmuir* **2000**, *16*, 7777–7782.
55. Bartell, F. E.; Shepard, J. W. *J. Phys. Chem.* **1953,** *57,* 211–215.
56. Sun, M. H.; Luo, C. X.; Xu, L. P.; Ji, H.; Qi, O. Y.; Yu, D. P.; Chen, Y. *Langmuir* **2005**, *21*, 8978–8981.
57. Qu, M.; Zhao, G.; Wang, Q.; Cao, X.; Zhang, J. *Nanotechnology* **2008**, *19*, 55707–55711.
58. Zhang, L.; Sun, J. *Macromolecules* **2010**, *43*, 2413–2420.
59. Hozumi, A.; Cheng, D.F.; Yagihashi, M. *J. Colloid Interface Sci.* **2011**, *353*, 582–587.
60. Liu, X.; Dai, B.; Zhou, L.; Sun, J. J. Mater. Chem. 2009, 19, 497–504.
61. Yao, L.; Zheng, M.; He, S.; Ma, L.; Li, M.; Shen, W. *Appl. Surf. Sci.* **2011**, *257*, 2955–2959.
62. Hsieh, C. T.; Chen, W. Y.; Wu, F. L. *Carbon* **2008**, *46,* 1218–1224.
63. Zimmermann, J.; Reifler, F. A.; Fortunato, G.; Gerhardt, L. C.; Seeger. S. *Advanced Functional Mat.* **2008**, *18,* 3662−3669.
64. Sun, M.; Luo, C.; Xu, L.; Ji, H.; Ouyang, Q.; Yu, D.; Chen. Y. *Langmuir* **2005**, *21*, 8978–8981.
65. Lau, K. K. S.; Bico, J.; Teo, K. B. K.; Chhowalla, M.; Amaratunga, G. A. J.; Milne, W. I.; McKinley, G. H.; Gleason, K. K. *Nano Letters* **2003**, *3*, 1701–1705.
66. Li, S.; Li, H.; Wang, X.; Song, Y.; Liu, Y.; Jiang, L.; Zhu, D. *J. Phys. Chem. B* **2002,** *106,* 9274−9276.
67. Decher, G.; Hong, J. Berich. B. *Gesell.* **1991**, *95*, 1430−1434.
68. Decher, G.; Hong, J. D. *Makromol. Chem. Macromol. Symp.* **1991**, *46*, 321–327.
69. Decher, G. *Science* **1997**, *277*, 1232−1237.
70. Lee, S. W.; Kim, B. S.; Chen, S.; Horn, Y. S.; Hammond. P. T. *J. Am. Chem. Soc*. **2009**, *131*, 671–679.
71. Zhang, Y.; Arugula, M. A.; Williams, S. T.; Minteer, S. D.; Simonian. A. L. *Journal of Electrochemical Society* **2016,** *163*, 449–454.
72. Kong, B. S.; Geng. J.; Jung. H. T. *Chem. Commun*. **2009**, 2174–2176.
73. Kulkarni, D. D.; Choi, I.; Singamaneni, S. S.; Tsukruk, V. V. *ACS Nano* **2010**, *4*, 4667−4676.

74. Hu, M.; Mi. B. *Journal of Membrane Science* **2014,** *469,* 80–87.
75. Ahn, E.; Lee,T.; Gu, M.; Park, S.; Min, H.; Kim, B S. *Chem. Mater.* **2017**, *29*, 69−79.
76. Zhuk, A.; Mirza, R.; Sukhishvili, S. *Acs Nano* **2011**, *5***,** 8790–8799.
77. Lee, H.; Lee, Y.; Statz, A. R.; Rho, J.; Park, T. G.; Messersmith, P. B. *Adv Mater.* **2008**, *20*, 1619–1623.
78. Tang, Z.; Wang,Y.; Podsiadlo, P.; Kotov, N. A. *Adv. Mater*. **2006**, *18*, 3203–3224.
79. Zhai, L.; Cebeci, F. C.; Cohen, R. E.; Rubner, M. F. *Nano Lett*. **2004***, 4*, 1349–1353.
80. Ji, J.; Fu, J.; Shen, J. *Adv. Mater.* **2006**, *18*, 1441–1444.
81. Li, Y.; Chen, S.; Wu, M.; Sun, J. *Adv. Mater.* **2014,** *26,* 3344–3348.
82. Shang, H.M.; Wang, Y.; Limmer, S. J.; Chou, T.P.; Takahashi, K.; Cao, G. Z. *Thin Solid Films 472*, **2005**, 37–43.
83. Sia, Y.; Guo, Z. *Nanoscale* **2015**, *7*, 5922–5946.
84. Tadanaga, K.; Morinaga, J.; Matsuda, A.; Minami, T. *Chem. Mater*. 2000, *12*, 590–592.
85. Manca, M.; Cannavale, A.; Marco, L. D.; Arico, S.A.; Cingolani, R.; Gigli, G. *Langmuir* **2009**, *25*, 6357–6362.
86. Xu, Q.F.; Wang, J. N.; Sanderson, K. D. *ACS Nano* **2010**, *4*, 2201–2209.
87. Shang, H.M.; Wang, Y.; Limmer, S. J.; Chou, T. P.; Takahashi, K.; Cao, G. Z. *Thin Solid Films*, **2005**, *472,* 37–43.
88. Ma, W.; Wu, H.; Higaki, Y.; Otsuka, H.; Takahara, A. *Chem. Commun*. **2012**, *48*, 6824–6826.
89. Brinker, C.J.; Keefer, K.D.; Schaefer, D.W.; Ashley, C. S. *J. Non-Crystalline Solids* **1982**, *48*, 47–64.
90. Li, M.; Zhai, J.; Liu, H.; Song, Y.; Jiang, L.; Zhu, D. *J. Phys. Chem. B* **2003,** *107,* 9954-9957.
91. Erbil, H. Y.; Levent D. A.; Avcı, Y.; Mert, O. *Science* **2003,** *299*, 1377
92. Jiang, L.; Zhao, Y.; Zhai, J. *Angew. Chem. Int. Ed*. **2004**, *43*, 4338–4341.
93. Liu, Z. J.; Wang, H. Y.; Wang, E. Q.; Zhang, X. G.; Yuan, R. X.; Zhu, Y. J. *Polymer* **2016**, *82*, 105–113.
94. Park, S. H.; Lee, S. M.; Lim, H. S.; Han, J. T.; Lee, D. R.; Shin, H. S.; Jeong, Y.; Kim, J.; Cho, J. H. *ACS Appl. Mater. Interfaces* **2010**, *3,* 658–662.
95. Genzer, J.; Efimenko K. *Science* **2000,** *290,* 2130–2133.
96. Tian, X.; Verho, T.; Ras, R. H. A. *Science* **2016**, *352*, 142–143.
97. Verho, T.; Bower, C.; Andrew, P.; Franssila, S.; Ikkala, O.; Ras, R. H. A. *Adv. Mater*. **2011**, *23*, 673–678.
98. Li, Y.; Li, L.; Sun, J. *Angew. Chem. Int. Ed.* **2010**, *49*, 6129–6133.

99. Zhu, X. T.; Zhang, Z. Z.; Men, X. H.; Yang, J.; Wang, K.; Xu, X. H.; Zhou, X. Y.; Xue, Q. J. *J. Mater. Chem*. **2011***, 21*, 15793–15797.
100. Levkin, P. A.; Svec, F.; Frechet, J. M. *J. Adv. Funct. Mater.* **2009**, *19*, 1993–1998.
101. Yohe, S. T.; Colson, Y. L.; Grinstaff, M. W. *J. Am. Chem. Soc*, **2012**, *134*, 2016–2019.
102. Manna, U.; Lynn, D. M. *Adv. Mater.* **2013**, *25*, 5104−5108.
103. Deng, R.; Shen, T.; Chen, H.; Lu, J.; Yang, H. C.; Li, W. *J. Mater. Chem. A* **2020**, 8, 7536–7547.
104. Li, X.; Wang, G.; Zhan, B.; Li, S.; Han, Z.; Liu, Y. *Adv. Mater. Interfaces* **2019**, *6*, 1900864
105. Boreyko, J. B.; Polizos, G.; Datskos, P. G.; Sarles, S. A.; Collier, C. P. *PNAS*, **2014**, *111*, 7588–7593.
106. Yang, S.; Qiu, R.; Song, H.; Wang, P.; Shi, Z.; Wang, Y. *Appl. Surf. Sci.* **2015**, *328*, 491–500.
107. Zhang, P.; Chen, H.; Zhang, L.; Zhang, Y.; Zhang, D.; Jiang, L. *J. Mater. Chem. A* **2016**, *4*, 12212–12220.
108. Wei, C.; Zhang, G.; Zhang, Q.; Zhan, X.; Chen, F. *ACS Appl. Mater. Interfaces* **2016**, *8*, 34810–34819.
109. Huang, X.; Chrisman, J. D.; Zacharia, N. S. *ACS Macro Lett. 2013*, *2*, 826–829.
110. Manabe, K.; Nishizawa, S.; Kyung, K. H.; Shiratori, S. *ACS Appl. Mater. Interfaces* **2014**, *6*, 13985–13993.
111. Sunny, S.; Vogel, N.; Howell, C.; Vu, T. L.; Aizenberg, J. *Adv. Funct. Mater*. **2014**, *24*, 6658–6667.
112. Chen, X. C.; Ren, K. F.; Wang, J.; Lei, W. X.; Ji, J. *ACS Appl. Mater. Interfaces* **2017**, *9*, 1959–1967.
113. Huang, W. P.; Chen, X.; Hu, M.; Hu, D. F.; Wang, J.; Li, H. Y.; Ren, K. F.; Ji, J. *Chem. Mater*. **2019**, *31*, 834–841.
114. Badv, M.; Jaffer, I. H.; Weitz, J. I.; Didar, T. F. *Sci. Rep*. **2017**, *7*, 11639.
115. Heale, F. L.; Parkin, I. P.; Carmalt, C. J. *ACS Appl. Mater. Interfaces* **2019**, *11*, 41804–41812.
116. Yang, H. C.; Waldman, R. Z.; Chen, Z.; Darling, S. B. *Nanoscale*, **2018**, *10*, 20505–20513.
117. You, I.; Lee, T. G.; Nam, Y. S.; Lee, H. *ACS Nano* **2014**, *8*, 9016–9024.
118. Zhang, J.; Wang, A.; Seeger, S. *Adv. Funct. Mater*. **2014**, *24*, 1074–1080.
119. Ma, W.; Higaki, Y.; Otsuka, H.; Takahara, A. *Chem. Commun*. **2013**, *49*, 597–599.
120. Manna, U.; Lynn, D. M. *Adv. Mater*. **2015**, *27*, 3007–3012.
121. Wang, Y.; Zhang, H.; Liu, X.; Zhou, Z. *J. Mater. Chem. A* **2016**, *4*, 2524–2529.

122. Wang, N.; Xiong, D.; Lu, Y.; Pan, S.; Wang, K.; Deng, Y.; Shi, Y. *J. Phys. Chem. C* **2016**, *120*, 11054–11059.
123. Liu, Q.; Yang, Y.; Huang, M.; Zhou, Y.; Liu, Y.; Liang, X. *Appl. Surf. Sci*. **2015**, *346*, 68–76.
124. Wu, J.; Zhang, B.; Wang, B.; Li, J. *Chem Nano Mat* **2017**, *3*, 869–873.
125. Yuan, S.; Li, Z.; Song, L.; Shi, H.; Luan, S.; Yin, J. *ACS Appl. Mater. Interfaces* **2016**, *8*, 21214–21220.
126. Blossey, R. *Nat. Mater.* **2003**, *2,* 301−306.
127. Parkin, I. P.; Palgrave, R. G. *J. Mater. Chem.* **2005**, *15,* 1689−1695.
128. Wang, P.; Chen, M.; Han,H.; Fan, X.; Liua, Q.; Wang, J. *J. Mater. Chem. A* **2013**, *4*, 7869–7874.
129. Zhiqing, Y.; Hong, C.; Jide, Z.; Dejian, Z.; Yuejun, L.; Xiaoyuan, Z.; Song, L.; Pu, S.; Jianxin, T.; Xin, C. *Sci. Technol. Adv. Mater.* **2008,** *9*, 045007–045012.
130. Nakajima, A.; Hashimoto K.; Watanabe T. *Langmuir* **2000**, *16*, 7044-7047.
131. Lu, Y.; Sathasivam, S.; Song, J.; Crick, C. R.; Carmalt, C. J.; Parkin, I. P. *Science* **2015**, *6*, 1132–1135.
132. Zhang, Z.; Wang, H.; Liang Y.; Li, X.; Ren, L.; Cui. Z.; Luo, C. *Scientific Reports* **2018**, *8,* 3869.
133. Bua, Y.; Huangb, J.; Zhanga, S.; Wanga, Y.; Gua, S.; Caob, G. C.; Yanga, H.; Yea, D.; Zhoua, Y.; Xu, W. *Applied Surface Science* **2018**, *440,* 535–546.
134. Feng, L.; Zhang, Z.; Mai, Z.; Ma, Y.; Liu, B.; Jiang, L.; Zhu, D. *Angew. Chem. Int. Ed.* **2004**, *43,* 2012 –2014.
135. Gui, X.; Wei, J.; Wang, K.; Cao, A.; Zhu, H.; Jia, Y.; Shu, Q.; Wu, D. *Adv. Mater.* **2010**, *22,* 617–621.
136. Ruan, C.; Ai, K.; Li, X.; Lu, L. *Angew. Chem. Int. Ed.* **2014***, 53*, 5556–5560.
137. Manna, U.; Kratochvil, M. J.; Lynn, D. M. *Adv. Mater*. **2013**, *25,* 6405–6409.
138. Wolinsky, J. B.; Yohe, S. T.; Colson, Y. L.; Grinstaff, M. W. *Biomacromolecules* **2012**, *13*, 406−411.
139. Xiang, T.; Zheng, S.; Zhang, M. Sadig, H. R.; Li, C. *ACS Sustainable Chem. Eng.* **2018**, *6*, 10960−10968.
140. Zhang, J.; Gu, C.; Tu, J. *ACS Appl. Mater. Interfaces* **2017**, *9*, 11247−11257.
141. Song, F.; Wu, C.; Chen, H.; Liu, Q.; Liu, J.; Chen, R.; Liad, R.; Wang, J. *RSC Adv.* **2017**, *7*, 44239.

142. Liu, K. S.; Zhang, M. L.; Zhai, J.; Wang, J.; Jiang, L. *Appl. Phys. Lett*. **2008**, *92,* 183103−183106.
143. Xu, W.; Song, J.; Sun, J.; Lu, Y.; Yu, Z. *ACS Appl. Mater. Interfaces* **2011**, *3*, 4404−4414.
144. Ishizaki, T.; Saito, N. *Langmuir* **2010**, *26,* 9749−9755.
145. Liu, Q.; Chen, D.; Kang, Z. *ACS Appl. Mater. Interfaces* **2015**, *7*, 1859–1867.
146. Huang, Z. B.; Zhu, Y.; Zhang, J. H.; Yin, G. F. *J. Phys. Chem. C* **2007**, *111*, 6821–6825.
147. Caitlin, H.; Vu, T. L.; Lin, J. J.; Kolle, S.; Juthani, N.; Watson, E.; Weaver, J. C.; Alvarenga, J.; Aizenberg, J. *ACS Appl. Mater. Interfaces* **2014**, *6*, 13299−13307.
148. Amini, S.; Kolle, S.; Petrone, L.; Ahanotu, O.; Sunny, S.; Sutanto, C. N.; Hoon, S.; Cohen, L.; Weaver, J.C.; Aizenberg, J.; Vogel, N.; Miserez, A. Science **2017**, *357*, 668–673.
149. Darmanin, T.; Givenchy, E. T. D.; Amigoni, S.; Guittard, F.; Celia, E. *J. Colloid Interface Sci.,* **2013,** *402*, 1-18.
150. Fan, H. L.; Chen, P. P.; Qi, R. M.; Zhai, J.; Wang, J. X.; Chen, L.; Chen, L.; Sun, Q. M.; Song, Y. L.; Han, D.; Jiang, L. *Small* **2009***, 5*, 2144–2148.
151. Sun, T. L.; Tan, H.; Han, D.; Fu, Q.; Jiang, L. *Small* **2005**, *1*, 959–963.
152. Cho, E. C.; Jian, C. W. C.; Chen, H. C.; Chuang, K. S.; Zheng, J. H.; Hsiao, Y. S.; Lee, K. C.; Huang, J. H. *Chem. Eng. J.* **2017**, *314*, 347–357.
153. Cao, L.; Jones, A. K.; Sikka, V. K.; Wu, J.; Gao, D. *Langmuir* **2009**, *25*, 12444–12448.
154. Lo, C. W.; Sahoo, V.; Chang, M. *ACS Nano* **2017,** *11*, 2665–2674.
155. Kim, A.; Lee, C.; Kim, H.; Kim, J. *ACS Appl. Mater. Interfaces* **2015,** *7*, 7206–7213.
156. Jung, S.; Tiwari, K. M.; Doan, N. V.; Poulikakos, D. *Nature Communications* **2012**, *3*, 1-8.
157. Kim, P.; Wong, T. S.; Alvarenga, J.; Kreder, M. J.; Adorno-Martinez, W. E.; Aizenberg, J. *ACS Nano* **2012**, *6*, 6569–6577.
158. Garrod, R. P.; Harris, L. G.; Schofield, W. C. E.; McGettrick, J.; Ward, L. J.; Teare, D. O. H.; Badyal, J. P. S. *Langmuir* **2007,** *23,* 689−693.
159. Yu, Z.; Yun, F. F.; Wang, Y.; Yao, L.; Dou, S.; Liu, K.; Jiang, L.; Wang, X. *small* **2017**, 13, 1701403.
160. Park, K.-C.; Kim, P.; Grinthal, A.; He, N.; Fox, D.; Weaver J. C.; Aizenberg, J. *Nature* **2016**, *531*, 78–82.
161. Dai, X.; Sun, N.; Nielsen, S. O.; Stogin, B. B.; Wang, J.; Yang, S.; Wong, T.-S. *Sci. Adv.* **2018**, *4*, eaaq0919.
162. Mumm, F.; V.; Helvoort, A. T. J.; Sikorski, P. *ACS Nano* **2009, 3,** 2647−2652.
163. Das, A.; Megaridis, C. M.; Liu, L.; Wang, T.; Biswas, A. *Appl. Phys. Lett.* **2011,** *98,* 174101.

164. Park, Y. B.; Im, H.; Im, M.; Choi, Y. K. *J. Mater. Chem.* **2011,** *21,* 633-636.

165. Watanabe, K.; Udagawa, Y.; Udagawa, H. *J. Fluid Mech.* **1999,** *381,* 225−238.

166. Rather, A. M.; Manna, U. *Chem. Mater*. **2016**, *28*, 8689−8699.

167. Parbat, D.; Manna, U. *Chem. Sci*., **2017**, *8*, 6092–6102.

Title: Synthesis of Scalable and Durable Superhydrophobic Melamine Sponge for Efficient Oil/Water Separation *

In the past, lotus leaf-inspired extreme water-repellency property was strategically incorporated on various commercially available porous sponges to develop selective oil absorbents. However, most of the earlier reported materials either lacked physical and chemical durability or associated with complex fabrication procedures, limiting their applicability in practically harsh environments. In this regard, a reusable and stable dispersion of chemically reactive polymeric nano-complex (CRPNC) was successfully synthesized and utilized to achieve a chemically reactive polymeric coating on the highly compressible and commertially available melamine sponge. The post-covalent functionalization of the chemically reactive coated melamine sponge through catalyst-free 1,4-conjugate addition reaction at room temperature yielded a superhydrophobic melamine sponge (SMS). The durability of the embedded extreme non-wetting property in the SMS has been thoroughly tested. The synthesized material was exposed to several relevant physical/chemical insults and prolonged UV irradiation for examining its tolerance at outdoor conditions. The highly abrasion tolerant SMS was then employed as an efficient oil absorbent wherein oily phases with different densities and surface tensions could be selectively recovered from an oil/water mixture with high (e.g., 137 gg^{-1} for chloroform and 83 gg^{-1} for diesel) oil absorption capacity. Moreover, the selective oil absorption capacity of the as-synthesized material remained unaffected at practically relevant severe chemical and physical settings, and the extreme water repellence of the material remains intact even after repetitive (at least 50 cycles) use for oil/water separation.

*Shome, A.; **Maji, K**.; Rather, A. M.; Yashwanth, A.; Patel, D. K.; Manna, U. *Chem. Asian J.* 2019, *14*, 4732 – 4740.

2.1 Introduction

The growth of human civilization has raised some serious environmental concerns. As the global demand for energy rises, regular oil spill accidents and industrial oily wastewater discharge pollute the open water resources, including rivers and seashores, which perturbed aqua and its surrounding ecosystem. For instance, the Exxon Valdex oil spill accident resulted in widespread damages to nearly 3 lakh species breeding in that habitant.[1] Conventional remediation methods like skimming, mechanical collection, in situ burning of oils, use of chemical dispersants[2–4] have been used in the past to encounter these massive oil spill accidents. These methods are associated with various relevant drawbacks, including high operational costs, tedious and energy inefficient processes, secondary pollution caused due to burning of oils or chemical dispersants used. Therefore, the design of environment-friendly and energy-efficient materials for oil/water separation is highly relevant in the current prospect. In this context, bio-mimicked lotus-leaf inspired extreme repellence of aqueous phase provided a highly promising basis for energy-efficient and environment-friendly oil/water remediation process.[5–9] In 2004, Feng et al. unprecedentedly introduced an extremely water-repellent interface for "proof of concept" demonstration of oil/water separation,[7] where a superhydrophobic mesh selectively allowed only the oil phase to penetrate in contrast, the water phase was extremely repelled by the mesh in a gravity-driven filtration process. However, these gravity-driven and filtration-based separation processes are inappropriate for cleaning up the oil-contaminated open and vast natural water reservoirs (e.g., oceans, rivers, seas, lakes, etc.) Later, this bio mimicked approach was further successfully extended for selective absorption-based oil/water separation, where porous superhydrophobic sponges and monoliths selectively absorbed floating or sediment oil phases from the respective aqueous phase. Since then, various synthetic approaches have been introduced for developing different superhydrophobic sponges and monoliths[10–23] for selective oil removal. However, these reported materials are associated with various limitations such as complicated synthetic procedures, poor tolerance to abrasive challenges, recyclability, use of chemicals that harm health and environment, labile chemistry limitting their applications at practically relevant severe and diverse settings.[24–30] The strategic modification of commercially available spongy substrates with essential physical and chemical parameters that confer superhydrophobicity, has recently been utilized for developing reusable and selective oil-absorbents. Moreover, the high compressibility provided a facile basis for energy-efficient and environment-friendly removal and collection of the absorbed oil, compared to the other existing approaches-such as refluxing, burning etc.[31, 32] The low density (=10 mg cm^{-3}), high porosity (average pore size of 150 ± 5 μm) of melamine sponge inherently allowed greater absorption of the oily phase, selectively, after embedding the selected spongy substrate with artificial

superhydrophobicity.[33–38] However, in the literature till date, the demonstration of oil/water separation at practically relevant severe settings has barely been demonstrated with the superhydrophobic MS sponge, likely due to the poor durability of the embedded superhydrophobicity in the reported materials. For instance, Li et al[39] synthesized the graphydene based melamine sponge for selective absorption of the oil phase. However, the embedded anti-wetting property of the synthesized material is compromised in harsh chemical media, and eventually, such design is inappropriate for practical application. In another report, Turng et al[40] synthesized a superhydrophobic MS by layer-by-layer deposition of various nanoparticles (silica, carbon nanotubes, and graphene oxide). Nevertheless, the anti-wetting property of the synthesized materials is susceptible to compromise under various physical and chemical settings. Despite considerable progress in the fabrication of superhydrophobic MS for oil/water separation in recent years, there is still a need to design 1) a physically and chemically durable superhydrophobic MS following 2) a simple and scalable synthetic procedure, and the synthesized superhydrophobic MS should be 3) capable of performing under various challenging scenarios. In this report, a commercially available compressible melamine sponge (MS) has been decorated with a chemically reactive coating-following a simple and rapid Michael addition reaction between amine and acrylate groups at ambient conditions. The rational post-chemical modification of the reactive coating with hydrophobic alkylamine provided highly tolerant superhydrophobicity with a water contact angle of 159^0. The embedded water repellence on the MS remained intact even after severe physical and chemical abrasions, revealing the extreme durability of the chemically optimized extreme water repellence in the currently developed superhydrophobic MS (SMS). The as-fabricated SMS was extended for oil/water separation with both heavy and light oil-contaminated aqueous phases. The spongy superhydrophobic material repetitively (50 times) and successfully separated oil/oily phases from respective oil/water mixtures with a maximum absorption capacity of 137 gg^{-1}. The material exhibited excellent separation efficiency (above 98 %), irrespective of the densities and viscosities of the used oils. The oil absorption capacity and oil separation efficiency remained unaltered at various practically relevant challenging settings. Hence, the modified SMS with embedded extreme water-repellent property holds promising potential for use in practical applications.

2.2 Experimental Section

2.2.1 Materials

Branched poly (ethylenimine) (BPEI, MW~25000 Da), dipentaerythritol penta/hexa acrylate (5 siliconeAcl, MW=524.51 $gmol^{-1}$), octadecylamine were purchased from Sigma Aldrich (Bangalore India), and absolute ethyl alcohol (CAS 64-17-5, Lot 1005150) was purchased from TEDIA/Company (United States of America). Reagent grade THF was procured from RANKEM (Maharashtra).

Rhodamine 6G (Rh-6G), methylene blue, nile red dye, silicon oil was obtained from Sigma Aldrich (Bangalore, India). NaOH was purchased from Emparta (Merck Specialties Private Limited). Melamine sponge was purchased from AR Acoustics LLP Maharashtra. UV cabinet used for continuous exposure of UV radiations was purchased from Relitech (Bangalore, India). Hydrochloric acid (HCl) was purchased from Fisher Scientific (Hyderabad, India). Motor oil was obtained from Castrol India Limited. Dichloromethane (DCM) and chloroform were obtained from Merck Life Science Pvt Ltd (Bangalore, India). Diesel and petrol were obtained from the nearest Indian oil petrol pump in Guwahati (Assam, India). Kerosene oil was procured from a local shop in Guwahati city (Assam, India). River water collected from Brahmaputra River.

2.2.2 General Considerations

Glass vials used to prepare the polymer solutions were washed with acetone and ethanol prior to use. The contact angle measurements were taken using the KRUSS Drop Shape Analyser-DSA25 instrument with an automatic liquid dispenser at ambient conditions. Advancing and receding water contact angles were measured at three to four different locations for each sample. Field Emission Scanning electron microscope (FESEM) images were acquired using Sigma Carl Zeiss scanning electron microscope (samples were coated with a thin layer of gold prior to imaging). Fourier Transform Infrared Spectroscopy (FTIR) spectra were recorded using the PerkinElmer instrument at ambient conditions, wherein the sample was grinded with KBr to prepare the pellet before analysis. Digital pictures were acquired using a canon power shot SX420 IS digital camera. Deionized (DI) water was used for all experiments.

2.2.3 Synthesis of Superhydrophobic Melamine Sponge (SMS)

Prior to use, the melamine sponge (MS) (10 cm x 6 cm x 2 cm) was first rinsed with acetone and ethanol to remove the undesired contaminants from the surface. Solutions of 5-Acl and BPEI were prepared by dissolving 13.25 g of 5-Acl and 5 g of BPEI in 100 mL of ethanol separately. Then, 50 mL of 5-Acl and 15 mL of BPEI were mixed and kept for 1 h till the turbidity appeared. Next, the turbid milky polymeric solution was diluted with ethanol to half of its original concentration. Subsequently, the cleaned MS was dipped in the diluted turbid polymeric solution and kept undisturbed for 3 hours. Thereafter, the MS was washed with THF for 1 h and subsequently, transferred into octadecylamine (ODA) solution (5 mg/mL in THF) for 12 hours. After the post modification, the MS was further rinsed with THF to remove the loosely held ODA molecules and was dried at ambient conditions. Later, the anti-wetting property was examined through visual inspection and contact angle measurement.

2.2.4 Durability Tests

The superhydrophobic melamine sponge was subjected to various practically relevant challenging physical and chemical manipulations to examine the durability of the sponge. Details of each durability test are provided in the following section.

2.2.4.1 Sand Paper Abrasion: Sandpaper was fixed on the glass slide using adhesive tape. Next, a superhydrophobic melamine sponge (10 cm x 6 cm x 2 cm) was placed on the sandpaper with an external load of 500 g. The material was moved with the weight back-and-forth motion multiple (minimum 10 times) times on the sandpaper. Thereafter, the water wettability was measured through visual inspection and contact angle measurements.

2.2.4.2 Adhesive Tape Test: Here, an adhesive tape was fixed onto the post-modified sponge with a 500 g load on top of the adhesive tape to facilitate better contact between the substrate and adhesive tape. Then, the adhesive tape was peeled off from the material, and subsequently, the anti-wetting property was examined through digital images and contact angle measurements.

2.2.4.3 Sand Drop Test: In this abrasion test, 150 g of sand grains were poured from a height of & 20 cm over the superhydrophobic melamine sponge (tilted at ~ 45^0 horizontally). Thereafter, the anti-wetting property of the superhydrophobic MS was examined with digital images and contact angle measurements.

2.2.4.4 Scratch Test: Random scratches were made all over the superhydrophobic melamine sponge using a sharp-edged knife multiple times, and thereafter, the anti-wetting property was verified through both digital images and contact angle measurements on the physically damaged area.

2.2.4.5 ***Chemical Durability Tests:*** The chemical durability of the SMS was examined after exposing it to various harsh aqueous chemical conditions including extremes of pH (1 and 12), artificial seawater, surfactant (SDS, DTAB 1mM) contaminated water, river (Brahmaputra, Assam India) water for 20 days. Artificial Seawater was prepared by mixing $MgCl_2$ (0.226 g), $MgSO_4$ (0.325 g), NaCl (2,673 g), $CaCl_2$ (0.112 g) in 100 mL of de-ionized water in a volumetric flask. Digital images and contact angle measurements were acquired at regular intervals to examine the durability of the embedded liquid water wettability.

2.2.4.6 UV Durability Test: Here, the superhydrophobic melamine sponge (2 cm x 4 cm) was kept under UV radiation at both short (254 nm) and long (365 nm) wavelengths for 15 days. The anti-wetting property of the sponge was examined after every 5 days interval through contact angle measurements and digital images.

2.2.5 Absorption-based Oil/Water separation

Here, we have demonstrated the separation of various oils and organic solvents from respective oil/oily water mixtures. First, 20 mL of light oil was poured (red-dyed, for visual inspection) at the air/water interface in a petri-dish, and subsequently, SMS was placed at the oil/water interface, immediately the SMS selectively absorbed the oil phase while repelling the water phase extremely. The absorbed oil was collected separately by manually squeezing the sponge. The same experiment was repeated for the separation of light oil using the native sponge. The native MS absorbed both oil and aqueous phases during the process of separation of light oil from the oil/water mixture. The native MS and SMS were also explored for the separation of heavy oil (Dichloromethane, dyed red color for visual inspection) sediment at the bottom of the water. The SMS instantly soaked the oil phase without any traces of water although the sponge first came in contact with the water phase. The absorbed oil was re-collected through manual squeezing.

2.3 Results and Discussions

2.3.1 Synthesis and Characterization of Superhydrophobic Melamine Sponge (SMS)

In the recent past, a reactive polymeric gel has been introduced via the formation of chemically reactive nanocomplexes, where amine and acrylate groups of branched poly(ethyleneimine) (BPEI) and

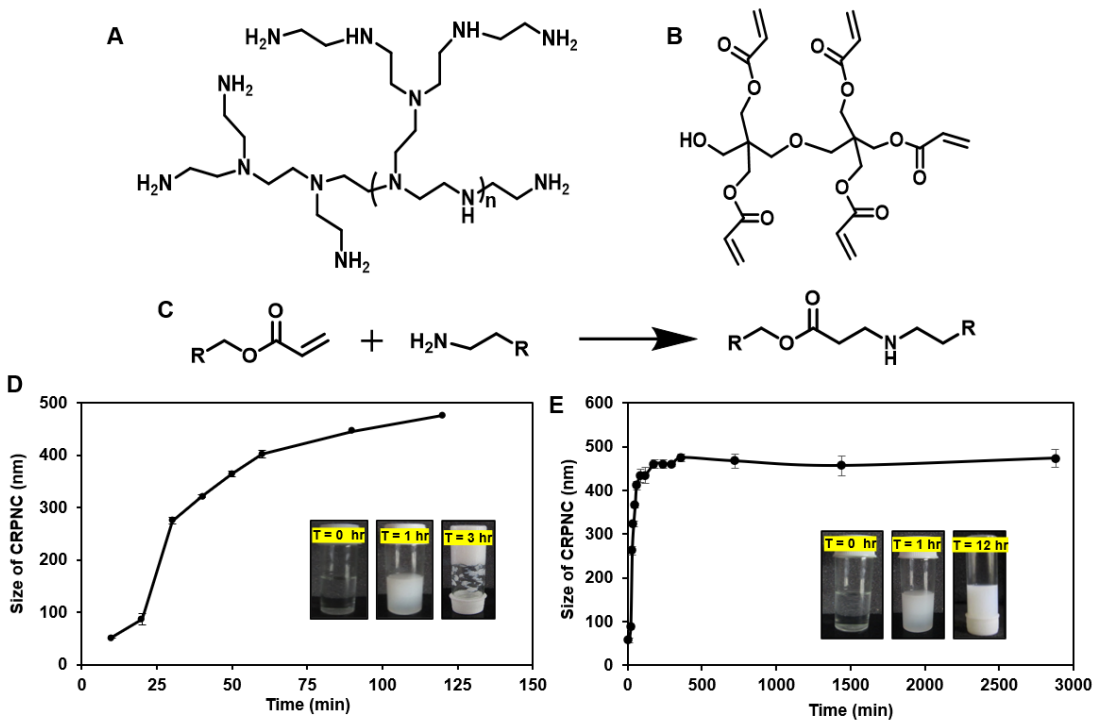

Figure 2.1. (A, B) Chemical structure of Branched poly (ethylenimine) (BPEI) (A) and dipentaerythritol penta acrylate 5-Acl (B). (C) Representation of 1,4-conjugate addition reaction between acrylate and amine groups. (D, E) DLS spectra of CRPNC without (D) and with dilution (E).

dipentaerythritol penta/hexa acrylate (5Acl), respectively, reacted through 1,4-conjugate addition reaction (Fig. 2.1 A-C).[41] The reaction mixture of BPEI and 5-Acl formed a milky turbid solution of nanocomplexes, which further reacted over time to transform into a chemically reactive polymeric gel after 3h (Fig 2.1 D). However, in this current work, a stable dispersion of chemically "reactive" polymeric nano-complexes was obtained by adopting a simple half dilution process to introduce a highly scalable synthetic process of superhydrophobic MS (SMS). The reaction mixture of Branched poly (ethylenimine) (BPEI) and dipentaerythritol penta acrylate (5-Acl) was diluted with ethanol after 1 h of mutual reaction between the reactants at ambient conditions. The dilution of the reaction mixture certainly reduced the uncontrolled aggregation of nanocomplexes in the solution. The size of the nanocomplex in the reaction mixture remained steady at 465 nm over 48 h (Fig 2.1 E). Then, a piece of commertially available melamine sponge (MS) was dipped in the stable dispersion of nanocomplexes for 3 h for developing essential features that conferred extreme water repellence, after covalent modification of chemically reactive coating with primary amine-containing small molecules. This residual chemical reactivity allowed post covalent modification of the nano-complex coated MS

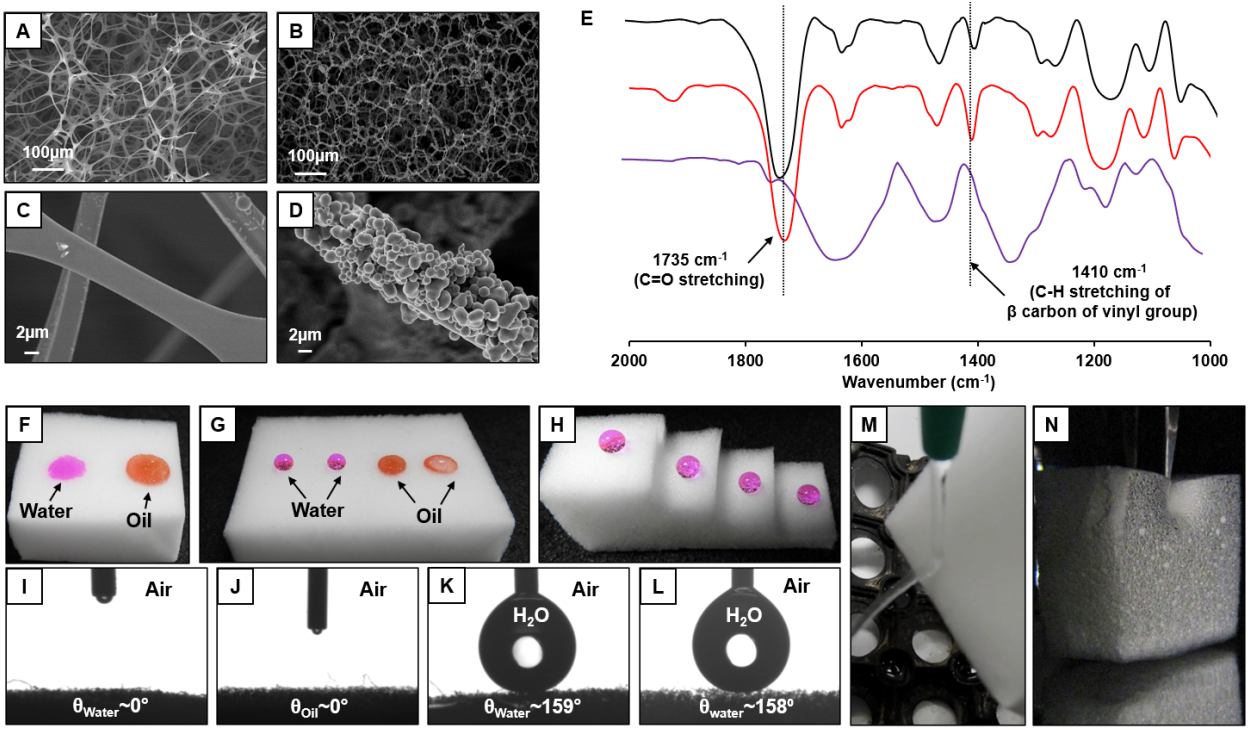

Figure 2.2. (A-D) FESEM of native melamine sponge (A, C) superhydrophobic melamine sponge (SMS) (B, D) at lower magnification (A, B) and higher magnification (C, D). (E) FTIR spectra of native MS (violet), CRPNC coated reactive MS (red) and superhydrophobic MS (black). (F, G) Digital images of beaded water (pink) and oil (orange) droplet on native MS (F) and superhydrophobic MS (G). (H) Digital image of the beaded water droplet on different position of the stair-cased superhydrophobic MS (H) to show bulk superhydrophobicity. (I, J) Contact angle images of beaded water (I) and oil (J) droplet on native MS. (K, L) Contact angle images of beaded water droplet on surface (K) and bulk (L) of the superhydrophobic MS. (M) Digital image of a stream of water jet bounced back from the SMS surface. (N) Digital image of shinny interface of SMS dipped into DI water.

with selected alkylamine to attain essential low surface energy in the material. After the post-chemical modification of the residual acrylate moieties with octadecylamine (ODA), the IR peak intensity at 1410 cm^{-1} of C-H stretching of β-carbon of vinyl group significantly depleted with respect to the normalized carbonyl stretching frequency at 1735 cm^{-1}, which unambiguously indicated the successful post covalent modification of the material through a 1,4-conjugate addition reaction. The pristine MS, which is inherently hydrophilic (Figure 2.2 F, I), became extremely water repellent with advancing contact angle ~ 159^0 and contact angle hysteresis ~ 6^0 (Figure 2.2 K) after the immobilization of "reactive" polymeric nano-complexes followed by post chemical modification with ODA. As expected, the oil droplet beaded with contact angle 0^0 on the SMS as is shown in Figure 2.2 J. The contrasting wettability of water and oil on the modified MS appeared to be beneficial for the selective collection of oil from the oil/water mixture. The anti-wetting property was not limited only to the surface but was present all throughout the material. In this context, the SMS was arbitrarily cut into a staircase shape to expose the interiors of the material. The water droplets were placed at different freshly-exposed interior regions, and it was found that the water droplets beaded with a contact angle of 158^0 as shown in Figure 2.2 H, L. Thus, the covalently crosslinked polymeric network provided appropriate hierarchical (micro/nano) topography and the postmodification with ODA gave essential low surface energy coating both on the surface as well as in the bulk of the material. It is worth to mention here that the porosity of the coating is reduced from ~98 % to ~84 % on deposition of the polymeric nanocomplex. Moreover, the bouncing of a stream of water on the SMS surface revealed the existence of non-adhesive superhydrophobicity as shown in Figure 2.2 M. The heterogeneous wetting was arisen due to the presence of external meta-stable trapped air as an essential criterion to exhibit superhydrophobic property[48, 49] where the trapped metastable air layer ensures minimum contact between the surface and liquid droplet. When the SMS was submerged underwater, the surface of the material exhibited a shiny silver mirror-like appearance without any wetting by water (Figure 2.2 N). It is due to the presence of metastable trapped air layer indicating the existence of Cassie–Baxter state.

2.3.2 Physical and Chemical Durability Performance

Next, the as-synthesized SMS was exposed to various physical manipulations to examine its durability for potential competence in practical settings. Primarily, the SMS was subjected to an adhesive tape peeling test, wherein SMS was fixed onto a glass slide, and subsequently, the top surface was peeled off manually using a freshly exposed adhesive tape (Figure 2.3A). The exposed interior of the substrate continued to exhibit unperturbed water repellence with an advancing and receding contact angle of ~

158^0 and ~ 150^0 respectively as shown in Figure 2.3 B–D. In another severe abrasive test, the SMS was rubbed back and forth multiple (minimum 10 times) times on sandpaper under an applied load of

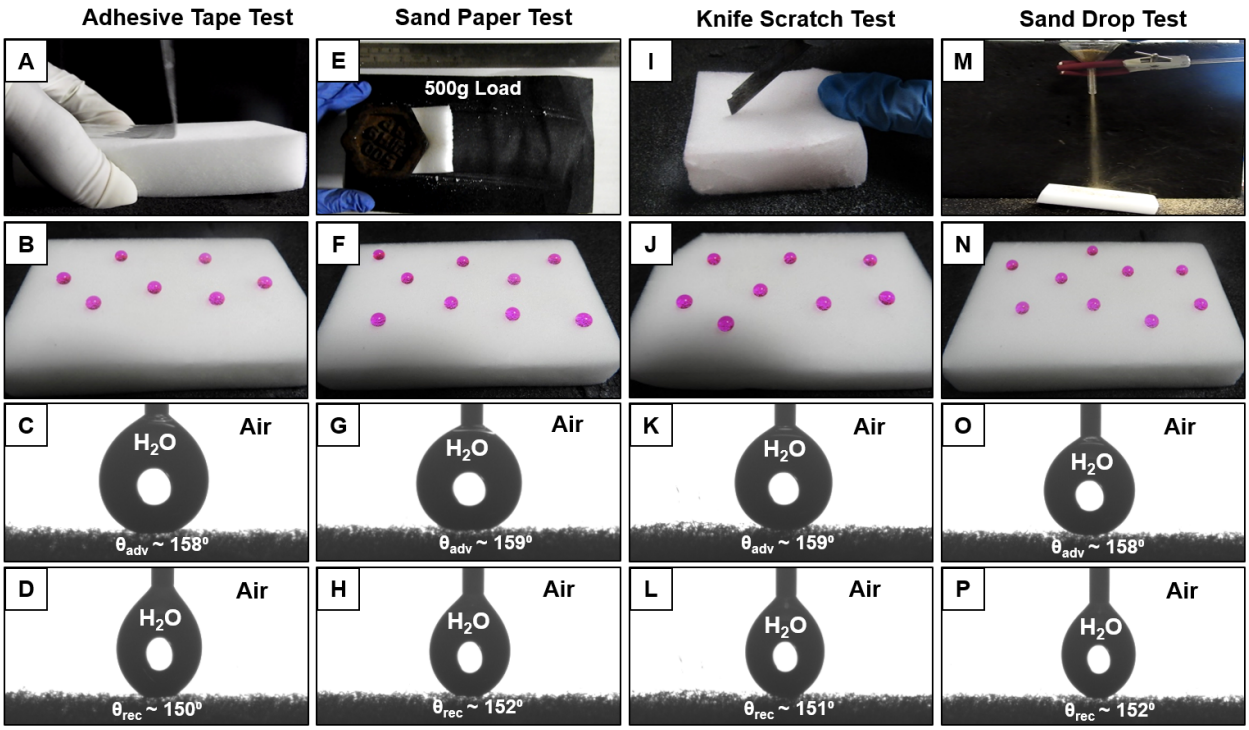

Figure 2.3. (A, E, I, M) Digital snapshot images for the process of adhesive tape test (A), sandpaper test (E), knife scratch test (I) and sand drop test (M). (B, F, J, N) Digital images of the beaded water droplets of the SMS after adhesive tape test (B) sandpaper test (F), knife scratch test (J) and sand drop test (N). (C, G, K, O) Advancing water contact angle of the SMS after incurring after adhesive tape test (C) sandpaper test (G), knife scratch test (K) and sand drop test (O). (D, H, L, P) Advancing water contact angle of the SMS after incurring after adhesive tape test (D) sandpaper test (H), knife scratch test (L) and sand drop test (P).

500g, as shown in Figure 2.3 E.

The digital image and contact angle measurement revealed that the embedded superhydrophobicity remained intact even after severe sandpaper abrasions for multiple times and the aqueous droplet beaded with an advancing contact angle of 159^0 as shown in Figure 3F, G. Furthermore, the SMS was deeply scratched with a sharp-edged knife over a large area (Figure 2.3 I). Interestingly, the physically damaged interface repelled the beaded aqueous droplet extremely with an advancing and receding contact angle of 159^0 and 151^0, respectively, as shown in Figure 2.3J–L. The sand drop test was carried out to investigate further another standard physical durability where 150 g of sand grains were poured onto the SMS from a height of 20 cm, however, the embedded anti-wetting property remained unperturbed with both advancing and receding contact angle above 150^0 and contact angle hysteresis below 10^0 as is noted in Figure 2.3N–P. Thus, the as-synthesized SMS retained its water-repellent property against various practically relevant physical abrasions. The mechanical robustness of superhydrophobic interfaces is an essential criterion for their utility in practical applications. In that

context, the cyclic compressive stress-strain curve behavior of SMS to maximum 60% strain was analyzed, as shown in Figure 2.4A. In the cyclic compressive test, the collapse of the porous network of SMS was not observed, and the SMS retained its mechanical strength as indicated by a slight change in the compressive stress even after 2000 cycles of compression. The SMS remained highly compressible without compromising the embedded anti-wetting property, even after applying repetitive (2000 times) high (80%) compressive strain as shown in Figure 2.4B, confirming its excellent mechanical robustness and durable anti-wetting property. This ability of high and repetitive deformation of SMS provided a facile basis for re-collection of the absorbed oil/oily phase by simple manual squeezing of the material illustrated in the following section. Moreover, the SMS synthesized following the facile 1,4-conjugate addition reaction was exposed to short (265 nm) and long (384 nm) wavelength UV radiation for 15 days continuously. The anti-wetting property of the SMS was examined at regular time intervals, and it was found the SMS displayed uninterrupted water repellence with advancing contact angle above 150^0 and contact angle hysteresis below 10^0 as shown in Figure 2.4C. Furthermore, the SMS was exposed to different practically relevant harsh aqueous chemical conditions, including extremes of pH (1 and 12) surfactant (SDS, DTAB; 1mM) contaminated water,

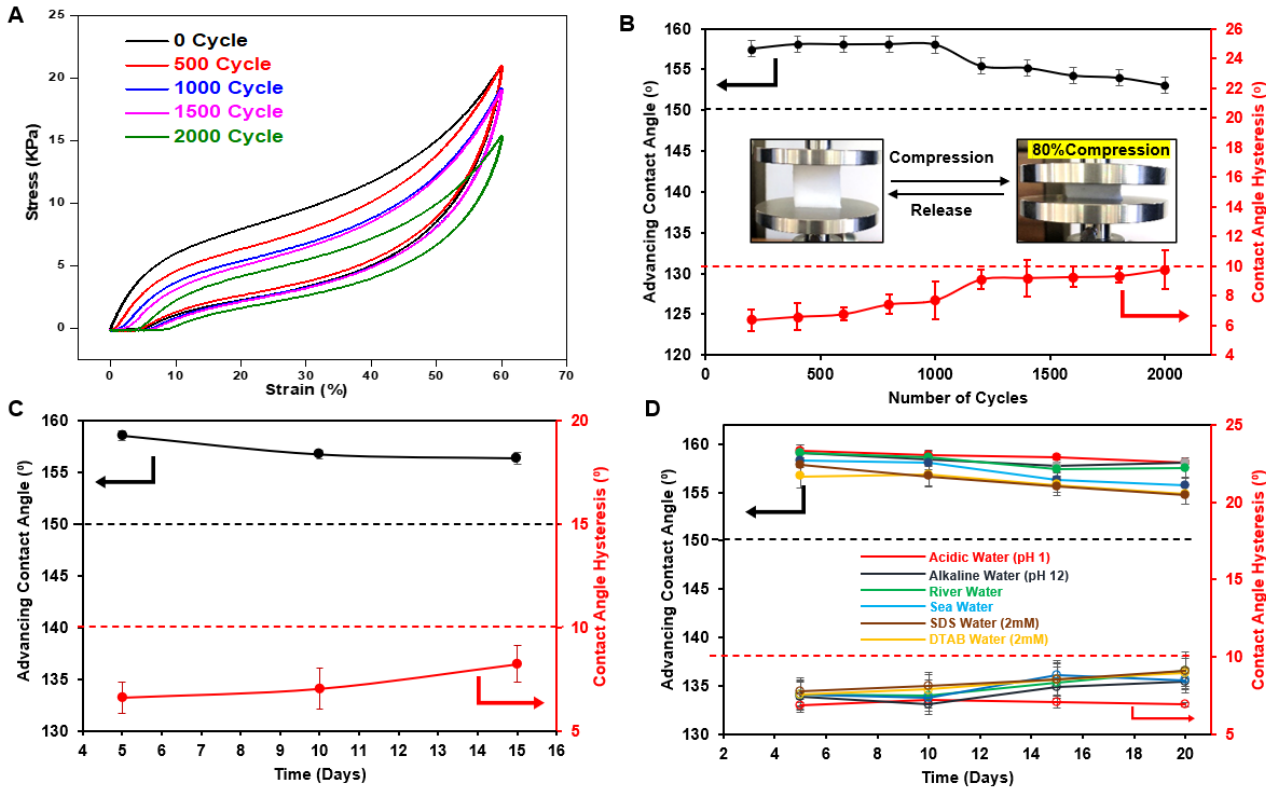

Figure 2.4. (A) A plot illustrating stress-strain curve up to 2000 cycles for SMS at 60% compression. (B) A plot describing minimal change of advancing and contact angle hysteresis up to 2000 cycle of mechanical compression at 80% deformation. (C) Plot showing effect on advancing and contact angel hysteresis after prolonged expouser to UV irradiation (C). (D) A plot accounting change in advancing and contact angle hysteresis after several various chemical abrasions.

artificial seawater, river (Brahmaputra Assam) water for 30 days. On examining the contact angles at regular intervals, it was found that the extreme water-repellent property of the SMS remained unperturb with an advancing contact angle above 150^0 and contact angle hysteresis below 10^0, as noted in Figure 2.4D. This impeccable physical and chemical durability can be attributed to the strategic use of facile and robust Michael addition reaction between amine and acrylate moieties at ambient conditions for optimizing both appropriate topography and essential low surface energy.

2.3.3 Separation of Oil from Oil/Water Mixture

The embedded extreme water repellence along with excellent mechanical and chemical durability of the SMS allowed to demonstrate selective absorption-based oil/water separation. The oil/water separation performance of both MS and SMS has been compared as shown in Figure 2.5 A-P. As a proof-of-concept demonstration, diesel having a density less than water was poured at the air/water interface. Subsequently, a piece of SMS was placed at the oil/water interface, and it was observed that the SMS selectively absorbed the oil phase without any traces of water, even after direct exposure to the aqueous phase as shown in Figure 2.5I–L. The absorbed oil was re-collected separately (Figure 2.5L) by simple manually squeezing process, in comparison to refluxing and burning process.[31, 32] However, when the uncoated MS was placed at the oil/water interface, it absorbed the water instantly and hence, remained inefficient to absorb the oil as shown in Figure 2.5A–D. Furthermore, the absorption-based separation principle was extended for model sediment oil, dichloromethane (DCM, model heavy oil). Subsequently, when the SMS was immersed underwater, it selectively absorbed only the oil phase as shown in Figure 2.5M–P. The absorbed oil was re-collected by manually squeezing the substrate without any traces of water (Figure 5P). Hence, the SMS efficiently and selectively separated the oil/oily phases from the water phase. The uncoated MS was completely wetted by water even before it came in contact with the oily layer underwater and hence, remained unable to remove any traces of oil present at the bottom of the water, as shown in Figure 2.5E–H. The presence of a three-dimensional porous network in SMS allowed it to absorb a large amount of oil from a oil/water mixture and displayed a high oil absorption capacity. The oil absorption capacity of SMS was calculated for various other oils, including chloroform, DCM, silicone oil, diesel, petrol as shown in Figure 2.6A. The absorption capacity was calculated according to the following equation

$$Q = (m_2-m_1)/m_1$$

Where m_1 and m_2 are the weight of MS before and after absorption of respective oil/oily phases. The maximum absorption capacity was measured to be 137 gg^{-1} for model heavy oil-chloroform, whereas

the absorption capacity was found to be above 70 gg^{-1} for different synthetic (silicon oil), refined (petrol, diesel) oils having a density less than water as shown in Figure 2.6A.

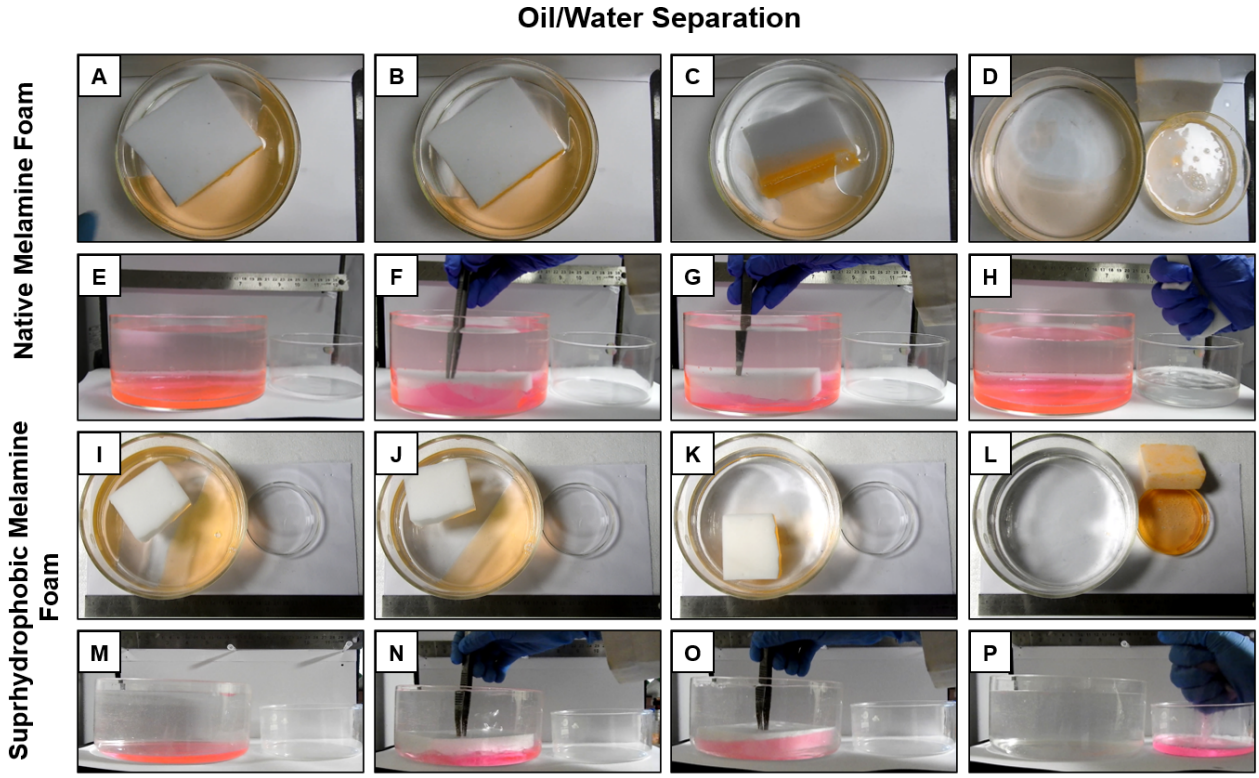

Figure 2.5. (A-H) Digital snapshot images of native MS during the process of separation of oil from oil/water mixture for both light oil (A-D) and heavy oil (E-H). (I-P) Snapshot photographs of superhydrophobic MS (SMS) for the process of separation and collection of oil from oil/water mixture for light oil (I-L) and heavy oil (M-P).

The prepared material can separate oil/oily phase irrespective of the change of surface tensions—provided that all the selected oil/oily phases are immiscible with aqueous phase. The oil absorption capacity of the as-synthesized SMS was found to be higher than the oil absorption capacities of most of the recently reported superhydrophobic carbon, cellulose, polyurethane sponges (Table 2.1).[50-61] Recyclability is an important parameter for the cost-effective utilization of SMS for practical applications as it reduces the operational cost for oil spill treatments. The oil absorption capacity of the SMS was calculated for 50 cycles using petrol and diesel. The oil absorption capacity remained consistent throughout 50 consecutive cycles, as shown in Figure 2.6B. Furthermore, the embedded water repellence of the SMS was examined after repetitive oil absorption/desorption cycles using diesel and petrol. Even after repeating this absorption/desorption cycles for 50 cycles, the embedded

superhydrophobicity remained unaltered with advancing contact angle above 150^0 and the contact angle hysteresis below 10^0. It revealed that the oil-absorbed SMS can also withstand 50 cycles of mechanical squeezing without compromising its lotus-leaf inspired non-adhesive antifouling property as shown in Figure 2.6C. Furthermore, the oil absorption capacity was calculated for diesel and petrol at different practically relevant harsh aqueous chemical scenarios including extremes of pH (1 and 12), surfactant (SDS, DTAB) contaminated water, artificial seawater, river (Brahmaputra, Assam India) water as shown in Figure 2.6D. The absorption capacity was found to be unaffected at different harsh

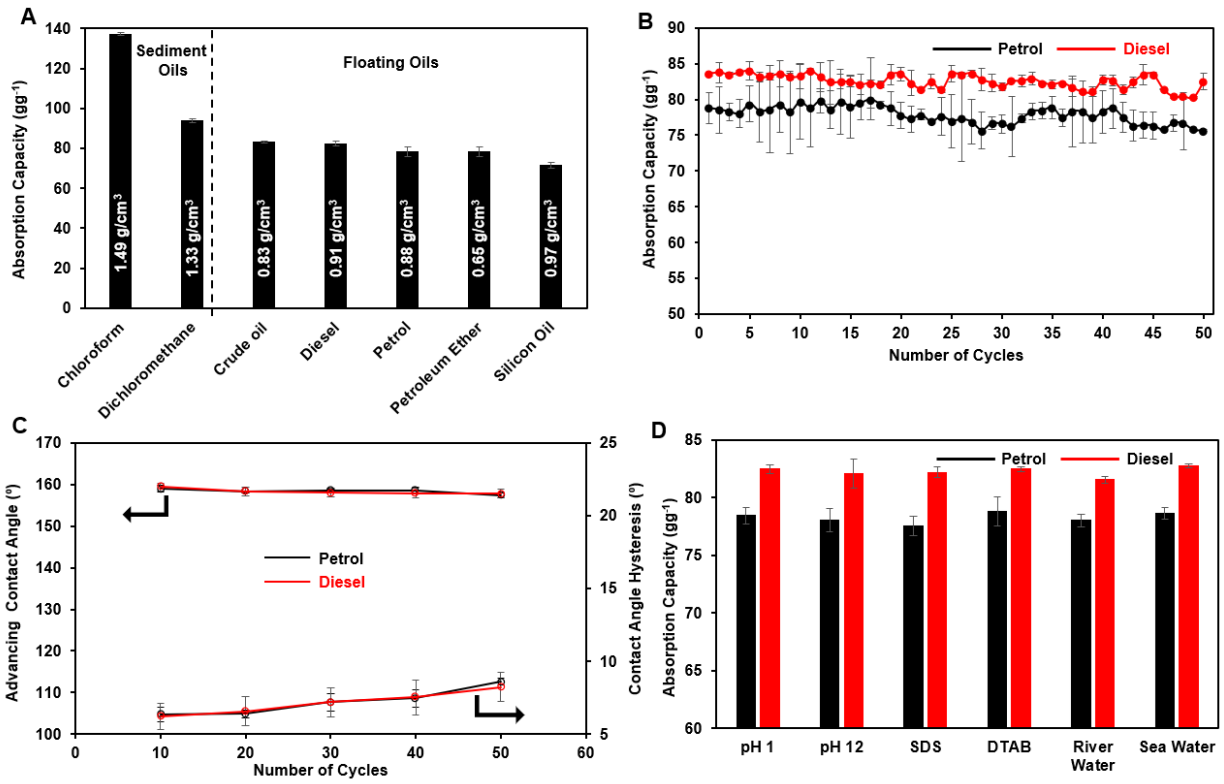

Figure 2.6. (A) A plot describing absorption capacity of superhydrophobic melamine for different water immiscible oily phases having different densities and viscosities. (B) A plot illustrating the trend in absorption capacity of the superhydrophobic MS for repetitive separation of petrol (black) and diesel (red) for 50 consecutive cycles. (C) A plot demonstrating the variation of advancing contact angle and contact angle hysteresis of the beaded water droplet of the SMS for 50 consecutive separation of petrol (black) and diesel (red). (D) Plot accounting absorption capacity of the SMS for petrol (black) and diesel (red) at several harsh aqueous media including acidic water (pH=1), basic water (pH=2), SDS and DTAB contaminated water, river water and artificial sea water.

settings (Figure 2.6D), likely due to the presence of durable superhydrophobicity in the as-synthesized SMS. Moreover, the performance of the synthesized SMS has been compared with earlier reported materials in the literature, as listed in Table 2.1. The prepared material displayed a high and selective oil-absorption capacity and remained efficient to perform at practically relevant challenging settings—including extremes of pH, artificial sea water, river water, surfactant contaminated water etc. In the

Sponge Type	Oil used	Absorption Capacity (gg^{-1})	Performance at Extreme Conditions*	Reference
PU–CNT–PDA–ODA	Soyabean Oil Silicon Oil	27 28	Performed	50
PU-Glue-TiO_2	N-Dodecane Methyl Oleate	6 4	Not Performed	51
SiO_2–PMMA–PU	Silicon Oil Hexane	23 18	Not Performed	52
EC-ECH-Si-CNTs	Soyabean Oil Hexane	40 30	Not Performed	53
Poly-Lactic Acid Foam	Silicon Oil Cyclohexane	25 13	Not Performed	54
MF-OTS-PNIPAAm	Hexane Pump Oil	30 40	Not Performed	55
MF-GO-Si NP-fCNT	Hexane Gasoline	45 40	Not Performed	56
MF/graphene/carbon black	Pump Oil Hexane	80 50	Not Performed	57
Fe-CNT	Gasoline Diesel	48 55	Not Performed	58
ZIF-8@rGO@Sponge	Silicon Oil Dibromomethane	24 32	Not Performed	59
Silylated Nanofibrillated Cellulose sponge	Silicon Oil Motor Oil	70 50	Not Performed	60
Co-MOFs/CF	Petroleum Ether N-Heptane	80 90	Not Performed	61
MS@CRPNC@ODA	Diesel Petrol	80 78	Performed	This Work

Table 1. Comparing the oil absorption capacity of superhydrophobic sponges and their performance of practically relavent diverse and severe conditions.

past, the performance of superhydrophobic materials at severe conditions have barely been demonstrated.

2.4 Conclusions

In conclusion, a facile and highly robust Michael addition reaction between amine and acrylate groups at ambient conditions was successfully extended in fabricating a physically/chemically durable

superhydrophobic melamine sponge (SMS). The deposition of chemically reactive nano-complex followed by post-covalent modification provided essential physical and chemical parameters to display extreme water repellence. The embedded superhydrophobic property in SMS remained intact even after exposure to various harsh physical, chemical abrasions and UV irradiation. The SMS was explored for successful oil/water separation of both light and heavy oils with high absorption capacity (e.g., 137 gg^{-1} for chloroform and 83 gg^{-1} for diesel). This oil/water separation was also demonstrated in different harsh conditions including extremes of pH, sea and river water, surfactant contaminated water. The selectively absorbed oil was collected back by adopting manual squeezing of the SMS. Moreover, the oil absorption capacity and the anti-wetting property remained intact after 50 absorption and desorption cycles. Therefore, the modified sponge might be a potential substitute over the existing ones for oil/water separation at the practical settings due to its ease in fabrication, involvement of robust covalent chemistry, and extreme physical and chemical durability of embedded superhydrophobicity.

2.5 References

1. Lahann, J.; *Nat. Nanotechnol.* **2008**, *3*, 320–321.
2. Schaum, J.; M. Cohen, Perry, S.; Artz, R.; Draxler, R.; Frithsen, J.B.; Heist, D.; Lorber, M.; Phillips, L. *Environ. Sci. Technol.* **2010**, *44*, 9383–9389.
3. Feng, C.; Yi, Z.; She, F.; Gao, W.; Peng, Z.; Garvey, C. J. *ACS Appl. Mater. Interfaces* **2016**, *8*, 9977–9985.
4. Kujawinski, E. B.; Kido Soule, M. C.; Valentine, D. C. L.; Boysen, A. K.; Longnecker, K.; Redmond, M. C. *Environ. Sci. Technol.* **2011**, *45*, 1298–1306.
5. Yao, X.; Song, Y.; Jiang, L. *Adv. Mater.* **2011**, *23*, 719–734.
6. Wang, S.; Liu, K.; Yao, X.; Jiang, L. *Chem. Rev.* **2015**, *115*, 8230–8293.
7. Feng, L.; Zhang, Z. Y.; Mai, Z. H.; Ma, Y. M.; Liu, B. Q.; Jiang, L.; Zhu, D. B. *Angew. Chem. Int. Ed*., **2004**, *43*, 2012.
8. Xue, Z. X.; Cao, Y. Z.; Liu, N.; Feng, L.; Jiang, L. *J. Mater. Chem. A* **2014**, *2*, 2445–2460.
9. Wang, B.; Liang, W.; Guo, Z.; Liu, W. *Chem. Soc. Rev.* **2015**, *44*, 336–361.
10. Yang, Y.; Tong, Z.; Ngai, T.; Wang, C. *ACS Appl. Mater. Interfaces* **2014**, *6*, 6351–6360.
11. Chen, S. L.; He, G. H.; Hu, H.; Jin, S. Q.; Zhou, Y.; He, Y.Y.; He, S. J.; Zhao, F.; Hou, H. Q. *Energy Environ. Sci.* **2013**, *6*, 2435–2439.
12. Sun, H. Y.; Xu, Z.; Gao, C. *Adv. Mater.* **2013**, *25*, 2554–2560.
13. Zhang, J.; Li, B.; Li, L.; Wang, A. *J. Mater. Chem. A* **2016**, *4*, 2069–2074.

14. Zheng, Q.; Cai, Z.; Gong, S. *J. Mater. Chem. A* **2014**, *2*, 3110–3118.
15. Korhonen, J. T.; Kettunen, M.; Ras, R. H. A.; Ikkala, O. *ACS Appl. Mater. Interfaces* **2011**, *3*, 1813–1816.
16. Song, X.; Lin, L.; Rong, M.; Wang, Y.; Xie, Z.; Chen, X. *Carbon* **2014**, *80*, 174–182.
17. Nguyen, D. D.; Tai, N. H.; Lee, S. B.; Kuo, W. S. *Energy Environ. Sci.* **2012**, *5*, 7908–7912.
18. Zhou, S.; Hao, G.; Zhou, X.; Jiang, W.; Wang, T.; Zhang, N.; Yu, L. *Chem. Eng. J.* **2016**, *302*, 155–162.
19. Gui, X. C.; Zeng, Z. P.; Lin, Z. Q.; Gan, Q. M.; Xiang, R.; Zhu, Y.; Cao, A. Y.; Tang, Z. K. *ACS Appl. Mater. Interfaces* **2013**, *5*, 5845–5850.
20. Dong, X. C.; Chen, J.; Ma, Y. W.; Wang, J.; Chan-Park, M. B.; Liu, X. M.; Wang, L. H. W.; Huang, P. Chen, *Chem. Commun.* **2012**, *48*, 10660–10662.
21. Zhu, Q.; Chu, Y.; Wang, Z.; Chen, N.; Lin, L.; Liu, F.; Pan, Q. *J. Mater. Chem. A* **2013**, *1*, 5386–5393.
22. Pham, V. H.; Dickerson, J. H. *ACS Appl. Mater. Interfaces* **2014**, *6*, 14181 –14188.
23. Li, J.; Yan, L.; Tang, X.; Feng, H.; Hu, D.; Zha. F. *Adv. Mater. Interfaces* **2016**, *3*, 1500770.
24. Zhang, J.; Seeger, S. *Adv. Funct. Mater*. **2011**, *21*, 4699–4704.
25. Wang, Z.; Wang, Y.; Liu, G. *Angew. Chem. Int. Ed.* **2016**, *55*, 1291–1294.
26. Mo, X.; Wu, Y.; Zhang, J.; Hang, T.; Li, M. *Langmuir* **2015**, *31*, 10850–10858.
27. Osicka, J.; Il˘cikov, M.; Popelka, A.; Filip, J.; Bertok, T.; Tkac, J.; Kasak, P. *Langmuir* **2016**, *32*, 5491–5495.
28. Wang, B.; Guo, Z. *Chem. Commun.* **2013**, *49*, 9416–9418.
29. Zhou, C.; Chen, Z.; Yang, H.; Hou, K.; Zeng, X.; Zheng, Y.; Cheng, J. *ACS Appl. Mater. Interfaces* **2017**, *9*, 9184–9194.
30. Han, Z.; Li, B.; Mu, Z.; Niu, S.; Zhang, J.; Ren, L. *Small* **2017**, *13*, 1701121–32.
31. Vibhute, A. M.; Muvvala, V.; Sureshan, K. M. *Angew. Chem. Int. Ed.* **2016**, *55*, 7782–7785.
32. Liang, H. –W.; Guan, Q. –F.; Chen, L. -F.; Zhu, Z.; Zhang, W. –J.; Yu, S. –H. *Angew. Chem. Int. Ed.* **2012**, *51*, 5101–5105.
33. Chen, C.; Zhu, X.; Chen, B.; *Environ. Sci. Technol.* **2019**, *53*, 1509−1517.
34. Ji, C.; Zhang, K.; Li, L.; Chen, X.; Hu, J.; Yan, D.; Xiao, G.; He, X. *J. Mater. Chem. A* **2017**, *5*, 11263–11270.
35. Ge, J.; Wang, F.; Yin, X.; Yu, J.; Ding, B. *ACS Appl. Mater. Interfaces* **2018**, *10*, 40274−40285.
36. Wang, C. –F.; Chen, L. –T. *Langmuir* **2017**, *33*, 1969−1973.
37. Yang, Y.; Yi, H.; Wang, C. *ACS Sustainable Chem. Eng.* **2015**, *3*, 3012−3018.

38. Lia, Z. –T.; Wua, H. –T.; Chena, W. –Y.; Hea, F. –A.; Lib, D. –H. *Separa. Purific. Techno.* **2019**, *212*, 40-50.
39. Li, J.; Chen, Y.; Gao, J.; Zuo, Z.; Li, Y.; Liu, H.; Li, Y. *ACS Appl. Mater. Interfaces* **2019**, *11*, 2591−2598.
40. Mi, H. -Y.; Jing, X.; Huang, H. –X.; Turng, L. –S. *ACS Appl. Mater. Interfaces* **2017**, *9*, 37529−37535.
41. Rather, A. M.; Manna, U. *Chem. Mater.* **2016**, *28*, 8689–8699.
42. Yang, J.; Wang, H.; Tao, Z.; Liu, X.; Wang, Z.; Yue, R.; Cui, Z. *Chem. Eng. J.* **2019**, *359*, 149-158.
43. Das, A.; Parbat, D.; Shome, A.; Manna, U. *ACS Sustainable Chem. Eng*. **2019**, *7*, 11350-11359.
44. Rather, A. M.; Mahato, S.; Maji, K.; Gogoi, N.; Manna, U. *Nanoscale* **2017**, *9*, 16154–16165.
45. Farrer, R. A.; LaFratta, C. N.; Li, L.; Praino, J.; Naughton, M. J.; Saleh, B. E. A.; Teich, M. C.; Fourkas, J. T. *J. Am. Chem. Soc.* **2006**, *128*, 1796–1797.
46. Weatherspoon, M. R.; Dickerson, M. B.; Wang, G.; Cai, Y.; Shian, S.; Jones, S. C.; Marder, S. R.; Sandhage, K. H. *Angew. Chem. Int. Ed.* **2007**, *46*, 5724–5727.
47. Bechler, S. L.; Lynn, D. M. *Biomacromolecules* **2012**, *13*, 15231532.
48. Sun, T. L.; Feng, L.; Gao, X. F.; L. Jiang, *Acc. Chem. Res.* **2005**, *38*, 644.
49. Feng, L.; Li, S. H.; Li, Y. S.; Li, H. J.; Zhang, L. J.; Zhai, J.; Song, Y. L.; Liu, B. Q.; Jiang, L.; Zhu, D. B. *Adv. Mater.* **2002**, *14*, 1857.
50. Wang, H.; Wang, E.; Liu, Z.; Gao, D.; Yuan, R.; Suna, L.; Zhua, Y. *J. Mater. Chem. A* **2015**, *3*, 266–273.
51. Wang, Y.; Zhu, Y.; Yang, C.; Liu, J.; Jiang, W.; Liang, B. *ACS Appl. Mater. Interfaces* **2018**, *10*, 24149−24156.
52. Zhang, J.; Meng, Z.; Liu, J.; Schlaich, C.; Yu, Z.; Deng, X. *J. Mater. Chem. A* **2017**, *5*, 16369–16375.
53. Lu.; Y, Yuan, W. *ACS Appl. Mater. Interfaces* **2017**, *9*, 29167−29176.
54. Wang, X.; Pan, Y.; Liu, X.; Liu, H.; Li, N.; Liu, C.; Schubert, D. W.; Shen, C. *ACS Appl. Mater. Interfaces* **2019,** *11*,14362-14367.
55. Lei, Z.; Zhang, G.; Deng, Y.; Wang, C. *ACS Appl. Mater. Interfaces* **2017**, *9*, 8967−8974.
56. Mi, H. –Y.; Jing, X.; Huang, H. –X.; Turng, L.-S. *ACS Appl. Mater. Interfaces* **2017**, 9, 37529−37535.
57. Ji, C.; Zhang, K.; Li, L.; Chen, X.; Hu, J.; Yan, D.; Xiao, G.; He, X. *J. Mater. Chem. A* **2017**, 5, 11263–11270.

58. Gui, X.; Zeng, Z.; Lin, Z.; Gan, Q.; Xiang, R.; Zhu, Y.; Cao, A.; Tang, Z.; *ACS Appl. Mater. Interfaces* **2013**, *5*, 5845−5850.
59. Gu, J.; Fan, H.; Li, C.; Caro, J.; Meng, H. *Angew. Chem. Int. Ed.* **2019**, *58*, 5297–5301.
60. Zhang, Z.; Sèbe, G.; Rentsch, D.; Zimmermann, T.; Tingaut, P. *Chem. Mater.* **2014**, *26*, 2659−2668.
61. Ge, X.; Qin, W.; Zhang, H.; Wang, G.; Zhang, Y.; Yu, C. *Nanoscale* **2019**, *11*, 12161–12168.

Title: Chemically Reactive Spray Coating for Achieving Durable and Bulk Superhydrophobicity*

The chemically-reactive porous polymeric coatings for designing various durable and smart materials through a robust covalent chemistry is challenging to achieve. In chapter 3, the chemically reactive polymeric nanocomplexes (CRPNC) with tailored sizes were synthesized in alcoholic solvents through a catalyst-free, 1,4-conjugate addition reaction, that was strategically exploited in developing a hierarchically featured and chemically reactive thick (254 ± 10 μm) polymeric coating for manipulating a special bio-inspired wettability- superhydrophobicity, three-dimensionally. The amine-reactive residual acrylate moieties in the porous polymeric thick coating provided a facile chemical avenue for modulating the essential chemistry and eventually yielded bulk polymeric coatings with chemically adjusted Cassie–Baxter and Cassie–Wenzel transitional states through controlled optimization of the metastable trapped air level in the bulk polymeric coating. The fraction of contact area between a beaded water droplet and trapped air in the polymeric coating was tailored from 0 to above 0.9 by varying the carbon chain length of the selected alkylamine. Thus, the same 'reactive' polymeric interface was capable of displaying both highly non-adhesive and controlled-adhesive superhydrophobicity. The biomimicked wettability remained unperturbed even after being subjected to severe physical and chemical exposures, including physical abrasion of material, prolonged (30 days) exposure to UV radiation, etc. This simple design was capable of coating a wide range of substrates, irrespective of their chemical compositions, geometries, and dimensions. Even some practically relevant flexible and complex objects, such as printing paper (A4 size) and shoes, were decorated with durable superhydrophobicity as an early demonstration for protecting handwritten and printed text from aqueous exposure and self-cleaning of dust-contaminated interfaces. This bulk optimization of essential chemistry could be useful in synthesizing various other smart materials for many relevant outdoor applications.

*Maji, K.; Manna, U. *J. Mater. Chem. A* **2018,** *6*, 6642-6653.

3.1 Introduction

Often, different and relevant physical properties of materials are controlled through appropriate optimization of physical and chemical parameters. In the past, the post-chemical manipulation of thin and featureless 'reactive' polymeric interfaces has been exploited in the synthesis of several functional materials.[1–6] However, the approach of controlled tailoring of various chemical functionalities three-dimensionally (including the top surface and interior) in hierarchically featured and thick polymeric coatings is rare in the literature and would be useful in the synthesis of various other smart and durable materials for diverse applications in practically relevant scenarios. In this context, the synthesis of artificial bio-inspired interfaces is highly relevant, where the biomimicking interfaces are generally developed by the appropriate integration of essential chemistry and hierarchical surface topography.[7–12] For example, several top-down and bottom-up approaches have been adopted[7–12] to achieve a classical and prospective bio-inspired wettability—commonly referred to as superhydrophobicity—which is well recognized for its wide range of prospective applications.[11–18] Such interfaces are mostly achieved by optimization the required surface chemistry (e.g., inert coating) at the top of the essential hierarchical topography.[7–12] In common practice, these chemical optimizations are mainly maintained over a few nanometers across the thickness of the coating, and can even be achieved by including some delicate chemistries (e.g. hydrogen bonding, electrostatic interaction, metal–thiol bonds, modifications with various analogues of silane, etc.),[7,8,11,12,19–22] which are susceptible to severe chemical/physical exposures, meaning that the embedded special wettability in the thin organic/ inorganic coatings is inherently inappropriate to tolerate the practically relevant harsh conditions.[23,24] To combat this poor durability aspect of artificial biomimicking wettability, some interesting and sophisticated designs have recently been introduced, including self-healing, post-repairing, and mechanically durable coatings.[25–31] Such designs are certainly capable of providing more stable wettability compared to the conventionally synthesized superhydrophobic materials; however, in most of the cases, the essential chemical optimization at the top of the appropriately decorated hierarchical topography remains restricted over a few nanometers across the thickness of such special biomimicking designs.[25–31] Thus, the severe physical damage (e.g., scratching) that altered the chemistry and topography at the top surface of the thin conventional coatings is likely to cause permanent damage to the embedded wettability. As a consequence, most of these synthesized materials remained inappropriate for outdoor applications in practically relevant complex scenarios.[23,24] In 2009, Fréchet and co-workers introduced a seminal report on a bulk superhydrophobic coating, which was found to be fundamentally different from other synthetic designs. This coating approach possessed both the optimum chemistry and the essential topography throughout the bulk of the material, including the top interface.[32] As a

consequence, such unique designs remained inherently durable and capable of withstanding various types of severe damage, including the removal of the top portion of the coating.[32–35] However, the demonstrations of such bulk superhydrophobicity are rare in the literature and most of them were synthesized using either a sophisticated instrumental setup or complex and tedious processes.[32–35] Thus, most of the reported bulk superhydrophobic coatings remained inappropriate for practical utility. So, further development on the synthesis procedures for the substrate independent (irrespective of shape, size, and chemical composition) durable and thick superhydrophobic bulk coatings through a facile and scalable approach is extremely important for materializing several prospective and smart applications of artificial biomimicking interfaces in practically relevant real-world scenarios. In chapter 3, a three-dimensionally 'chemically reactive' and porous polymeric coating has been introduced through the covalent and three-dimensional modulation of essential and desired chemistries in the porous polymeric coating for addressing various practically relevant durability issues. Furthermore, this design would be useful in achieving controlled adhesive superhydrophobicity, chemically patterned robust interfaces, etc. In this current demonstration, a catalyst-free, rapid, and mutual reactivity between amine and acrylate groups from branched poly(ethyleneimine) (BPEI) and dipentaerythritol penta acrylate (5Acl), respectively, was strategically applied in synthesizing a three-dimensionally chemically reactive, scalable and porous polymeric coating, where the prepared reaction mixture was spray deposited on various selected substrates. The choice of reaction medium played a crucial role in developing stable and porous polymeric coating. The synthesized porous and covalently cross-linked polymeric coating possessed 'chemically reactive" residual acrylate functionality three-dimensionally, including the surface and interior of the coating, and it was eventually possible to optimize the desired chemistry in the entire polymeric coating through a simple 1,4-conjugate addition reaction under ambient conditions. After appropriate and covalent chemical modification, the porous and covalently cross-linked polymeric coating exhibited bulk superhydrophobicity, which remained unaltered even after different types of physical abrasion and severe chemical exposure. Moreover, simple and covalent optimization of the appropriate chemistries in the porous polymeric coating conferred various other interesting special wettability through optimum and controlled tailoring of the fraction of contact area between the beaded water droplet and metastable trapped air in the polymeric bulk coating. A diverse set of substrates (concrete, wood, plastic, metal, glass, cellulose, etc.), irrespective of their shape, size, and texture, were successfully coated with such highly robust bulk-superhydrophobicity, and this substrate independent, robust coating approach would be useful in several practically relevant applications. A model flexible and large object, e.g., printer paper (A4 size), was coated with such bulk-superhydrophobicity, and exposed to various common physical

manipulations, and the coated paper was used in printing text using a regular printer machine; however, the embedded antifouling property was observed to be unperturbed. Furthermore, this facile and scalable spray coating approach was extended to coat a geometrically complex substrate, namely a shoe. This practically relevant substrate, which often gets dirty in real-world scenarios, was used to demonstrate the self-cleaning performance, without wetting the interface.

3.2 Experimental Section

3.2.1 Materials

Branched poly(ethyleneimine) (BPEI, MW ~ 25,000 Da), dipentaerythritol penta/hexa acrylate (5Acl, MW = 524.21 g mol^{-1}), octadecylamine (97%), dodecylamine (98%), decylamine (95%), octylamine (99%), heptylamine (99%), hexylamine (99%), and pentylamine (95%) were purchased from Sigma-Aldrich, Bangalore, India. Pentanol, butanol and propanol were procured from Alfa Aesar. Ethanol was purchased from TEDIA, USA. A-4 sized printing paper was acquired from J K Copier. Shoes (Ajanta, India, Model-8) were procured from a local store in Guwahati, India. Spray bottles (100 mL capacity, nozzle diameter ~ 400 µm) were obtained from Amazon India. Sandpaper (grit no. 400) was purchased from Million International, India. Glass slides (Boroleb, India), aluminum foil (Parekh Aluminex Ltd. India), and adhesive tape (Jonson tape Ltd. India) were acquired from different sources. Concrete, a wooden block, and sand were collected from a construction site at IIT Guwahati. Before experimental use, the sand was washed thoroughly using water.

3.2.2 General Considerations

Prior to the experiments, the glass slides (Model Substrate) were washed thoroughly using ethanol. The Fourier Transform Infrared Spectroscopy (FTIR) spectra were collected using a PerkinElmer instrument, using standard KBr pellets. The contact angles and roll-off angles of beaded water droplets on the materials were measured using a KRUSS Drop Shape Analyser-DSA25 instrument at ambient temperature. The dynamic contact angles were measured using 4 mL deionized water (DI water) droplet in four different locations for each polymeric coated sample. Field Emission Scanning electron microscope (FESEM) images were obtained using Sigma Carl Zeiss scanning electron microscope (each sample was coated with a conducting gold layer prior to imaging). Digital images were taken using a Canon Power Shot SX420 IS digital camera. The thickness of the coatings was measured using a Veeco Dektak 150 surface profilometer.

3.2.3 Fabrication of 'Reactive' Porous Polymeric Coating

The amine-reactive porous polymeric coatings were prepared by spray deposition of chemically reactive polymeric nanocomplexes (CRPNC) onto selected substrates (e.g., glass, wood, concrete, metal, shoe, plastic, cellulose paper, etc.). First, a reaction mixture was prepared in pentanol by mixing

10 mL of dipentaerythritol penta/hexa acrylate (5Acl) (1.325 g/10 mL) and 3 mL of Branched poly(ethyleneimine) (BPEI) (0.5 g/10 mL) in a spraying bottle and shaking vigorously for 5 minutes. Then, the turbid reaction mixture (13 mL) was sprayed uniformly onto the selected substrates over a 180 cm^2 area from a 15 cm distance. After the deposition of the reaction solution, the coated substrates were kept in the open air for solvent evaporation. A similar process was adopted for the spray coating of the same reaction mixtures that were prepared in lower analogs of pentanol. The effect of this solvent was found to be significant on the polymeric coating.

3.2.4 Post Functionalization with Amine-Containing Small Molecules

The polymeric spray coatings prepared using pentanol as reaction medium, were post functionalized with various amine-containing small molecules (octadecylamine, 2.5 mg mL^{-1}; dodecylamine, 2.5 mg mL^{-1}; decylamine, 0.2 mL mL^{-1}; octylamine, 0.2 mL mL^{-1}; heptylamine, 0.2 mL mL^{-1}; hexylamine, 0.2 mL mL^{-1}; pentylamine, 0.2 mL mL^{-1}). In general, the respective amount of alkylamine dissolved in ethanol and then the reactive coating were immersed in the solutions separately for 12 hours at ambient conditions.[36] After the post-chemical modification, the coated substrates were thoroughly washed with ethanol to remove the excess amount of the alkylamines, and the coated modified substrates were kept in the open air for drying.

3.2.5 Calculation of Fraction of Air/Liquid and Solid/Liquid Interfaces

According to the Cassie–Baxter model, the beaded water droplet on a superhydrophobic surface is in contact with both the metastable trapped air and the solid surface (in this case, solid polymeric coating). The area fraction of the air/water and solid/water interfaces can be estimated using equations (1) and (2). First, a featureless, smooth polymeric coating (10 bilayers, 40 nm thickness) was constructed by layer-by-layer deposition of branched poly(ethyleneimine) (BPEI) and dipentaerythritol penta/hexa acrylate (5Acl) following a procedure described in a previous report.[36] Then, the water contact angle (WCA; static) was measured on these featureless smooth coatings after post-modification with pentylamine (66^0), hexylamine (69^0), heptylamine (74^0), octylamine (76^0), decylamine (79^0), doceylamine (81^0) and octadecylamine (81^0). The same basic components (i.e., BPEI, 5Acl, and appropriate primary amine-containing small molecules) were used in developing the featureless smooth polymeric coating (LbL deposition) and porous polymeric coating (spray deposition). With reference to this WCA on both the smooth interfaces and porous polymeric coatings, the fraction of air/water and solid/water interfaces was estimated and represented in Fig. 3.4.

3.2.6 Physical and Chemical Durability of the Polymeric Coating

3.2.6.1 Sand Paper Abrasion Test

The polymeric coating on a glass substrate was abraded using 400 grit sandpaper under a 200 g applied load. First, the sandpaper (3 cm × 2 cm) was fixed on a glass slide with double-sided adhesive tape. Then, the polymeric coating (6 cm × 2.5 cm) was brought in contact with the abrasive sandpaper substrate with an applied load of 200 g, prior to rubbing the sandpaper manually across the coated substrate ten times back and forth. The superhydrophobic property was examined with visual inspection and contact angle measurements after performing the abrasive sandpaper test.

3.2.6.2 Sand drop Test

A 200 g of sand grains was poured from a height of 20 cm using a glass funnel onto the appropriately post-modified polymeric spray coating (6 cm × 2.5 cm), which was tilted at an angle of 45^0. After this treatment, the anti-wetting property was assessed by advancing contact angle measurements and visual inspection.

3.2.6.3 Scratch Test

The polymeric coating on a glass substrate was scratched manually using a sharp knife. Then, the water wettability was examined with visual inspection and contact angle measurements.

3.2.6.3 Adhesive Tape Test

The random fracture of the polymeric coating was induced with double-sided adhesive tape. The adhesive surface (2.5 cm × 1.5 cm) was first brought into contact with the polymeric coating (6 cm × 2.5 cm), and a 500 g load was applied for 5 min to improve the contact between the adhesive surface and the polymeric coating. Then, the adhesive tape was peeled off from the polymeric coating. During this tape removal process, some portion of the polymeric coating was transferred to the adhesive surface.

3.2.6.4 Chemical Durability

The coated glass substrates were submerged in different harsh aqueous media, including artificial seawater, river water, acidic water (pH = 1), and alkaline water (pH = 13) for 100 h. Then, the anti-wetting property was examined with contact angle measurements. Two identical polymeric coatings were also kept under UV irradiation with λ_{max} at 254 nm and 365 nm respectively for 30 days continuously, and after every 5 days, the water contact angle was measured to monitor the change in water wettability.

3.2.7 Self-Cleaning Performance

The self-cleaning of deposited dust and dirt on a coated shoe and printer (A-4) paper was performed by placing the dusty surface under a stream of water. Both the shoe and printer paper was cleaned immediately, without wetting the substrates, as the rolling water droplets collected all the dust from the contaminated interfaces.

3.2.8 Printing and Writing on Superhydrophobic Paper

The appropriately post-modified spray-coated printer paper (A-4 size) was processed with a commercial HP LaserJet (M1136 MFP) printing machine to print carbon ink. In another proof-of-concept demonstration, manual writing was performed on the coated paper with a fountain pen. During this writing process, some superficial damage was noticed. However, the artificial biomimicking interface protects the ink of the manually written text from spilling and spreading under exposure to water.

3.3 Results and Discussions

3.3.1 Synthesis of a Three-Dimensionally Chemically 'Reactive' and Porous Polymeric Coating

The spray deposition approach is unique for its ample simplicity and inherent ability to coat complex and large objects without a sophisticated instrumental setup. In the past, both spray-deposition-based organic and inorganic thin coatings have been introduced to synthesize biomimicking wettability.[36–41] In the earlier designs, chemically inert (referring to the inability of any catalyst-free covalent reaction under ambient conditions) nanomaterials were mainly spray-deposited to develop the essential topography, and the deposited nanomaterials were integrated following additional physical and chemical curing processes.[37–40] Such common spray depositions of chemically inert nanomaterials were useful in developing non-adhesive superhydrophobicity, but any further chemical modification

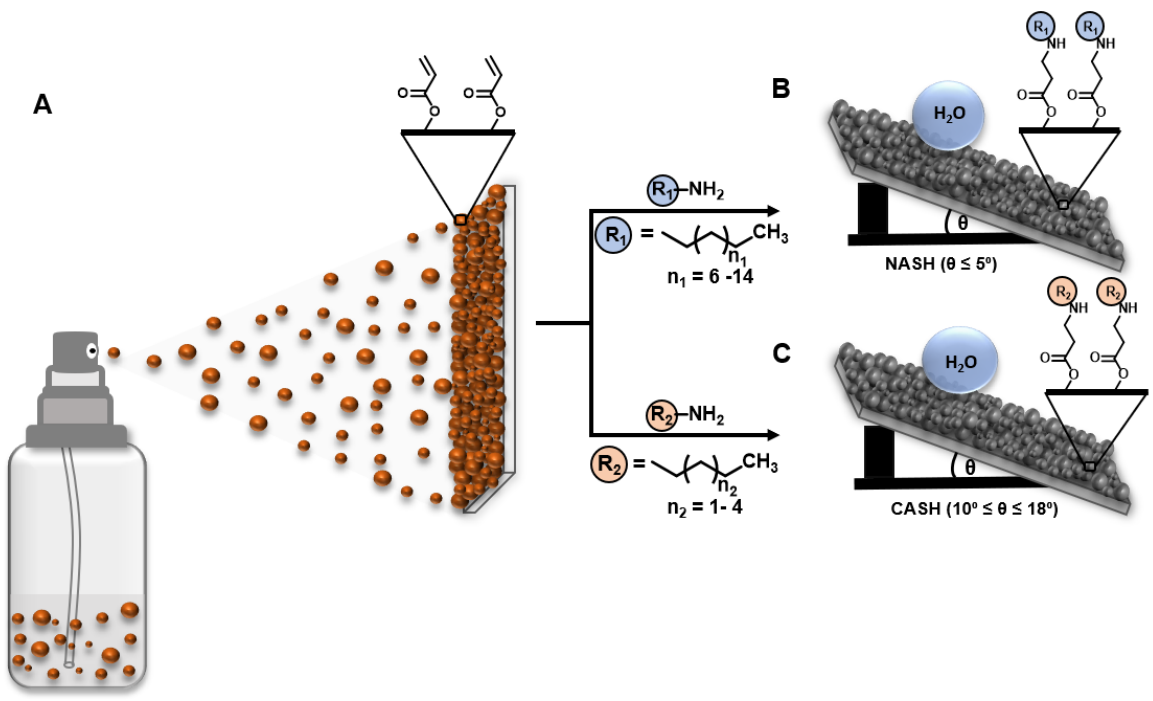

Figure 3.1. (A) Schematic representation of spray-deposition of chemically reactive polymeric nanocomplexes (CRPNCs) on a flat surface. (B, C) Illustrating the polymeric coating that displayed non-adhesive superhydrophobicity (NASH; B) and controlled adhesive superhydrophobicity (CASH; C) after appropriate post covalent modifications.

was restricted, and eventually, such approaches appeared to be inherently incapable of fabricating other important biomimicking interfaces.[37–41] Although some of those spray coatings were highly selective to certain substrates,[38,39] few mechanically durable and substrate independent thin surface coatings have been introduced through a multistep layer-by-layer (LbL) spray deposition process.[36,41] In this chapter, an unprecedented attempt to synthesize a 'chemically reactive' porous spray coating has been introduced with the strategic association of (1) catalyst-free & facile chemistry (i.e., 1,4-conjugate addition reaction) and (2) an inherently simple & scalable spray deposition process. Furthermore, the controlled and three-dimensional manipulation of this 'reactive' bulk coating with various chemical functionalities was achieved through the robust 1,4 conjugate addition reactions. In the recent past, the synthesis of functional nanostructures with desired shapes and sizes has emerged as an important tool for manipulating various relevant properties.[42,43] Chemically reactive polymeric nanocomplexes (CRPNC) have been introduced through the 1,4-conjugate addition reaction between branched poly(ethyleneimine) (BPEI) and dipentaerythritol penta-acrylate (5Acl) in an ethanolic solvent. [44] Earlier, these functional and 'reactive' nanocomplexes were strategically immobilized on a fibrous substrate or sponges for efficient oil/water separation and sustained release of loaded small molecules.[44,45] In the last chapter, I have adopted a strategy of in-situ dilutions of the reaction mixture for achieving stable dispersion of CRPNC. Such diluted and stable dispersion allowed to develop chemically reactive coating on spongy and porous substrates without compromising the mechanical property of the selected substrates. In contrast to the earlier approach, in this chapter, I have adopted a simple strategy to accelerate the sol-gel conversion process of the reaction mixture to achieve stable and uniform porous polymeric coating on flat substrates. Interestingly, the growth of the chemically reactive polymeric nanocomplex in the same reaction mixture was tailored by selecting the appropriate alcoholic solvent as a reaction medium (Fig. 3.2 A-D). The growth of the polymeric nanocomplexes was observed to be significantly faster in higher analogues of ethanol, as confirmed by digital snapshot images as well as dynamic light scattering (DLS) study (Fig. 3.2 E), even though the compositions of the BPEI/5Acl mixtures were kept identical in all of the alcoholic solvents. Here, in this present study, similar reaction mixtures (BPEI/5Acl) that contained chemically reactive polymeric nanocomplexes (CRPNC) were first prepared in various alcoholic solvents, prior to spray-deposition on a glass substrate. In the end, a stable, covalently cross-linked, porous, and chemically reactive polymeric coating was achieved, without involving any calcination or additional curing process. The transparent reaction mixture of BPEI/5Acl in pentanol became highly turbid within 5 minutes (Fig. 3.2 D) due to the formation of the polymeric nanocomplexes, and the average size of the nanocomplexes was estimated to be 429 ± 15 nm, whereas faint turbidity/no turbidity appeared for a similar reaction

mixture in lower analogues of pentanol within the same time interval (Fig. 3.2 A-D). This mixture of BPEI/5Acl in pentanol eventually formed a gel material after 15 minutes, whereas this gelation of the BPEI/5Acl mixture was slower in lower analogues of pentanol as evident from Fig. 3.2 A-D. Moreover, the residual chemical functionality in the CRPNCs was investigated by FTIR analysis, which is used as a standard tool to characterize the acrylate functionality in organic materials.[45,46] The polymeric nanocomplexes possessed acrylate moieties as confirmed from the FTIR signature at 1410 cm^{-1}, which corresponds to the symmetric stretching of the C–H bond of the β carbon of the vinyl group, and the IR peak at 1732 cm^{-1} revealed the presence of ester carbonyl stretching as shown in Fig. 3.2 F. These residual acrylate functional groups in the polymeric nanocomplexes were examined to be chemically reactive and were capable of mutually reacting with primary amine group-containing small molecules (i.e., propylamine, butylamine, amyl amine, hexylamine, heptylamine, octylamine, decylamine, dodecylamine, and octadecylamine) irrespective of their hydrocarbon tail length. The IR peak intensity at 1410 cm^{-1} was significantly reduced with respect to carbonyl stretching at 1732 cm^{-1} after the reaction of the CRPNCs with ODA molecules, as shown in Fig. 3.2 F. The carbonyl groups are expected to be unperturbed during the 1,4-conjugate addition reaction under ambient conditions.

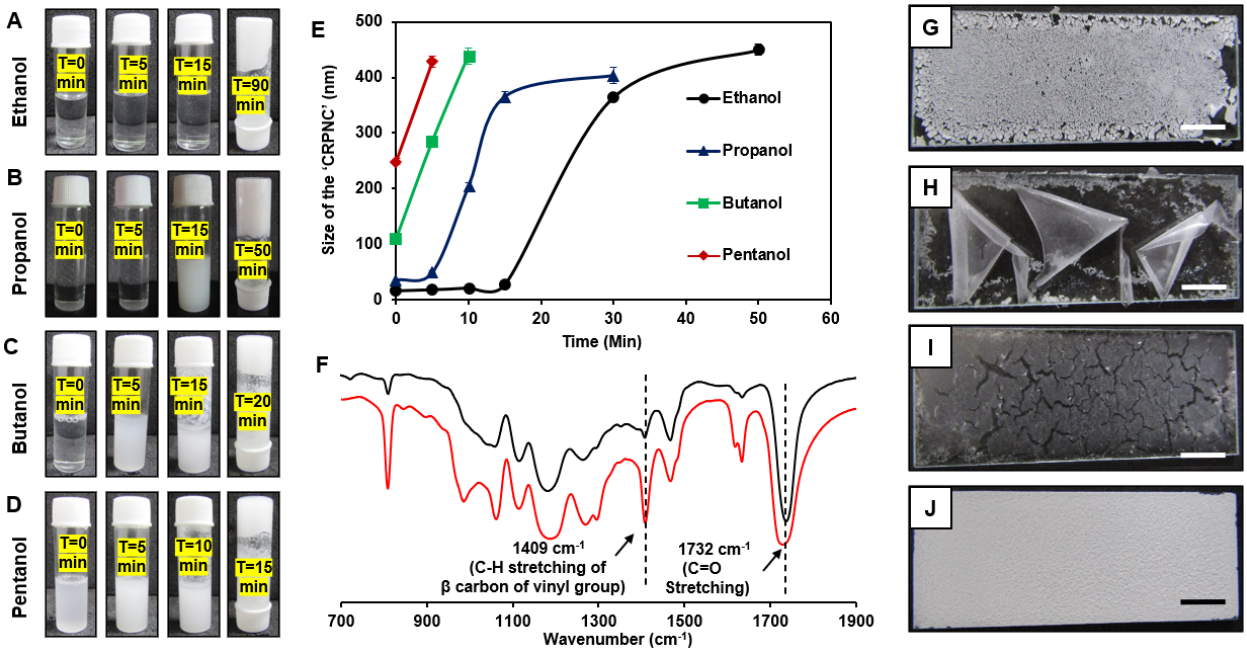

Figure 3.2. (A-D) Digital snapshot images depicting time dependent progress in gelation of the reaction mixture of branched poly(ethyleneimine) (BPEI)/dipentaerythritol penta-acrylate (5Acl) in different alcoholic solvents including ethanol (A), propanol (B), butanol (C) and pentanol (D). (E) Dynamic light scattering (DLS) plot of reaction mixture of BPEI/5Acl in pentanol (red), butanol (green), propanol (blue) and ethanol (black). This plot indicating growth of chemically reactive polymeric nanocomplex (CRPNC) with time in different alcoholic reaction mixture of same reactants. (F) Fourier transform infrared spectroscopy (FTIR) spectra of CRPNC before (red) and after (black) post-covalent modification with octadecylamine. (G-J) Digital images of spray deposited coating of chemically reactive polymeric nanocomplexes (CRPNCs) after air drying, where the respective reaction mixtures were prepared in different acholic media including ethanol (G), propanol (H), butanol (I) and pentanol (J).

Thus, the significant depletion of the IR peak at 1410 cm^{-1} (Fig. 3.2 F) unambiguously confirmed the existence of amine-reactive acrylate groups, which make the polymeric nanocomplexes "chemically-reactive". Before gelation of the reaction mixtures of BPEI/5Acl in pentanol, the turbid dispersion of the 'reactive' and growing nanocomplexes was spray-deposited onto glass substrates. After the air drying, the spray coating that was prepared from the reaction mixture in pentanol was capable of providing a uniform and stable polymeric coating (Fig. 3.2 J), whereas the other spray deposition of other reaction mixtures that were prepared in lower analogs of pentanol yielded inhomogeneous (ethanol) and severely damaged coatings, including cracking (butanol) and peeling (propanol), after air-drying of the deposited polymeric materials, as shown in Fig. 3.2 G-J. During the spray deposition process, both the rate of gelation and the volatility of the alcoholic medium influenced the formation of the stable polymeric coating. For example, the gelation of reaction mixture in ethanol is slow—but evaporation of the used solvent during spray deposition process is high. Hence, an incomplete gelation of the spray deposited reaction mixture led to a loosely bound and inhomogeneous coating. Whereas, a stable polymeric coating was achieved on replacing ethanol with pentanol—as the gelation of same reaction mixture in pentanol is significantly fast and volatility of pentanol is also low. Hence, the use of pentanol in the reaction mixture allowed the complete the gelation process—and eventually a stable coating was achieved. In the past, the computational study revealed that the de-solvation energy of used reactants in a selected solvent influenced the rate of Michael addition reaction.[47]

3.3.2 Characterization of Bulk and Controlled Chemical Optimizations in Porous and 'Reactive' Coatings

The residual reactivity of the polymeric coating, deposited using pentanol solvent, was characterized by FTIR analysis. The experiments were designed to examine the distribution of residual acrylate groups in the thick (254 ± 10 µm) polymeric coating, where the interior of the polymeric coating was randomly exposed with the application of a standard adhesive tape peeling process and characterized by FTIR. After application of the adhesive tape, the exposed interior of the polymeric coating was denoted as 'interior-1', and the thickness of the polymeric coating decreased from 254 ± 10 µm to 147 ± 5 µm. This thickness was further reduced to 65 ± 5 µm on the successive (twice) application of a fresh adhesive surface each time at the same location of the coating and the resulting interface was denoted as 'interior-2'. Irrespective of the physical damage that was strategically incurred on the polymeric coating through application of the adhesive tape peeling test, very similar IR signatures for acrylate groups appeared from different parts of the polymeric coating as shown in Fig. 3.3 B, which strongly suggested the existence of acrylate functionality three-dimensionally (including surface and interior) in the polymeric coating. As expected, the 'reactive' polymeric coating, which was found to

be inherently hydrophilic with a water contact angle (WCA) of 0^0 (Fig. 3.3 A), and after covalent modification with ODA molecules, the coating was capable of repelling water (Fig. 3.3 C) with an advancing water contact angle (WCA) of 162^0 (Fig. 3.3 D) and a roll-off angle of 3^0, including the top surface and interior (including the interfaces: 'interior-1' and 'interior-2', Fig. 3.2 B) of the polymeric coating, (Fig. 3.3 B) through the 1,4-conjugate addition reaction. The IR peak intensity of the polymeric coating at 1410 cm^{-1} was significantly reduced with respect to carbonyl stretching at 1732 cm^{-1} after the reaction of the same polymeric coating with ODA molecules in three different regions (surface, interior-1, interior-2), as shown in Fig. 3.3 B. The carbonyl groups are expected to be unperturbed during the 1,4-conjugate addition reaction under ambient conditions. Thus, the significant depletion of the IR peak at 1410 cm^{-1} unambiguously confirmed the existence of amine-reactive acrylate groups present three-dimensionally in the spray deposited polymeric coating. This simple

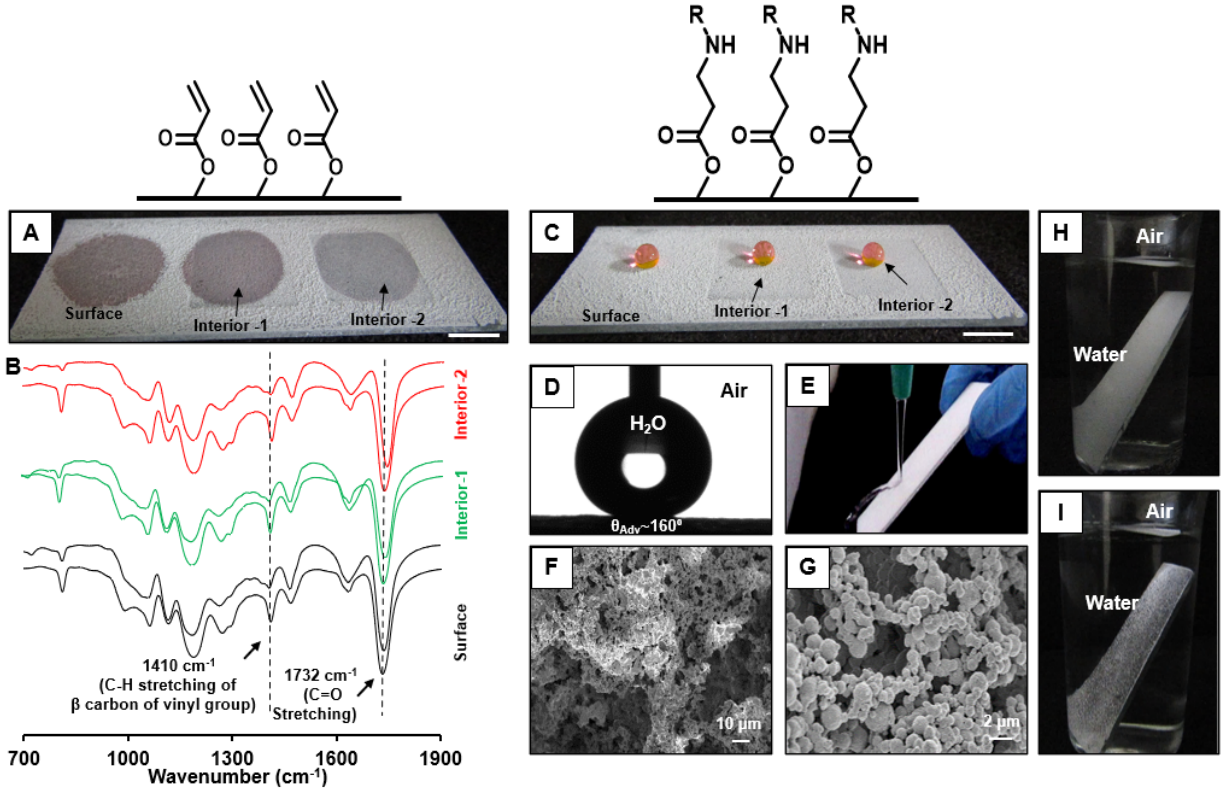

Figure 3.3. (A) Digital photograph of the soaked aqueous droplets on the chemically reactive polymeric coating at different regions including surface, interior-1 and interior-2 (interior-1 and interior-2 were developed by adopting single and successive adhesive tape peeling process). (B) FTIR spectra of the polymeric coating at three different regions (surface, interior-1, interior-2) before and after post chemical modification with octadecylamine. (C) Digital image of the beaded water droplets on the same polymeric coating after post-modified with octadecylamine at different regions (surface, interior-1 and interior-2) which unambiguously showed the existence of three-dimensional superhydrophobicity. (D) Advancing contact angle image of the beaded water droplet on the superhydrophobic coating. (E) Digital image of the water jet bounced off the superhydrophobic coating. (F, G) FESEM images of the superhydrophobic polymeric coating at low (F) and high (G) magnifications. (H, I) Digital image of the reactive (H) and ODA-treated (I) polymeric coating submerged under water. The shiny interface of the ODA-treated interface depicting presence of metastable trapped air.

demonstration further revealed the existence of chemically reactive acrylate groups three-dimensionally in the polymeric coating. A stream of aqueous phase exposed on this polymeric coating was immediately bounced off, as shown in Fig. 3.3 E, and this simple study revalidated the synthesis of a durable and non-adhesive superhydrophobicity. Furthermore, the chemical and physical durability of the embedded special wettability in the synthesized polymeric coating will be discussed in the following section. Next, the topography of the polymeric coating was examined by field emission scanning electron microscopy (FESEM), where the spray-based polymeric coating was found to have randomly aggregated granular domains (Fig. 3.3 F and G). This arbitrary association of polymeric granular domains provided a porous and hierarchical topography (Fig. 3.3 F, G), which made this polymeric coating extremely water-repellent, after the appropriate covalent modification of the residual acrylate groups with octadecylamine through a 1,4- conjugate addition reaction. The underwater shiny interface of the modified polymeric coating revealed the presence of a trapped air layer (Fig. 3.3 I), which is instrumental in the heterogeneous wetting according to the Cassie–Baxter model. However, an aqueous phase immediately infiltrated into the reactive polymeric coating once submerged as shown in Fig. 3.3 H-I.

3.3.3 Controlled Manipulation of the Solid/Liquid Contact Area

The residual amine-reactive acrylate functionalities that were distributed three-dimensionally in the polymeric coating were strategically exploited in controlled manipulation of both the Cassie–Baxter, and Cassie–Wenzel transitional states, which essentially confer various important biomimicking wettabilities. In the past, adhesive superhydrophobicity (interfaces with advancing WCA ~ 150^0 and CA hysteresis > 10^0) was well recognized for its immense potential in the no-loss transfer of tiny water droplets, and this approach would be highly useful in open microfluidics applications.[13] The tailored adhesive superhydrophobicity mainly arises because of the Cassie–Wenzel transitional state. In the past, such interfaces were developed by adopting (1) delicate chemistry (metal–ion interactions, metal–thiol bonds, etc.) and/or (2) complex topography.[48–50] The delicate chemistries (e.g., metal– thiol interactions, metal ion interactions, etc.) that were involved in maintaining optimum chemical functionality in the reported materials for tailoring the Cassie–Wenzel transitional state are susceptible to be affected severely by the practically relevant harsh chemical conditions. On the other side, the manipulation of the essential topography, which is another alternative for achieving the Cassie–Wenzel transitional state, is an inherently complex and challenging process.[44–46] Hence, the demonstrations of facile and controlled regulation of adhesiveness between a beaded water droplet and a solid/air interface are rare. The synthesized chemically reactive polymeric coating was capable of providing a wide range of roll-off angles (from ~ 3^0 to 18^0) for the highly repelled ($\theta_{Adv.} > 150^0$) water droplet,

depending on the modulation of chemical functionalities in the polymeric coating through a 1,4-conjugate addition reaction. Thus, the strategic three-dimensional chemical modifications yielded polymeric interfaces that possessed both (a) NASH (with $\theta_{roll\text{-}off.}$ below 5^0) (after covalent integration

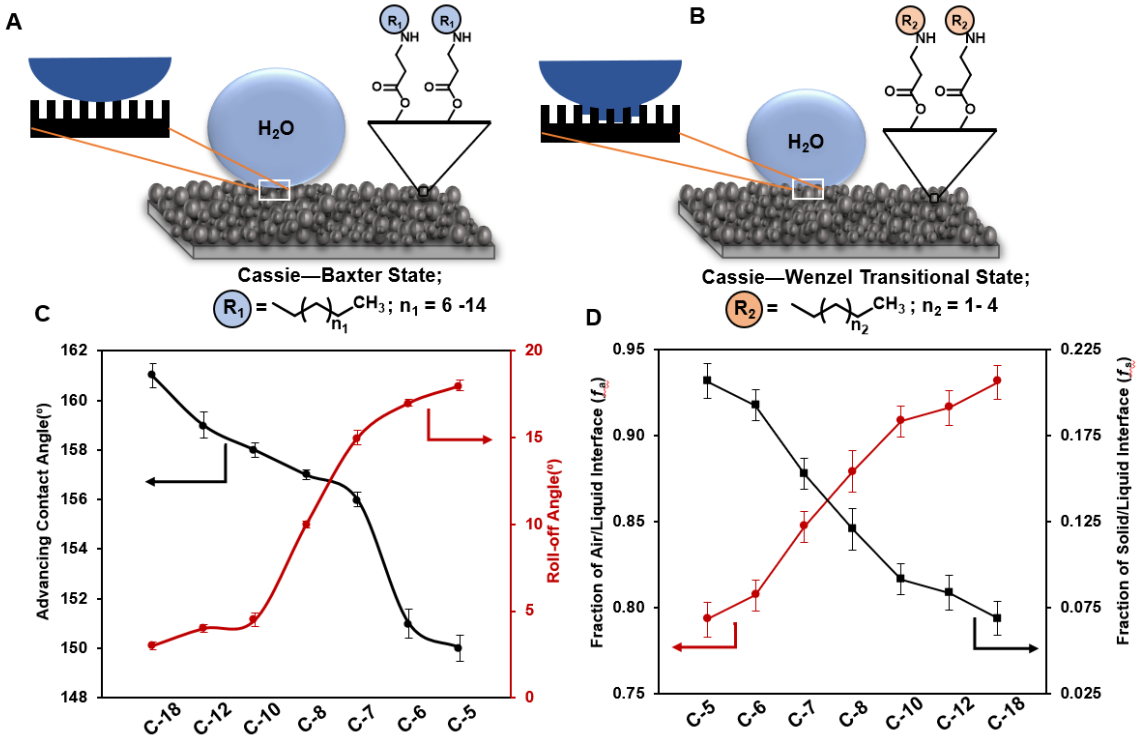

Figure 3.4. (A, B) Schematic representation of Cassie-Baxter (A) and Cassie-Wenzel transitional (B) states. (C) A plot showing decrease in advancing contact angle (black) and increase in roll-off angle (red) with the decrease in hydrocarbon chain length of the selected alkylamine. (D) A plot showing increase in fractional area of entrapped air/liquid (red) and decrease in fractional area of solid/liquid (black) with the increase in carbon chain length of the alkylamine.

of small molecules having long hydrocarbon tails (octadecylamine ($\theta_{roll\text{-}off.} \sim 3^0$), dodecylamine ($\theta_{roll\text{-}off.} \sim 4^0$), decylamine ($\theta_{roll\text{-}off.} \sim 5^0$)), and (b) CASH (with $\theta_{roll\text{-}off.}$ above 10^0) (after chemical modification with small molecules having comparatively shorter hydrocarbon tails (octylamine ($\theta_{roll\text{-}off.} \sim 10^0$), heptylamine ($\theta_{roll\text{-}off.} \sim 15^0$), hexylamine ($\theta_{roll\text{-}off.} \sim 17^0$), pentylamine ($\theta_{roll\text{-}off.} \sim 18^0$)), as shown in Fig. 3.4 C. Such demonstration of precisely chemically controlled adhesive interactions between the beaded water droplet and the polymeric interface is unprecedented in the literature. Furthermore, the fraction of contact area between the beaded water droplet and the porous polymeric coating was estimated using the following equations:[51,52]

$$cos\theta_{CB} = f_{solid}\, cos\theta_y - f_{air} \quad \text{..... (1)}$$

$$f_{solid} + f_{air} = 1 \quad \text{..... (2)}$$

The fraction of contact area of water/metastable trapped air was labelled as f_{air}, whereas f_{solid} denotes the fraction of contact area between the highly repelled water droplet and the porous polymeric coating, which was strategically modified with different and appropriate amine-containing small molecules to maintain similar chemical compositions. The change in the fraction of contact area (f_{air} and f_{solid}) was completely due to controlled and covalent chemical modification of the porous and reactive polymeric coating. No changes in the topography of the polymeric coatings were observed after post-chemical modifications. The chemically reactive porous polymeric coating was inherently hydrophilic with a water contact angle of ~ 0^0, which is due to the absence of any trapped air between the beaded water phase and the polymeric coating. This fraction of air contact area with the beaded water droplet on the polymeric coating significantly increased to 0.78 after the reaction of residual acrylate groups with pentylamine. However, this fraction of air/water contact area on the polymeric coating was further improved on covalent-chemical modifications with higher analogs of pentylamine as shown in Fig. 3.4 D. The fraction of air contact area with the highly repelled water droplet was calculated to be above 0.9 after modifying the porous polymeric coating with octadecylamine molecules (having long hydrocarbon tails). As a consequence, the contact area of the solid/water interfaces gradually decreased (Fig. 3.4 D), and the roll-off angle or adhesive interaction between the repelled water droplets on the porous polymeric coating was reduced. Thus, the facile chemical modification of the 'reactive' interfaces through 1,4-conjugate addition reaction allowed to modulate both the Cassie–Baxter, and Cassie–Wenzel transitional in the porous polymeric coating.

3.3.4 Substrate Independent Bulk Polymeric Coatings

Further, this approach was extended to coat various other substrates including flexible (e.g., aluminum foil, polymeric film, etc.) and rigid (e.g., surface of concrete, wood, etc.) objects, which would allow the strategic use of bio mimicking special interfaces in practical settings. The current spray-based 'reactive' polymeric coating allowed various substrates to be coated with superhydrophobicity ($\theta_{Adv.} > 150^0$ and $\theta_{roll\text{-}off.} \sim 6^0$), irrespective of their texture (smooth or rough), wettability (hydrophilic, hydrophobic), and chemical composition (metal, polymer, etc.) as shown in Fig. 3.5 A–D. Furthermore, this facile synthetic process was adopted to decorate commercially relevant objects with large dimensions (printing paper, A-4 size) Fig. 3.5 E. After coating the printing paper (hydrophilic) with an appropriately post-modified polymeric porous film, the interface was capable of displaying extreme water-repellent properties with $\theta_{Adv.}$ of 160^0 and $\theta_{roll\text{-}off.}$ of 4^0, even after printing carbon ink on the superhydrophobic interface using a regular laser printer, as shown in Fig. 3.5 F. The extreme anti-wetting property of the coated objects was observed by measuring the both advancing and receding contact angles of the beaded water droplets as shown in Fig. 3.5 G-N.

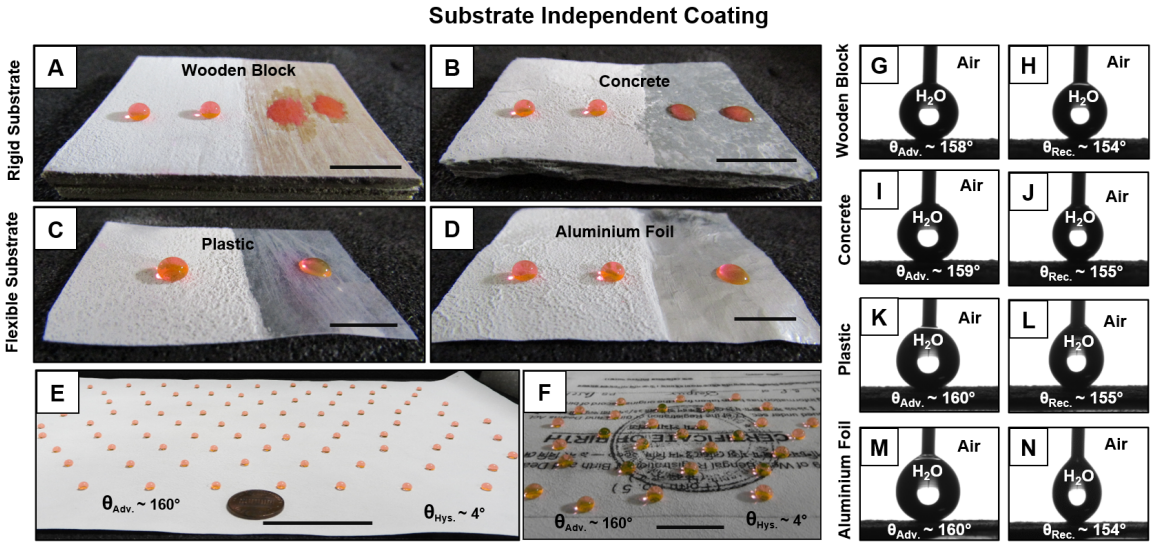

Figure 3.5. (A-D) Digital photographs of the beaded aqueous droplets on various substrates (wooden block, A; concrete, B; plastic, C; aluminium foil, D) which were decorated with non-adhesive superhydrophobicity. (E) Digital image of the beaded water droplets on commercially available A-4 size paper which was decorated with non-adhesive superhydrophobicity. (F) Digital image of the beaded water droplets on superhydrophobic paper after printing. (G-N) Advancing and receding contact angle images of the beaded water droplet on coated substrates (wooden block, G-H; concrete, I-J; plastic, K-L; aluminium foil, M-N).

Next, a fountain pen was used to manually write on this superhydrophobic coated paper, and during this process, some physical damages were incurred, but the anti-wetting property remained intact (the physical durability aspect of the polymeric coating has been separately discussed in the following section in detail). This extremely water-repellent interface was capable of protecting the written text even from any spilling and spreading of ink under a stream of water, unlike the uncoated printer paper as shown in Fig. 3.6 A-F). The written text on the bare printing paper was found to be significantly damaged due to the spreading and spilling of the ink all around the uncoated paper on exposure to the stream of an aqueous phase, as shown in Fig. 3.6 A-C. Next, a geometrically complex object e.g., shoe (Ajanta, India, Model no. 8) was successfully decorated with artificial non-adhesive superhydrophobicity. This coated shoe was used to demonstrate the self-cleaning of a dust-contaminated interface. First, the superhydrophobic shoe (Fig. 3.6 J) was contaminated with a substantial amount of dust particles, as shown in Fig. 3.6 J. Upon exposure to a stream of the aqueous phase, the dust-contaminated interface self-cleaned and remained dry (Fig. 3.6 J-L) due to the inherent ability of the biomimicking wettability. In comparison, the uncoated shoe with deposited dust was found to be muddy after identical treatment with an aqueous stream as shown in Fig. 3.6 G-I. Thus, the current design of artificial biomimicking wettability made it possible to develop some smart materials for convenient and relevant uses in practically relevant scenarios.

3.3.5 Physical/Chemical Durability Tests

Both the physical and chemical durability of this embedded wettability were investigated in detail using the standard abrasion tests that have been commonly used in the literature. [14] First, the adhesive surface of adhesive tape was strategically applied with an external load of 500 g on the superhydrophobic coating (Fig. 3.7 A), and after manual peeling of the adhesive tape from the

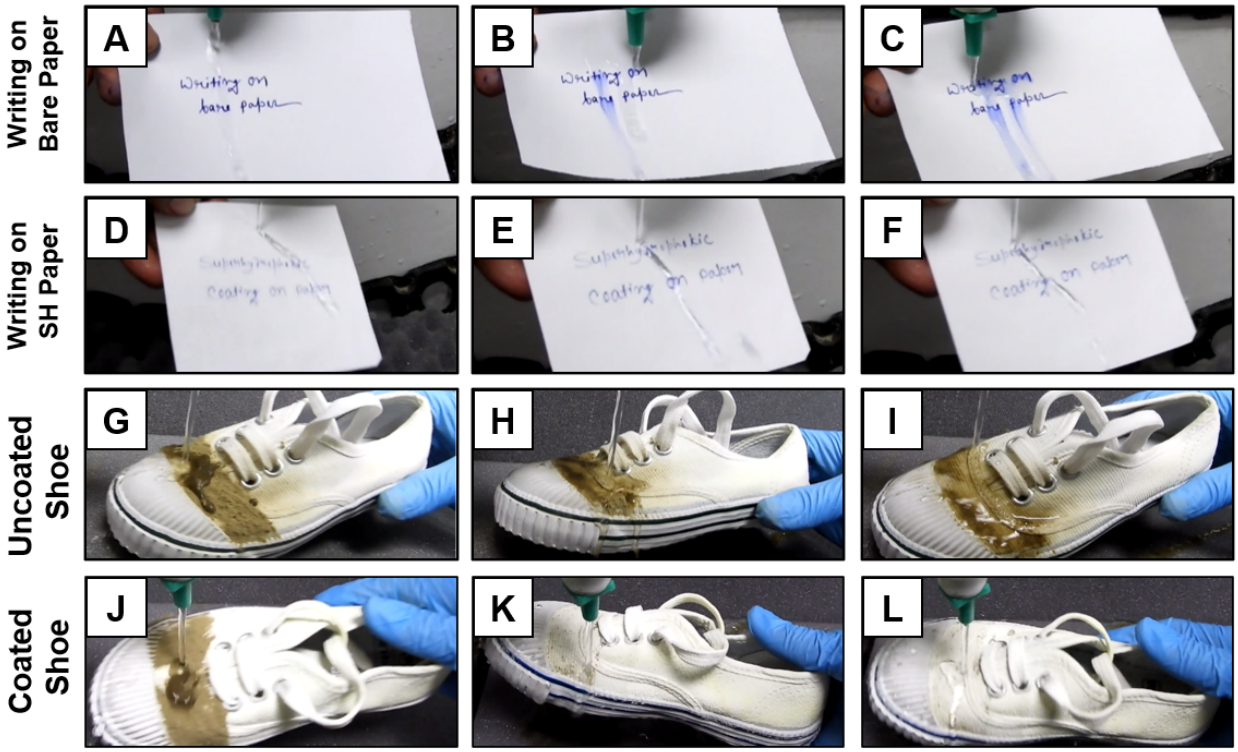

Figure 3.6. (A-F) Snapshot images illustrating the responses of hard written ink on bare paper (A-C) and superhydrophobic paper (D-F) under the exposure of stream of water. (G-L) Uncoated shoe became muddy and wetted under the stream of water (G-I) whereas contaminated dust particles cleaned away from coated superhydrophobic shoe (J-L) under the same experiment and remained cleaned and dry.

polymeric coating, the top portion of the film was transferred to the adhesive surface and eventually provided a randomly fractured interior. However, after this obvious physical abrasion, the embedded antifouling property was observed to be unperturbed (Fig. 3.7 B-C) with $\theta_{Adv.} \sim 159^0$ and $\theta_{roll\text{-}off.} \sim 3^0$, mainly due to the existence of appropriate and three-dimensional chemical optimization of the porous polymeric coating as discussed in earlier sections. This simple demonstration further independently revalidated the existence of three-dimensional superhydrophobicity. The presence of this three-dimensional special wettability was also confirmed by performing other abrasive tests, including a scratch test (Fig. 3.7 F), a sandpaper abrasion test, and a sand drop test (Fig. 3.7 D, G), etc. Even after severe physical damage of the polymeric coating during the performance of these abrasive tests, the

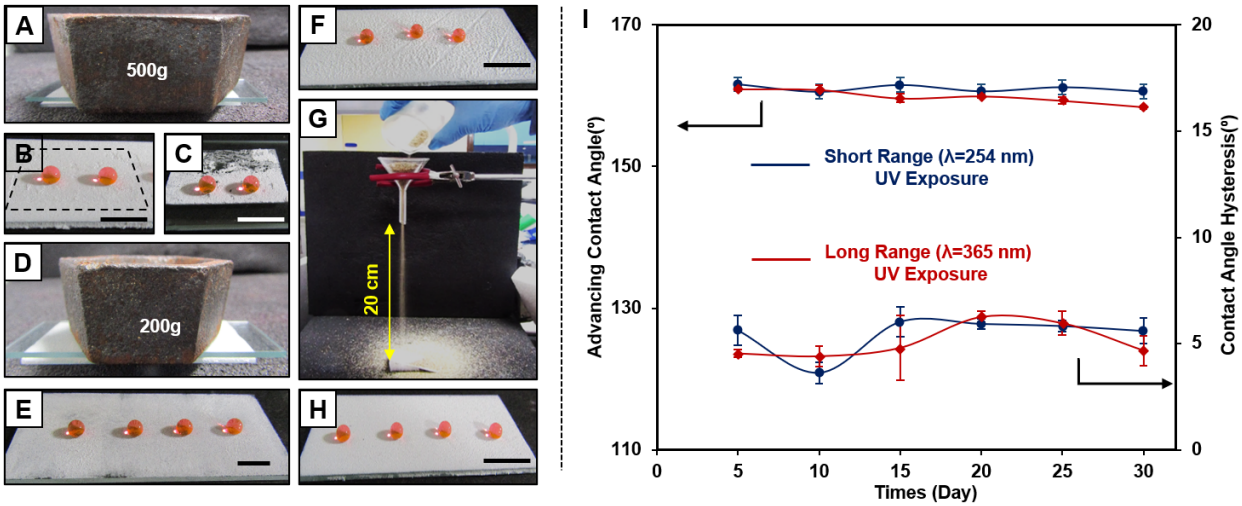

Figure 3.7. (A) Digital image for the set-up of adhesive tape test. (B, C) Digital photograph of beaded aqueous droplets on adhesive tape abraded superhydrophobic polymeric coating (dotted region; B) and superhydrophobic polymeric coating which was transferred to the adhesive tape during the abrasion (C) (scale bar ~ 1 cm). (D) A 200 g of load applied during the sand paper abrasion test. (E-F) Digital images of beaded aqueous droplets on octadecylamine treated polymeric after incurring sand paper abrasion (E) and scratch test (F) (scale bar ~ 1 cm). (G) Digital snapshot image for the sand drop test. (H) Digital image of the beaded aqueous droplets after sand drop test. (scale bar ~ 1 cm). (I) A plot illustrating the change in advancing contact angle and contact angle hysteresis of a beaded water droplet on the polymeric coating after prolonged exposure to UV irradiation (with l_{max} = 254 nm, (blue line) and l_{max} = 365 nm (red line)); the lines on the graph are only for guiding the eyes.

bulk polymeric coating continued to display extreme water repellence with $\theta_{Adv.} > 155^0$ and $\theta_{roll\text{-}off.} \sim 5^0$ as observed from digital images of beaded water droplets on the damaged interface as shown in Fig. 3.7 E, H. These different abrasive tests allowed to mimic various kinds of physical insults, and the polymeric coating was found to be highly capable of sustaining all of such severe physical damage. Then, this three-dimensional superhydrophobic coating was kept under exposure to UV light both at high (λ_{max} = 365 nm) and low (λ_{max} = 254 nm) wavelengths for 30 days, and after regular intervals, the water wettability was investigated on the polymeric coating as shown in Fig. 3.7 I. The embedded antifouling property was found to be unperturbed with $\theta_{Adv.}$ above 160^0 and $\theta_{roll\text{-}off.} \sim 5^0$ even after UV exposures for 30 days, likely due to the association of the robust 1,4-conjugate addition reaction during the synthesis of (a) synthesizing covalently cross-linked porous polymeric coatings and (b) optimization of the appropriate chemical functionality in the entire polymeric coating. Furthermore, this polymeric coating was exposed to various chemically complex aqueous phases, including extremes of pH, artificial seawater, and river water (Brahmaputra, Assam, India) for 100 h continuously, and the polymeric interface remained highly efficient in repelling water droplets even

after such harsh aqueous exposures with an advancing contact angle ~ 158^0 and contact angle hysteresis ~ 5^0 (Fig. 3.8 A-H).

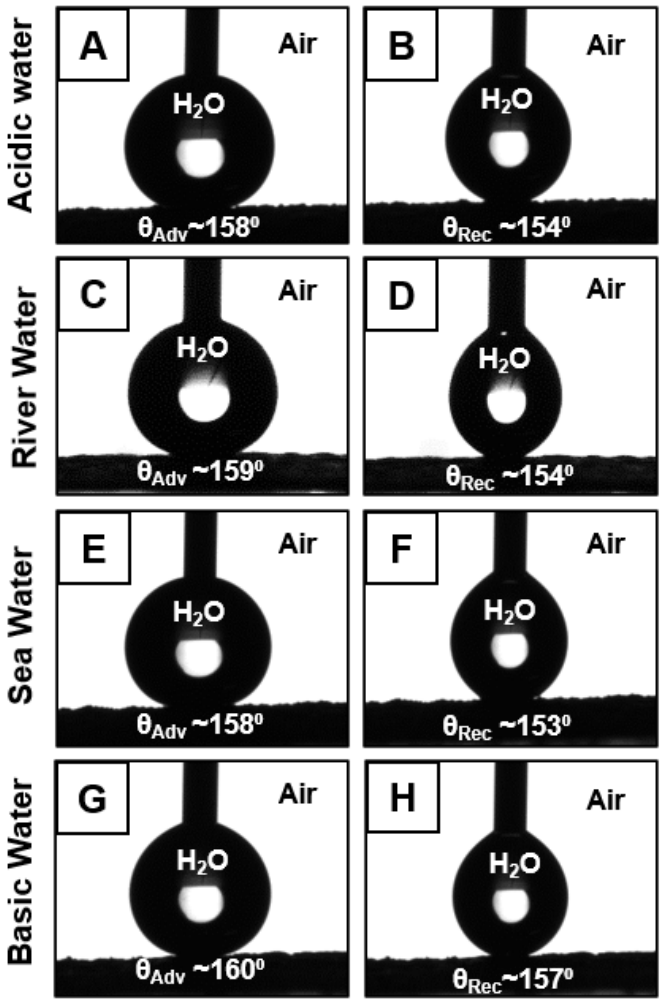

Figure 3.8. A-H) Advancing (A, C, E, G) and receding (B, D, F, H) contact angles of beaded water droplet on ODA modified polymeric coatings after 100 h incubation in different harsh aqueous phases including acidic water (A, B), river water (C, D), sea water (E, F) and basic water (G, H).

3.4 Conclusions

In conclusion, in chapter 3, a facile and rapid chemical reaction (1,4- conjugate addition) between a polymer (BPEI) and a small molecule (5Acl) was strategically used to develop a three-dimensional hierarchically featured and 'covalently reactive' polymeric bulk coating. This facile and scalable approach provided a unique chemical basis to tailor both the Cassie– Baxter state and Cassie–Wenzel transitional state through controlled manipulation of the metastable trapped air level (fraction of air/water contact area varied from 0 to above 0.9) in the polymeric coating, which conferred various important biomimicking special interfaces. Furthermore, this simple and scalable approach allowed bulk superhydrophobic coatings to be synthesized on a variety of relevant substrates, independent of

their geometry, dimensions, and chemical compositions. The embedded superhydrophobicity was found to have impeccable physical and chemical durability and was capable of surviving various forms of severe physical damages to the polymeric coating. Furthermore, regular printing of carbon ink was processed on coated superhydrophobic paper (A-4 size) without affecting the extreme water repellence. On the other hand, a shoe decorated with this robust antifouling property remained highly efficient in self-cleaning the deposited dust and dirt without wetting the material. Thus, this facile approach has an immense ability to coat large and complex objects with highly durable biomimicking wettability for smart and relevant applications in 'real-world' scenarios.

3.5 References

1. Lahann, J.; Balcells, M.; Rodon, T.; Lee, J.; Choi, I. S.; Jensen, K. F.; Langer, R. *Langmuir* **2002,** *18,* 3632–3638.
2. Buck, M. E.; Zhang, J.; Lynn, D. M. *Adv. Mater.* **2007,** *19,* 3951–3955.
3. Deng, X.; Friedmann, C.; Lahann. J. *Angew. Chem. Int. Ed.* **2011,** *123,* 6652 –6656.
4. Spruell, J. M.; Wolffs, M.; Leibfarth, F. A.; Stahl, B. C.; Heo, J.; Connal, L. A.; Hu, J.; Hawker, C. J. *J. Am. Chem. Soc.* **2011,** *133,* 16698–16706.
5. Carter, M. C. D.; Jennings, J.; Speetjens, F. W.; Lynn, D. M.; Mahanthappa, M. K. *Macromolecules* **2016,** *49,* 6268−6276.
6. Liu, P.; Zhang, H.; He, W.; Li, H.; Jiang, J.; Liu, M.; Sun, H.; He, M.; Cui, J.; Jiang, L.; Yao, Xi. *ACS Nano* **2017,** *11,* 2248−2256.
7. Li, X. M.; Reinhoudt, D.; Crego-Calama, M.; *Chem. Soc. Rev.* **2007,** *36,* 1350–1368.
8. Wang, S.; Liu, K.; Yao, X.; Jiang, L. *Chem. Rev.* **2015,** *115,* 8230.
9. Manna, U.; Carter, M. C. D.; Lynn, D. M. *Adv. Mater.* **2013,** *25,* 3085–3089.
10. Nishimura, R.; Hyodo, K.; Sawaguchi, H.; Yamamoto, Y.; Nonomura, Y.; Mayama, H.; Yokojima, S.; Nakamura, S.; Uchida, K. *J. Am. Chem. Soc.* **2016,** *138,* 10299–10303.
11. Feng, X.; Jiang, L. *Adv. Mater.* **2006,** *18,* 3063-3078.
12. Yan, Y. Y.; Gao, N.; Barthlott, W. *Adv. Colloid. Interface Sci.* **2011,** *169,* 80–105.
13. Hong, X.; Gao, X.; Jiang, L. *J. Am. Chem. Soc.* 2007, **129,** 1478–1479.
14. Yao, X.; Song, Y.; Jiang, L. *Adv. Mater.* **2011,** *23,* 719–734.
15. Yohe, S. T.; Colson, Y. L.; Grinstaff, M. W. *J. Am. Chem. Soc.* **2012,** *134,* 2016–2019.
16. Ueda, E.; Levkin, P. A. *Adv. Mater.* 2013, **25,** 1234–1247.
17. Wen, L.; Tian, Y.; Jiang, L. *Angew. Chem. Int. Ed.* **2015,** *54,* 3387–3399.
18. Gao, A.; Wu, Q.; Wang, D.; Ha, Y.; Chen, Z.; Yang, P. *Adv. Mater.* 2016, **28,** 579–587.

19. Osicka, J.; Ilcikova, M.; Popelka, A.; Filip, J.; Bertok, T.; Tkac J.; Kasak, P. *Langmuir*. **2016,** *32,* 5491–5499.
20. Zhou, C.; Chen, Z.; Yang, H.; Hou, K.; Zeng, X.; Zheng, Y.; Cheng, J. *ACS Appl. Mater. Interfaces.* **2017,** *9,* 9184–9194.
21. Wu, M.; Ma, B.; Pan, T.; Chen, S.; Sun, J. *Adv. Funct. Mater.* **2016,** *26,* 569–576.
22. Zang, D.; Zhu, R.; Zhang, W.; Yu, X.; Lin, L.; Guo, X.; Liu, M.; Jiang, L. *Adv. Funct. Mater.* **2017,** *27,* 1605446.
23. Verho, T.; Bower, C.; Andrew, P.; Franssila, S.; Ikkala, O.; Ras, R. H. A. *Adv. Mater.* **2011,** *23,* 673–678.
24. Tian, X.; Verho, T.; Ras, R. H. A. *Science* **2016,** *352,* 142–143.
25. Deng, X.; Mammen, L.; Zhao, Y.; Lellig, P.; Müllen, K.; Li, C.; Butt, H. -J.; Vollmer, D. *Adv. Mater.* **2011,** *23,* 2962–2965.
26. Mates, J. E.; Bayer, I. S.; Palumbo, J. M.; Carroll, P. J.; Megaridis, C. M. *Nat. Comm.* **2015,** *6,* 8874.
27. Paven, M.; Fuchs, R.; Yakabe, T.; Vollmer, D.; Kappl, M.; Itakura, A. N.; Butt, H. -J. *Adv. Funct. Mater.* **2016,** *26,* 4914–4922.
28. Zhu, X. T.; Zhang, Z. Z.; Men, X. H.; Yang, J.; Wang, K.; Xu, X. H.; Zhou, X. Y.; Xue, Q. J. *J. Mater. Chem.* **2011,** *21,* 15793–15797.
29. Wu, M.; Li, Y.; An, N.; Sun, J. *Adv. Funct. Mater.* **2016,** *26,* 6777–6784.
30. Li, Y.; Li, L.; Sun, J. *Angew. Chem. Int. Ed.* **2010,** *49,* 6129–6133.
31. Wang, H. X.; Xue, Y. H.; Ding, J.; Feng, L. F.; Wang, X. G.; Lin, T. *Angew. Chem. Int. Ed.* **2011,** *50,* 11433–11436.
32. Levkin, P. A.; Svec, F.; Frechet, J. M. *Adv. Funct. Mater.* **2009,** *19,* 1993–1998.
33. Manna, U.; Broderick, A. H.; Lynn, D. M. *Adv. Mater.* **2012,** *24,* 4291–4295.
34. Yohe, S. T.; Freedman, J. D.; Falde, E. J.; Colson, Y. L.; Grinstaff, M. W. *Adv. Funct. Mater.* **2013,** *23,* 3628–3637.
35. Santhosh Kumar, K. S.; Kumar, V.; Nair, C. P. R. *J. Mater. Chem. A* **2014,** *2,* 15502–15508
36. Li, Y.; Chen, S.; Wu, M.; Sun, J. *Adv. Mater.* **2014,** *26,* 3344–3348.
37. Chen, Q.; de Leon, A.; Advincula, R. C. *ACS Appl. Mater. Interfaces* **2015,** *7,* 18566–18573.
38. Baidya, A.; Ganayee, M. A.; Ravindran, S. J.; Tam, K. C.; Das, S. K.; Ras, R. H. A.; Pradeep, T. *ACS Nano* **2017,** *11,* 11091–11099.
39. Hu, X.; Tang, C.; He, Z.; Shao, H.; Xu, K.; Mei, J.; Lau, W. M. *Small* 2017, **13,** 1602353.
40. Zhang, J.; Yu, B.; Gao, Z.; Li, B.; Zhao, X. *Langmuir* **2017,** *33,* 510–518.

41. Liu, Z.; Wang, H.; Zhang, X.; Lv, C.; Wang, C.; Zhu, Y. *Adv. Mater. Interfaces* 2017, **4,** 1601202.
42. Chen, Y.; Yoon, Y. J.; Pang, X.; He, Y.; Jung, J.; Feng, C.; Zhang, G.; Lin, Z. *Small* **2016**, *12*, 6714–6723.
43. Chen, Y.; Yang, D.; Yoon, Y. J.; Pang, X.; Wang, Z.; Jung, J.; He, Y.; Harn, Y. W.; He, M.; Zhang, S.; Zhang, G.; Lin, Z. *J. Am. Chem. Soc*. **2017**, *139*, 12956–12967.
44. Rather, A. M.; Mahato, S.; Maji, K.; Gogoi, N.; Manna, U. *Nanoscale* **2017**, *9*, 16154–16165.
45. Rather, A. M.; Jana, N.; Hazarika, P.; Manna, U.; *J. Mater. Chem. A* **2017**, *5*, 23339–23348.
46. Bechler, L.; Lynn, D. M. *Biomacromolecules* **2012**, *13*, 1523–1532.
47. Rather, A. M.; Jana, N.; Begum, S.; Srivastava, H. K.; Manna, U. *Green Chem.* **2017**, *19*, 4527–4532.
48. Lai, Y.; Gao, X.; Zhuang, H.; Huang, J.; Lin, C.; Jiang, L. *Adv. Mater.* **2009**, *21*, 3799–3803.
49. Zhu, H.; Guo, Z.; Liu, W. *Chem. Commun.* **2014**, *50*, 3900–3913.
50. Tan, C.; Cai, P.; Xu, L.; Yang, N.; Xi, Z.; Li, Q. *Appl. Surf. Sci.* **2015**, *349*, 516–523.
51. Yang, S.; Chen, S.; Tian, Y.; Feng, C.; Chen, L. *Chem. Mater.* **2008**, *20*, 1233–1235.
52. Cassie, A. B. D.; Baxter, S. *Trans. Faraday Soc.* **1944**, *40*, 546–551.

Title: Design of Chemically Reactive Slippery Liquid Infused Porous Surface*

The design of Nepenthes pitcher-inspired slippery liquid-infused porous surface (SLIPS) appeared as an important avenue for various potential and practically relevant applications. In general, a hydrophobic/superhydrophobic matrix infused with selected liquid lubricants for developing chemically inert SLIPS. In chapter 4, an inherently hydrophilic (soaked beaded water droplet with ~20° within a couple of minutes), porous and thick (above 200 μm) polymeric coating, loaded with chemically reactive acrylate moieties yielded a chemically reactive SLIPS, where residual acrylate groups in the synthesized hydrophilic and porous interface provided essential chemical compatibility and hence stability to the infused lubricants. The chemically reactive porous polymeric coating was capable of reacting with the solution of primary amine-containing nucleophiles in organic solvent through 1,4-conjugate addition reaction, both in the presence (referred to as "in situ" modification) and absence (denoted as premodification) of lubricated phase. Such amine-reactive SLIPS was further extended to (1) examining the impact of different chemical modifications on the performance of SLIPS and (2) developing a spatially selective and "in situ" post-modification with primary amine-containing nucleophiles through a 1,4-conjugate addition reaction. Such a principle will undoubtedly be helpful for spatially selective covalent immobilization of water-insoluble functional molecules/polymers directly from organic solvents, which would be of potential interest for various applied and fundamental contexts. Moreover, the chemically reactive SLIPS could sustain various physical abrasions and prolonged (up to 10 days) exposure to different complex and harsh aqueous phases.

*Maji, K.; Das, A.; Hirtz, M.; Manna, U. *ACS Appl. Mater. Interfaces* **2020**, *12*, 14531−14541.

4.1 Introduction

Modulating essential topography and appropriate chemistry remained a primary basis for developing various functional and smart interfaces.[1–4] In 2011, Aizenberg and co-workers introduced a Nepenthes pitcher-inspired slippery liquid infused porous surface (SLIPS) through the strategic use of a porous fluorinated matrix and fluorine-based liquid lubricant, where the chemical compatibility between the infused lubricant and the matrix was hypothesized to be a key and essential parameter for achieving a non-adhesive slippery interface for various probe liquids.[5] Since then, this hypothesis has been followed for synthesizing a bioinspired SLIPS, where hydrophilic hierarchically featured/porous interfaces (denoted as a base layer) were routinely hydrophobized with long-tail hydrocarbons, aromatic groups, fluorinated molecules, and so forth, following chemical and physical deposition processes, prior to infusing with selected fluorinated/nonfluorinated lubricants.[6–29] In another approach, inherent hydrophobic base layers were developed by associating hydrophobic polymers or nanomaterials to prepare advanced and different stimuli-responsive SLIPS [30–43] for printing assisted functionalization,[30] programable droplet manipulation, [31,32] developing patterned interface,[33] controlled switching of liquid wettability,[34–37] controlled transfer of gas, and so on.[38–43] However, eventually, chemically inert and highly hydrophobic interfaces were mostly used to prepare SLIPS. Was this modification with a hydrophobic and inert base layer required to achieve SLIPS? As per my knowledge, there was no report in the literature to address this fundamental concern on SLIPS that have immense prospects for widespread practically relevant applications, including tissue engineering, gas, and liquid transport, anti-corrosion, water harvesting, drug delivery, and so forth.[5–43] To address this important aspect of the bio mimicked interface, a design of a readily chemically reactive, hydrophilic, and porous interface was essential, where the chemically reactive porous interface would allow systematic post covalent modification with small molecules having different hydrocarbon tail lengths. Routinely, either highly hydrophobic or superhydrophobic base layers were developed for stabilizing infused lubricants in the porous interface of the SLIPS. However, the minimal chemical requirements have not been systematically examined due to the lack of suitable substrates with porosity, hydrophilicity, and ready chemical reactivity. In the past, few chemically reactive and porous coatings were introduced in the literature, but most of them were inherently superhydrophobic and were generally utilized in synthesizing interfaces displaying patterned extreme water wettabilities.[44–46] The embedded extreme water repellence in the reported chemically reactive bioinspired coatings[44–46] makes such an interface inappropriate for evaluating the minimal and necessary chemical requirement that is required for stabilizing the lubricant phase in the liquid-infused porous interfaces. Even though, both the topography and chemistry were hypothesized to be crucial fundamentals behind designing the

bioinspired SLIPS.[5] Only the role of topography on the bioinspired SLIPS was examined thoroughly, where it was proven that the hierarchical topography was not an essential criterion for synthesizing a liquid-infused slippery interface, even interfaces with only nanometer-scale features were also capable of displaying slippery properties.[47,48] However, progress on designing appropriate experiments capable of evaluating the exact role of chemistry for designing the SLIPS was few, likely due to the challenge in synthesizing hydrophilic yet chemically reactive porous interfaces. Besides the above-mentioned challenge, recently, a few porous polymeric coatings were spatially modulated with hydrophobic and hydrophilic chemical moieties for developing interfaces with patterned wettability.[49–52] After infusion with selected liquid lubricants, the portion of the porous interface selectively modified with long-tail hydrocarbon/fluorinated molecules provided SLIPS, and the area of coating modified with a hydrophilic moiety failed to display such bioinspired property.[49–52] This study strongly suggested that the macroscale perturbation in chemistry is likely to scarify the slippery property in SLIPS. Even though the mobility of lubricants in SLIPS can self-heal abrasions in the order of micro-scale, [5] but most of the reported SLIPS that were developed based on the post-modification on the top of hydrophilic hierarchical features (base layer) with the thin layer (in the order of nm) of hydrophobic coating [6–25] are fundamentally inappropriate to tolerate macroscale (in order of few cm and more) physical abrasion. It is likely due to the damage of the appropriate chemical makeup that is mostly optimized only over few nanometers across the thickness of the reported SLIPS.[6–25] Thus, any macroscale (in order of mm/cm) physical abrasions on the conventional design of the SLIPS was expected to expose the hydrophilic interior, misbalancing the chemical compatibility between the featured interface and infused lubricant, and eventually, most of the reported SLIPS were therefore unlikely to perform in practically relevant different physical abrasive settings. However, recently, self-healing SLIPS were developed by the strategic association of supramolecular polymers, and such designs were found to be appropriate for sustaining large physical damages.[53–55] In this chapter, a hydrophilic and chemically reactive porous polymeric coating loaded with residual acrylate groups, has been introduced for systematically evaluating the impact of chemistry on designing SLIPS, as shown in Fig. 4.1 A. Surprisingly, during the course of the study, the direct lubrication of the chemically reactive and hydrophilic interface with a range of natural and synthetic liquid lubricants allowed to develop SLIPS without requiring any prior hydrophobization (Fig. 4.1 B). However, in the past literature, hydrophobic post modification, prior to lubrication, was routinely adopted as the essential component for designing SLIPS. In such a design of SLIPS, it was experimentally validated that the residual acrylate groups helped to anchor the water-immiscible lubricated phase, even though the entire porous polymeric coating remained highly hydrophilic [with a water contact angle (WCA)

of ~20°]. Furthermore, the readily amine-reactive acrylate groups available in the chemically reactive porous polymeric coating allowed for systematic modulation with various alkyl amines having different hydrocarbons tail lengths, as shown in Fig. 4.1 D, E. Moreover, various standard and severe macroscale (order of few cm) physical abrasions (e.g., sand-paper abrasions, adhesive tape test, etc.) were strategically imposed on the synthesized slippery polymeric coating for exposing the interior of the polymer coating randomly over a large area (in the scale of cm). However, upon infusing liquid lubricants, this physically damaged polymeric interface displayed Nepenthes pitcher-inspired liquid wettability, even though no post covalent modulation was involved in the currently synthesized SLIPS unlike the conventional designs. Moreover, the design of chemically reactive SLIPS was successfully extended for in situ and spatially selective covalent modification with selected nucleophiles that too using organic solvents in the presence of the lubricated phase in the porous polymeric coating.

4.2 Experimental Section

4.2.1 Materials

Branched polyethyleneimine (BPEI, MW ≈ 25 000 Da) and dipentaerythritol penta/hexa acrylate (5 Acl, MW ≈ 524.21 g mol^{-1}) were purchased from Sigma Aldrich. Silicon oil (AR 20), octadecylamine (97%), dodecylamine (98%), decylamine (95%), octylamine (99%), heptylamine (99%), hexylamine (99%), pentylamine (95%), and propylamine (98%) were bought from Sigma- Aldrich. Butylamine (98%) was purchased from Spectrochem. Glucamine (95%) and Nile red were procured from TCI Chemicals, India. Fluorescein was obtained from Loba Chemie. Pentanol was obtained from Alfa Aesar. Microscope slides acquired from Zenith India. A spray bottle (capacity ≈ 100 mL, nozzle diameter ≈ 400 μm) was purchased from Amazon India. Adhesive tape, paper, aluminum foil, and sandpaper (300 grit) were procured from a local stationary shop. Concrete and wooden blocks were collected from a local construction site. Glass slides were thoroughly washed using ethanol prior to experiments.

4.2.2 Characterization

All FTIR spectra were obtained using standard KBr plate by PerkinElmer instruments. All FESEM images were acquired using a Carl Zeiss scanning electron microscope (prior to the experiment each sample was coated with a thin layer of conducting gold). The microscopic images were obtained by an OLYMPUS BX51 microscope. All contact angles were measured using a Drop shape Analyser-DSA25 at 25 °C. The advancing/receding angles were taken with Milli-Q water droplets, respectively, at four different regions of each surface. The surface free energy was calculated using a Drop Shape Analyser-DSA25 at 25 °C, where water and hexane were used as polar and dispersive phases,

respectively. Digital photographs were taken using a Nikon COOLPIX, B700 point shot camera. The thickness of the coating was measured by a Veeco Dektak 150 surface profilometer.

4.2.3 Fabrication of Reactive Polymeric Coating

The "reactive" porous polymeric coatings were prepared by spray deposition of chemically reactive polymeric nanocomplex (CRPNC) onto the glass substrates, using a commercially available spray bottle. The chemically reactive polymeric nano-complexes (CRPNC) were prepared first by mixing two solutions of mutually reactive reactants, which were 10 mL of 5 Acl (0.1325 g/mL) and 3 mL of BPEI (0.05 g/mL) in pentanol. After mixing, the reaction medium was kept under vigorous agitation for 5 min. Then, a turbid reaction mixture (13 mL) solution was manually sprayed onto selected substrates over an area of 200 cm^2 from a distance of 15 cm using a commercially available spraying bottle. After deposition of CRPNC, the substrates were kept in the open air for the evaporation of the reaction medium. The selection of reaction media played a crucial role in achieving stable coating. The lower analog of pentanol failed to provide a stable coating.

4.2.4 Post Chemical Modification

The "reactive" polymeric coatings were further postmodified with primary amine containing small molecules, for example, octadecylamine (2.5 mg/mL), dodecylamine (5 mg/mL), decylamine (0.1 mL/mL), octylamine (0.1 mL/ mL), heptylamine (0.1 mL/mL), hexylamine (0.1 mL/mL), pentylamine (0.1 mL/mL), and glucamine (2.5 mg/mL) through 1,4 conjugate addition reaction at ambient condition. After post modification, the post functionalized substrates were thoroughly washed with ethanol/water and kept in open air for drying.

4.2.5 Infusion of Selected Lubricants into the Polymeric Matrix

Both chemically reactive and post-modified porous polymeric coatings (7.5 cm × 2.5 cm) were infused with different lubricants (silicone oil, soybean oil, olive oil, etc.). In brief, 200 µL of selected lubricant spread to a porous matrix using a weighing paper over an area of 18.75 cm^2, and the excess oil was removed by vertically placing the substrates for 15 min.

4.2.6 Physical and Chemical Durability of the Reactive SLIPS

All the physical/chemical durability tests were performed on the reactive porous polymeric coating. An adhesive tape test was carried out by placing an adhesive surface (3 cm × 2.5 cm) onto the polymeric coating with a weight of 500 g, and after 5 min, the tape was taken out randomly. Some visual damages were noted on the coating, but the sliding behavior of water droplets remains unperturbed after the infusion of the selected lubricant. Sandpaper abrasion was performed by placing sandpaper (grit no-300, 3 cm × 2 cm) fixed on a glass slide, on half of the polymeric coating using an external pressure, and rubbed the surface back and forth 10 times. Random damages occurred as some

portion of the reactive coating came out with the sandpaper and water sliding behavior examined by contact angle measurements and digital photographs after silicone oil infusion. For the chemical durability test, silicone oil-infused polymeric surfaces (glass as model substrate) were submerged in different aqueous environments, for example, acidic water (pH = 1), alkaline water (pH = 13), river water, and artificial seawater for 10 days. The liquid water wettability was examined by contact angle measurements for each substrate. Further, the porous polymeric coatings on a glass substrate were kept continuously under UV irradiation for 10 days, and on every 5 days of interval, the water wettability was examined by contact angle measurements.

4.3 Result and Discussions

4.3.1 Synthesis and Characterization of Chemically Reactive SLIPS.

In the previous chapters, I introduced a facile and catalyst-free approach for synthesizing chemically reactive polymeric nano-complexes (CRPNC) with residual acrylate groups that were readily chemically reactive towards different alkylamines through 1,4 conjugate addition reaction at ambient conditions.[56,57] Such nano-complexes were strategically exploited further for developing chemically reactive polymeric coatings on both spongy as well flat substrates, and the residual chemical reactivity was rationally extended for achieving extremes of water repellence in air. [57–60] In this chapter, the CRPNC prepared in pentanol was spray deposited to develop a thick (245 ± 10 µm) polymeric coating

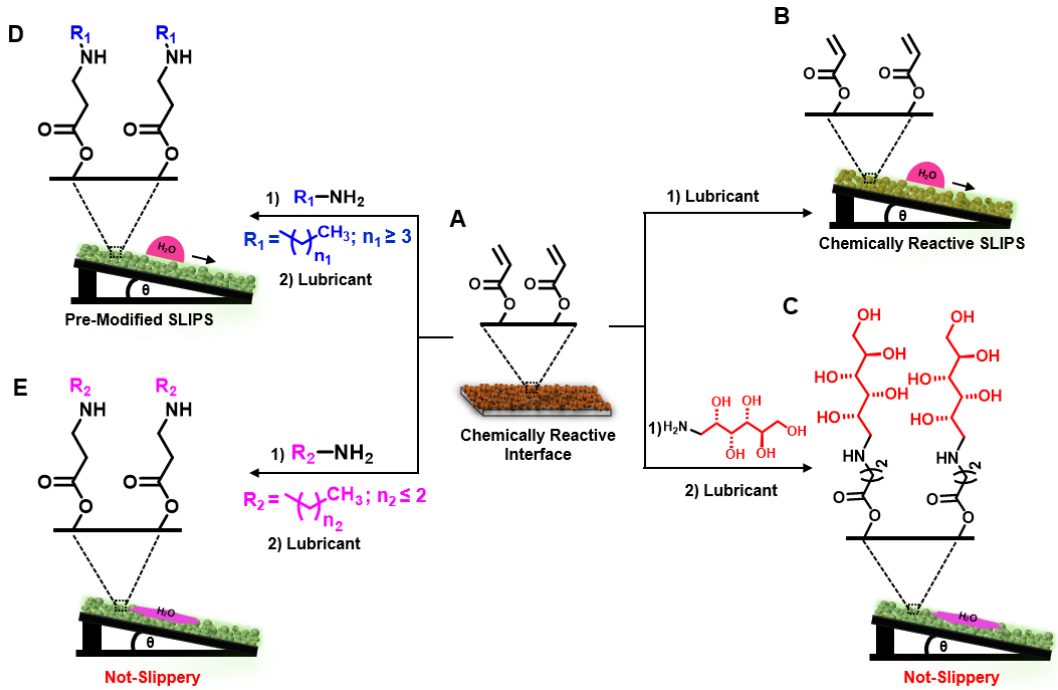

Figure 4.1 (A, B) Schematic representation of chemically reactive porous polymeric coating (A) and chemically reactive SLIPS (B). (C) The polymeric coating fails to show slippery property after post-modification with glucamine prior to lubrication. (D, E) The polymeric coating showed slippery behaviour after post covalent modification with higher analogues of butylamine (D), whereas no slippery property was noticed for polymeric coating that was treated with butylamine and its lower analogue (E).

that was inherently hydrophilic. The as-synthesized polymeric coating was highly hydrophilic, where a beaded water droplet (4 μL) is gradually and continuously soaked by the polymeric coating with a WCA of 20° within 2 min, as shown in Fig. 4.2 1 A−C. The scanning electron microscopy study on the synthesized polymeric coating revealed the existence of random and covalent aggregation of nano-complexes, as shown in Fig. 4.2 D, E and eventually, provided a porous topography. Porosity in the polymeric coating allowed to store selected lubricants three-dimensionally. The chemical compatibility of the lubricants with the porous matrix was an anticipated challenge before adopting nature-inspired slippery property. Interestingly residual acrylate moiety in the currently synthesized porous polymeric coating provided a simple basis for chemical compatibility that confer the slippery property. The existence of residual acrylate groups was confirmed with Fourier transform infrared (FTIR) spectral analysis, as shown in Fig. 4.2 F. The appearance of IR peaks at 1732 and 1411 cm^{-1} in the synthesized polymeric coating, due to vibrational stretching of carbonyl and symmetric stretching of the C−H bond of β-carbon of the vinylic group respectively, unambiguously confirmed the presence of residual acrylate groups in the hydrophilic polymeric coating. [57–60] The normalized (with respect to IR peak at 1732 cm^{-1}) IR peak intensity at 1411 cm^{-1} significantly depleted after the mutual reaction with a primary amine-containing small molecule (i.e., glucamine) through 1,4-conjugate addition reaction, where the carbonyl group remained intact, and vinyl groups were consumed. Thus, standard FTIR analysis revealed the existence of chemically reactive acrylate groups in the synthesized porous polymeric coating. This residual reactivity provided essential hydrophobic anchoring points for stabilizing the lubricated phase in the porous polymeric coating. Moreover, this residual chemical reactivity was extended for a systematic investigation to study the impact of different chemical functionalities on bioinspired liquid-infused slippery properties. The chemically reactive and inherently hydrophilic porous polymeric coating was lubricated with silicone oil (AR 20), before examining the slipping behavior of a beaded aqueous droplet (red color aids visual inspection). The optically opaque polymeric coating instantly became translucent after lubricating with silicone oil. Then, the polymeric coating with both the dry (top opaque portion, Fig. 4.2 G) and the lubricated (translucent) region was kept at a tilting angle of 4°, before beading two aqueous droplets at two different portions of the coating. The aqueous droplet that beaded on the dry polymeric interface remained stationary and slowly started spreading (Fig. 4.2 H−J), whereas the aqueous droplet that beaded on the lubricated portion of the polymeric coating with a WCA of ~83°, immediately slipped away from the initial position and traveled along the downslope of the inclined SLIPS, as shown in Fig. 4.2 H−J. Thus, the same polymeric interface that soaked the aqueous phase (Fig. 4.2 A−C) could also display slippery properties after the infusion of silicone oil. In the conventional design of SLIPS,

inert and hydrophobic post-modification was routinely adopted to achieve the chemical compatibility between the lubricated phase and polymeric coating for obtaining the slippery property. The current study experimentally validated that this additional introduction of high hydrophobicity with long-tail hydrocarbons or fluorinated moieties does not always essential to achieve SLIPS. In the synthesized SLIPS, the residual acrylate groups are self-sufficient for stabilizing the lubricant phase, and the aqueous phase readily slipped off from the tilted interface. Further, experiments were designed to validate the stabilization of the lubricant in chemically reactive SLIPS, where the chemically reactive polymeric coating loaded with residual acrylate groups was post-modified with a hydrophilic small molecule (glucamine), replacing the acrylate groups with multiple hydroxyl moieties (hydrophilic groups) of glucamine. The successful covalent modulation of the polymeric coating with glucamine

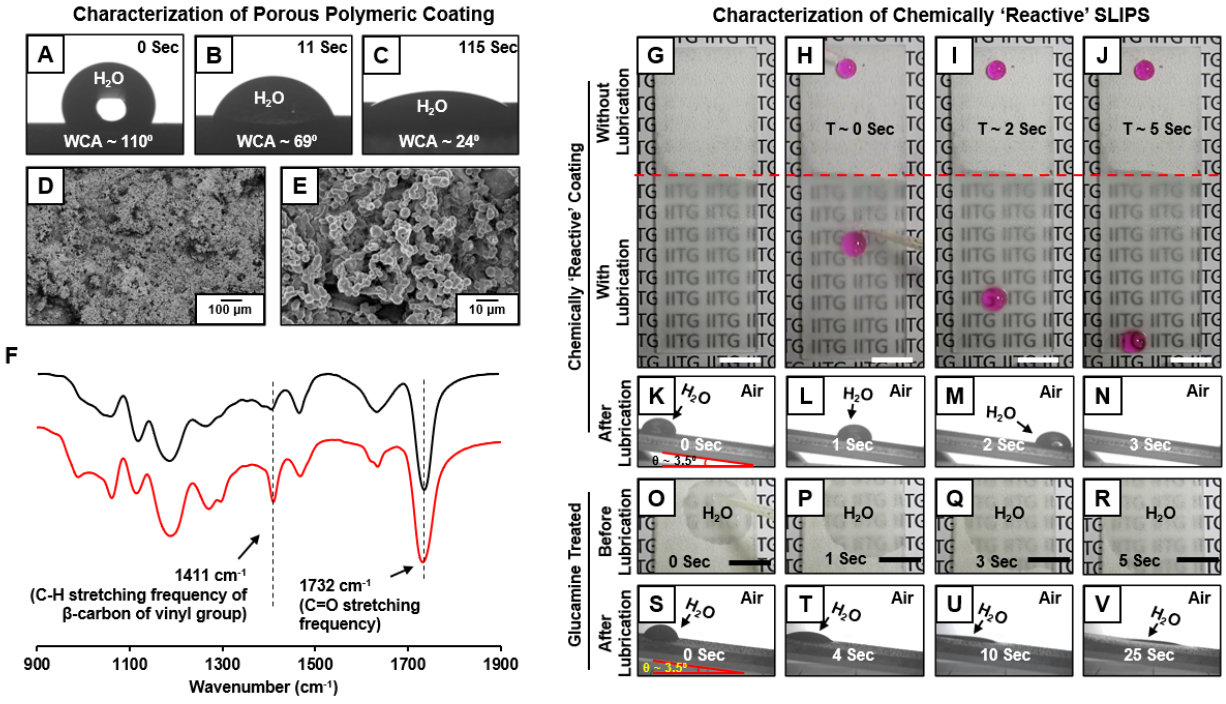

Figure 4.2 (A−C) Digital snapshots of wetting and spreading of a beaded water droplet (4 µL) on chemically reactive porous polymeric coating. (D, E) FESEM images of the reactive polymeric coating in low (D, scale bar: 100 µm) and high (E, scale bar: 10 µm) magnifications. (F) FTIR spectra of reactive polymeric coating before (red) and after (black) post-chemical modification with glucamine. (G−J) Digital images comparing the behaviour of beaded aqueous droplets on the chemically reactive polymeric coating with (bottom portion) and without (top portion) lubrication (scale bar 1 cm) with silicone oil (AR 20). (K−N) Snapshot images illustrating the movement of beaded water droplet on the tilted (with tilting angle of 3.5°) chemically reactive SLIPS. (O−V) Snapshot photographs depicting rapid spreading and spilling of beaded water droplets on the glucamine treated polymeric coatings both before (O−R) and after (S−V) lubrication with silicone oil.

was confirmed by FTIR analysis (Fig. 4.2 F). A drastic change in liquid wettability was noted for such glucamine-modified polymeric coating. Aqueous droplets were instantly soaked by the glucamine-treated polymeric coating with WCA of 0°, as shown in Fig. 4.2 O−R. Moreover, the lubricated phase in the glucamine-treated polymeric coating became unstable upon exposure to probe liquid, which

resulted in the spreading of the beaded aqueous phase on lubricated polymeric coating (Fig. 4.2 S-V). Thus, the controlled study unambiguously revealed that the residual acrylate group was instrumental for achieving the desired chemical compatibility in the synthesized chemically reactive SLIPS. Nevertheless, in the current design, any additional post-covalent modification was not required to achieve SLIPS, such demonstration was unprecedented in the literature.

4.3.2 Investigation of Chemical Compatibility between the Porous Substrate and Infused Lubricants

The synthesis of SLIPS with the hydrophilic interface without adopting any post-modification with the hydrophobic coating was highly unusual in the literature. However, during the study, it was found that the chemically reactive hydrophilic interface transformed into SLIPS after lubrication with silicone oil as discussed in the above section. This superior chemical compatibility of the as-synthesized hydrophilic and chemically reactive polymeric coatings with the selected lubricant phase over probe liquid (i.e., aqueous phase) was further independently revalidated with another controlled study. At first, the synthesized chemically reactive coating was submerged in the aqueous phase (added fluorescein dye aids visual inspection) for 30 s to allow infiltration of the aqueous phase, as shown in Fig 4.3 A, C. This impregnation of the aqueous phase in the hydrophilic polymeric coating was confirmed by both visual inspection and fluorescence microscopy. The fluorescence signal appeared due to the penetration of the dyed aqueous phase into the porous and hydrophilic polymeric coating (Fig 4.3 C). Next, the wet (by aqueous phase) polymeric interface was transferred into the Nile-red (water-immiscible dye)-dyed silicone oil (model lubricant), followed by washing with deionized (DI) water for removing loosely held silicone oil (Fig 4.3 B) from top of the interface. In the end, the polymeric coating appeared to be completely red as the Nile-red added silicone oil rapidly infiltrated into the polymeric coating, replacing the aqueous phase. Furthermore, the fluorescence microscopic study (Fig 4.3 D) also confirmed the complete removal of the aqueous phase by the water-immiscible lubricated phase from the polymeric coating. Only the fluorescence signal for Nile-red dye (only soluble in the oily phase) was noted, whereas no trace of fluorescence for the water-soluble dye (fluorescein) was observed from the polymeric coating (Fig 4.3 D). As expected, the beaded aqueous phase (blue color aids visual inspection) readily slipped off from the tilted polymeric interface that was exposed to both, probe liquid (aqueous) phase, and subsequently, the lubricant (silicone oil) phase (Fig 4.3 I-K). In a separate control study, the same demonstration was repeated with glucamine-treated polymeric coating, where acrylate groups were consumed through a 1,4-conjugate addition reaction and hydroxyl groups were introduced in place of the acrylate groups. The outcome of the demonstration with glucamine-treated polymeric coating was completely different in comparison to

the as-synthesized chemically reactive and hydrophilic coatings. The glucamine-treated polymeric coating immediately soaked the dyed aqueous phase as confirmed by visual inspection and fluorescence microscopic images in Fig 4.3 E, G. However, the model lubricant phase (Nile-red added silicone oil) failed to displace the infiltrated aqueous phase. As a result, no fluorescence signal for Nile red dye was observed from the glucamine-treated polymeric coating even after submerging the coating in dyed (with Nile-red) silicone oil phase for 30 s (Fig 4.3 H). This controlled study confirmed that the glucamine-treated polymeric coating was chemically more compatible with the probe liquid than the lubricant phase. Therefore, the polymeric coating that was post modified with glucamine completely failed to display slippery properties, and the beaded water droplet completely spread on the interface, as shown in Fig 4.3 L–N. Even though the as-synthesized chemically reactive polymeric coating remained overall highly hydrophilic in the air with a WCA of 20° (Fig 4.2 A), but the affinity for the

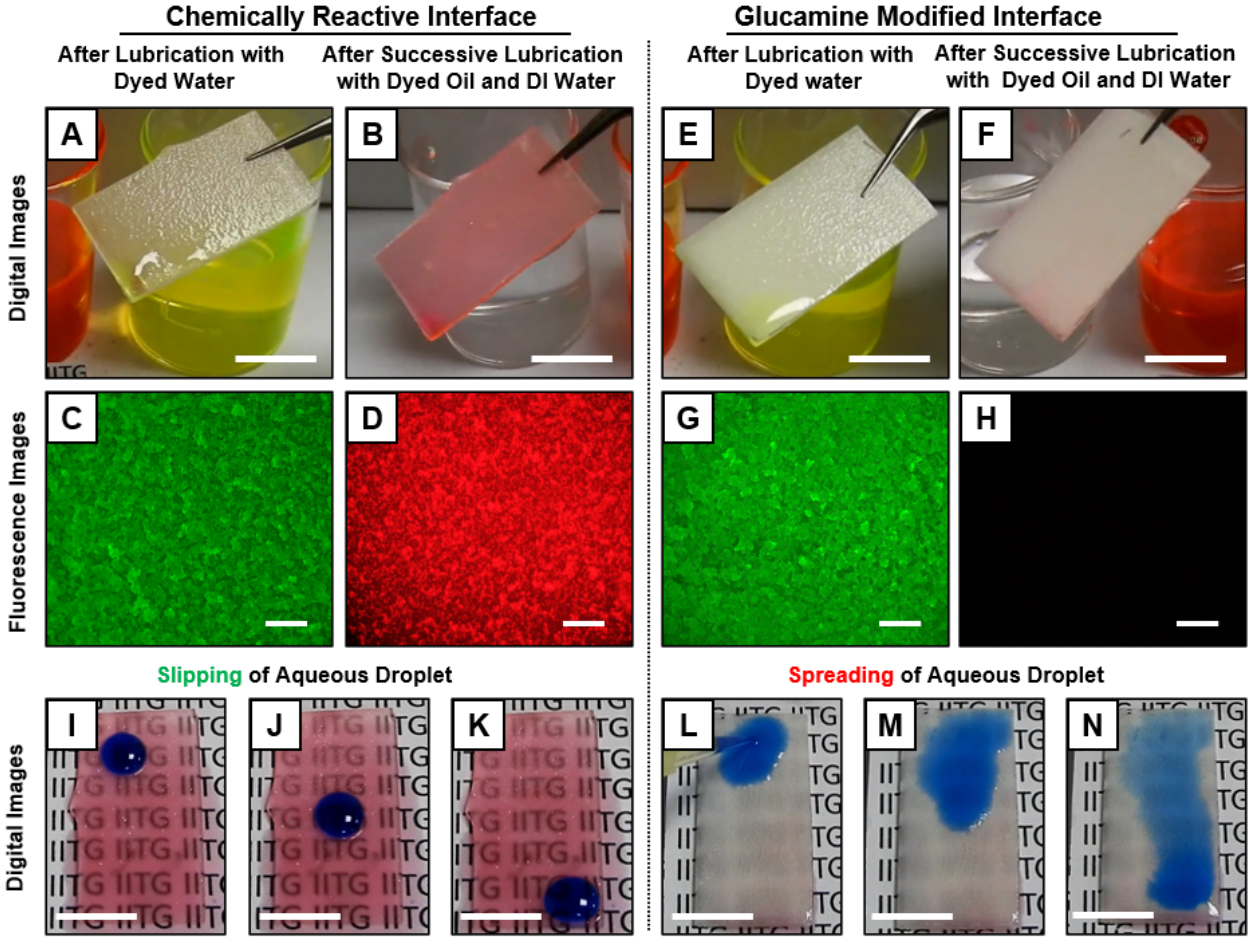

Figure 4.3 (A-D) Digital (A, B; scale bar 1 cm) and fluorescence (C, D; scale bar 500 µm) images of the reactive polymeric coating after lubrication with dyed water (A, C) followed by lubrication with dyed oil and washing with DI water (B, D). (E-H) Digital (E, G; scale bar 1 cm) and fluorescence (F, H; scale bar 500 µm) images of the reactive polymeric coating after lubrication with dyed water (E, G) followed by lubrication with dyed oil and washing with DI water (F, H). (I-N) Digital snapshot images of sliding behaviour of aqueous droplet on reactive polymeric coating (I-K) and glucamine treated polymeric coating (L-N) after lubrication with dyed water followed by successive lubrication with dyed oil and DI water (scale bar 1 cm).

oily phase was found to be superior, likely due to the presence of the residual hydrophobic acrylate groups. This demonstration unambiguously and unprecedentedly revealed that the conventional post-modification with long-tail hydrocarbon or fluorinated molecules at the top of the SLIPS is not an essential chemical criterion for achieving the slippery property. Further, the residual acrylate groups in the synthesized porous polymeric coating provided the essential chemical compatibility with various other synthetic and natural lubricated phases, including vegetable oil, olive oil, silicone oil, and eventually, the polymeric coating became slippery after infusion of selected lubricants. Moreover, various practically relevant substrates (e.g., wood, concrete, paper, aluminum foil, etc.) were successfully coated with such chemically reactive SLIPS as shown in Fig. 4.4 A-I.

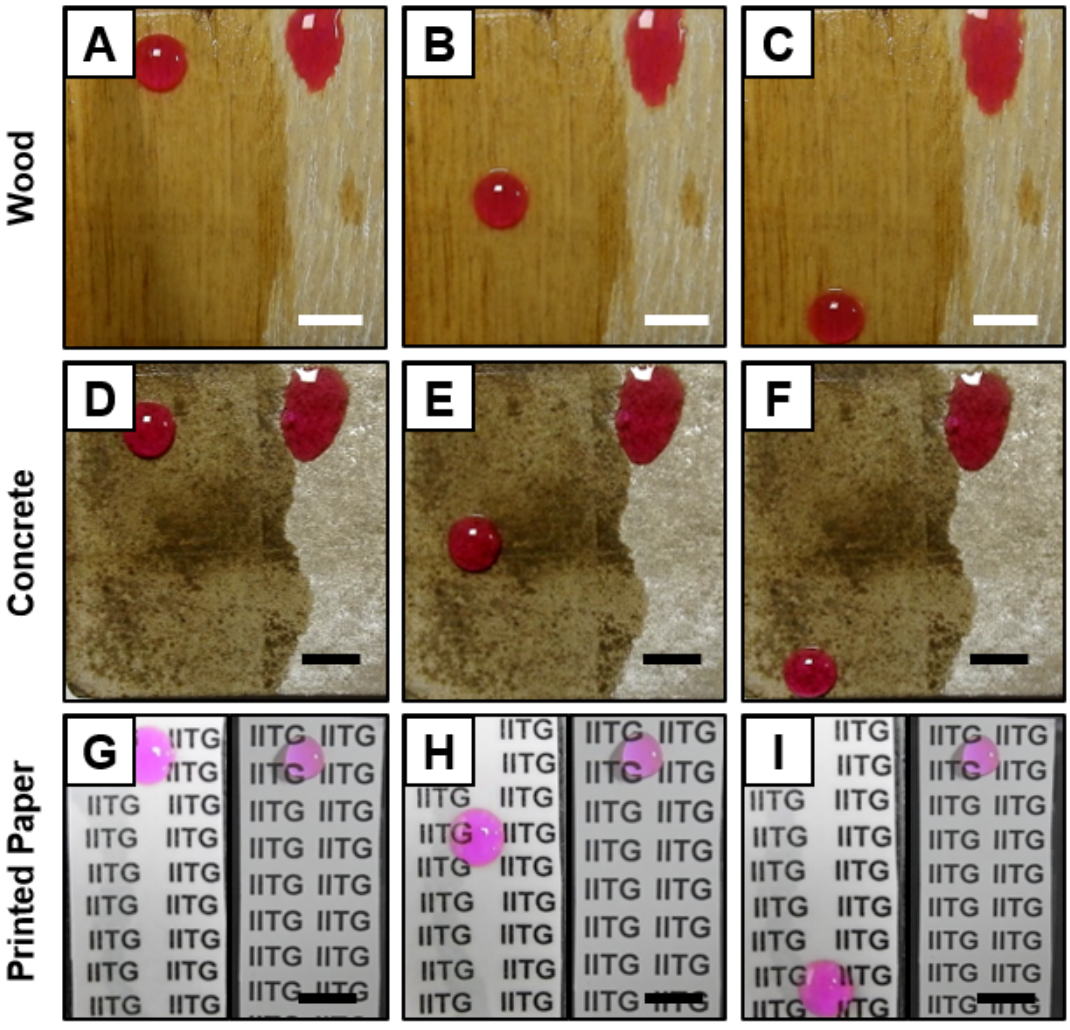

Figure 4.4. A-K) Snapshot images of moving water droplet on polymeric coated objects (wooden block, A-C; concrete, D-F; paper, G-I).

4.3.3 Physical and Chemical Durability of Chemically Reactive SLIPS

Next, different standard physical and chemical durability tests were performed on the as-synthesized SLIPS to examine its tolerance at practically relevant challenging physical settings. In the past,

primarily micrometer-scale scratches were introduced to mimic practically relevant harsh abrasive challenges, and the tolerance toward such minor damages was commonly examined with the previously reported SLIPS.[5] However, the demonstration for analyzing the impact of large-scale (over centimeters) physical damages, which is more relevant for practical scenarios, is rare in literature. In general, any physical abrasion over a large scale is likely to remove the thin hydrophobic coating from the top of the hydrophilic hierarchical interface in most of the conventional reported SLIPS, and the lack of chemical compatibility between the lubricated phase and freshly exposed hydrophilic interior in earlier reported materials was a major threat for its survival under practically relevant and severe physical challenges. The slippery interfaces, introduced in this chapter 4, were fundamentally different from the conventional approach. Compared to previous relevant literature, in our current design, the chemically reactive slippery interface does not require any post-chemical hydrophobization on top of the featured interface. Thus, the essential chemical compatibility between the chemically reactive polymeric coating and the lubricated phase should be remained intact at physically abraded interfaces. Some standard and severe abrasive tests were performed on the polymeric coating for investigating the impact of physical abrasions on the embedded slippery property. An abrasive surface of sandpaper (grid no-300) was manually rubbed on the polymeric coating 10 times, with an applied pressure of 3.27 kPa. During this abrasion process, a white powdery material piled up at the edges of the coating, and the thickness of the coating significantly reduced from 240 ± 8 μm to 170 ± 4 μm. However, the embedded slippery property remained intact, and a beaded water droplet (color aids visual inspection) on the physically abraded polymeric coating (kept with a tilting angle of ~4°) was observed to move down the surface, as shown in Fig 4.5 A−C. The topography of the abraded interface was further examined with field emission scanning electron microscopy (FESEM), confirming the existence of a random association of granular polymeric domains as shown in Fig 4.5 D, E. Moreover, the sandpaper abraded polymeric coating with freshly exposed interior remained loaded with residual acrylate groups as confirmed from standard FTIR analysis. Thus, the abraded interface remained efficient in displaying bioinspired slippery properties after lubrication with silicone oil. In another abrasion process, a freshly exposed adhesive surface was brought in contact with the polymeric coating with an applied load of 500 g. The applied external pressure secured uniform and facilitated contact between the adhesive surface and the top of the polymeric coating. Duringthe process of adhesive tape peeling from the polymeric coating, a top portion of the porous polymeric coating was fractured randomly and transferred onto the adhesive tape surface. The interior of the polymeric coating was exposed arbitrarily after this abrasion test, but the slippery property was found to be unaltered (Fig 4.5 F−H). Further, the physically damaged interface remained highly porous (Fig 4.5 I, J) to store infused

lubricant. In another type of physical manipulations, a reactive polymeric coated aluminum foil was arbitrarily bent and creased, and some random damages were found to occur during the process of these physical insults (Fig 4.5 K−O). Irrespective of such damages the coated aluminum foil was able to show slippery property towards dyed aqueous phase after lubrication with silicone oil as shown in Fig 4.5 M−O. Further, the as-synthesized polymeric coating was intentionally exposed to various other practically relevant conditions, including extremes of pH, artificial seawater, river water, and UV

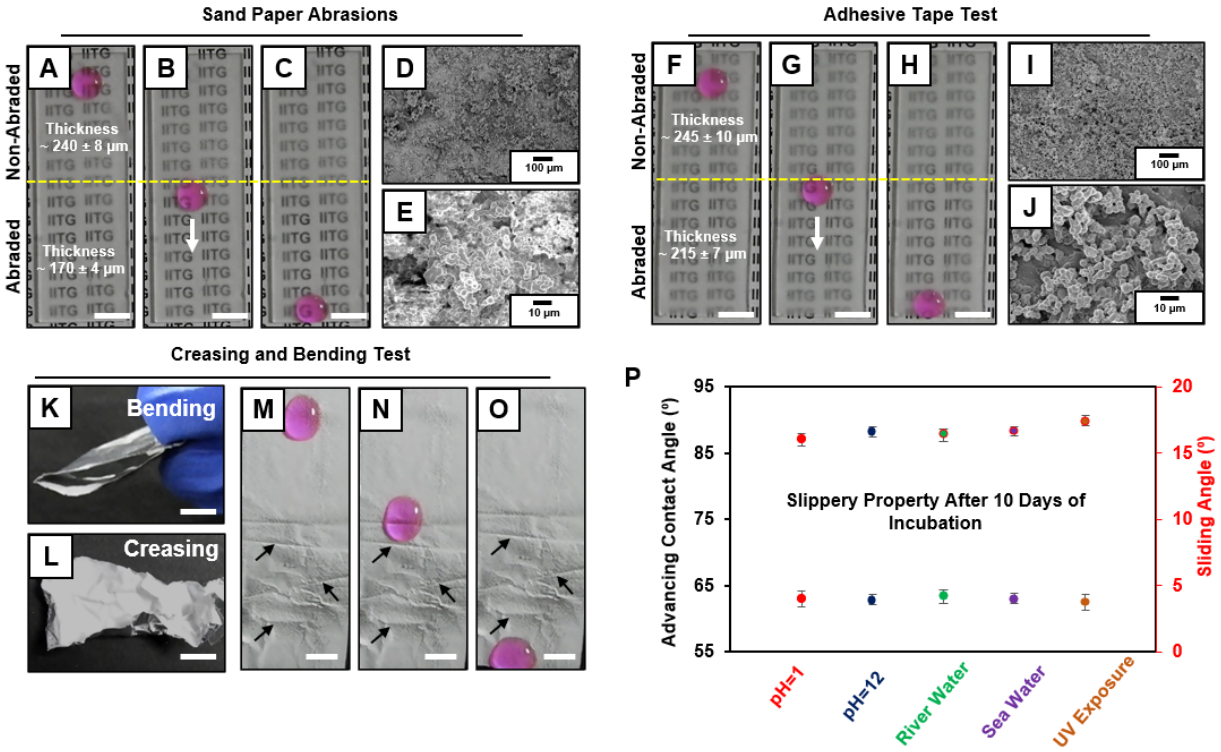

Figure 4.5 (A-C) Digital snapshot images of slipping behaviour of aqueous droplet on both sand paper abraded and non-abraded regions (scale bar: 1 cm) (D-E) FESEM images of the polymeric coating after abrasions with sand paper at low (D: scale bar 100 µm) and high magnifications (E: scale bar 10 µm). (F-H) Aqueous droplet freely slipped away on both adhesive tape abraded and non-abraded regions after infusion of silicone oil (dotted line separated the non-abraded regions from the abraded one). (I-J) FESEM images of adhesive-tape abraded region at low (I: scale bar 100 µm) and high magnifications (I: scale bar 10 µm). (K-L) Digital images (scale bar: 1 cm) for the process of bending (K) and creasing (L). (M-O) Sliding behaviour of aqueous droplet on the coated aluminium after bending and creasing, (arrows signified the portions which were bended/creased) (P) A plot accounting advancing contact angle and sliding angle of beaded water on as-synthesized SLIPS that was exposed to practically relevant various harsh aqueous and UV exposure.

irradiation for the prolonged (10 days) duration. However, the embedded water wettability remained intact in the synthesized SLIPS, as phases and relevant liquid food products, including highly acidic (pH 1) and alkaline (pH 13) aqueous shown in Fig 4.5 P. As-synthesized SLIPS was found to be

antifouling in a various complex aqueous phase, hot (85 °C) coffee, cold (5 °C) orange juice, and honey (Fig 4.6 A−P).

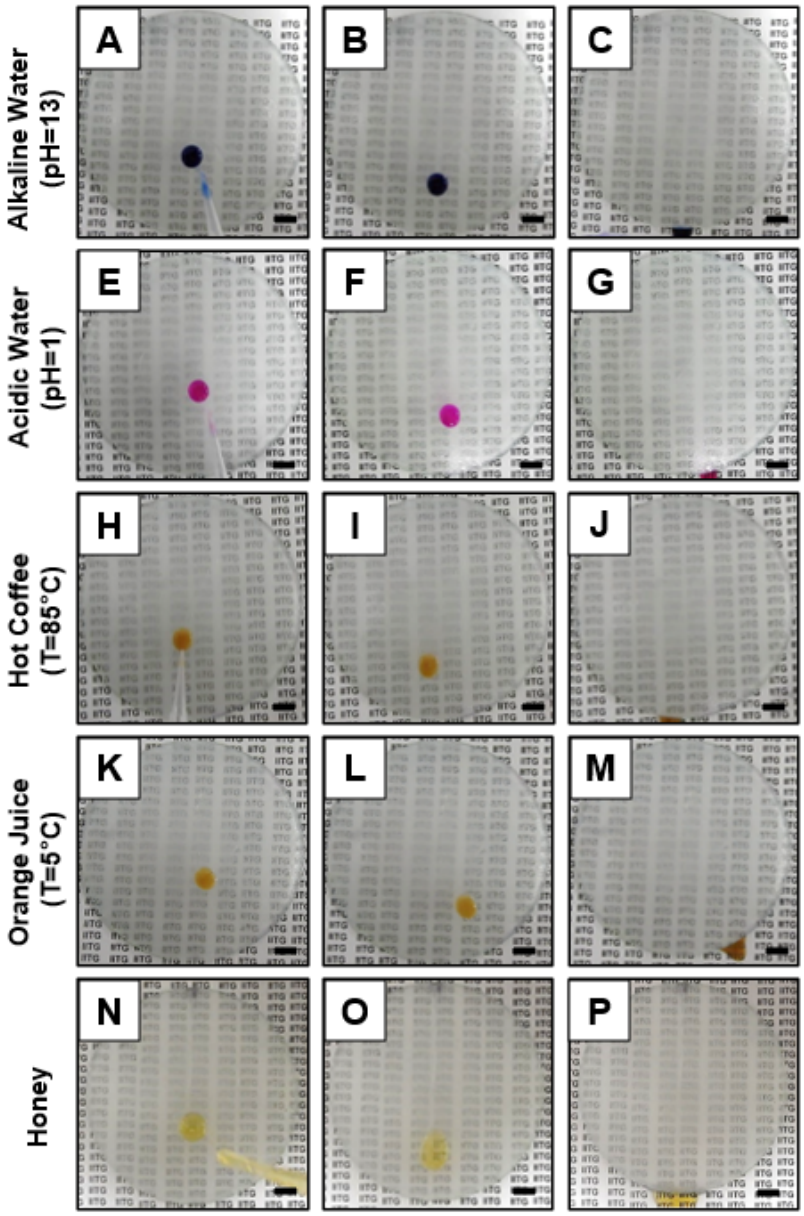

Figure 4.6 (A-P) Digital images illustrating movement of different complex aqueous probe liquids, including highly alkaline (pH 13; A−C) and acidic (pH 1; D−F) aqueous phase, hot coffee (85 °C; G−I), cold orange juice (5 °C; J−L), and honey (M−O) on silicone oil-infused polymeric coating on a watch glass.

4.3.4 Impact of Different Chemical Modifications on SLIPS

In the past, reported SLIPS remained mostly chemically inactive due to the optimization of the top of the interface with a chemically inert layer of either long-tail hydrocarbon or fluorinated derivatives. On the other hand, there are few reports of chemically reactive porous interfaces, but most of them were inherently adopted with superhydrophobicity. Thus, the detailed examination of the impact of

different chemical functionalities on the slippery property remained a challenge. Here, the chemical reactive and hydrophilic porous interface became SLIPS, immediately after lubrication with selected oils, was further extended to study the exact role of water wettability and surface free energy for designing the liquid-infused slippery interface. The residual acrylate groups were allowed to adopt various functional groups through simple 1,4 conjugate addition reactions at ambient conditions, without the generation of any side products. Before lubricating with silicone oil, the reactive porous polymeric coatings (having WCA ≈ 20°) were individually post modified with various alkyl amines with the gradually increasing length of the hydrocarbon tail starting from propylamine to octadecylamine. The successful post-covalent modifications of the chemically reactive polymeric coating with different alkyl amines were characterized by FTIR analysis and surface energy calculation, as shown in Fig. 4.7 A and Fig. 4.7 B, respectively. The surface energy significantly changed depending on the selection of post-covalent modifications, as noted in Fig. 4.7 B. With the increment of hydrocarbon length of the selected alkylamine, the contact between the aqueous phase and the polymeric coating decreases, and therefore surface energy decreases as shown in Fig. 4.7 B. The polymeric coating that is treated with a lower analog of pentylamine (i.e., propylamine and butylamine) remained extremely hydrophilic with a WCA of 0°. Unfortunately, even after lubrication, these post-modified interfaces failed to display the slippery property, and beaded water droplets spread on the lubricated interface. However, the chemical post modification of the same polymeric interface with pentylamine lead to a sharp rise in WCA from 0 to 147° in the porous polymeric coating, and the

A

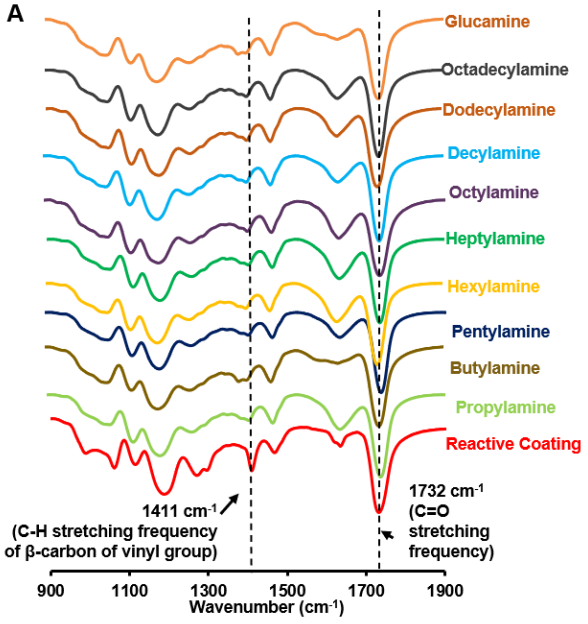

B

Different Post-Chemical Modification	Surface Energy (mN/m)
Propylamine	61.2 ± 0.8
Butylamine	52.1 ± 0.9
Pentylamine	11.6 ± 0.1
Hexylamine	11.4 ± 0.1
Heptylamine	11.1 ± 0.1
Octylamine	10.9 ± 0.1
Decylamine	10.7 ± 0.1
Dodecylamine	10.6 ± 0.1
Octadecylamine	10.6 ± 0.1
Glucamine	68.3 ± 0.4

Figure 4.7 (A) FTIR spectra of the polymeric coating without and with post-modifications with different alkylamines. (B) Accounting the change in surface energy with post covalent modification of the chemically reactive porous coating with different alkylamines.

lubricated interface displayed slippery properties with advancing WCA of ~86° and sliding angle of ~2°, as shown in Fig 4.8 A. Further, an increase in the hydrocarbon chain length of the selected alkyl amines for post chemical modification of the chemically reactive porous coating provided porous polymeric coating with higher WCA. However, the change in hydrophobicity of the porous polymeric

Coating With or Without Post-Chemical Modifications	Water Contact Angle (°)	Water Wettability After Infusion of Silicone Oil	
		θ_{CA}(°)	Sliding Angle (°)
Reactive Coating	20.3 ± 0.5	85.7 ± 0.3	2.1 ± 0.3
Propylamine	0	Spreading	NA
Butylamine	0	Spreading	NA
Pentylamine	147.4 ± 0.5	85.9 ± 0.4	1.8 ± 0.6
Hexylamine	148.5 ± 0.5	86.1 ± 0.3	1.9 ± 0.3
Heptylamine	149.4 ± 0.6	86.2 ± 0.4	1.8 ± 0.2
Octylamine	151.7 ± 0.4	86.3 ± 0.4	1.8 ± 0.7
Decylamine	154.3 ± 0.4	87.5 ± 0.4	1.8 ± 0.4
Dodecylamine	154.1 ± 0.7	87.5 ± 0.6	1.7 ± 0.4
Octadecylamine	155.7 ± 0.7	87.7 ± 0.5	1.5 ± 0.5

Figure 4.8 Accounting the water wettability of the reactive and post-modified polymeric coating before and after lubrication with silicone oil (AR 20).

coating has minimum impact on slippery property after infusion of silicone oil as shown in Fig 4.8. The interfaces modified with higher analouges of pentylamine remained equally efficient to attain require chemical compatibility with selected lubricant, i.e. silicone oil. Both the slip angles and WCAs remained very similar for all polymeric coatings that were treated with higher analogs of pentylamine and lubricated with silicone oil.

4.3.5 In Situ and Spatially Selective Covalent Modification of the Chemically Reactive SLIPS.

The infused lubricant protected the residual acrylate groups of porous polymeric coating from aqueous exposure; however, the residual acrylate groups in the chemically reactive SLIPS became readily reactive towards the organic phase having amine-containing small molecules. In general, an aqueous ink was used for spatially selective and contact-based post covalent modification to achieve the patterned interface with specific functional groups that display hydrophilicity/slippery wettability. However, a report of the spatially selective modification directly using organic solvents is yet to be

reported as the organic liquids with low surface tension can arbitrarily spill and spread on a commonly used solid and dry interface in air. Accordingly, spatially selective deposition of any water-insoluble functional molecules (i.e., conductive polymer, catalyst, etc.) is a persistent challenge. In general, the conventional SLIPS is chemically inert as the post modifications with long-tail hydrocarbons or fluorinated molecules were mandatorily associated, prior to the lubrication process. The currently synthesized chemically reactive porous polymeric coating acted as a base layer to infuse a selected lubricant could react with primary amine-containing small molecules through 1,4-conjugate addition reaction in the organic medium following two independent processes. The covalent modification performed before lubrication of the chemically reactive polymeric coating was referred to as pre-modified SLIPS, and the modification of the lubricated polymeric coating was denoted as "in situ" modified SLIPS. In this study, the synthesized chemically reactive SLIPS was unprecedentedly extended for spatially selective and "in situ" covalent modification with a primary amine-containing nucleophile, even in the presence of the lubricated phase in the porous polymeric coating. The lubricant-infused chemically reactive interface was directly and spatially selectively exposed to

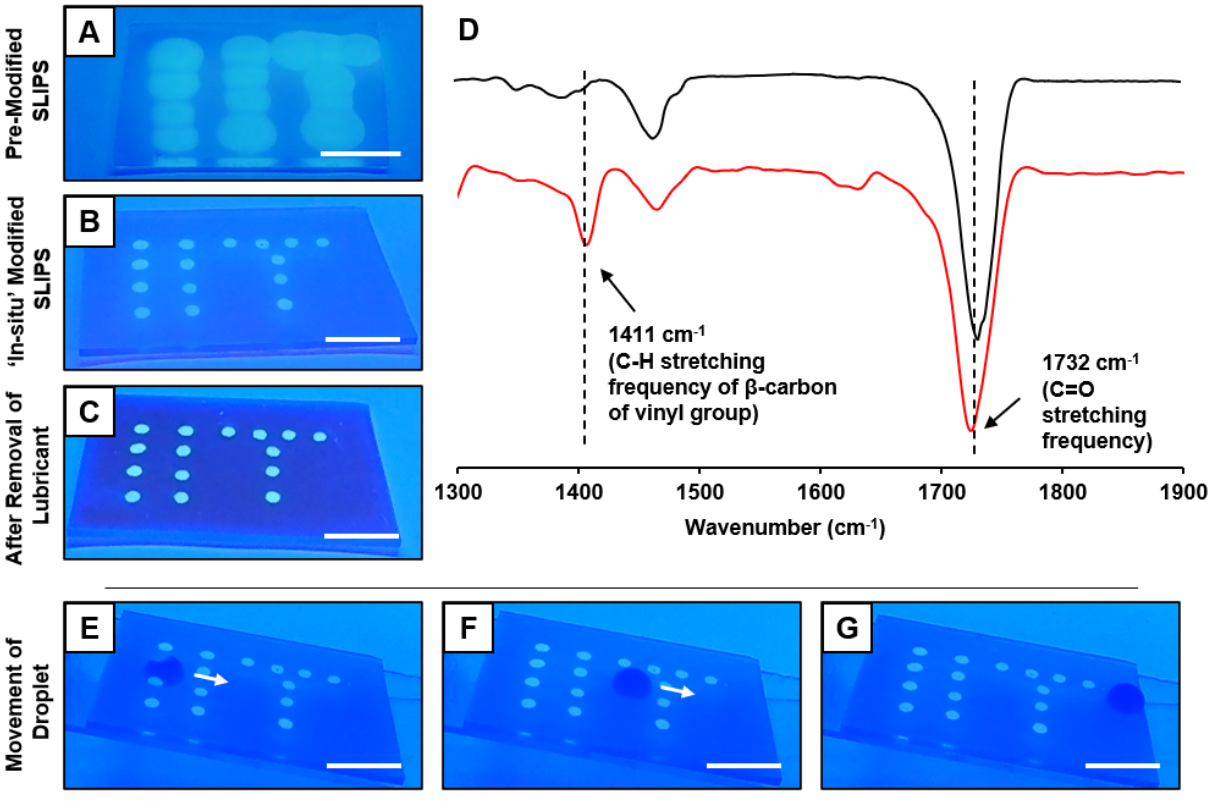

Figure 4.9 Digital images of chemically reactive SLIPS that are premodified (A, modification before lubrication) and in situ-modified (B, modification directly on lubricated surface) with solution of dansyl cadaverine (DC) in methanol. (C) Digital image of in situ modified SLIPS after the removal of lubricate phase. (D) FTIR spectra of chemically reactive SLIPS with (black) and without (red) in situ chemical modification through 1,4 conjugate addition reaction with DC. (E−G) Digital images illustrating the translation of beaded aqueous droplet on in situ modified SLIPS. All the digital images are acquired under UV light. Scale bars are 1 cm.

solutions of selected nucleophiles in an organic solvent having low surface tension. In the current study, two different approaches (a) premodification and (b) in situ-modification of chemically reactive SLIPS were adopted for direct comparison of its ability in developing spatially selective post covalent modification. The pattern in the form of "IIT" was generated on a chemically reactive SLIPS by transferring a series of droplets (0.7 μL) of dansyl cadaverine (DC) solution in methanol (MeOH) at different locations of the chemically reactive polymeric coating before (denoted as pre-modification) and after (referred as in situ-modification) lubrication. Before lubrication, the solution of DC in MeOH randomly and immediately spread on the dry polymeric coating, as revealed under UV light (Fig 4.8). However, the polymeric coating remained slippery after the infusion of the lubricant. In comparison, after lubrication, a chemically reactive SLIPS was exposed to a solution of DC in MeOH to prepare a spatially selective post modification through 1,4 conjugated addition reaction at ambient condition. In the end, a pattern of "IIT" was generated with well-defined circular spots as observed under UV light (Fig 4.9 B). Moreover, this pattern remained stable even after removing the lubricant phase from the polymeric coating, as shown in Fig 4.9 C. This simple study confirmed the successful transfer of DC to the polymeric coating through the lubricant phase without any arbitrary spillage. Further, the exposure of DC solution to chemically reactive SLIPS caused a significant depletion of the IR peak at 1411 cm^{-1} in the polymeric coating, which revealed the in situ 1,4 conjugate addition reaction between amine of DC and residual acrylate groups of the SLIPS at ambient condition (Fig 4.9 D). Even after the in-situ modification of the SLIPS with the selected nucleophile, the slippery property remained intact, as shown in Fig 4.9 E− G. Thus, the current design provided a simple basis for well-defined and spatially selective in situ modification of the chemically reactive SLIPS with primary amine-containing nucleophiles. This principle can be used for developing multifunctional SLIPS.

4.4 Conclusions

In summary, a chemically reactive SLIPS was rationally introduced through the strategic association of residual acrylate groups in the inherently hydrophilic porous polymeric spray coating, where acrylate groups not only allowed the adaptation of chemical reactivity through simple 1,4-conjugate addition reaction at ambient condition but also provided essential chemical compatibility towards various selected lubricants, without requiring any hydrophobization. Eventually, after selected lubrication, the hydrophilic polymeric coating loaded with chemically reactive residual functionality displayed slippery properties. The as-synthesized chemically reactive SLIPS remained highly tolerant towards various physical and chemical challenges. The impact of different chemical modulation was investigated through post-covalent modification of the residual acrylate groups with selected alkyl

amines. Further, various nucleophiles could be strategically and covalently embedded following an in-situ modification process for developing different functional SLIPS.

4.5 References

1. Li, X.-M.; Reinhoudt, D.; Crego-Calama, M. *Chem. Soc. Rev.* **2007**, *36*, 1350−1368.
2. Chu, Z.; Feng, Y.; Seeger, S. *Angew. Chem., Int. Ed.* **2015**, *54*, 2328−2338.
3. Su, B.; Tian, Y.; Jiang, L. *J. Am. Chem. Soc.* **2016**, *138*, 1727−1748.
4. Lai, Y.; Huang, Z.; Ge, M.; Zhang, K.-Q.; Chen, Z.; Chi, L.; Chi. *Small* **2016**, *12*, 2203−2224.
5. Wong, T.-S.; Kang, S. H.; Tang, S. K. Y.; Smythe, E. J.; Hatton, B. D.; Grinthal, A.; Aizenberg, J. *Nature* **2011**, *477*, 443−447.
6. Anand, S.; Paxson, A. T.; Dhiman, R.; Smith, J. D.; Varanasi, K. K. *ACS Nano* **2012**, *6*, 10122−10129.
7. Kim, P.; Wong, T.-S.; Alvarenga, J.; Kreder, M. J.; Adorno-Martinez, W. E.; Aizenberg, J. *ACS Nano* **2012**, *6*, 6569−6577.
8. Yao, X.; Hu, Y.; Grinthal, A.; Wong, T.-S.; Mahadevan, L.; Aizenberg, J. *Nat. Mater.* **2013**, *12*, 529−534.
9. Subramanyam, S. B.; Azimi, G.; Varanasi, K. K. *Adv. Mater. Interfaces* **2014**, *1*, 1300068.
10. Manabe, K.; Kyung, K.-H.; Shiratori, S. *ACS Appl. Mater. Interfaces* **2015**, *7*, 4763−4771.
11. Wang, Y.; Zhang, H.; Liu, X.; Zhou, Z. *J. Mater. Chem. A* **2016**, *4*, 2524−2529.
12. Guo, J.; Fang, W.; Welle, A.; Feng, W.; Filpponen, I.; Rojas, O. J.; Levkin, P. A. *ACS Appl. Mater. Interfaces* **2016**, *8*, 34115−34122.
13. Park, K.-C.; Kim, P.; Grinthal, A.; He, N.; Fox, D.; Weaver, J. C.; Aizenberg, J. *Nature* **2016**, *531*, 78−82.
14. Yu, L.; Chen, G. Y.; Xu, H.; Liu, X. *ACS Nano* **2016**, *10*, 1076−1085.
15. Wu, Y.; Zhou, S.; You, B.; Wu, L. *ACS Nano* **2017**, *11*, 8265−8272.
16. Dai, X.; Sun, N.; Nielsen, S. O.; Stogin, B. B.; Wang, J.; Yang, S.; Wong, T.-S. *Sci. Adv.* **2018**, *4*, No. eaaq0919.
17. McBride, S. A.; Dash, S.; Varanasi, K. K. *Langmuir* **2018**, *34*, 12350−12358.
18. Park, K.-C.; Kim, P.; Grinthal, A.; He, N.; Fox, D.; Weaver, J. C.; Aizenberg, J. *Nature* **2016**, *531*, 78−82.
19. Howell, C.; Grinthal, A.; Sunny, S.; Aizenberg, M.; Aizenberg, J. *Adv. Mater.* **2018**, *30*, 1802724.
20. Kreder, M. J.; Alvarenga, J.; Kim, P.; Aizenberg, J. *Nat. Rev. Mater.* **2016**, *1*, 15003.

21. Wang, W.; Timonen, J. V. I.; Carlson, A.; Drotlef, D.-M.; Zhang, C. T.; Kolle, S.; Grinthal, A.; Wong, T.-S.; Hatton, B.; Kang, S. H.; Kennedy, S.; Chi, J.; Blough, R. T.; Sitti, M.; Mahadevan, L.; Aizenberg, J. *Nature* **2018**, *559*, 77−82.
22. Hou, X.; Li, J.; Tesler, A.; Yao, Y.; Wang, M.; Min, L.; Sheng, Z.; Aizenberg, J. *Nat. Commun.* **2018**, *9*, 733.
23. Rapoport, L.; Solomon, B. R.; Varanasi, K. K. *ACS Appl. Mater. Interfaces* **2019**, *11*, 16123−16129.
24. Manabe, K.; Matsubayashi, T.; Tenjimbayashi, M.; Moriya, T.; Tsuge, Y.; Kyung, K.-H.; Shiratori, S. *ACS Nano* **2016**, *10*, 9387−9396.
25. Chen, X.-c.; Ren, K.-f.; Wang, J.; Lei, W.-x.; Ji, J. *ACS Appl. Mater. Interfaces* **2017**, *9*, 1959−1967.
26. Scarratt, L. R. J.; Zhu, L.; Neto, C. *Langmuir* **2019**, *35*, 2976−2982.
27. Xiang, T.; Zhang, M.; Sadig, H. R.; Li, Z.; Zhang, M.; Dong, C.; Yang, L.; Chan, W.; Li, C. *Chem. Eng. J.* **2018**, *345*, 147−155.
28. Kratochvil, M. J.; Welsh, M. A.; Manna, U.; Ortiz, B. J.; Blackwell, H. E.; Lynn, D. M. *ACS Infect. Dis.* **2016**, *2*, 509−517.
29. Tenjimbayashi, M.; Togasawa, R.; Manabe, K.; Matsubayashi, T.; Moriya, T.; Komine, M.; Shiratori, S. *Adv. Funct. Mater.* **2016**, *26*, 6693−6702.
30. He, W.; Liu, P.; Jiang, J.; Liu, M.; Li, H.; Zhang, J.; Luo, Y.; Cheung, H.-Y.; Yao, X. *J. Mater. Chem. A* **2018**, *6*, 4199−4208.
31. Wang, J.; Gao, W.; Zhang, H.; Zou, M.; Chen, Y.; Zhao, Y. *Sci. Adv.* **2018**, *4*, No. eaat7392.
32. Guo, P.; Wang, Z.; Heng, L.; Zhang, Y.; Wang, X.; Jiang, L. *Adv. Funct. Mater.* **2019**, *29*, 1808717.
33. Paulssen, D.; Hardt, S.; Levkin, P. A. *ACS Appl. Mater. Interfaces* **2019**, *11*, 16130−16138.
34. Huang, Y.; Stogin, B. B.; Sun, N.; Wang, J.; Yang, S.; Wong, T.-S. *Adv. Mater.* **2017**, *29*, 1604641.
35. Wang, Z.; Liu, Y.; Guo, P.; Heng, L.; Jiang, L. *Adv. Funct. Mater*. **2018**, *28*, 1801310.
36. Manabe, K.; Matsubayashi, T.; Tenjimbayashi, M.; Moriya, T.; Tsuge, Y.; Kyung, K.-H.; Shiratori, S. *ACS Nano* **2016**, *10*, 9387−9396.
37. Zhan, K.; Hou, X.; Microscale, T. *Small* **2018**, *14*, 1703283.
38. Bazyar, H.; Lv, P.; Wood, J. A.; Porada, S.; Lohse, D.; Lammertink, R. G. H. *Soft Matter* **2018**, *14*, 1780−1788.
39. Hou, X. *Natl. Sci. Rev.* **2020**, *7*, 9.

40. Liu, W.; Wang, M.; Sheng, Z.; Zhang, Y.; Wang, S.; Qiao, L.; Hou, Y.; Zhang, M.; Hou, X. *Ind. Eng. Chem. Res.* **2019**, *58*, 11976−11984.
41. Chen, Z.; Wang, H.; Tang, Y.; Wang, M.; Huang, L.; Min, L.;Meng, H.; Chen, S.; Jiang, L.; Hou, X. *Sci. Adv.* **2018**, *4*, No. eaao6724.
42. Bazyar, H.; Javadpour, S.; Lammertink, R. G.H. *Adv. Mater. Interfaces* **2016**, *3*, 1600025.
43. Hou, X. *Adv. Mater.* **2016**, *28*, 7049−7064.
44. Buck, M. E.; Schwartz, S. C.; Lynn, D. M. *Chem. Mater*. **2010**, *22*, 6319−6327.
45. Manna, U.; Broderick, A. H.; Lynn, D. M. *Adv. Mater.* **2012**, *24*, 4291−4295.
46. Li, J.; Li, L.; Du, X.; Feng, W.; Welle, A.; Trapp, O.; Grunze, M.; Hirtz, M.; Levkin, P. A. *Nano Lett.* **2015**, *15*, 675−681.
47. Kreder, M. J.; Alvarenga, M. J.; Kim, J.; Aizenberg, J. *Nat. Rev. Mater.* **2016**, *1*, 15003.
48. Kim, P.; Kreder, M. J.; Alvarenga, J.; Aizenberg, J. *Nano Lett.* **2013**, *13*, 1793−1799.
49. You, I.; Lee, T. G.; Nam, Y. S.; Lee, H. *ACS Nano* **2014**, *8*, 9016−9024.
50. Vogel, N.; Belisle, R. A.; Hatton, B.; Wong, T. S.; Aizenberg, J. *Nat. Commun.* **2013**, *4*, 2176.
51. Manna, U.; Lynn, D. M. *Adv. Mater.* **2015**, *27*, 3007−3012.
52. Huang, W.-P.; Chen, X.; Hu, M.; Hu, D.-F.; Wang, J.; Li, H.-Y.; Ren, K.-F.; Ji, J. *Chem. Mater.* **2019**, *31*, 834−841.
53. Wei, Q.; Schlaich, C.; Prévost, S.; Schulz, A.; Böttcher, C.; Gradzielski, M.; Qi, Z.; Haag, R.; Schalley, C. A. *Adv. Mater.* **2014**, *26*, 7358−7364.
54. Liu, M.; Wang, Z.; Liu, P.; Wang, Z.; Yao, H.; Yao, X. *Sci. Adv.* **2019**, *5*, No. eaaw5643.
55. Zhou, J.; Han, P.; Liu, M.; Zhou, H.; Zhang, Y.; Jiang, J.; Liu, P.; Wei, Y.; Song, Y.; Yao, X. *Angew. Chem., Int. Ed*. **2017**, *56*, 10462−10466.
56. Bechler, S. L.; Lynn, D. M. *Biomacromolecules* **2012**, *13*, 1523−1532.
57. Rather, A. M.; Manna, U. *Chem. Mater*. **2016**, *28*, 8689−8699.
58. Parbat, D.; Manna, U. *Chem. Sci*. **2017**, *8*, 6092−6102.
59. Rather, A. M.; Mahato, S.; Maji, K.; Gogoi, N.; Manna, U. *Nanoscale* **2017**, *9*, 16154−16165.
60. Maji, K.; Manna, U. *J. Mater. Chem. A* **2018**, *6*, 6642−6653.

Title: Design of Chemically Patterned Hydrophilic SLIPS for Achieving Efficient Water Harvesting *

Efficient water harvesting with a robust interface is important for realistic applications. Here, a dual chemically reactive porous polymeric interface has been introduced to adopt various bio-inspired interfaces for the direct comparison of their water-harvesting performances using an identical experimental setup. An improved water-harvesting performance (1100 mg cm^{-2} h^{-1}) was observed when an edible oil (olive oil)-infused hydrophilic and slippery interface was used, in comparison to both hydrophobic slippery liquid-infused porous surface (SLIPS, 800 mg cm^{-2} h^{-1}) and superhydrophobic interface (250 mg cm^{-2} h^{-1}). Furthermore, the strategic physical confinement of the hydrophilic-slippery interface and the specific arrangement of chemically modulated hydrophilic patterns on a hydrophilic-slippery background accelerated the shedding of condensed water droplets from 107 s to only 15 s. Eventually, a physically confined hydrophilic SLIPS with chemically modulated patterns yielded a highly efficient (4400 ± 190 mg cm^{-2} h^{-1}) water-harvesting SLIPS.

*Maji, K.; Das, A.; Dhar, M.; Manna, U. *J. Mater. Chem. A* **2020**, *8*, 25040–25046.

5.1 Introduction

Enhanced condensation, the rapid growth of water droplets, and the immediate shedding of the mature droplets are the primary basis for efficient water harvesting and various other relevant applications.[1–8] For example, an acute worldwide shortage of potable water has been recognized as a challenge to remedy, and the design of an unconventional yet effective alternative could be a wise approach to solving this severe problem.[7–9] In the past, various bio-mimicked wettability and bio-inspired architectures were rationally associated to achieve faster growth of condensed water droplets and rapid shedding of water droplets.[9–17] However, there have been few studies that successfully produced durable bio-inspired interfaces that displayed a satisfactory water-harvesting performance.[3,9–18] In the past, superhydrophobic interfaces are associated with different patterns to increase water-harvesting efficiency.[9–13] However, the superhydrophobic interfaces, loaded with metastable trapped air,[19] were an inappropriate choice for the realistic application of water harvesting due to the inherent intolerance of superhydrophobicity in highly humid environments.[15,20,21] During the course of the water-harvesting process, a continuous invasion of humid air occurs in the empty space of the hierarchical features of the superhydrophobic interface, followed by the condensation of tiny water droplets in the hierarchically featured interface, and this is expected to displace the metastable trapped air that conferred the Cassie–Baxter state.[15,20,21] A loss of meta-stable trapped air from the superhydrophobic interface would compromise the heterogeneous (Cassie–Baxter) wettability, and the adhesiveness of the interface to the beaded water droplets would increase.[22] Thus, delayed shedding of the condensed water droplet on a superhydrophobic interface is expected, and this would affect significantly the water-harvesting performance in practical settings. As an alternative approach, the slippery liquid-infused porous surfaces (SLIPS), which was inspired by the Nepenthes pitcher plant, was integrated with different geometrical patterns for achieving efficient water-harvesting interfaces.[3,14–18] The general approach for preparing a SLIPS is the lubrication of a chemically inert and hydrophobic porous matrix with a liquid that remains immiscible with the probe liquid.[3,14–18,23–25] In 2012, Varanasi and co-workers' introduced a seminal report which described the enhanced condensation of water droplets on such SLIPS.[3] Later, Aizenberg and co-workers' extended this same bio-inspired slippery interface for fast shedding of condensed water droplets through the association of asymmetric bumps that mimicked the structure of Namib Desert beetles and cacti.[14] However, the water-harvesting ability remained very low when compared to previously reported hydrophobic SLIPS.[14,16–18] Inspired by the rice leaf, Wong and co-workers' introduced a hydrophilic and directional SLIPS by infusing a synthetic hydrophilic (hydroxy-terminated PDMS) lubricant in an array of hierarchically featured micropillars,[15] and such an interface harvested water from the artificial fog with an efficiency of approximately 435

mg cm^{-2} h^{-1}, which was approximately 144 times higher than that of conventional hydrophobic (Krytox infused) SLIPS.[15] Even after the association of such complex and different topography with durable SLIPS, overall, the water harvesting ability of the reported SLIPS remained mostly below 2000 mg cm^{-2} h^{-1}.[3,14–18] Recently, various smart SLIPS, including patterned SLIPS, hydrophobic SLIPS, and hydrophilic SLIPS, have been introduced through (a) a strategic and spatially selective modulation of chemistry in the porous matrix and (b) an appropriate selection of lubricants.[26–28] In the past, chemically patterned SLIPS were mostly extended for droplet manipulations and bioengineering applications; [26–29] however, such interfaces were yet to be examined for water-harvesting applications. Moreover, in the past, different synthetic lubricants (Krytox and silicone oil) were commonly infused in hydrophobic or superhydrophobic interfaces for achieving hydrophobic (water contact angle (WCA) above 90^0) SLIPS.[3,14–18,21–24] In contrast to earlier approaches,[14–16,18] here, we selected a natural and edible oil for preparing hydrophilic SLIPS. Thus, even if the collected water becomes contaminated with a tiny amount of edible and natural oil, it is not necessary to purify the collected water. In this chapter, a dual chemically reactive and porous polymeric interface (DCRPPI) has been extended for preparing various bio-mimicked interfaces, including (i) a superhydrophobic interface (SHI), (ii) hydrophobic SLIPS (HB-SLIPS), and (iii) hydrophilic SLIPS (HL-SLIPS), as shown in Fig. 5.1 A. Furthermore, a spatially selective controlled chemical modulation on a chemically reactive interface allowed us to develop an (iv) chemically patterned superhydrophobic interface (CP-SHI), and furthermore, the selection of appropriate lubrication yielded (v) chemically patterned hydrophobic SLIPS (CPHB- SLIPS) and (vi) chemically patterned hydrophilic SLIPS (CPHL- SLIPS), as shown in Fig. 5.1 A. These different bio-inspired interfaces with and without spatially selective chemical patterns were examined in the presence and absence of appropriate lubrication for comparing the water-harvesting performance under a common experimental setup (Fig 5.1 B). Interestingly, a strategic association of chemically modulated hydrophilic patterns (WCA approximately 6^0) on hydrophilic SLIPS (CP-HL-SLIPS; WCA approximately 80^0) facilitated (a) faster growth of water droplets and (b) rapid shedding of those water droplets in comparison to other bio-inspired interfaces. Eventually, such interfaces enabled water to be harvested from the artificial fog with an efficiency of 2950 ± 210 mg cm^{-2} h^{-1}, which was significantly higher than that obtained with other reported water-harvesting SLIPS.[3,14–18] Moreover, an arrangement of a single array of hydrophilic spots on a physically confined hydrophilic SLIPS allowed to improve the water-harvesting performance with an unprecedented efficiency of 4400 ± 190 mg cm^{-2} h^{-1}.

5.2 Experimental Sections

5.2.1 Materials

Branched poly(ethyleneimine) (BPEI, MW ~ 25 000 Da), dipentaerythritol penta/hexa acrylate (5 Acl, MW ~ 524.21 g mol^{-1}), octadecyl acrylate, rhodamine cadaverine (Rh-NH_2), fluorescein isothiocyanate (FITC) purchased from Sigma-Aldrich, Bangalore, India. D-glucamine (>95%) was obtained from TCI (Tokyo Chemical Industry). Krytox Oil (Dupont KrytoxR GPL 103) was procured from H Costenoble GmbH & Co. KG (Eschborn, Germany). Pentanol procured from Alfa Aesar. Ethanol, THF was procured from Merck Specialties Private Limited, India. A-4 sized printing paper was acquired from J K Copier. Spray bottles (100 mL capacity, nozzle diameter 400 mm) and ultrasonic cool mist humidifier (Crane, EE-5301) were obtained from Amazon India. Sandpaper (grit no. 400) was purchased from Million International, India. Olive oil (Borges Extra Virgin Olive Oil), Fountain Pen (Legend Executive Fountain Pen), Glass slides (Boroleb, India), and adhesive tape (Jonson tape Ltd. India) were acquired from different local sources. The sand was thoroughly washed with water before the experimental use.

5.2.2 General Considerations

All Attenuated total reflection infrared (ATR-IR) spectra were recorded using PerkinElmer UATR Two at ambient conditions. The contact angles, roll-off angles, sliding angles were obtained from Kruss drop-Shape Analyser-DSA25 instrument at laboratory temperature (~25°C). The FESEM images were acquired using Sigma Carl Zeiss scanning electron microscope (each sample was coated with a conducting gold layer prior to imaging). All fluorescence microscopic images were captured using a ZEISS Axio Vert.A1 inverted microscope with a 10X objective. The contact angles were taken using 5µl water droplets at four different locations of the same synthesized interface. The Fog harvesting was carried out by using an ultrasonic cool mist humidifier (Crane, EE-5301). The Digital images and videos were captured using a Nikon Coolpix b700 digital camera.

5.2.3 Fabrication of Dual Chemically Reactive Porous Polymeric Interface (DCRPPI)

The dual chemically reactive porous polymeric interface (DCRPPI) was prepared following the previously reported method. In brief, the reactive reaction mixture was prepared by mixing 10 mL 5Acl solution (0.252M in pentanol) and 3 mL BPEI solution (0.105M in pentanol with respect to the polymer repeat unit). The reaction mixture agitated vigorously for 5 minutes, which yielded a milky turbid solution. Then, the turbid reaction mixture (13 mL) was sprayed uniformly onto the A4 Size paper at an angle of nearly 90° over a 623.7 cm^2 area from a distance of 15 cm using a commercially available spraying bottle. Then, the coated substrates were kept in the air overnight for solvent

evaporation. The coated paper was washed thoroughly with THF for 15 minutes and kept in the air for drying.

5.2.4 Post Covalent Modification of DCRPPI

The dual residual chemically reactivities of DCRPPI were strategically exploited for post covalent modifications—which were essential to achieve various bioinspired wettability. For example, superhydrophobic interface (SHI) was prepared through the post chemical modification of DCRPPI with octadecyl acrylate (ODAC), where residual amine of DCRPPI readily reacted with acrylate group of ODAC through 1,4-conjugate addition reaction at ambient condition. Firstly, the chemically reactive interface (DCRPPI) was submerged in a THF solution of octadecyl acrylate (5 mg/mL) for 12 h followed by washing the coated substrate thoroughly with fresh THF multiple times to remove excess and loosely deposited octadecyl acrylate. Finally, the post-modified coating was kept in a vacuum for drying. The octadecyl acrylate treatments provided the desired superhydrophobicity. Further, treatment of this ODAC-treated coating with D-glucamine yielded a hydrophilic interface, where residual acrylate groups of DCRPPI readily reacted with primary amines of D-glucamine through 1,4-conjugate addition reaction. An ODAC-treated coating was subsequently treated with the solution of D-glucamine (5 mg/ml) in 25% ethanol solution for dual post covalent modification. A similar protocol was followed for single and dual post-modification of DCRPPI with Rh-NH_2 and FITC.

5.2.5 Fabrication of Chemically Patterned Superhydrophobic Interface (CP-SHI)

At first, the desired pattern was printed on a paper prior to depositing a chemically reactive superhydrophobic coating, where the DCRPPI on the pre-printed substrate (which contains an array of black dots aligned with the certain spacing) was treated with ODAC and the residual acrylate groups were exploited to develop spatially selected chemical modulation with D-glucamine. The chemically reactive SHI interface was fabricated on a pre-printed paper. The pre-printed each black spot guided to transfer the solution of D-glucamine (5 mg/mL in 25 % ethanol solution) on the SHI using a fountain pen and kept the interface as it was for 6 h. After that, substrates were washed thoroughly with ethanol for 1 h and kept in the air for drying. The spatially selected chemical modification with D-glucamine provided the hydrophilic patterns on the superhydrophobic interface—which was denoted as CP-SHI.

5.2.6 Fabrication of HL-SLIPS, HB-SLIPS, CP-HL-SLIPS, and CP-HB-SLIPS

HL-SLIPS, CP-HL-SLIPS were prepared through the infusion of olive oil to the SHI and CP-SHI respectively. Similarly, HB-SLIPS, CP-HB-SLIPS were fabricated through the infusion of synthetic krytox oil to the SHI and CP-SHI respectively. In brief, 20 µL of lubricant spread on the respective

polymeric coating using a tracing paper over an area of 6 cm^2, and the excess lubricant was removed by vertically placing the substrates for 10 min.

5.2.7 Fog Harvesting Set-up

An ultrasonic cool mist humidifier (Crane, EE-5301) with a flow rate of 100 mL/h was used for the fog harvesting set up to evaluate the water harvesting performance of i) superhydrophobic interface (SHI), ii) hydrophobic-SLIPS (HB-SLIPS), and iii) hydrophilic-SLIPS (HL-SLIPS), iv) chemically patterned superhydrophobic interface (CP-SHI), and further, the selection of appropriate lubrication yielded v) chemically patterned hydrophobic-SLIPS (CP-HB-SLIPS) and vi) chemically patterned hydrophilic-SLIPS (CP-HL-SLIPS). All above-mentioned interfaces were placed at a fixed distance (5 cm) from the outlet of the humidifier and the bio-inspired interfaces were kept with a tilting angle ~ 45° from the horizontal plane. A clean and dry beaker was placed under the bio-mimicked interfaces at a distance of 10 cm for collecting the water droplets from the bio-inspired interface. The weight of the collected water droplets was measured after every certain interval of time. The experimental temperature was maintained at 25 ± 2°C. The water collection efficiency (WCE) was calculated using the formula: WCE = w/A.t where w is the weight of collected water in mg, A is the fog capture area in cm^2, and t is the collection time in h. The entire setup was covered with a wooden box.

5.3 Results and Discussions

5.3.1 Synthesis and Characterization of Various Bio-inspired Water Wettability

In chapter 4, I have introduced a chemically reactive, durable, and hydrophilic SLIPS through lubrication of silicone oil in a hydrophilic and chemically reactive porous polymeric coating, where the residual acrylate groups were exploited for spatially selective and in situ chemical modulation using a lubricant-soluble organic phase.[30] However, such an inherently hydrophilic (WCA approximately 20^0) and chemically reactive interface are inappropriate for spatially selective chemical modification with an aqueous solution of hydrophilic (water-soluble) small molecules.[30] Rather, a hydrophobic and chemically reactive interface would be appropriate to restrict unwanted spilling of the beaded aqueous phase during the contact-based spatially selective chemical modulation. During the course of the current study, the same porous polymeric coating, which was prepared by spray deposition of the reaction mixture of branched poly(ethyleneimine) (BPEI) and dipentaerythritol penta acrylate (5Acl), was found to be loaded with two distinct and residual chemical groups—amine and acrylate. As shown in Fig. 5.1 A, this coating was denoted as dual chemically reactive porous polymeric interface (DCRPPI) for the remainder of this text. The existence of these two residual functional groups (acrylate and amine) and their chemical reactivity towards appropriate small

molecules were characterized with standard attenuated total reflectance and Fourier transform infrared (ATR-FTIR) analysis and a fluorescence imaging study, as shown in Fig. 5.2. The DCRPPI was initially treated with Rh–NH_2 (tetramethylrhodamine) where amine moiety of Rh–NH_2 reacted through 1,4 conjugate addition reaction with the residual acrylate of the DCRPPI and the amine groups present in the DCRPPI remained unperturbed. The Rh–NH_2-modified DCRPPI was then treated with fluorescein isothiocyanate (FITC) where the isothiocyanate (–N=C=S) group readily reacted with residual amine groups of the Rh–NH_2 treated DCRPPI. The post-chemical functionalization with Rh–NH_2 and FITC was examined under a fluorescence microscope (Fig. 5.2 B, C). The appearance of both

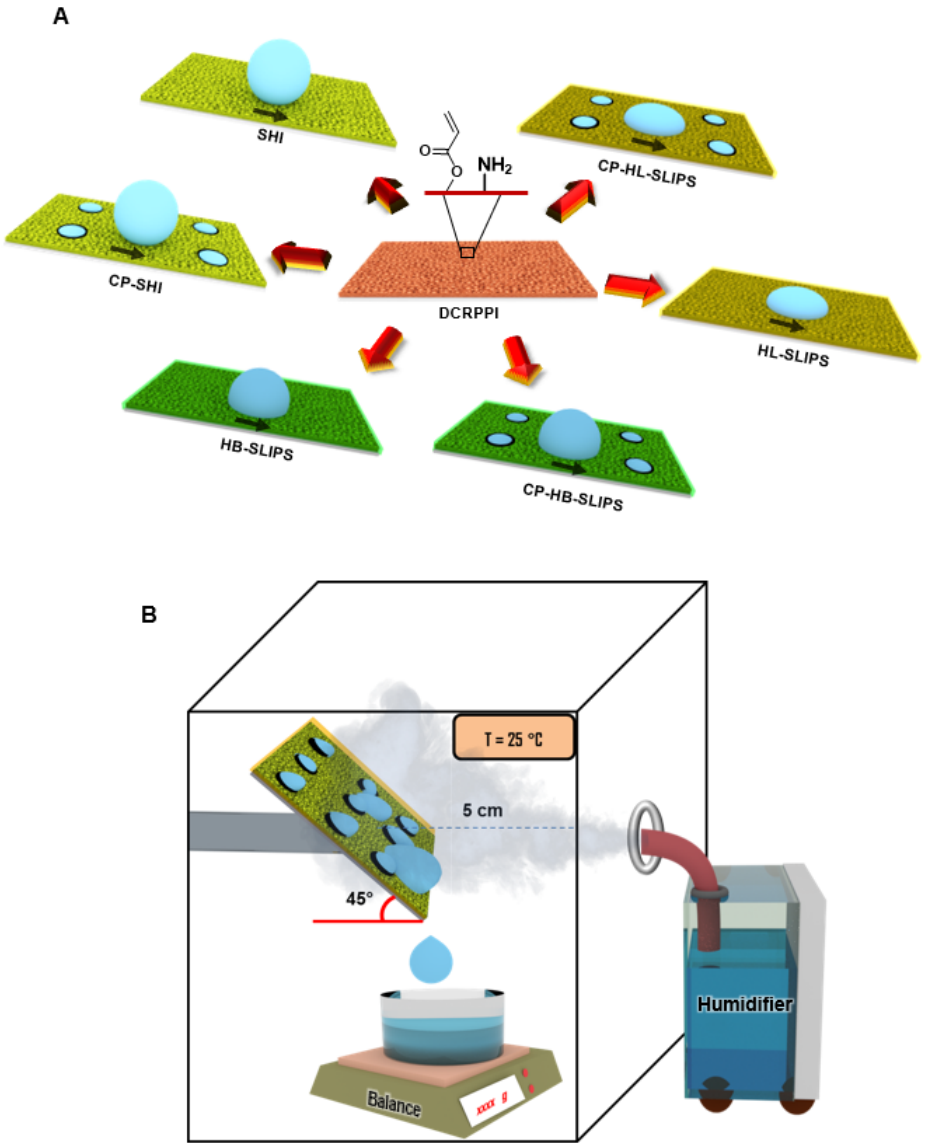

Figure 5.1 (A) A schematic diagram depicting the derivation of various bio-inspired interfaces, including a superhydrophobic interface (SHI), chemically patterned SHI (CP-SHI), hydrophobic/hydrophilic slippery liquid infused porous surface (HB-SLIPS/HL-SLIPS), and chemically patterned SLIPS (CP-HB-SLIPS/CP-HL-SLIPS) from a dual chemically reactive porous polymeric interface (DCRPPI). (B) A schematic diagram illustrating the common experimental setup for evaluating the water harvesting performances of various bio-inspired interfaces.

green and red fluorescence revalidated the successful post-covalent modification of the DCRPPI with two distinct dyes as shown in Fig. 5.2 B, C. However, the DCRPPI that was consecutively pre-treated with D-glucamine and octadecyl acrylate prior to exposing in the respective solutions of Rh–NH_2 and FITC completely failed to display such fluorescence signals, as shown in Fig. 5.2 E, F. It is worth to mention that the pre-treatment of DCRPPI with D-glucamine and octadecyl acrylate led to consumption of both the residual functionalities (primary amine and acrylate) of DCRPPI. The presence of dual residual groups in the DCRPPI also confirmed by FTIR study. The appearance of

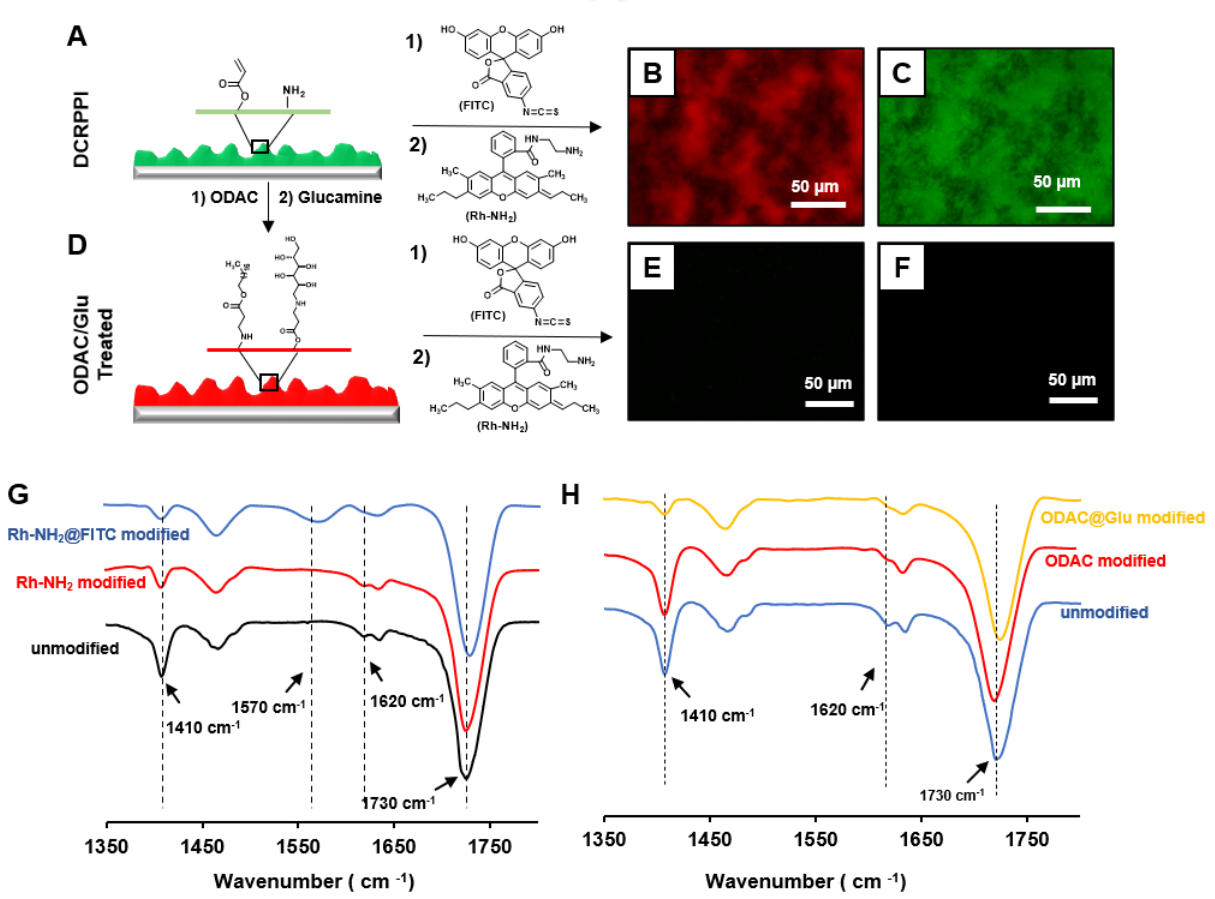

Figure 5.2 (A, D) Schematic representation of DCRPPI before (A) and after (D) consecutive treatments with both ODAC and D-glucamine (denoted as Glu). (B, C) Fluorescence images of the DCRPPI after the sequential treatments with both Rh-NH_2 and FITC. (E, F) Fluorescence images of the DCRPPI that was pre-treated with ODAC and Glu, prior to treatment with both Rh-NH_2 and FITC. The pre-modification of DCRPPI with ODAC and D-glucamine, consumed all the residual reactivates and it failed to react with both Rh-NH_2 and FITC. Eventually, no fluorescence signal was noted. (G) The ATR-IR spectra before (black) and after single (with Rh-NH_2; red) and dual (successive treatments with Rh-NH_2 and FITC; blue) post-modifications of dual chemically reactive porous polymeric coating (DCRPPI), where the characteristic IR peaks at 1730 cm^{-1} and 1410 cm^{-1} were corresponded to the carbonyl stretching and symmetric deformation of the C–H bond for the β carbon of the vinyl group, respectively. Further, the appearance of IR peak at 1570 cm^{-1} confirms the mutual chemical reaction between isothiocyanate group of FITC and residual amine of DCRPPI. (H) ATR-IR spectra of dual chemically reactive porous polymeric coating (DCRPPI) before (blue) and after single (ODAC; red) & dual (successive treatments with both ODAC and D-glucamine; yellow) post covalent modifications. The IR peaks at 1410 cm^{-1}, 1620 cm^{-1} and 1730 cm^{-1} appeared due to symmetric deformation of the C-H stretching of β-carbon of the vinyl group, primary N-H bending of the residual amine and stretching of the carbonyl groups respectively.

characteristic IR signatures at 1410 cm^{-1} (C–H deformation of the β carbon of the vinyl group) and 1730 cm^{-1} (carbonyl groups) validated the existence of residual acrylate groups in the porous polymeric coating. The treatment of this polymeric coating with rhodamine-amine ($Rh–NH_2$) led to significant depletion of the IR peak at 1410 cm^{-1} with respect to another IR signature at 1730 cm^{-1}. The vinyl moiety of the acrylate group readily compromised on reaction with the primary amine of $Rh–NH_2$ through a 1,4-conjugate addition reaction. Next, the existence of residual amine was verified by examining the IR spectra of the porous polymeric coating after the treatment with fluorescein isothiocyanate (FITC), where isothiocyanate groups of FITC readily reacted with residual amine groups. The appearance of a characteristic IR peak at 1570 cm^{-1} for the –N=C=S bond and the depletion of the IR peak at 1620 cm^{-1} (for N–H bending) confirmed the covalent bond formation between isothiocyanate and amine groups. Therefore, the DCRPPI possessed two distinct residual chemical functionalities—which remained chemically reactive. The dual chemical reactivity of the DCRPPI was utilized for adopting various bio-inspired water wettability which will be discussed in the next section. Furthermore, this DCRPPI possessed two distinct chemically reactive groups that were extended to optimize different degrees of bio-inspired liquid wettability through appropriate selection of the post chemical modifications and (or) lubricants. The DCRPPI (Fig. 5.3 A, B) inherently displayed hydrophilicity with a water contact angle (WCA) of approximately 20^0 and became superhydrophobic with a WCA of approximately 154^0 after the post covalent modification with octadecyl acrylate (ODAC), as shown in Fig. 5.3 D, E. A beaded water droplet (6 mL) readily rolled off after the interface was tilted by 9^0. Moreover, this superhydrophobic coating remained chemically reactive, as the residual acrylate group (see Fig. 5.2 H) remained unaffected during the treatment with ODAC. Thus, further treatment of the ODAC-treated superhydrophobic coating with D-glucamine (referred to as Glu-treatment) yielded a highly hydrophilic (WCA approximately 6^0) interface, as shown in Fig. 5.2 G and H. However, no change in topography was noted after incurring these post-covalent modifications (ODAC and Glu) through 1,4 conjugate addition reactions, as evident from field emission scanning electron microscopy (FESEM) images in Fig. 5.3 C, F, and I. Thus, this sharp change in the water wettability in the DCRPPI was due to the selection of appropriate residual reactivity for essential post-covalent modifications. Furthermore, the embedded superhydrophobicity and residual acrylate groups in the ODAC-treated polymeric coating allowed the development of a hydrophilic/superhydrophobic patterned interface (denoted as CP-SHI) through spatially selective chemical modification of the SHI, without having any arbitrary spilling or spreading of the aqueous solution of selected small molecules (i.e., D-glucamine), as shown in Fig. 5.3 J. The hydrophilic spots on the superhydrophobic background were obtained by spatially selective transfer of tiny aqueous

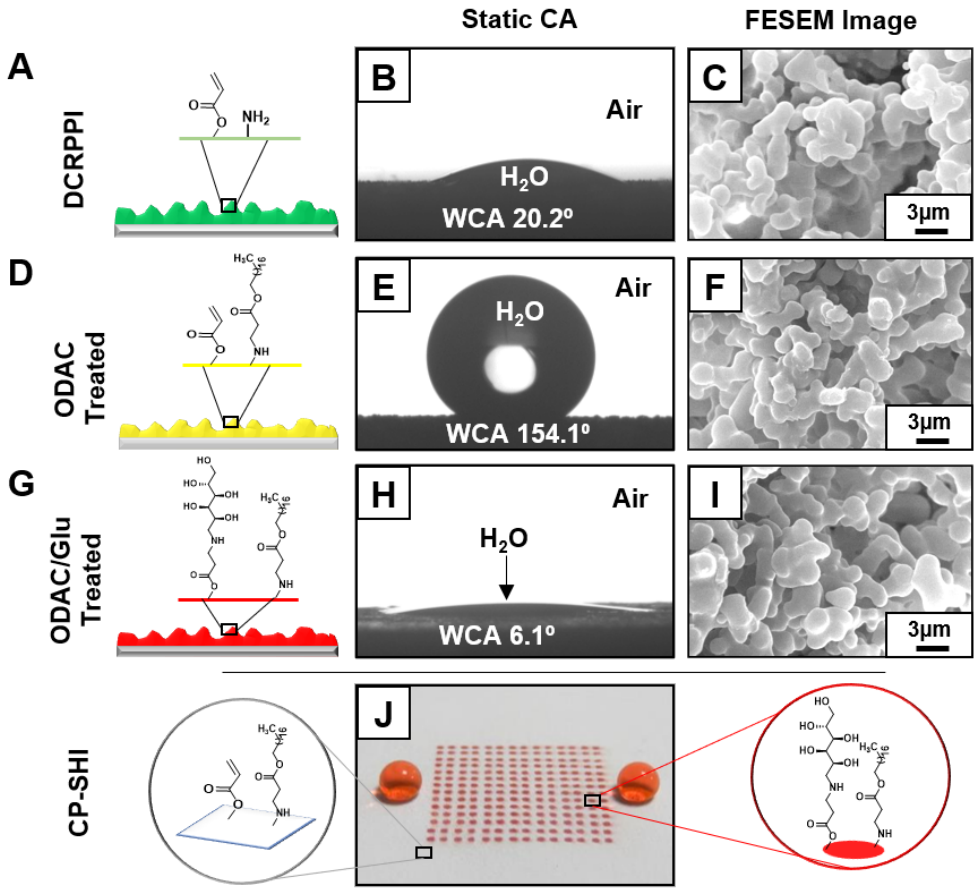

Figure 5.3 (A–I) Schematic representations (A, D and G), contact angle images (B, E and H), and FESEM images (C, F and I) of a dual chemically reactive porous polymeric interface (DCRPPI) before (A–C) and after single (octadecylacrylate: ODAC) (D–F) and dual (consecutive treatment with ODAC and D-glucamine: Glu) (G–I) post-covalent modifications. (J) A digital image of a chemically patterned superhydrophobic interface (CP-SHI), where hydrophilic spots were achieved on a superhydrophobic background via spatially selective chemical modifications. As denoted in the schematic diagrams, the red-coloured aqueous phase aids visual inspection.

solutions (doped with 25% ethanol) of D-glucamine on the SHI using a fountain pen, where primary amine of selected hydrophilic small molecules, i.e., D-glucamine, readily reacted with residual acrylate groups of SHI through a 1,4-conjugate addition reaction. The addition of 25% ethanol to the aqueous solution was essential to facilitate the transfer of aqueous solution from the fountain pen to SHI, where the added (25%) ethanol lowered the contact angle of the beaded aqueous phase to 130^0. Such hydrophobicity ensured both a) the spatially selective transfer of ink and b) unwanted spilling and spreading of the beaded aqueous solution of D-glucamine during the spatially selective post-covalent modification process through a 1,4- conjugate addition reaction. This same chemical approach was extended to achieve HL-SLIPS, HB-SLIPS, and chemically patterned different (hydrophilic and hydrophobic) SLIPS. Thereafter, DCRPPI (hydrophilic with WCA approximately 20^0), SHI (ODAC-treated), and CP-SHI were individually infused with two distinct (natural and synthetic) lubricants—olive oil (natural) and Krytox (synthetic) prior to investigating the water wettability. Interestingly, after

lubrication of hydrophilic DCRPPI with Krytox, a hydrophobic (WCA of approximately 112^0, Fig. 5.3 A) slippery interface was achieved, where a beaded water droplet (30 mL) slipped with a tilting angle of 21.5^0 (Fig. 5.4 B). Unlike past reports, such a design did not demand any conventional post-modification with fluorinated molecules. [3,14–18,21–24] Similarly, after infusion with Krytox, the SHI (ODAC treated) displayed another hydrophobic (WCA of approximately 113^0, Fig. 5.4 C) slippery interface—with a significant lowering of sliding angle (7^0, Fig. 5.4 N). However, the olive oil lubrication in both the DCRPPI- (hydrophilic) and ODAC treated coatings (superhydrophobic) yielded hydrophilic (WCA approximately 79^0 for DCRPPI- and approximately 81^0 for the ODAC-treated coating, Fig. 5.4 E and G) slippery interfaces with a sliding angle below 10^0, as shown in Fig. 5.4 F and H. Thereafter, CP-SHI was separately lubricated with Krytox and olive oil to achieve two distinct chemically patterned SLIPS—i.e., CP-HB-SLIPS and CP-HL-SLIPS. During the sliding of a red-

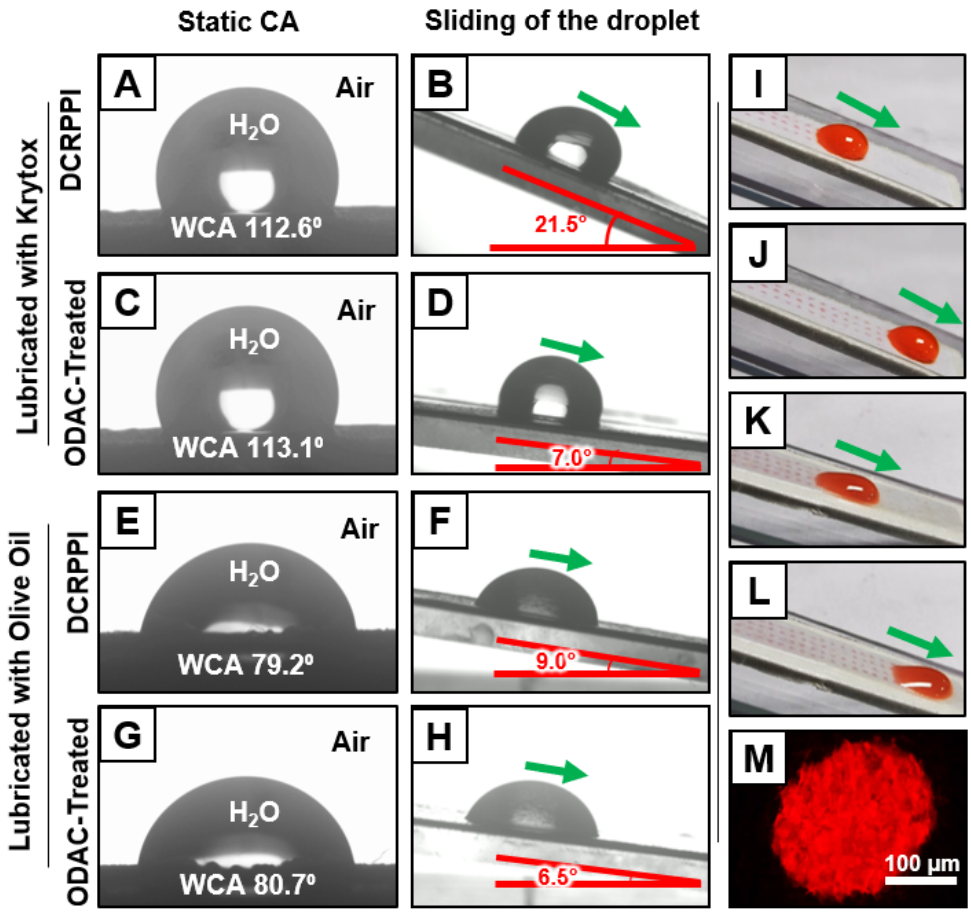

Figure 5.4 (A–H) Contact angle images depicting the wetting (A, C, E and G) and sliding (B, D, F and H) of beaded water droplets on both hydrophobic (HB-SLIPS; A–D) and hydrophilic (HL-SLIPS; E–H) slippery interfaces after the independent infusion of Krytox (A–D) and olive oil (E–H) in both untreated (A, B and E, F) and ODAC-treated (C, D and G, H) DCRPPI. (I–L) Digital images depicting the sliding of a beaded (dyed water aids visual inspection) water droplet on both CP-HB-SLIPS (I and J) and CP-HL-SLIPS (K and L), where the chemically modulated and spatially selected hydrophilic spots selectively wet during the passage of the beaded aqueous droplet. (M) A red fluorescence image showing one of the chemically patterned hydrophilic spots that captured dye in the aqueous phase, while no such fluorescence signal was observed from the lubricated slippery background.

colored aqueous droplet on the CP-HB-SLIPS, the chemically modulated hydrophilic spots selectively captured the aqueous phase, as shown in Fig. 5.4 I and J. Similarly, a CP-HL-SLIPS was achieved by infusing olive oil the CP-SHI, as shown in Fig. 5.4 K and L. Due to the embedded hydrophilicity, an aqueous droplet of the same size (30 mL) was beaded on the CP-HL-SLIPS with more contact area. The chemically modulated and spatially selected hydrophilic spots that got exposed to beaded aqueous droplets, were readily captured some portion of aqueous phase during the sliding of the beaded aqueous droplet on the CP-HL-SLIPS, as shown in Fig. 5.4 K and L. The microscopic image in Fig. 5.3 M shows the size of a hydrophilic spot on the slippery background of the patterned SLIPS.

5.3.2 Water Harvesting Performance of Different Bio-inspired Interfaces

Next, the water harvesting performance of these interfaces was investigated in detail (Fig. 5.5). Similar to the past demonstration,[15] both the growth and the shedding of condensed water droplets were accelerated for the synthesized HL-SLIPS (Fig. 5.5 F–J) in comparison to both SHI (Fig. 5.5 K-O) and HB-SLIPS (Fig. 5.5 A-E). The shedding of the water droplets on HL-SLIPS was observed right after 107 s of exposure to artificial fog, whereas more than double time (230 s) was required to achieve the shedding of water droplets on HB-SLIPS under identical experimental conditions (Fig. 5.5 A–E).

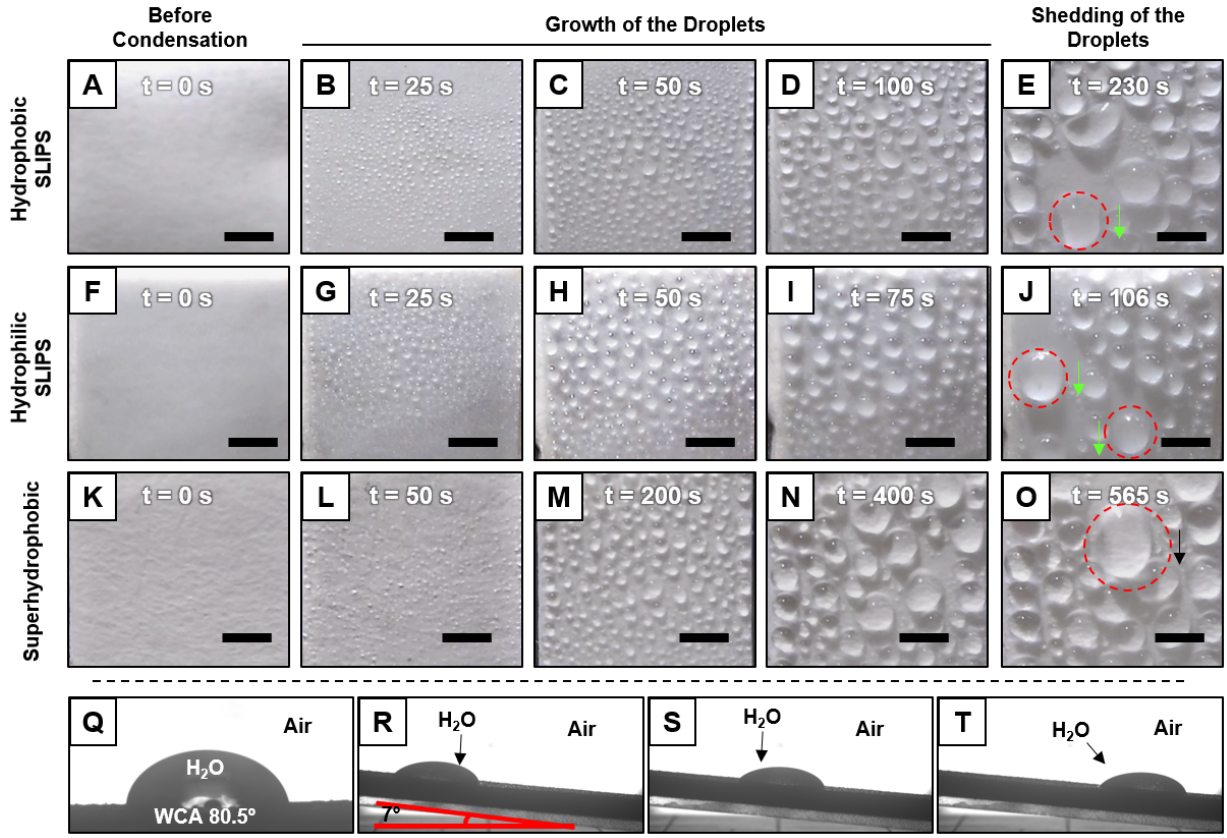

Figure 5.5 (A-O) Digital images illustrating the process of water harvesting on hydrophobic-SLIPS (HB-SLIPS; A-E, scale: 3 mm), hydrophilic-SLIPS (HL-SLIPS; F-J, scale: 3 mm) and superhydrophobic interface (SHI; K-O, scale: 3 mm). (Q-T) The contact angle images depicting the static water contact angle and slipping of beaded water droplet on hydrophilic SLIPS after fog collection.

Therefore, the time required to reach the maximum and steady water harvesting was greater for HB-SLIPS. The water-harvesting ability was significantly lower for the synthesized superhydrophobic interface (SHI) due to the pinning of condensed water droplets (Fig. 5.5 K–O). The condensed water droplets were known to pin on the superhydrophobic interface due to the conversion of the Cassie–Baxter state to the Wenzel state.[22] Eventually, the shedding of water droplets was delayed (Fig. 5.5 K–O) on the SHI. The superhydrophobic property has been found to be inefficient for water harvesting from the artificial fog as the flooding of the interface was noted whereas the slippery property of SLIPS remained unaltered after the performance of fog collection. The beaded aqueous droplet freely slipped away along the downslope on the HL-SLIPS after one hour of artificial fog collection as shown in Fig. 5.5 Q-T. Furthermore, the rapid shedding of water droplets contributed to achieving an improved water-harvesting performance for HL-SLIPS (1100 mg cm^{-2} h^{-1}), in comparison to HB-SLIPS (800 mg cm^{-2} h^{-1}) and SHI (250 mg cm^{-2} h^{-1}), as shown in Fig. 5.7 B.

5.3.3 Effect of Spatially Selective Patterns on Water harvesting Performance

The nucleation rate is higher for an interface with high surface energy (i.e. hydrophilic surface) but, the flooding of hydrophilic surface with water layer, prevented the fresh nucleation of water vapor. Eventually, the water harvesting performance was observed to be very poor on uniformly hydrophilic interfaces. To avoid this flooding issue, many research groups introduced bio-inspired wettability-where the heterogeneous nucleation was observed, but rapid shedding of mature water droplet allowed a continuous and repetitive nucleation on same interface—and prevented the flooding of the water harvesting interfaces.

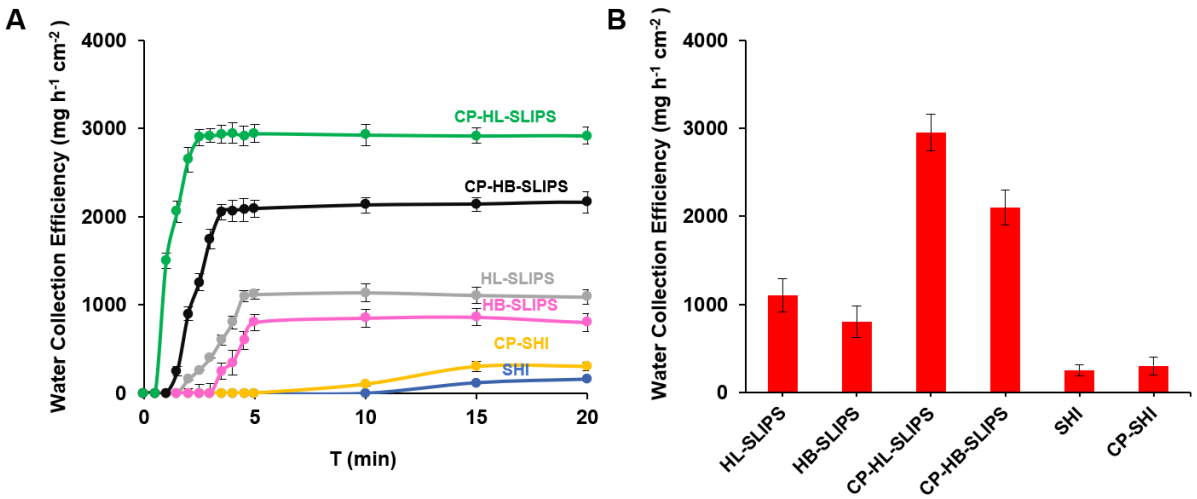

Figure 5.6 (A and B) Plots illustrating the initial rate of water collection (A) and the water harvesting efficiency (B) for different bio-mimicking interfaces, including SHI, CP-SHI, HL-SLIPS, HB-SLIPS, CP-HB-SLIPS, and CP-HL-SLIPS.

Slippery interface is already known for high rate of nucleation,[3] the only challenge is to achieve faster shedding of droplets.[14-15] In this chapter, spatially selective hydrophilic patterns were introduced on both hydrophilic-SLIPS and hydrophobic-SLIPS for achieving an improved water harvesting performance. Interestingly, when the hydrophilic spots were incorporated onto both hydrophobic

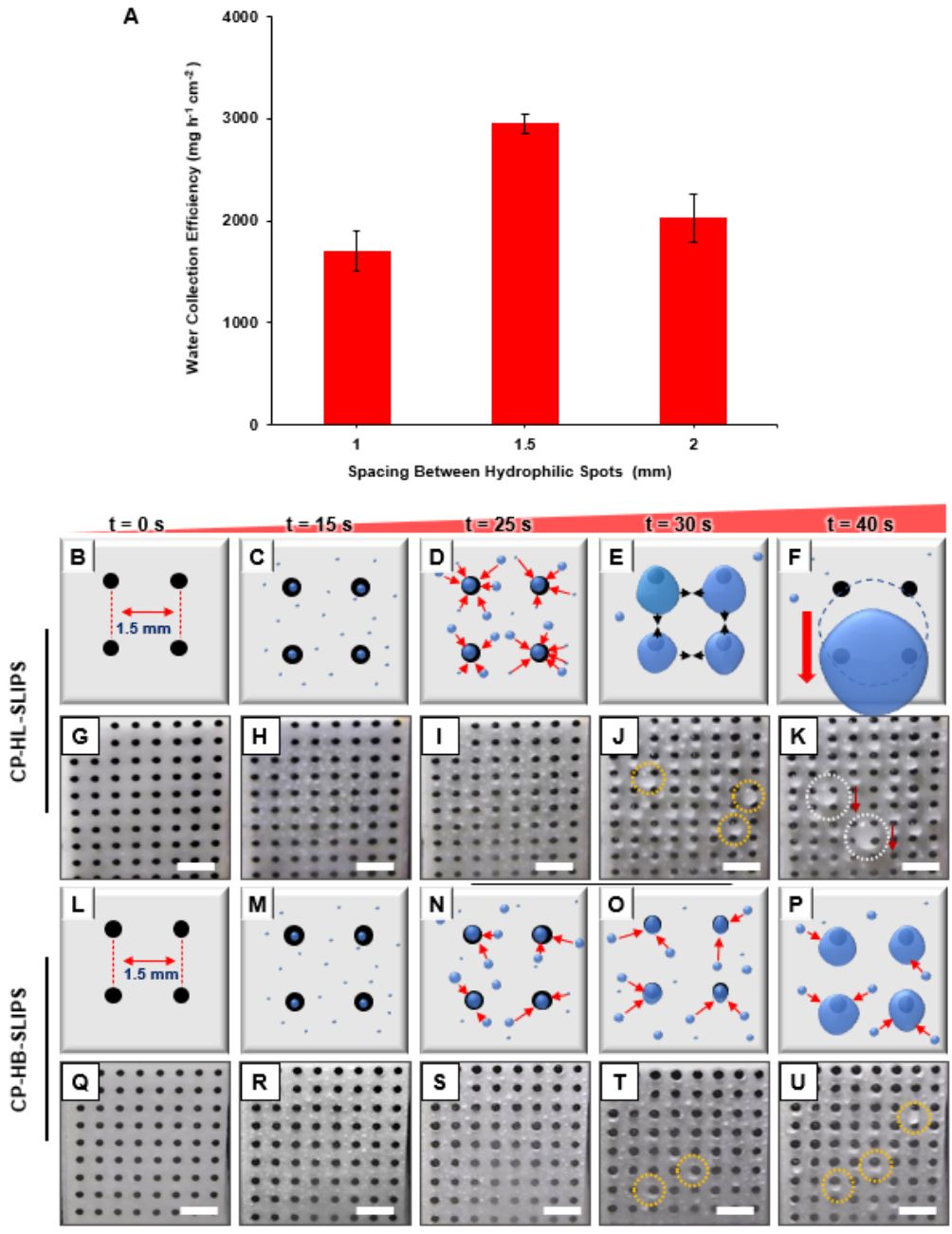

Figure 5.7 (A) A plot accounting the impact of change in the spacing between hydrophilic spots of CP-HL-SLIPS on the water harvesting ability. (B–U) Schematic representations (B–F and L–P) and digital images (G–K and Q–U) depicting different stages of the water-harvesting process on both CP-HL-SLIPS (B–K) and CP-HB-SLIPS (L–U), where each black spot indicates the location of the hydrophilic spot on the chemically patterned slippery interfaces. Initially, water condensation was observed everywhere on the patterned interface (C and M). Then, water droplets began to accumulate (I, J and S, T) on hydrophilic spots, and, finally, the shedding (K) of water droplets was noted on CP-HL-SLIPS. The shedding of water droplets is indicated with white dotted circles. Such shedding was not observed on CP-HB-SLIPS after 40 s because the water droplet shedding was significantly delayed (84 s). Scale bar: 3 mm.

SLIPS (HB-SLIPS) and hydrophilic SLIPS (HL-SLIPS) through spatially selected chemical modulation with D-glucamine, a rapid shedding of water droplets found to be observed as compared to both HB-SLIPS and HL-SLIPS respectively. In fact, the time required for continuous shedding of aqueous droplets for CP-HL-SLIPS was lesser than that of CP-HB-SLIPS. Therefore, a better and improved water harvesting efficiency was observed for CP-HL-SLIPS as compared to CP-HB-SLIPS as shown in Fig. 5.6 B. Each black dot that was pre-printed on the paper prior to depositing the chemically reactive porous polymeric coating assisted in (1) associating spatially selective chemical modification with D-glucamine, prior to lubrication and (2) identifying the hydrophilic spots on both the CP-HL-SLIPS/CP-HB-SLIPS during the water-harvesting process. The arrangement of hydrophilic spots on HL-SLIPS played a crucial role in achieving a fast shedding (approximately 40 s) of water droplets via the accelerated accumulation of condensed water droplets at hydrophilic spots, as evident from Fig. 5.7 A. Optimum (1.5 mm) spacing between hydrophilic spots provided highly efficient (2950 mg cm^{-2} h-1) water-harvesting SLIPS (Fig. 5.7 A), whereas either an increment or decrement of the spacing between two adjacent hydrophilic spots on CP-HL-SLIPS resulted in a compromise of the water-harvesting ability (Fig. 5.7 A). Thereafter, the water-harvesting process of CP-HL-SLIPS was compared with CP-HB-SLIPS, where the spacing between the two adjacent hydrophilic spots was maintained at 1.5 mm, as shown in Fig. 5.7 B–K and Fig. 5.7 L–U. The shedding of water droplets on CP-HB-SLIPS was significantly slower (by more than two times: 84 s) with respect to CP-HL-SLIPS. However, it remained faster in comparison to only HB-SLIPS (having no hydrophilic spot). Furthermore, with respect to CP-HL-SLIPS, a sluggish accumulation of water droplets at hydrophilic spots and the fusion of large droplets at hydrophilic spots were observed for CP-HB-SLIPS (Fig. 5.7 Q–U), which was likely due to the restricted spreading of condensed water droplets on the hydrophobic slippery background of CP-HB-SLIPS.

5.3.4 Effect of Physical Confinement on Water Harvesting Performance

Overall, each and every hydrophilic spots on the liquid infused slippery background of SLIPS (either hydrophobic or hydrophilic) contributed to faster growth of condensed droplets, which was followed by rapid shedding of the accumulated droplets that eventually conferred a more efficient water harvesting performance (Fig. 5.6 A, B). Furthermore, these hydrophilic spots were arranged on the physically confined (Fig. 5.8 A–M) CP-HB-SLIPS and CP- HL-SLIPS so that the impact of this confinement on water-harvesting efficiency could be investigated. This was accomplished by aligning an array of hydrophilic spots in a single line with the spacing of 1.5 mm, and the edge-to-edge distance of the respective slippery background was varied from 1 mm to 3 mm (Fig. 5.8 M). Interestingly, the

physical confinement of the hydrophilic spots with an end-to-end edge distance of 2 mm resulted in the most synergistic changes with respect to both the growth and the shedding of the condensed water droplets (Fig. 5.8 E–L). The rapid accumulation of the condensed water droplets in the hydrophilic

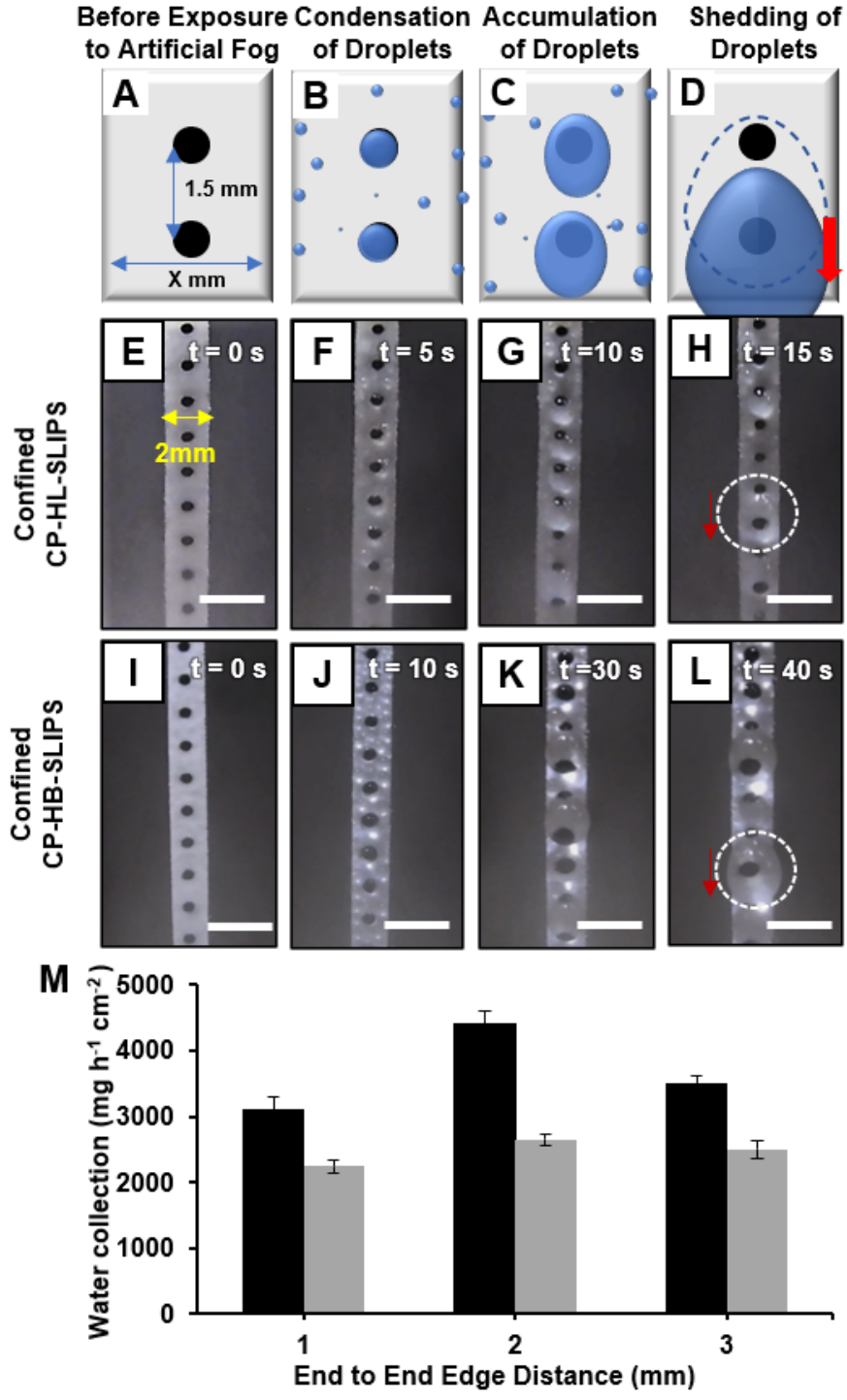

Figure 5.8 (A–D) Schematic representations of the process of water harvesting on a physically confined patterned interface, where the spacing in between hydrophilic spots was maintained at 1.5 mm, and the edge-to-edge distance of the slippery surface was varied from 1 mm to 3 mm. (E–L) Digital images showing the water harvesting process from artificial fog on physically confined CP-HL-SLIPS (E–H, scale: 3 mm) and CP-HB-SLIPS (I–L, scale: 3 mm). (M) A plot showing the water-harvesting efficiency for CP-HL-SLIPS (black) and CP-HB-SLIPS (grey), where the impact of the edge-to-edge distance (mm) on the water-harvesting ability was investigated.

spots contributed to the fast growth of the droplets, as shown in Fig. 5.8 E–H, which resulted in ultra-fast (within 15 s) shedding of droplets from physically confined CP-HL-SLIPS. However, the growth and shedding of the droplets were relatively slow for physically confined CP-HB-SLIPS. Eventually, a record (4400 ± 190 mg cm^{-2} h^{-1}) water-harvesting efficiency was achieved for inherently durable pitcher plant-inspired SLIPS. Furthermore, if there was any increment (3 mm) or decrement (1 mm) of edge-to-edge distances of a chemically patterned slippery interface, the shedding of the water droplets was significantly delayed for both the CP-HB-SLIPS and CP-HL-SLIPS as shown in Fig. 5.8 M). Thus, this simple design provides a more realistic solution for efficient water harvesting. If the edible lubricant significantly contaminates the harvested water and the situation demands, the aqueous phase could be separated from the oil contamination following a reported underwater superoleophobicity assisted facile and environmentally friendly oil and water separation process.[32]

5.4 Conclusions

In summary, two important issues are addressed through the current research study. First, a dual chemically reactive and porous polymeric coating has been appropriately and chemically modulated to adopt different bio-inspired interfaces, including superhydrophobic, patterned-superhydrophobic, hydrophobic SLIPS, hydrophilic SLIPS, chemically patterned hydrophilic SLIPS, and chemically patterned hydrophobic SLIPS, through a 1,4-conjugate addition reaction. Furthermore, the water-harvesting abilities of these interfaces were compared under an identical experimental set-up. Second, the current study revealed that an appropriate arrangement of a chemically modulated pattern and the physical confinement of hydrophilic SLIPS led to the rapid shedding (from 107 s to 15 s) of condensed water droplets, which eventually provided a highly efficient (4400 ± 190 mg cm^{-2} h^{-1}) water-harvesting SLIPS.

5.5 References

1. Daniel, S.; Chaudhury, M. K.; Chen, J. C. *Science* **2001**, *291*, 633–636.
2. Zheng, Y.; Bai, H.; Huang, Z.; Tian, X.; Nie, F.-Q.; Zhao, Y.; Zhai, J.; Jiang, L. *Nature* **2010**, *463*, 640–643.
3. Anand, S.; Paxson, A. T.; Dhiman, R.; Smith J. D.; Varanasi, K. K. *ACS Nano* **2012**, *6*, 10122–10129.
4. Miljkovic, N.; Enright, R.; Nam, Y.; Lopez, K.; Dou, N.; Sack J.; Wang, E. N. *Nano Lett.* **2013**, *13*, 179–187.
5. Xiao, R.; Miljkovic, N.; Enright, R.; Wang, E. N. *Sci. Rep.* **2013**, *3*, 1988.
6. Mouterde, T.; Lehoucq, G.; Xavier, S.; Checco, A.; Black, C. T.; Rahman, A.; Midavaine, T.; Clanet C.; Qu´er´e, D. *Nat. Mater.* **2017**, *16*, 658–663.

7. Malik, F. T.; Clement, R. M.; Gethin, D. T.; Krawszik W.; Parker, A. R.; *Bioinspiration Biomimetics* **2014**, *9*, 031002.
8. Clus, O.; Ortega, P.; Muselli, M.; Milimouk, I.; Beysens, D. *J. Hydrol.* **2008**, *361*, 159–171.
9. Lei, J.; Guo, Z. *Nanoscale* **2020**, *12*, 6921–6936.
10. Parker, A. R.; Lawrence, C. R. *Nature* **2001**, *414*, 33–34.
11. Bai, H.; Wang, L.; Ju, J.; Sun, R.; Zheng, Y.; Jiang, L. *Adv. Mater*. **2014**, *26*, 5025–5030.
12. Zhang, L.; Wu, J.; Hedhili, M. N.; Yang, X.; Wang, P. *J. Mater. Chem. A* **2015**, *3*, 2844–2852.
13. Zhu, H.; Guo, Z. *Chem. Commun*. 2016, *52*, 6809–6812.
14. Park, K.-C.; Kim, P.; Grinthal, A.; He, N.; Fox, D.; Weaver, J. C.; Aizenberg, J. *Nature* **2016**, *531*, 78–82.
15. Dai, X.; Sun, N.; Nielsen, S. O.; Stogin, B. B.; Wang, J.; Yang, S.; Wong, T.-S. *Sci. Adv.* **2018**, *4*, eaaq0919.
16. Luo, H.; Lu, Y.; Yin, S.; Huang, S.; Song, J.; Chen, F.; Chen, F.; Carmalt, C. J.; Parkin, I. P. *J. Mater. Chem. A* **2018**, *6*, 5635–5643.
17. Ang, B. T. W.; Zhang, J.; Lin, G. J.; Wang, H.; Lee, W. S. V.; Xue, J. *ACS Appl. Mater. Interfaces* **2019**, *11*, 27464–27469.
18. Feng, R.; Xu, C.; Song, F.; Wang, F.; Wang, X.-L.; Wang, Y.-Z. *ACS Appl. Mater. Interfaces* **2020**, *12*, 12373–12381.
19. Cassie, A. B. D.; Baxter, S. *Trans. Faraday Soc.* **1944**, *40*, 546–551.
20. Wier, K. A.; McCarthy, T. J. *Langmuir* **2006**, *22*, 2433–2436.
21. Cheng, Y.-T.; Rodak, D. E. *Appl. Phys. Lett*. **2005**, *86*, 144101.
22. Koishi, T.; Yasuoka, K.; Fujikawa, S.; Ebisuzaki, T.; Zeng, X. C. *Proc. Natl. Acad. Sci. U. S. A.* **2009**, *106*, 8435–8440.
23. Wong, T.-S.; Kang, S. H.; Tang, S. K. Y.; Smythe, E. J.; Hatton, B. D.; Grinthal A.; Aizenberg, J. *Nature* **2011**, *477*, 443–447.
24. Villegas, M.; Zhang, Y.; Jarad, N. A.; Soleymani, L.; Didar, T. F. *ACS Nano* **2019**, *13*, 8517–8536.
25. Chapman, S. P.; Hong, J. K.; Waterhouse, A.; Neto, C. *Chem. Soc. Rev.* **2020**, *49*, 3688–3715.
26. Manna, U.; Lynn, D. M. Adv. Mater. **2015**, *27*, 3007–3012.
27. Li, J.; Ueda, E.; Paulssen, D.; Levkin, P. A. *Adv. Funct. Mater.* **2019**, *29*, 1802317–1802329.
28. Paulssen, D.; Hardt, S.; Levkin, P. A. *ACS Appl. Mater. Interfaces* **2019**, *11*, 16130–16138.
29. Jiang, J.; Gao, J.; Zhang, H.; He, W.; Zhang, J.; Daniel, D.; Yao, X. *Proc. Natl. Acad. Sci. U. S. A*. **2019**, *116*, 2482–2487.

30. Maji, K.; Das, A.; Hirtz, M.; Manna, U. *ACS Appl. Mater. Interfaces* **2020**, *12*, 14531–14541.
31. Yu, Z.; Yun, F. F.; Wang, Y.; Yao, L.; Dou, S.; Liu, K.; Jiang, L.; Wang, X. *small* **2017**, *13*, 1701403.
32. Chu, Z.; Feng, Y.; Seeger, S. *Angew. Chem. Int. Ed.* **2015**, *54*, 2328–2338.

Conclusions and Future Plan

In chapter 6, I have summarized the thesis work demonstrated in each chapter and further, I have provided possible future plans which are related to this thesis work. In general, conventional approaches for the development of bio-mimicked special wettable interfaces including lotus-leaf inspired superhydrophobic surface (SHS) and nepenthes-pitcher plant-inspired slippery liquid infused porous surfaces (SLIPS), were fabricated using expensive chemicals through weak/delicate chemical bondings/interactions, complex/tedious methods, inert chemistries. Therefore, these associated limitations of existing approaches restrict its applications in practically relevant scenarios. The current thesis work highlighted facile synthetic procedures for the various scalable and durable bio-mimicked interfaces for relevant applications. In my thesis work, I have tailored the growth of chemically reactive polymeric nanocomplex (CRPNC) which was synthesized through catalyst-free 1,4 conjugate addition reaction between branched poly(ethyleneimine) (BPEI) and dipentaerythritol penta/hexa acrylate (5 Acl) for the preparation of reactive polymeric coating on various substrates for desired anti-wetting interfaces. Moreover, I have introduced a simple dilution method for the preparation of stable dispersion of CRPNC in ethanolic solvent for dip coating for multiple cycles with the same deposition solution. Then a dip-coating process was adopted to coat a commercially available spongy material, melamine sponge (MS) using the synthesized stable dispersion of CRPNC to develop a chemically reactive polymeric coating on the selected substrate. A desired post-covalent modification with long-tail alkylamine produced physically and chemically abrasion tolerant compressible superhydrophobic melamine sponge (SMS). This highly deformable and robust superhydrophobic melamine sponge (SMS) that selectively absorbed oil/oily phase with the capacity of 70 gg^{-1}, was extended for separating oil-spillages from the aqueous phase. Furthermore, the oil/water separation performance remains unaltered at practically relevant different severe aqueous mediums. Also, I have developed solvent-dependent accelerated growth of CRPNC to synthesize three-dimensional chemically reactive polymeric coating onto various substrates including flat and geometrically complex objects following a facile and scalable spray deposition process. The inherently hydrophilic chemically reactive polymeric coating yielded both controlled-adhesive superhydrophobicity (CASH) and non-adhesive superhydrophobicity (NASH) through appropriate post-chemical functionalization with different alkylamines through 1,4 conjugate addition reaction at ambient conditions. Furthermore, the fractional contact area between the beaded water droplet and the polymeric coating was tailored by adopting appropriate post-chemical modifications. The synthesized coating survived severe physical abrasions and exposures to harsh aqueous phases. Moreover, the self-cleaning performance of the robust superhydrophobic coatings was demonstrated using a coated superhydrophobic shoe. The same

hydrophilic reactive polymeric coating having residual acrylate groups three-dimensionally showed slippery behavior towards aqueous phases after infusion of silicone oil without incurring any prior hydrophobization which has been conventionally regarded as an essential parameter for achieving SLIPS. The presence of residual acrylate groups in the chemically reactive polymeric coating provided essential chemical compatibility between selected lubricants and porous polymeric matrix even though the overall coating remained hydrophilic. Therefore, the essential criteria for synthesizing artificial SLIPS were revisited and revalidated with the help of the residual chemical reactivity of the porous polymeric coating. However, the chemical reactivity of the polymeric coating was not perturbed even after the infusion of selected lubricants. Eventually, a spatially selective in situ covalent modification was demonstrated from organic solvents. The reactive porous polymeric coating which has been synthesized through spray deposition of CRPNC using pentanol as a reacting medium possessed two distinct reactive residual groups, acrylate, and amine. The dual chemical reactivities of the porous polymeric coating and the appropriate selection of lubricants allowed to adopt various bio-inspired water wettability including a reactive superhydrophobic interface (SHI), chemically patterned superhydrophobic interface (CP-SHI), hydrophilic SLIPS (HL-SLIPS), hydrophobic SLIPS (HB-SLIPS), chemically patterned hydrophilic SLIPS (CP-HL-SLIPS), chemically patterned hydrophobic SLIPS (CP-HB-SLIPS). Further, the water harvesting performance of all of these interfaces was examined under an identical experimental set-up. The specific arrangement of chemically modulated hydrophilic patterns on hydrophilic-slippery background accelerated both the growth and shedding of the condensed water droplets. Finally, physical confinement on chemically patterned hydrophilic SLIPS (CP-HL-SLIPS) helped to achieve a record water harvesting efficiency of 4400 ± 190 mg cm^{-2} h^{-1}.

Thus, it is clearly realized that current thesis work can be further extended to develop various smart materials for many possible realistic applications. For instance, the synthesized SMS could be integrated with some robotic devices for oil/water separation in practical settings. In the recent past, bulk superhydrophobic materials are an alternative material for the controlled and sustained release of embedded drug-like small molecules. The presence of metastable trapped air layer (presence of Cassie-Baxter state) at the surface and in the interior of bulk superhydrophobic materials provides the means for the slow infiltration of water and thereby promotes the slow and controlled release of embedded drug-like small molecules. Hence, the synthesized polymeric material having different post-chemical modifications for controlled water wettability in the current thesis has an immense prospective for the controlled and sustained release of small molecules. The controlled adhesiveness of the superhydrophobic polymeric coating could be further exploited for the transportation of tiny aqueous

droplets which are very relevant in bio-medical applications and tissue-engineerings. Further, the reactive slippery interfaces will be useful for anti-platelet adhesion, marine biofouling, and anti-corrosion coatings. The various architecture can also be integrated with different bio-inspired interfaces for atmospheric water collection at low humid conditions which could be useful for remediating the crisis of fresh-water. Further, the incorporation of hydrophilic MOF within the patterned interfaces might lead to the enhancement of water harvesting efficiency. Thus, the controlled growth of CRPNC and its scalable deposition to achieve chemically reactive coating on diverse substrates could be useful in developing various functional materials for different perspectives in the near future.

List of acronyms used throughout the thesis

5 Acl	Dipentaerithritol penta acrylate
BPEI	Branched polyethyleneimine
ODA	Octadecylamine
ODAC	Octadecylacrylate
DI	Deionized
DTAB	Dodecyl trimethyl ammonium bromide
SDS	Sodium dodecyl sulfate
DCM	Dichloromethane
FTIR	Fourier-transform infrared
FESEM	Field emission scanning electron microscope
WCA	Water contact angle
CRPNC	Chemically reactive polymeric nanocomplex
MS	Melamine sponge
SMS	Superhydrophobic melamine sponge
CASH	Controlled-adhesive superhydrophobicity
NASH	Non-adhesive superhydrophobicity
SLIPS	Slippery liquid-infused porous surfaces
DCRPPI	Dual chemically reactive porous polymeric interface
SHI	Superhydrophobic interface
HB-SLIPS	Hydrophobic slippery liquid-infused porous surfaces
HL-SLIPS	Hydrophilic slippery liquid-infused porous surfaces
CP-SHI	Chemically patterned superhydrophobic interface
CP-HB-SLIPS	Chemically patterned hydrophobic slippery liquid-infused porous surfaces
CP-HL-SLIPS	Chemically patterned hydrophilic slippery liquid-infused porous surfaces

List of Publications

1. Shome, A.; **Maji, K**.; Rather, A. M.; Yashwanth, A.; Patel, D. K.; Manna, U. *Chem. Asian J.* **2019**, *14*, 4732 – 4740.
2. **Maji, K**.; Manna, U. *J. Mater. Chem. A* **2018,** *6*, 6642 − 6653.
3. **Maji, K**.; Das, A.; Hirtz, M.; Manna, U. *ACS Appl. Mater. Interfaces* **2020**, *12*, 14531−14541.
4. **Maji, K**.; Das, A.; Dhar, M.; Manna, U. *J. Mater. Chem. A* **2020**, *8*, 25040–25046.
5. Das, A.; **Maji, K**.; Naskar, S.; Manna, U. *Chem. Sci.,* **2020**, *11*, 6556 −6566.
6. Parbat, D.; Das, A.; **Maji, K**.; Manna, U. *J. Mater. Chem. A* **2020**, *8*, 97 −106.
7. Rather, A.M.; Mahato, S.; **Maji, K**.; Gogoi, N.; Manna, U. *Nanoscale*, **2017**, *9*, 16154–16165

List of Patents

1. Uttam Manna, V. Nandakumar, Karthick R, **Kousik Maji**, Arpita Shome, Adil Majeed Rather, 'Selective and Super Oil Absorbent for Remediation of Oil Spills' Submitted as: Indian Patent (Application No 201841029004, application date: Aug 1, 2018), Applied.

2. Uttam Manna, V. Nandakumar, Karthick R, Avijit Das, **Kousik Maji**, Arpita Shome 'A process for preparation of a superhydrophobic membrane', Submitted as: Indian Patent (Application No 202041005525, application date: Feb 7, 2020), Applied.

Conferences/Seminars Attended

- Presented Model based on "Stretchable and Porous Superhydrophobic Fibrous Substrate for Oil Spill Clean-up" in '**Research Conclave' (2018)** organized by Students' Academic Board (SAB), IIT Guwahati.
- Presented poster entitled "Covalent and Bulk 'Optimization' of Chemical Functionalities in Porous Organic Coating" in **'Research Conclave' (2018)** organized by Students' Academic Board (SAB), IIT Guwahati.
- Presented poster entitled "Covalent and Bulk 'Optimization' of Chemical Functionalities in Porous Organic Coating" in the International Conference - **'Frontiers in Chemical Sciences (FICS 2018)** organized by Department of Chemistry, IIT Guwahati.
- Presented poster entitled "Covalent and Bulk 'Optimization' of Chemical Functionalities in Porous Organic Coating" in the International Conference -**Reflux 7.0 (2019),** organized by Department of Chemical Engineering, IIT Guwahati.